FIBER OPTIC SENSORS

FUNDAMENTALS AND APPLICATIONS

Fourth Edition

FIBER OPTIC SENSORS

FUNDAMENTALS AND APPLICATIONS

Fourth Edition

David Krohn
Trevor MacDougall
Alexis Mendez

SPIE PRESS
Bellingham, Washington USA

Library of Congress Cataloging-in-Publication Data

Krohn, D. A. (David A)
Fiber optic sensors : fundamentals and applications / D.A. Krohn. Fourth edition.
pages cm
Includes bibliographical references and index.
ISBN 978-1-6284-1180-5
1. Optical fiber detectors. 2. Optical fibers Industrial applications. I. Title.
TA1815.K76 2014
681'.25 dc23

2014009882

Published by

SPIE
P.O. Box 10
Bellingham, Washington 98227-0010 USA
Phone: 360.676.3290
Fax: 360.647.1445
Email: Books@spie.org
www.spie.org

Printed in the United States of America
First printing

Cover images courtesy of Shutterstock.

SPIE.

To my grandson, Matthew Trotta, who at a very young age is showing a keen interest in science and engineering; and who has already made contributions to fiber optic sensor design.

D.K.

Many things must come together for one to have the opportunity to contribute towards the writing of a book. I have been very fortunate to find myself in such a position. Thanks are owed to my parents for their unselfish sacrifice, to my wife, Laurie, for always being everything to me, and to my three children, Kristin, Jesse, and Robyn, who always provide endless happiness and inspiration.

In addition, I would like to thank all of my colleagues at 3M, CiDRA, Weatherford, and Petrospec/QOREX, whose creative work and enormous talents deepened my understanding of much of this material and whose world class ingenuity turned much of this technology into real life products and commercial successes. No one can ever do these things alone.

T.M.

To my daughter Ariane—my little angel, with all my love.

A.M.

Table of Contents

Preface

Fiber optic sensor technology is not new, but is continuing to evolve after over 60 years of development and commercialization. The sensing designs are not based on a single concept but on a variety of optical phenomena that can be used to measure a broad range of physical and chemical parameters.

In early industrial applications, single point fiber optic sensors were used as an alarm to indicate the absence or presence of an object. As the technology evolved, the functionality increased to accurately determine the position of an object. Many of the sensing concepts that will be discussed throughout this book will be for single point sensors, which operate by detecting changes in the intensity of light (see Chapters 3, 8, and 9). They operate by altering the transmitted or reflected light intensity in a manner proportional to the parameter being sensed such as temperature, strain, or displacement (position). The sensing functionality can be expanded to monitor electric and magnetic field measurements using polarization concepts. As an example, certain materials exhibit Faraday rotation, which alters the plane of polarization and the resulting transmitted light intensity in the presence of a magnetic field. Polarization-based sensors are discussed in Chapter 7.

Interferometric sensors compare the phase of light in a sensing fiber to a reference fiber. Small phase shifts can be detected with extreme accuracy. The phase shifts are generated by changes in strain and/or temperature in the sensing fiber. This family of sensors has been especially useful in monitoring dynamic strain (vibration) (see Chapter 4). Also, a Sagnac interferometer is an interferometric sensor configured to be sensitive to rotation (Chapter 17). Two examples of successful commercialization of interfermetric-based sensors are hydrophones for submarine detection and fiber optic gyroscopes for advanced navigation systems. Both are for military applications primarily and have performed well for over 30 years with thousands of systems deployed.

A wavelength or spectral shift is another sensing approach. By introducing coatings on the fiber or a target that fluoresces, under certain conditions (usually related to chemical interaction or temperature fluctuation), a chemical reagent can be detected or temperature can be monitored. A more widely used spectral shift approach uses Bragg gratings, which are reviewed in detail in Chapter 5. A Bragg grating is characterized by having a

resonant wavelength that is reflected as light is transmitted through the grating. The reflected light is very sensitive to the grating spacing and the index of refraction of the grating material. Temperature and strain alter both of these parameters. As a result, Bragg gratings can function as temperature or strain sensors. While Bragg gratings have been used as single point sensors, they have had great utility as quasi-distributed sensors in which multiple sensors are located along a single fiber.

Bragg gratings, which have been in development for over 25 years are in wide commercial use. They have been especially effective in enabling smart civil structures and as pressure and temperature sensors in smart oil wells. Bragg gratings have evolved to handle the very harsh environment associated with energy applications.

Light-scattering phenomena have emerged in the last 10 years to be a key family of technologies to enable fully distributed fiber optic sensing systems. Distributed sensing systems allow any point along a fiber to function as a sensor, with virtually thousands of sensing points along a single fiber that may exceed 30 km in length. The basic sensing mechanisms are Raman scattering, Rayleigh scattering, and Brilloiun scattering. Detailed descriptions of how these sensors work are given in Chapters 6 and 18. Briefly, Raman scattering is sensitive to temperature but not strain, and makes an excellent distributed temperature sensor referred to as DTS. Brillioun scattering is sensitive to temperature and strain and is the basis for distributed temperature and strain sensors referred to as DTSS. Rayleigh scattering is sensitive to acoustic vibrations and is used a distributed acoustic sensor referred to as DAS. DTS and DAS approaches have been especially effective for oil and gas applications.

A very important point that is understated is that fiber optic sensing systems have enabled smart oil and gas wells that are allowing North America to gain energy independence. Fiber optic sensor technology has a long history of development and commercialization successes. The technology has not yet reached maturity and will likely expand and create many new applications and commercialization opportunities.

Chapter 1
Fiber Optic Fundamentals

1.1 Refraction and Total Internal Reflection

Refraction occurs when light passes from one homogeneous isotropic medium to another; the light ray will be bent at the interface between the two media. The mathematical expression that describes the refraction phenomena is known as Snell's law,

$$n_0 \sin\phi_0 = n_1 \sin\phi_1, \tag{1.1}$$

where

n_0 = the index of refraction of the medium in which the light is initially travelling,
n_1 = the index of refraction of the second medium,
ϕ_0 = the angle between the incident ray and the normal to the interface, and
ϕ_1 = The angle between the refracted ray and the normal to the interface.

Figure 1.1(a) shows the case of light passing from a high-index medium to a lower-index medium. Even though refraction is occurring, a certain portion of the incident ray is reflected. If the incident ray hits the boundary at ever-increasing angles, a value of $\phi_0 = \phi_c$ will be reached, at which no refraction will occur. The angle ϕ_c is called the critical angle. The refracted ray of light propagates along the interface, not penetrating into the lower-index medium as shown in part Fig. 1.l(b). At that point, sin ϕ_c equals unity. For angles ϕ_0 greater than ϕ_c, the ray is entirely reflected at the interface, and no refraction takes place [see Fig. 1.1(c)]. This phenomenon is known as total internal reflection (see Fig. 1.2).

In Fig. 1.2, a ray of light incident upon the end of the fiber at an angle θ will be refracted as it passes into the core. If the ray travels through the high-index medium at an angle greater than ϕ_c, it will reflect off of the cylinder wall, will have multiple reflections, and will emerge at the other end of the optical fiber. For a circular fiber, considering only meridional rays (which will be discussed later in this chapter), the entrance and exit angles are equal.

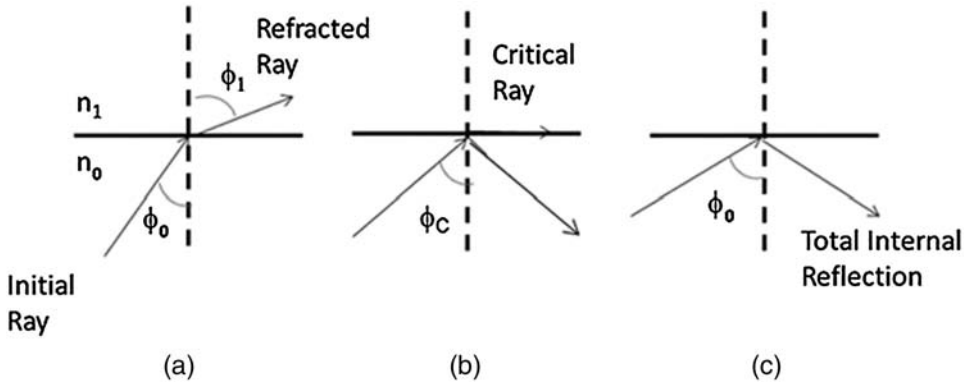

Figure 1.1 Ray incident at a plane interface between a low- and high-index medium.

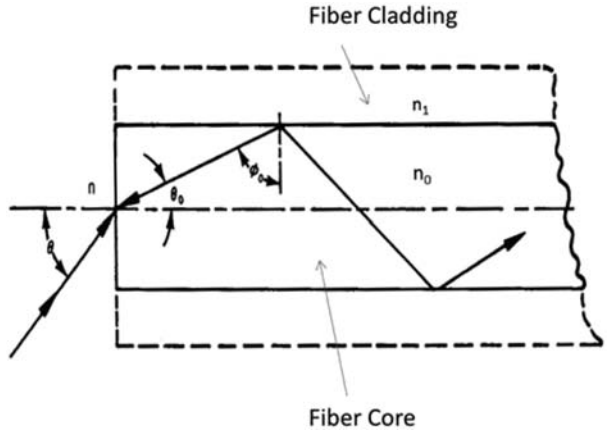

Figure 1.2 Ray passage along a flat-ended optical fiber.

Considering Snell's law for the optical fiber, core index n_0, cladding index n_1, and the surrounding media index n,

$$\begin{aligned} n\sin\theta &= n_0 \sin\theta_0 \\ &= n_0 \sin\left(\frac{\pi}{2} \quad \phi_c\right) \\ &= n_0\left[1 \quad (n_1 \quad n_0)^2\right]^{1/2} \\ &= (n_0^2 \quad n_1^2)^{1/2} = \text{ Numerical Aperture.} \end{aligned} \tag{1.2}$$

The quantity $\sin\theta$ is defined as the numerical aperture (NA). (For $\phi_0 = \phi_c$, $\phi_1 =$ 90 deg; therefore, $\sin_c = n_1/n_0$.) The NA is determined by the difference between the refractive index of the core and that of the cladding. It is a measure of the light-acceptance capability of the optical fiber. As the NA increases, so does the ability of the fiber to couple light into the fiber, as shown in Fig. 1.3(a). The larger NA allows the fiber to couple in light from more severe grazing angles

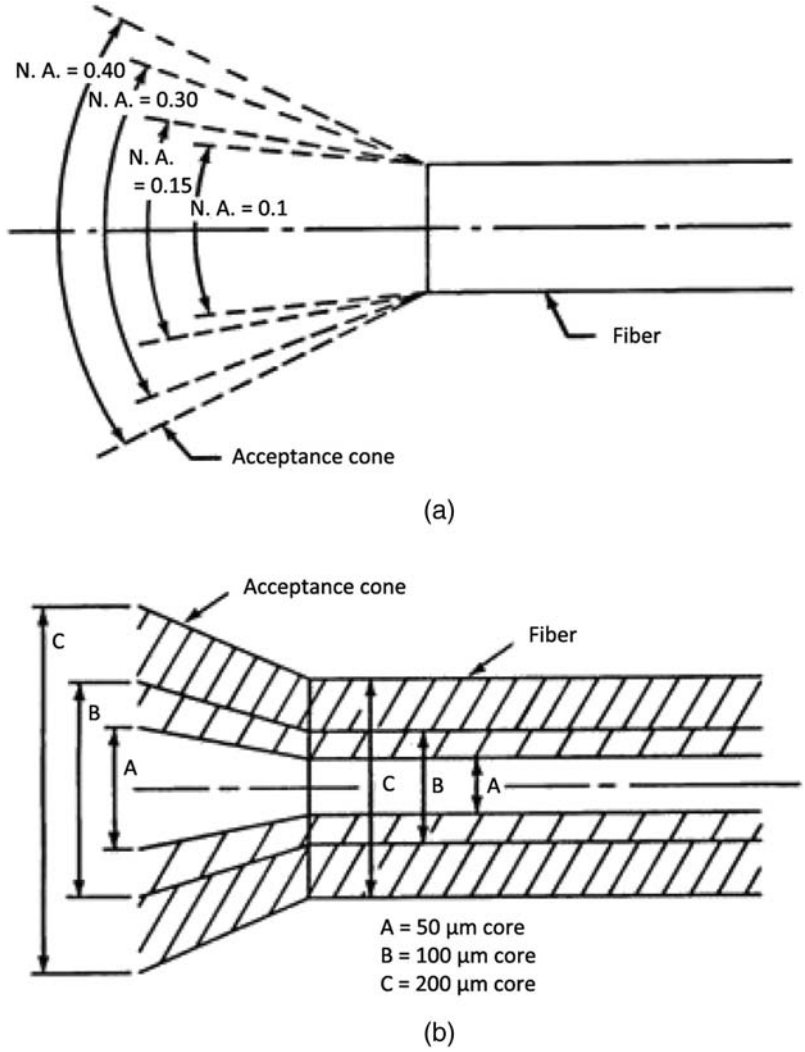

Figure 1.3 Acceptance angle associated with (a) numerical aperture and (b) core size.

thereby increasing the acceptance angle and the acceptance cone of light entering the fiber. Coupling efficiency also increases as the fiber diameter increases, since the large fiber can capture more light [see Fig. 1.3(b)].[1] Therefore, the maximum light-collection efficiency occurs for large-diameter-core fibers and large-NA fibers.

1.2 Meridional Rays

The definitions of total internal reflection and numerical aperture have been based on meridional ray analysis (i.e., the ray path, through its numerous reflections, as it passes through the longitudinal axis of the fiber). Using

Fig. 1.2 as a reference, it can be shown that the length of a meridional ray in a fiber in air ($n = 1$) is[2]

$$l(\theta) = \frac{L}{\left[1 \quad (\sin\theta/n_0)^2\right]^{1/2}} = L\sec\theta_0, \tag{1.3}$$

where $l(\theta)$ is the length of the optical path for a ray inclined to the fiber axis at an angle θ_0, and L is the length of the fiber measured along the fiber axis. It is interesting to note that the length of the optical path for an incident ray depends only on the fiber length, the angle of incidence, and the refractive index of the fiber core, while being independent of the fiber diameter. The number of reflections, however, is dependent on fiber diameter. The larger the diameter of the fiber, the fewer the number of reflections,[2]

$$N = \left(\frac{L}{d}\right)\tan\theta_0, \tag{1.4}$$

where N is the number of reflections at the core–cladding interface, and d is the fiber diameter.

1.3 Skew Rays

In general, meridional rays describe very simplified ray propagation. Often rays are skewed in nature and dominate the optical properties of the fiber. These rays affect the "real" ray propagation and alter the simplified definition of numerical aperture, ray path length, and number of reflections.

Skew rays travel along a helical path as illustrated in Fig. 1.4. For simplicity, however, this book will use meridional ray analysis. A more detailed treatment of skew rays is given in Ref. 2.

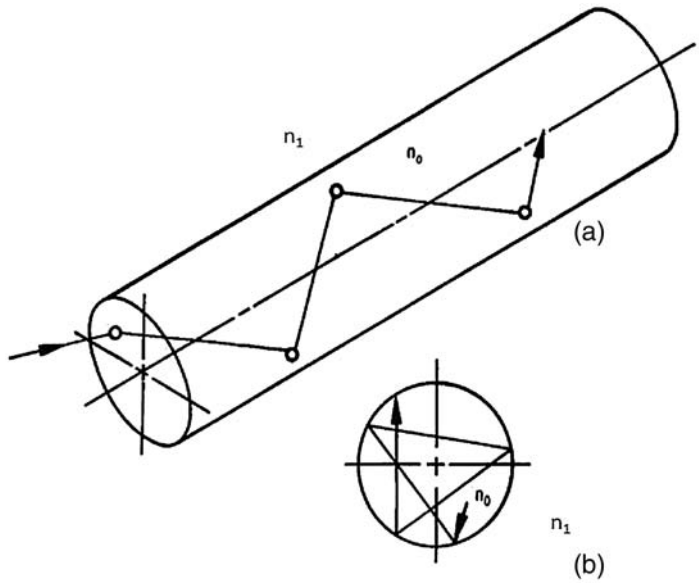

Figure 1.4 Skew rays.

1.4 Bent Fibers

Figure 1.5 shows the effect of bending on a meridional ray travelling in a fiber. For a straight fiber, the angle between the light ray and the normal to the plane of reflection is defined by the angle ϕ. However, as shown in Fig. 1.5, when the fiber is bent, the plane of reflection and the reflective ray rotate by the angle δ. Therefore, for a curved fiber, the angle between the reflected ray and the tangent at the reflection point is ϕ δ. In a straight fiber, for $\phi > \phi_c$, the rays will be totally internally reflected. In a bent fiber, the effective critical angle is reduced by δ. Therefore, rays incident between ϕ_c and ϕ_c δ will be lost through the cladding of the fiber. The effective critical angle is reduced in a bent fiber, as is the amount of light that can be injected into the fiber.

Figure 1.6 illustrates a curved fiber with rays traced through several internal reflections. The multiple reflections in a bent fiber with a constant radius of curvature do not increase the bending loss since the steepness of the rays as they hit the sidewalls of the fiber does not increase

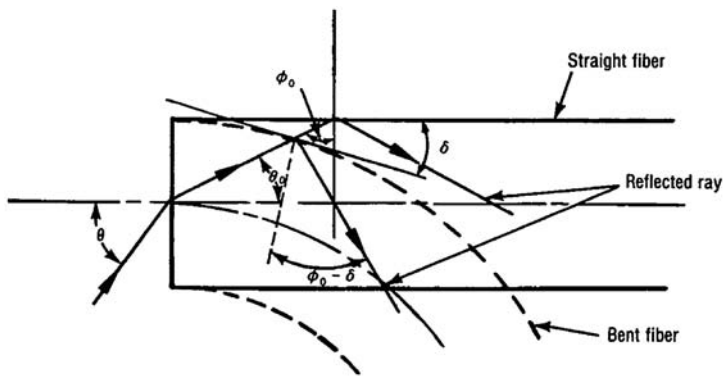

Figure 1.5. Bending effects on a critical angle.

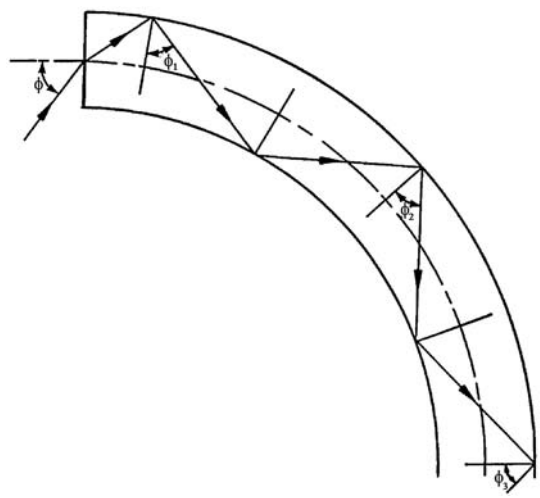

Figure 1.6 Multiple reflections in a bent fiber.

(i.e., $\phi_1 = \phi_2 = \phi_3$). The bending loss occurs primarily at the transition from the straight to the bent section (a change in one curvature to another curvature for multiple bending points).

1.5 Mechanisms of Attenuation

Attenuation or loss is defined by the following equation:

$$A = \quad 10 \log \frac{P_o}{P_i}, \tag{1.5}$$

where A is the attenuation, and P_i and P_o are the input power and output power, respectively. The negative sign arises from the convention that attenuation is negative. Attenuation is measured in decibels (dB) per unit length, typically dB/km.

Loss can vary from 1 to 1000 dB/km in useful fibers with the various causes of loss often being wavelength dependent. The causes for loss are absorption, scattering, microbending, and end loss due to reflection, as shown in Fig. 1.7.[3]

Figure 1.8 shows a typical attenuation curve for a single-mode fiber. Fibers for telecommunication applications use wavelengths in the C band, centered around 1550 nm. The loss decreases at higher wavelengths because inherent Rayleigh scattering losses are decreased, since the scattering is proportioned to $1/\lambda^4$, where λ is the wavelength.

Sensors are often required to work over a broad wavelength range. Figure 1.9 shows a transmission-versus-wavelength curve for synthetic silica. The transmission range is 180 nm in the ultraviolet (UV) spectrum to over 2 μm in the near-infrared (IR) spectrum. If the water content is reduced [less (OH)], the infrared transmission is improved (see Fig. 1.9). Bundle fibers, which are very useful in sensors, have typical transmission-versus-wavelength curves as shown in Fig. 1.10.[4] The transmission level is approximately 400 600 dB/km. In most applications, bundle fibers are limited to 3 to 10 m before loss becomes excessive. The loss in bundle fiber is associated with high transition metal concentrations in the fibers.

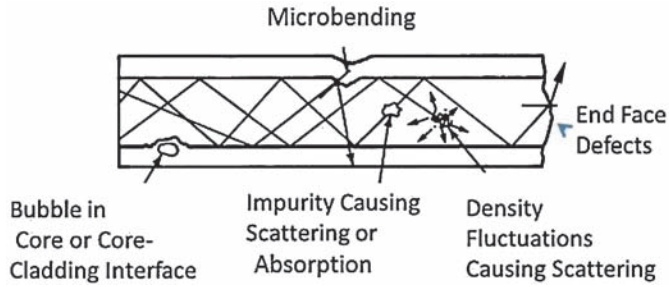

Figure 1.7 Causes for attenuation in an optical fiber.

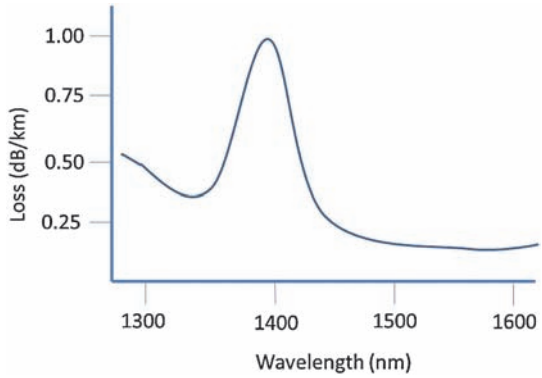

Figure 1.8 Attenuation curve for a typical low-loss fiber.

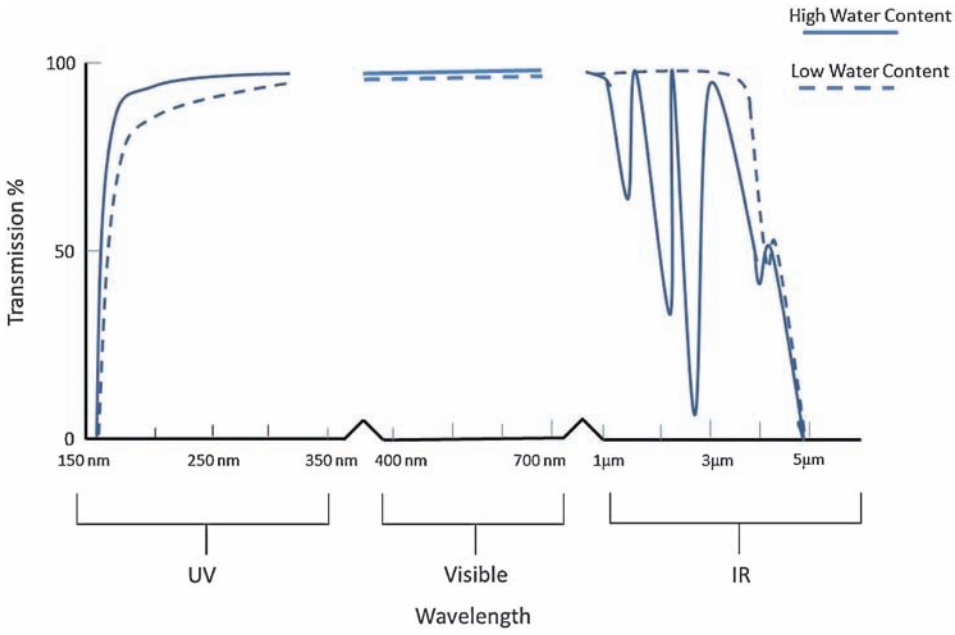

Figure 1.9 Transmission characteristics of silica.[5]

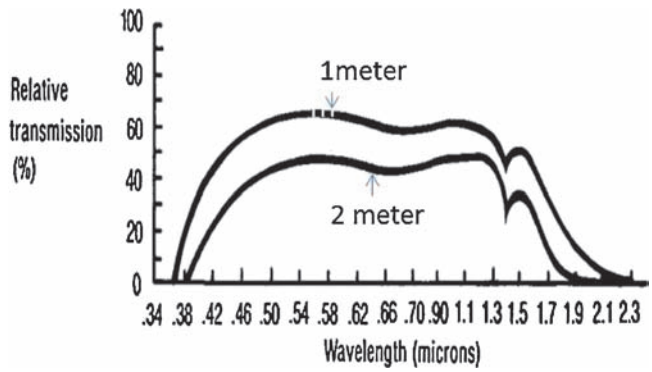

Figure 1.10 Transmission-versus-wavelength for bundle fiber.

Losses associated with microbending in the fiber will be discussed in depth in Chapter 3, since the microbending mechanism is quite useful in sensor design. The following characteristics of fiber loss ranges are useful:[3]

- Ultralow loss: less than 1 dB/km
- Low loss: less than 10 dB/km
- Medium loss: 10 to 100 dB/km
- High loss: greater than 100 dB/km

In addition to losses in the fiber itself, there are losses at the ends of the fiber due to reflection. The refractive-index difference between the fiber and, usually, an interface leads to Fresnel reflection losses. As a result, small amounts of energy are reflected back into the fiber. These losses occur in connections between the fiber and optical devices or other fibers and must be considered in overall system losses.

The Fresnel reflection loss R is defined for a glass–air interface by

$$R = \left[\frac{n_0 \quad 1}{n_0 + 1}\right]^{1/2}, \tag{1.6}$$

where n_0 is the index of refraction of the core material. Using the classical definition of absorption,

$$P_{\mathrm{o}} = P_{\mathrm{i}} e^{\ \alpha L}, \tag{1.7}$$

where P_{o} and P_{i} are the output power and input power, respectively, α is the attenuation coefficient (units/length), and L is the length. Transmission T in percent is given by

$$T = (1 \quad R)^2 e^{\ \alpha L}. \tag{1.8}$$

The term $(1 \quad R)^2$ is the reflection loss for the entrance and exit ends of the fiber.

The effect of reflections is multiplicative and therefore accounts for the square term since there are two surfaces (exit and entrance).

1.6 Waveguide Propagation

For the case of sensors, most fibers have a step-index profile (shown in Fig. 1.16). The step fiber has an index of refraction constant in the core, constant in the cladding, and discontinuous at the interface. Depending on the core size and numerical aperture, the fiber will transmit many modes (rays) of light and be referred to as multimode fiber. It may also be limited to a single mode.

Modal performance is mathematically defined by Maxwell's equation for cylindrical boundary conditions as follows:[6,7]

$$\frac{d^2\psi}{d\rho^2} + \frac{1}{\rho}\frac{d\psi}{d\rho} + \frac{1}{\rho^2}\frac{d\psi}{d\phi}(k^2 \quad \beta^2) = 0, \tag{1.9}$$

where
ρ = the radial parameter,
ψ = the wave function of the guided light,
k = the bulk medium wave vector,
β = the wave vector along the fiber axis, and
ϕ = the azimuthal angle.

If the wave function is assumed to be of the form

$$\psi = AF(\rho)e^{iv\phi}, \tag{1.10}$$

then Maxwell equation (1.9) becomes a Bessel equation. The boundary conditions require that on the axis ($\rho = 0$), the field has a finite value. However, the field becomes zero at infinity ($\rho = \infty$). The resulting longitudinal components of the field functions are as follows:

$$\begin{aligned} &AJ_v(ur/a)e^{iv\phi},\ \rho < a\ \text{(core)} \\ &BK_v(wr/a)e^{iv\phi},\ \rho < a\ \text{(cladding)}, \end{aligned} \tag{1.11}$$

where J_v (ur/a) and K_v (wr/a) are Bessel functions of the first and second kind, respectively:

$$\begin{aligned} u^2 &= \left(k_1^2 \quad \beta^2\right)a^2 \\ k^1 &= \frac{2\pi n_1}{\lambda_0} \\ w^2 &= \left(\beta^2 \quad k_2^2\right)a^2 \\ k_2 &= \frac{2\pi n_1}{\lambda_0}. \end{aligned} \tag{1.12}$$

The subscripts 1 and 2 denote the core and the cladding, respectively, while a is the radius of the core. The V parameter is defined in the following equation:

$$w^2 + u^2 = \left(\frac{2\pi a}{\lambda_0}\right)^2 (n^2 \quad n_2^2) = V^2. \tag{1.13}$$

The term $w^2 + u^2$ is a constant for all modes and is characteristic of the optical fiber. The parameter V represents the number of modes in the fiber and is related to the numerical aperture as follows (see Fig. 1.11):

$$V = \frac{2\pi a}{\lambda_0}\,(\text{NA}). \tag{1.14}$$

The relationship clearly follows the previously developed concept for numerical aperture [i.e., as the NA increases, so does the number of rays (modes) that can be accepted]. It is important to note that the mathematical solutions to Maxwell's equation have allowed values; therefore, there are allowed modes. Modes that do not fit the mathematical solutions are not allowed. As a result, modes can be considered to be quantized. For the simplest case of a single-mode fiber, where $v = 0$, only the TE and TM modes

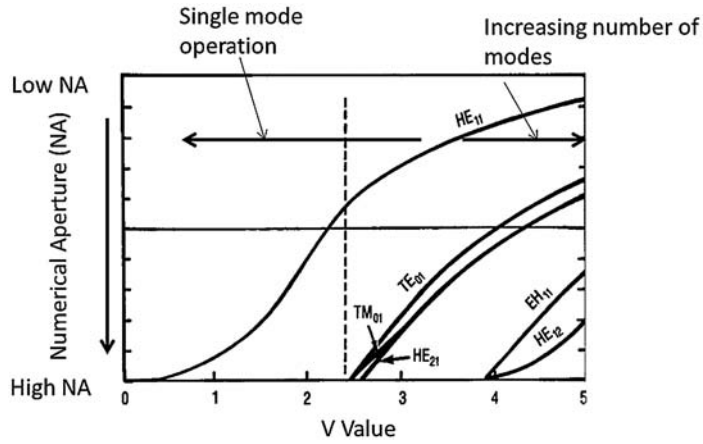

Figure 1.11 Mode formation with V value.

are present. Two modes exist in a single-mode fiber because the mode can degenerate due to polarization. For higher modes, where $v \neq 0$, the modes contain x, y, and z field components, which are referred to by the notation HE_{mn} ($n = v$) or EH_{mn}, depending on the dominance of magnetic or electric characteristics. The subscript n defines further mathematical solutions due to the behavior of Bessel functions. The field varies in a periodic fashion with ϕ, and skew rays that have a ϕ component result in a power concentration away from the fiber axis near the cladding.

At $V < 2.405$, the fiber can support only a single mode, designated as HE_{11}. At $V > 2.405$, other modes can exist, with the number increasing as V increases. The wavelength at which the optical fiber can only support the HE_{11} mode is defined as the second mode cutoff wavelength and is the point at which, for these operating wavelengths, the waveguide is defined as single-mode. This is a legacy term borrowed from the analysis of metallic waveguides that was used to define a cutoff frequency, which would be the frequency above which the waveguide would not support any low-loss transmission. It is important to point out here that cylindrical dielectric waveguides do not have a fundamental mode cutoff; this is different from the metallic waveguide case. In addition, each of the modes is doubly degenerate (for perfect circular symmetric waveguides) due to polarization, since in circular waveguides, two orthogonal polarization states (modes) exist for the same wave number. As will be discussed later in this chapter, elliptical core geometric considerations can eliminate the degeneracy.

It is clear from Eq. (1.14) that single-mode transmission requires small core size and low values of numerical aperture. However, if the V value is small due to a very low NA, the single ray is loosely guided and susceptible to bending losses.

Figure 1.12 is a plot of wavelength versus attenuation for a single-mode and multimode fiber. Single-mode fibers have strong wavelength dependence,

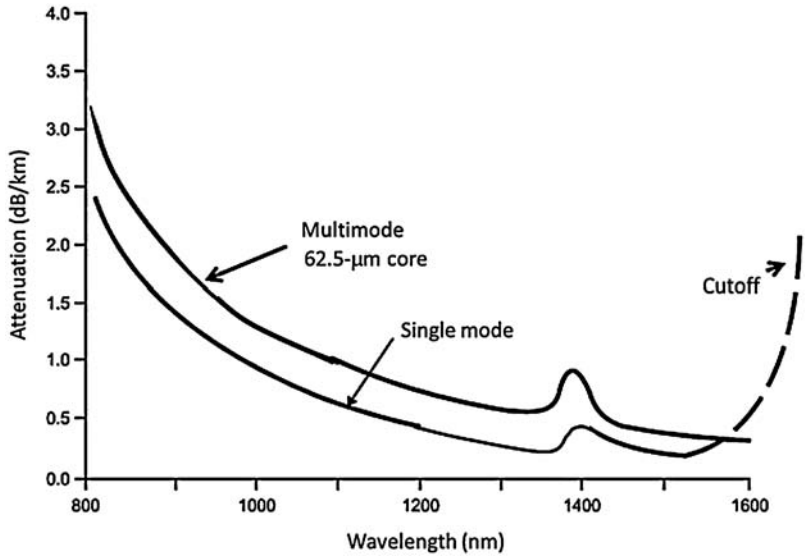

Figure 1.12 Fiber attenuation as a function of wavelength.

while multimode fibers are relatively insensitive to wavelength changes.[7] For a single-mode fiber, as λ_0 increases, V decreases. The ray is less tightly guided and tends to enter the cladding, where it is scattered if the fiber experiences any bending. This condition, referred to as cutoff, is shown in figure 1.12. The cutoff wavelength can vary depending on fiber parameters. As mentioned earlier, the fundamental HE_{11} mode has no cutoff in cylindrical dielectric waveguides and will continue to propagate. However, as the wavelength is increased, the mode field diameter will increase, causing an additional propagation loss. Multimode fibers in which large numbers of modes are propagating because of their core size and NA will have a cutoff wavelength that is extremely long and will not be practically reached. Multimode fibers in which large numbers of modes are propagating do not experience a cutoff wavelength (see Fig. 1.12).

1.7 Evanescent Wave

Energy is carried in the cladding as well as the core of the fiber. This is referred to as the evanescent wave phenomena. There is an exponential loss of energy in the fiber cladding as the distance from the fiber core is increased. Fig. 1.13(a) shows a wave incident on the core–cladding interface. The wavefronts (planes of constant phase) are shown as dotted lines. The arrows represent the wave normals.

The direction of the arrows indicates the flow of energy. The superposition of incident and reflected beams results in a wave where the wavefront is perpendicular to the interface, as shown in Fig. 1.13. The energy distribution

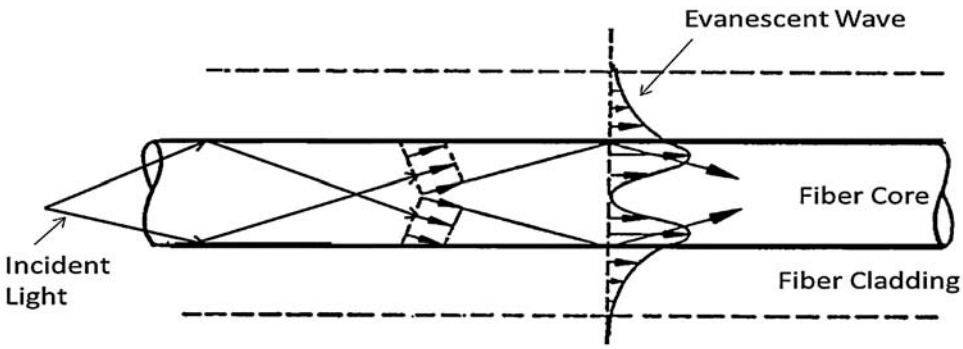

Figure 1.13 Evanescent wave phenomenon.

in the core has its maximum near the interface. The energy in the cladding falls off exponentially.

1.8 Cross Coupling

Cross coupling involves the transfer of light from one adjacent fiber to another. The extent of coupling between two adjacent fibers in close proximity is a function of the following: the diameter of the fibers; the spacing between the fibers; the length in which the fibers are in close proximity; the index of the fiber core, the cladding and the index of surrounding media; the thickness of the cladding; the wavelength of light in the fiber; and the particular modes excited in the fiber.

Clearly, a precise mathematical expression for the phenomenon is quite complex.[2] By properly selecting the various parameters, it is possible to completely transfer all of the energy in one fiber to an adjacent fiber. The length required for the transfer is referred to as the *beatlength*. For large fiber diameters, the energy transfer is limited over some length; a state of equilibrium will be reached. For small fibers, when the radiation is coherent, almost all of the energy will be transferred from one fiber to the other in a length $X/2$ and then return to the original fiber in an $X/2$ interval, where X is the beatlength. This phenomenon is known as beating. Beatlength is also used to describe observed light and dark bands in polarizing-maintaining fiber, which is discussed in Section 1.12 of this chapter.

It has been found that as the wavelength increases, the beatlength decreases. As a result, the relative intensity of energy in adjacent coupling fibers will vary with wavelength, as shown in Fig. 1.14.

1.9 Scattering

Rayleigh scattering was briefly discussed in Section 1.7. In addition to Rayleigh scattering, there are other scattering mechanisms, all of which have been very useful in optical-fiber-based sensing technology. Rayleigh scattering is a linear elastic scattering process that causes light to reflect back along the fiber due to

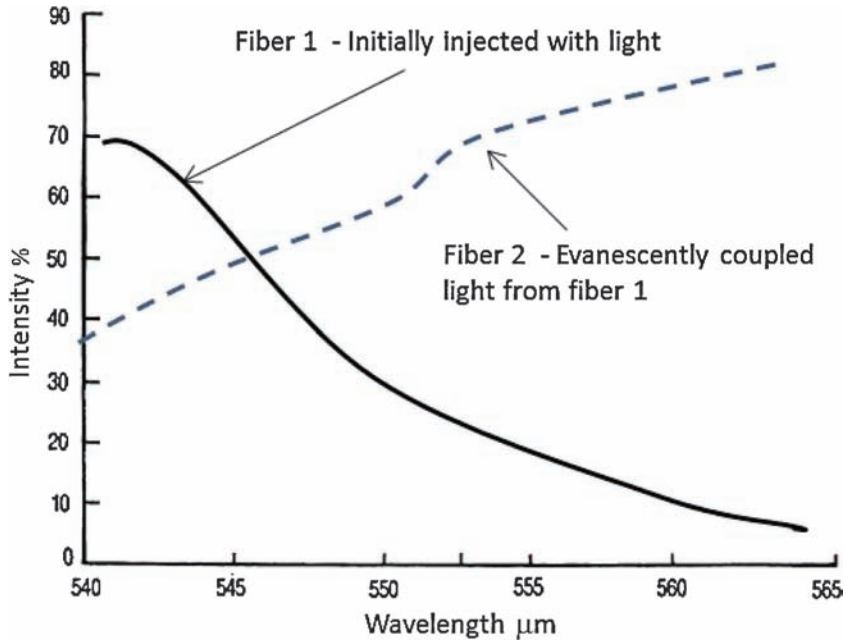

Figure 1.14 Plot intensity of the excited fiber and the coupled fiber as a function of wavelength of incident radiation.

submicroscopic inhomogenities in the composition and density of the glass. Other scattering mechanisms, including Raman scattering and Brillioun scattering, are associated with nonlinear inelastic processes that involve the interaction of optical energy with vibration energy that can alter the reflected wavelength and intensity due to perturbations at any point along the fiber.[8]

1.10 Mode Patterns

As discussed previously, not all rays are allowed to propagate in an optical fiber because certain boundary conditions and Maxwell's equation (Eq. 1.9) must be satisfied. Therefore, if the light emitting from a fiber were projected on a screen, it would not give a uniform illumination, even for a fiber with only one or a few modes. Rather, a geometrical pattern of light and dark is observed, corresponding to the complex energy distribution associated with the various modes. For fibers with large NA values, the individual modes are not visible due to modal interaction, but distinct patterns are possible, such as concentric rings and the so-called speckle pattern. The use of the mode patterns has had limited use in sensor technology. However, a more detailed analysis is given by Kapany.[2] The amount of energy carried in the cladding depends on the excited modes in the core. As the modes that are closer to the critical angle are excited, more energy is propagated in the cladding as is shown in Fig. 1.13.

1.11 Fiber Types

Figure 1.15 shows characteristics of the two basic fiber configurations.[3] The multimode step-index and single-mode step-index fibers have similar refractive-index profiles, but the single-mode fiber has a much smaller core. The single-mode fiber has much less dispersion and a sharp output pulse. The graded-index fiber has an intermediate output pulse.

The multimode graded-index fibers are used to increase bandwidth (i.e., information-carrying capacity) as compared to multimode step-index fibers. However, they will not play a great role in sensor technology. Most of the emphasis will be on step-index fibers, both single-mode and multimode. Step-index fibers have an index of refraction that is constant in the core and the cladding and stepped at the core–cladding interface. Table 1.1 lists some of the fiber types and their various properties. Refs. 9–18 will also be useful as background information. A comparison of a single-mode and multimode fiber is illustrated in Fig. 1.16.

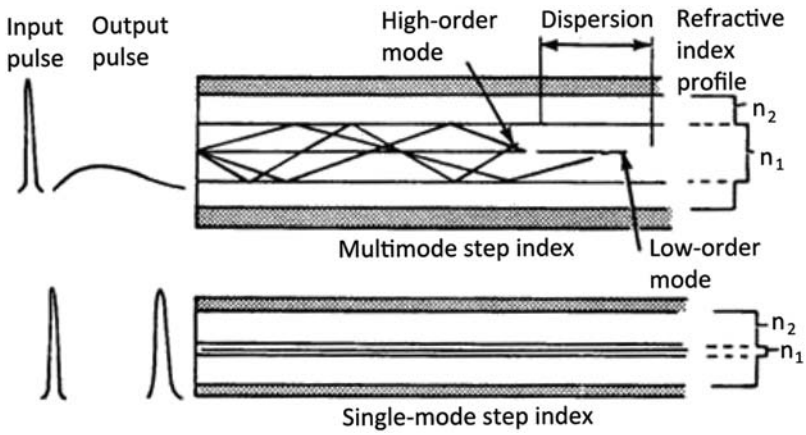

Figure 1.15 Core size and refractive index determine the light propagation characteristics of the fiber. Multimode: higher input power, microbending loss resistant, higher loss and higher dispersion. Single mode: lower loss, lower dispersion and higher microbending loss.

Table 1.1 Typical properties of various fiber types.

Type	Loss (dB/km)	NA	Core Size (O.D. Microns)	Core-to-Cladding Ratio	Bandwidth (MHz-km)
Multimode Step Index Glass Clad Glass (Bundle)	400 600	0.4 0.6	(50 70)	0.9 0.95	20
Plastic Clad Silica	3 10	0.3 0.4	200 600	0.7	20
Glass Clad Glass (Low Loss)	2 6	0.2 0.3	50 200	0.4 0.8	20
Single Mode	<1	0.15	5 8	0.04	>1000

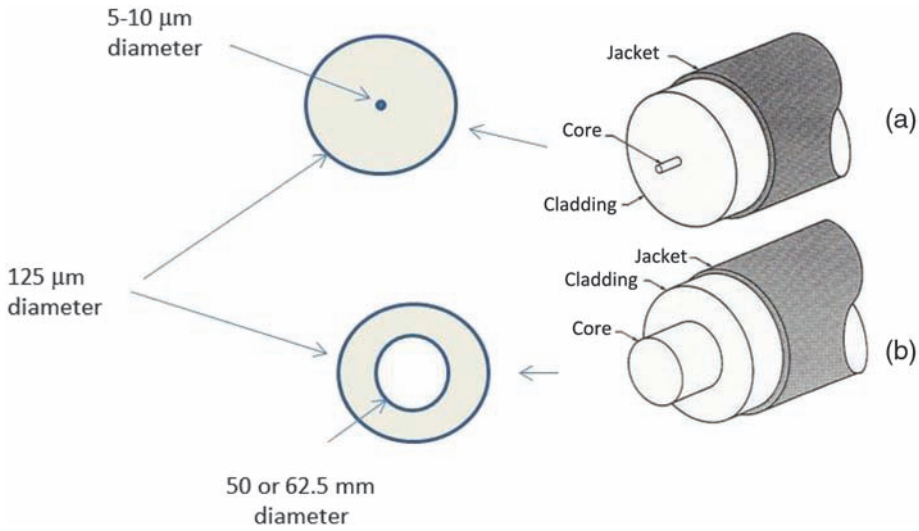

Figure 1.16 Comparison between (a) single-mode and (b) multimode optical fibers.

As optical fiber technology has advanced, a broad range of fibers have been developed to increase performance, especially for extreme environments. Ultralow-loss fiber with minimized water peak absorption is commercially available, as well as fiber that is insensitive to microbending. In addition to the fiber composition and structure, advanced coatings have enabled optical fiber to be functional in extremely harsh environments. Figure 1.17 is a very basic fiber optic cable. It consists of a buffer layer over the fiber, a strength member, and an outer jacket. As the environmental requirements become more severe, the cable construction becomes more complex.

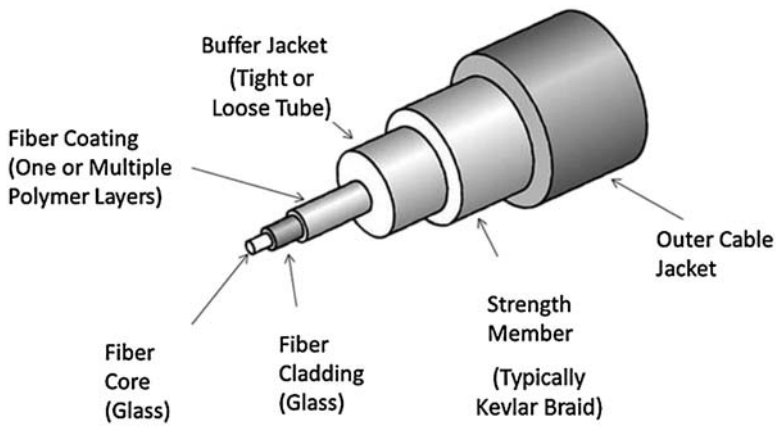

Figure 1.17 Basic elements of a fiber optic cable.[15]

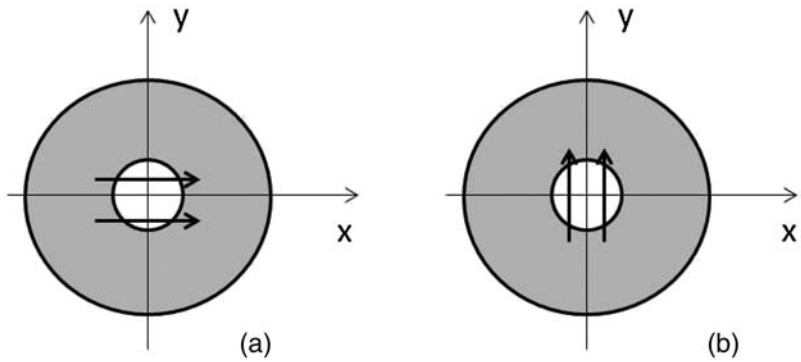

Figure 1.18 The two polarizations of the fundamental HE_{11} mode in a single-mode fiber: (a) H-Mode and (b) V-Mode.

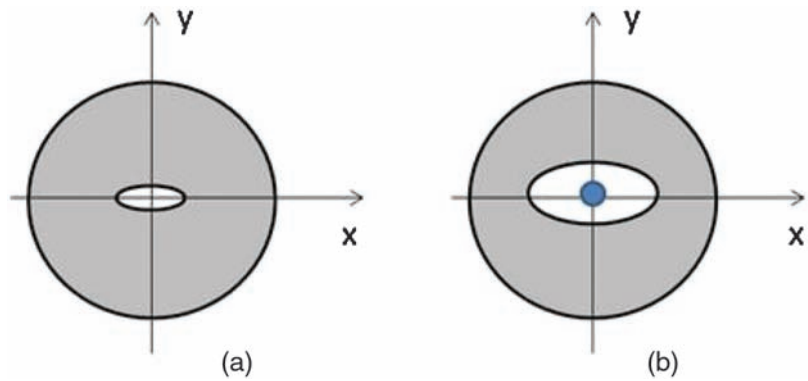

Figure 1.19 Birefringence from waveguide geometry. (a) Non circular core, (b) elliptical cladding generating asymmetrical stress in core (Other fiber geometries can generate as asymmetrical stress in the core).

1.12 Polarization-Maintaining Fibers

In the case of interferometric fiber optic sensors, the description assumes a single-mode fiber in which phase shifts between a sensing and a reference fiber can be determined. In reality, single-mode fibers are dual-mode fibers due to the fact that there are two possible degenerate polarization modes.[19 22] The fundamental HE_{11} mode can be separated into the horizontal or H-mode and the vertical or V-mode, as shown in Fig. 1.18. To achieve the desired sensing properties, preservation of polarization in single-mode fibers is required. Two approaches can be used to eliminate the degeneracy: a circumferential stress, due to an expansion mismatch, and/or a noncircular core. These fiber configurations are shown in Fig. 1.19.

The modes in the vertical and horizontal directions propagate at different phase velocities in polarization-maintaining fibers and, as such, have high

effective indices of refraction in these directions. The difference between the indices defines modal birefringence B:

$$B = n_{\mathrm{V}} \quad n_{\mathrm{H}}, \tag{1.15}$$

where n_{V} and n_{H} are the indices in the vertical and horizontal directions, respectively.

The effect of birefringence on the guided light is shown in Fig. 1.20. Light linearly polarized at 45 deg to the horizontal and vertical directions is injected into the fiber. The polarization state changes continuously along the fiber due to the fact that as the light propagates, the V-mode slips in phase relative to the H-mode. The linear polarization goes to elliptically polarized light and then circularly polarized light at a phase shift of $\pi/2$. The circularly polarized light goes through the elliptical state and to linear polarization at a phase shift of π. However, the polarization vector is now 180 deg out of phase with the initial polarization state.

Figure 1.21 helps to further clarify the effects of birefringence. If properly positioned at 0 deg and 2π rotation, scattered light is visible through the sides of the fiber. The distance L for a complete rotation of the polarization state is defined as the beatlength:

$$L = \lambda/B. \tag{1.16}$$

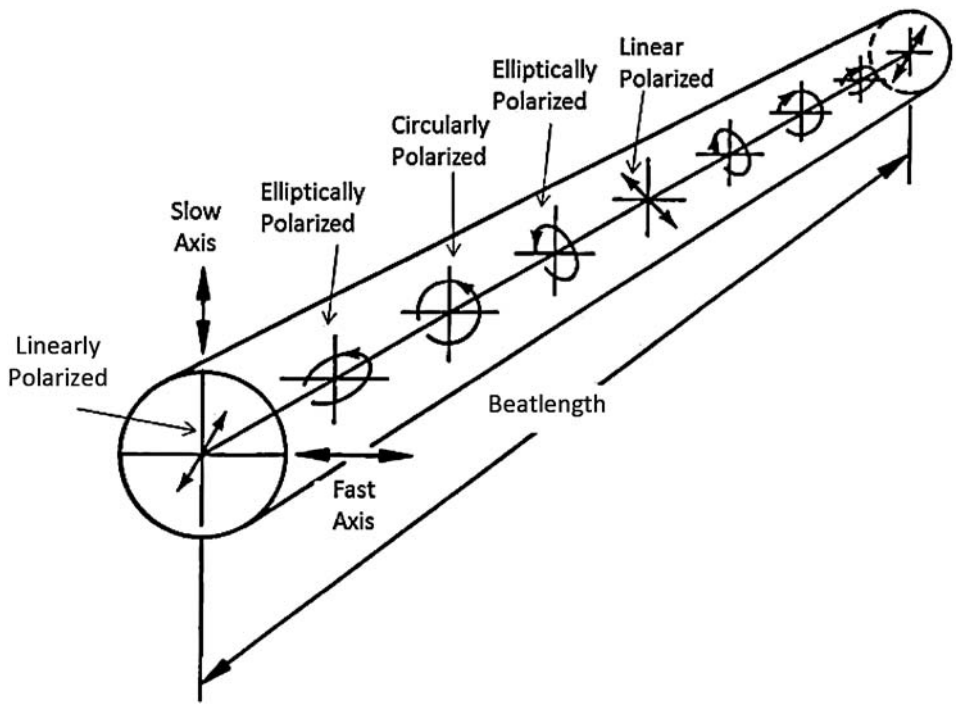

Figure 1.20 The effect of uniform birefringence on the state of polarization of initially linearly polarized light injected at 45 deg to the fiber's principal axes.

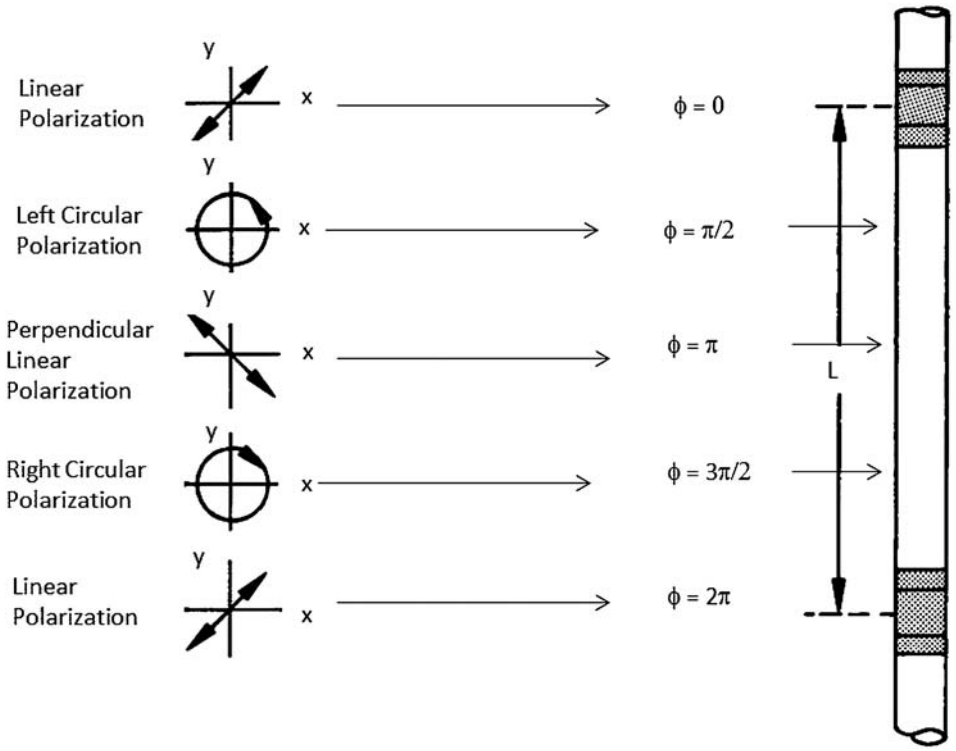

Figure 1.21 The effects of birefringence on polarized light in an optical fiber.[23]

(Note that the beatlength term here is defined differently from the term described earlier in this chapter.)

Typical beatlengths are between 10 cm and 2 m. A more important parameter to characterize polarization-maintaining fiber is the *h*-parameter, the so-called polarization-maintaining property of the fiber that describes the cross coupling of power injected in the H-mode to the V-mode. The power cross coupled is given by

$$\frac{P_{\mathrm{V}}}{P_{\mathrm{V}} + P_{\mathrm{H}}} = \frac{1}{2}(1 \quad e^{\ 2hL}), \tag{1.17}$$

where P_{V} and P_{H} are the powers in the vertical and horizontal polarization modes, respectively. It is clear that as the length of the fiber increases, the cross-coupled power increases. To achieve the desired "true" single-mode operation, P_{V} should approach zero and h should be very small. Typical values of h for good-quality, polarizing-maintaining fibers range from 5×10^{-6}/m to 2×10^{-5}/m. An h value of 10^{-5}/m results in 1% of cross-coupled power for a fiber 1 km long.

If constructive interference is to occur in applications with interferometric sensors, it is necessary that the output beam be matched not only in amplitude but also in polarization direction. Polarization-maintaining fibers[23] improve

sensitivity using fiber with high birefringence, short beatlength, and low *h*-values. It is important to note that fiber with high birefringence can have structural perturbations that can increase both cross coupling and *h*-values. The ability of fiber to hold a polarization state minimizes the possibility of degenerate modes that degrade sensitivity.

References

1. R. F. Coulombe, "A practical approach to plant data bus networks utilizing fiber optics," *Proc. ISA* **40**, pp. 1027–33 (1985).
2. M. S. Kapany, *Fiber Optics: Principles and Applications,* Academic Press, New York (1967).
3. Amp Inc., *Designers Guide to Fiber Optics, publisher:* AMP, Inc., Harrisburg, PA (1982).
4. Welch Allyn, Product Specification – Fiber Bundle Transmission, www.welchallyn.com 2000.
5. Heraeus Amersil, Product Specification – Silica Transmission, www.heraeus-quarzglas.com 2000.
6. C. M. Davis et al., *Fiber Optic Sensor Technology Handbook,* Dynamic Systems, Reston, VA (1982).
7. T. G. Giallorenzi, "Optical communications research and technology: fiber optics," *Proc. IEEE* **66**(7), pp. 744–80 (1978).
8. J. P. F. Wooler, FIBERPAEDIA, Fiber optics – Key Parameters Explained, Fibercore, 2009.
9. W. S. Boyle, "Light-wave communications," *Scientific American* **237**(2), pp. 40–48 (August 1977).
10. H. F. Wolf, *Handbook of Fiber Optics: Theory and Applications*, Garland STPM Press, New York, p. 63 (1979).
11. A. W. Snyder and J. D. Love, *Optical Waveguide Theory*, Chapman and Hall, New York (1983).
12. J. E. Midwinter, *Optical Fibers for Transmission*, Wiley, New York (1970).
13. D. Marcuse, *Principles of Optical Fiber Measurements*, Academic Press, New York (1981).
14. J. C. Poly, Ed., *Fiber Optics*, CRC Press, Boca Raton, FL (1984).
15. AFL, "Fiber Optic Cable Products" www.aflglobal.com 2013.
16. J. Gowar, *Optical Communications Systems*, Prentice/Hall International, Englewood Cliffs, NJ (1984).
17. J. M. Senior, *Optical Fiber Communications: Principles and Practice*, Hall International, Englewood Cliffs, NJ (1985).
18. OFS Fitel, LLC, "Optical Fiber," www.ofsoptics.com, 2013.

19. S. C. Rashleigh and R. H. Stolen, "Preservation of polarization in single mode fibers," Presented at the annual meeting of the Optical Society of America (1982).
20. J. F. Wahl, "Characterization of special fibers," *Guidelines*, Corning, NY, p. 3 (1985).
21. R. H. Stolen, "Polarizing: preserving fiber optics," SPIE's—O-E LASE, Tutorial Text 26, (1986).
22. AT&T, "Polarizing maintaining fiber," *AT&T Technical Memorandum*, p. 1014 (1989).
23. I. P. Kaminow, "Polarization in optical fibers," *IEEE Journal of Quantum Electronics* **QE-17**(1), 15–22 (1981).
24. W. K. Burns, R. P. Moeller, C. A. Villarruel, and M. Abebe, "Fiber optic gyroscope with polarizing-holding fibers," *Optics Letters* **9**(12), 570–572 (1984).

Chapter 2
Fiber Optic Sensor Fundamentals

2.1 Background

Optical fibers play an important role in many applications beyond communications, including sensing, control, and instrumentation.[1,2] In these areas, optical fibers have made a significant impact and continue to be the subject of substantial research. In general, for these applications, fibers are made more sensitive and susceptible to the very external mechanisms that would render telecommunications fibers ineffective. In its simplest form, an optical fiber sensor is composed of a light source, an optical fiber, a sensing element, and a detector (see Fig. 2.1).

The principle of operation of a fiber sensor is that the sensing element modulates some parameter of the optical system (intensity, wavelength, polarization, phase, etc.), which gives rise to a change in the characteristics of the optical signal received at the detector. Figure 2.2 depicts the various changes that can be introduced to the light traveling along the fiber.

A fiber optic sensor (FOS) can affect one or more of the light-guiding characteristics of the transmitting fiber and correlate the particular parameter of interest (e.g., temperature, strain, pressure, chemical species, etc.) to these particular light changes. Hence, the fundamental principle is to measure an external physical parameter by inducing changes in one or more of the optical properties of a light beam traveling inside and along an optical fiber. The fiber is thus both the sensing element and transmission medium.

Fiber optic sensors represent a technology base that can be applied to a multitude of sensing applications. The following are some characteristic advantages of fiber optics that make their use especially attractive for sensors:

- Nonelectrical
- Explosion proof
- Often do not require contact
- Remotable

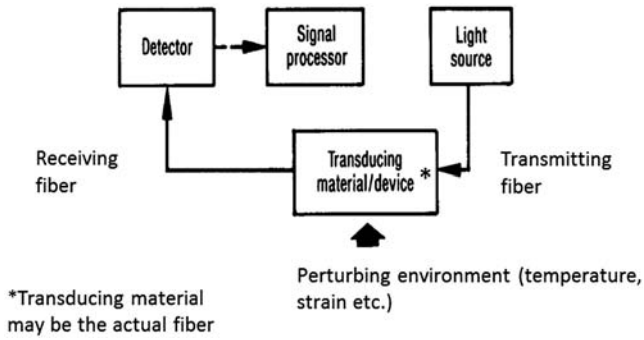

Figure 2.1 Basic elements of a fiber optic sensor.[3]

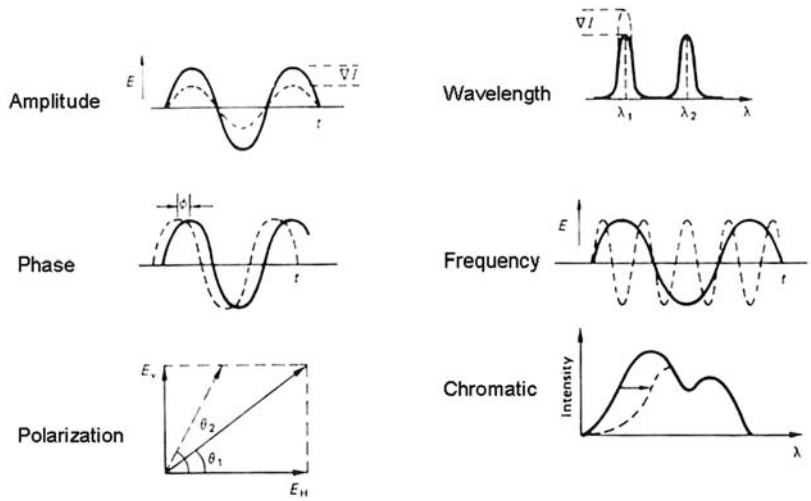

Figure 2.2 Light modulation effects used by fiber sensors to detect a physical parameter (reprinted from Ref. 4 with permission).

- Small size and lightweight
- Allow access into normally inaccessible areas
- Potentially easy to install
- Immune to radio frequency interference (RFI) and electromagnetic interference (EMI)
- Solid-state reliability
- High accuracy
- Can be interfaced with data communication systems
- Secure data transmission
- Resistant to ionizing radiation
- Can facilitate distributed sensing

Most physical properties can be optically sensed with fibers. Light intensity, displacement (position), temperature, pressure, rotation, sound, strain,

Table 2.1 Sensors for various applications.

Applications	Sensor
Automated production lines (steel, paper, etc.)	Position, thickness, limit switch, break detection, velocity
Process control	Temperature, pressure, flow, chemical analysis
Automotive	Temperature, pressure, torque, gas detection, acceleration
Machine tool	Displacement, tool break detection
Avionic	Temperature, pressure, displacement, rotation, strain, liquid level
Smart structures	Temperature, static and dynamic strain
Petrochemical	Flammable and toxic gases, leak detection, liquid level
Military, Homeland Security	Sound, rotation, radiation, vibration, position, temperature, pressure, chemical, biotoxin
Energy oil and gas	Temperature, pressure, flow
Energy wind and geothermal	Strain, temperature
Utility smart grid	Temperature, displacement, electric and magnetic field
Biomedical	Temperature, pressure, biotoxin, chemical

magnetic field, electric field, radiation, flow, liquid level, chemical analysis, and vibration are just some of the phenomena that can be sensed. Table 2.1 lists some typical applications and the associated sensors required. All of those listed can be addressed with fiber optics.[1,2]

Fiber optic sensors are classified as intrinsic or extrinsic. If the modulation takes place directly in the fiber, it is an intrinsic sensor. The sensing process is extrinsic if the modulation is performed by some external transducer (Fig. 2.3).

Historically, applications utilizing fiber optics were oriented toward the very simple sensors, such as card readers for computers and outage indicators to determine if the lights in automobiles were blown out. Technology has taken fiber optic sensors to the other extreme. Ultrasophisticated sensors using interferometric techniques have been developed and are in wide use. Compared to conventional displacement sensors, these devices have four to five orders of magnitude higher resolution. In general, such high

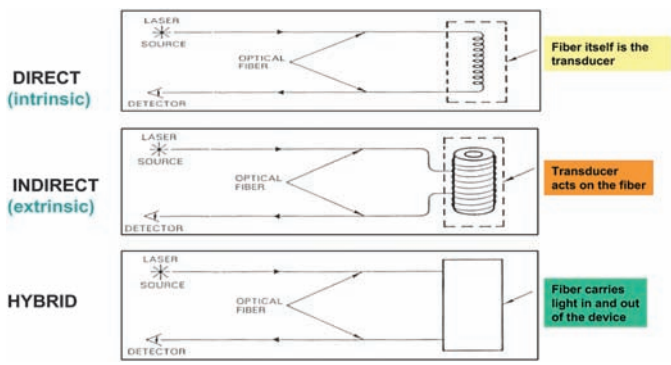

Figure 2.3 Classification of optical fiber sensors by transducing approach (Ref. 5).

sensitivities are not required for most applications except for military hydrophone and gyroscope use. Most industrial sensors fall somewhere between these extremes.

2.2 Sensor Categories

Fiber optic sensors can be divided into five basic categories: phase-modulated sensors, intensity-modulated sensors, wavelength-modulated sensors, scattering-based sensors, and polarization-based sensors.[3,4 6 17] Intensity-modulated sensors generally are associated with displacement or some other physical perturbation that interacts with the fiber or a mechanical transducer attached to the fiber. The perturbation causes a change in received light intensity, which is a function of the phenomenon being measured. Phase-modulated sensors compare the phase of light in a sensing fiber to a reference fiber in a device known as an interferometer. Phase difference can be measured with extreme sensitivity. Phase-modulated sensors are much more accurate than intensity-modulated sensors and can be used over a much larger dynamic range. However, they are often much more expensive. For the most part, interferometers have found applications in military systems where cost is not necessarily a major consideration. On the other hand, intensity-modulated sensors are well suited for widespread industrial use. In the third category, wavelength-modulated sensors experience wavelength change associated with displacement, temperature, or the presence of chemical species, which causes fluorescence. Scattering-based sensors are associated with three types of light scattering: Rayleigh, Raman, and Brillouin.[14] Anomalies along the fiber are detected by changes in the scattered light back-reflected along the fiber to a detector that is incorporated into a form of optical time-domain reflectometer. The perturbation of the scattered light may cause an intensity change or wavelength shift caused by the parameter being sensed, typically temperature or strain. Polarization-based sensors are based on phenomena such as Faraday rotation or birefringence that can alter the polarization state, hence altering the intensity of transmitted light.

In subsequent chapters, the different sensor categories will be discussed in detail, but it is useful here to further define the basic sensing mechanisms. Intensity-modulated sensors detect the amount of light that is a function of the perturbing environment, as shown in Fig. 2.4.[3] The light loss can be associated with transmission, reflection, microbending, or other phenomena such as absorption, scattering, or fluorescence, which can be incorporated in the fiber or in a reflective or transmissive target. Intensity-modulated sensors normally require more light to function than do phase-modulated sensors; as a result, they use large-core multimode fibers (or bundles of fibers). Transmission, reflection, and microbending sensor concepts are the most widely used. In essence, they are displacement sensors. Examples of how fiber optics can be used to detect position (displacement) and relate the movement to a physical

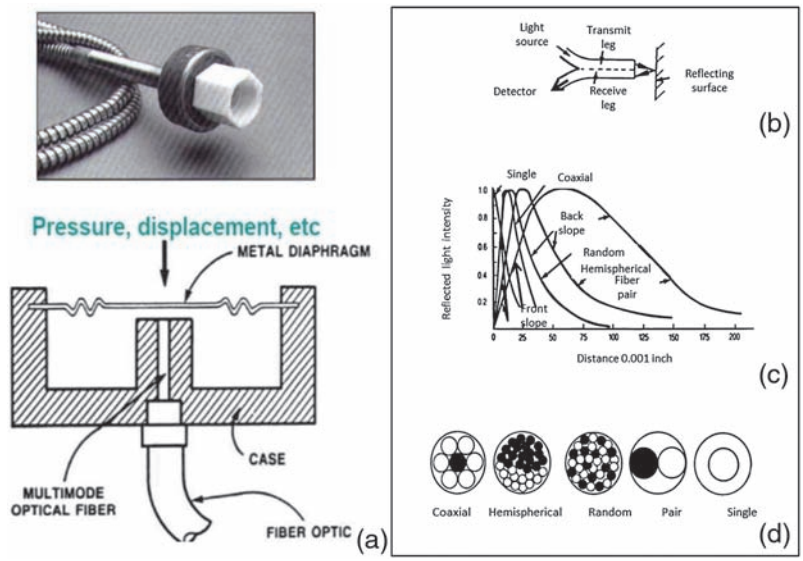

Figure 2.4 A simple intensity-based fiber optic pressure sensor (Source: EOTec Ref. 1). (a) Pressure sensor, (b) sensor arrangement, (c) output versus distance, (d) probe configuration.

property include the movement of a diaphragm for pressure or the movement of a bimetallic element for temperature. An example of an actual, intensity-modulated, fiber optic sensor is shown in Fig. 2.4. This device could be considered an extrinsic type, since it relies on a metallic deformable diaphragm to modulate the light intensity reflected back into a single fiber or fiber bundle. The magnitude of the external pressure applied can be determined by the intensity of the reflected light coupled back into the return fiber(s). Notice that two separate regions of operation are possible, each with a trade-off between dynamic range and pressure sensitivity.

Phase-modulated sensors use interferometric techniques to detect pressure, rotation, and magnetic field, the first two applications being the most widely developed. Figure 2.5 shows a schematic representation of a Mach–Zehnder interferometer. The laser light source has its outgoing beam split such that light travels in the reference single-mode fiber and the sensing fiber, which is exposed to the perturbing environment. If the light in the sensing fiber and the light in the reference fiber are exactly in phase upon recombining, they constructively interfere with an increase in light intensity. If they are out of phase, destructive interference occurs, and the received light intensity is lower. Such devices experience a phase shift if the sensing fiber under the influence of the perturbing environment has a length or refractive index change, or both.

Wavelength-modulated sensors can be the result of fluorescence. However, a broad-based concept using wavelength modulation is accomplished with Bragg gratings. Figure 2.6 shows a schematic representation of a

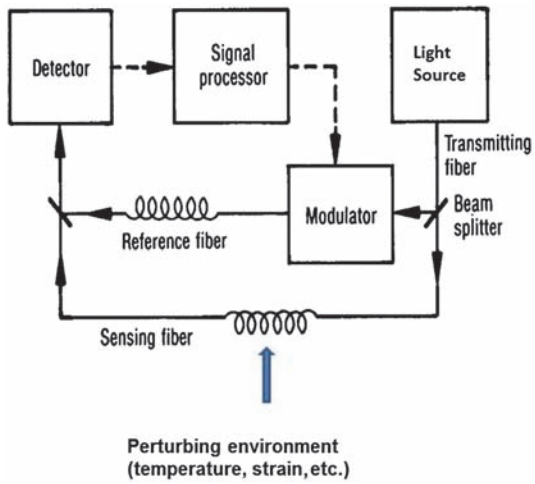

Figure 2.5 Phase sensor (Ref. 3).

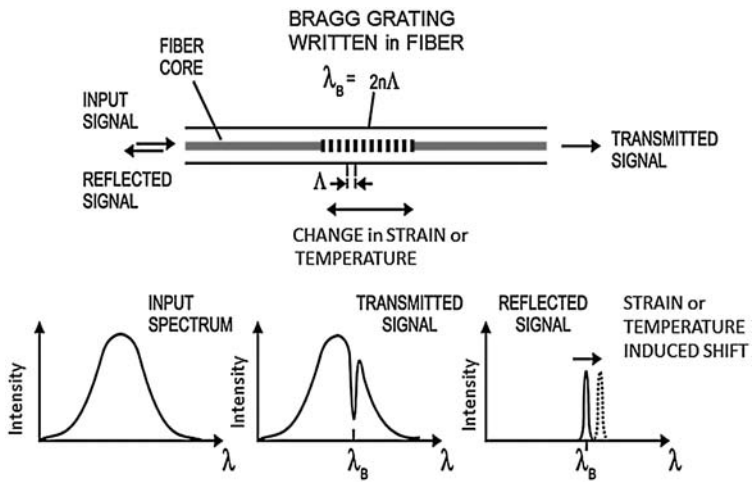

Figure 2.6 Fiber Bragg grating sensor system.[17]

Bragg grating-based sensing system.[17] The Bragg grating has a resonance condition at a specific wavelength. Light at that wavelength is reflected. However, change in strain or temperature perturbs the grating and causes the reflected light to have a wavelength shift, which is a direct measure of the change in strain and/or temperature.

The concept of scattering-based sensors is shown in Fig. 2.7.[14 16,19 21] Perturbations to the reflected signal over time show the magnitude of the parameter being sensed as well as location.

While polarization-based sensors can use external optics such as Faraday rotators to alter the transmitted light, intrinsic polarization-based fiber optic

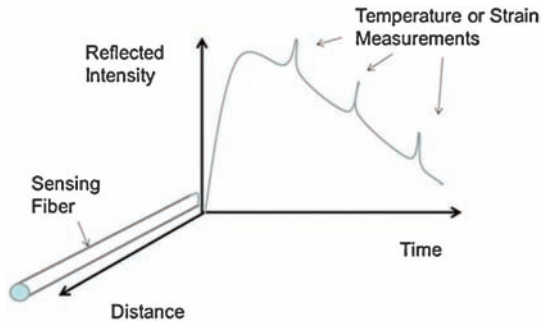

Figure 2.7 Concept of fiber optic distributive sensors based on scattering. (Anomalies along the fiber are detected by the changes in the properties of scattered light back-reflected to the interrogator.)

sensors use birefringence. Single-mode fibers actually have two modes associated with the two orthogonal polarization states. If linearly polarized light is injected in one mode of the orthogonal modes of the fiber, birefringence associated with strain or other perturbations to the fiber will cause a cross coupling of light to the other orthogonal mode. When passed through a second polarization filter (analyzer), the intensity change will correspond to the parameter that caused the birefringence change, such as temperature or strain. Since the parameter changes occur in real time, both static and dynamic measurements can be achieved.[18]

Figure 2.8 summarizes the common elements in a sensing system. Generally, all systems have a light source, an interface to an optical fiber, a modulator that alters the light in a manner proportional to the perturbing environment, and a photodetector.[22] The options to achieve the function of the elements are shown.

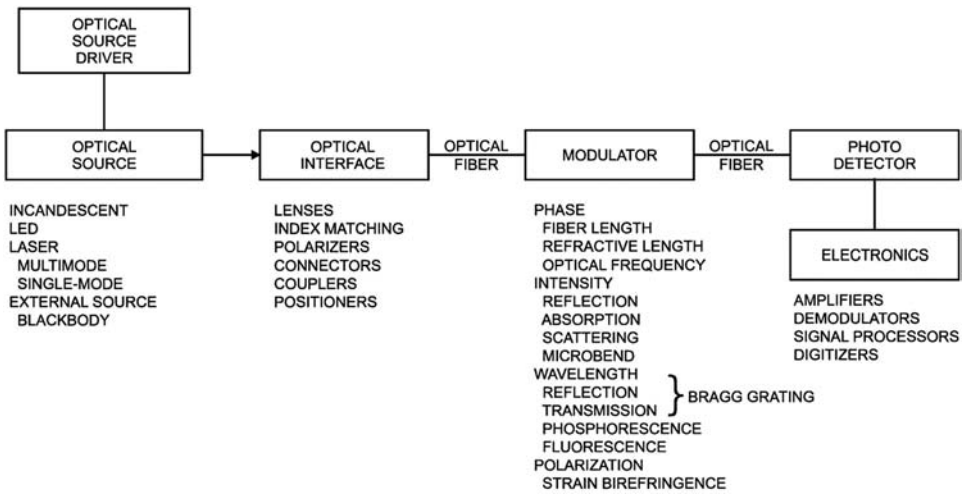

Figure 2.8 Components common to all fiber optic sensors.[1]

2.3 Distributed Fiber Optic Systems

Based on their topology and configuration, fiber optic sensors can be commonly classified as either single-point, multipoint, or distributed. Bragg grating sensors are single-point or multipoint (quasi-distributed). Interferometric sensors can fall into all three classifications. Scattering-based sensors are distributed. As illustrated in Fig. 2.9, in a single-point sensor, the sensing portion of the fiber is typically located at the tip and measures single or multiple parameters at that specific spatial point; whereas, a multipoint fiber optic sensor consists of two or more sensing regions along the length of a fiber, where each can detect the same or a different parameter. These sensing regions can be physically spaced from a few millimeters to several meters away, depending on the application requirements. Every portion along the length of a truly distributed fiber optic sensor is sensitive to one or more external parameter and is capable of effectively detecting these parameters over its entire length, which can be on the order of several tens of kilometers. This capability is unique to fiber optics and cannot be easily achieved using conventional sensors and sensing techniques; it would become extremely cumbersome given the cabling, power, and telemetry requirements, not to mention the high cost. Distributed fiber sensors are a specialized yet powerful technology that enables the possibility to measure a parameter along a spatially continuous region using solely an opto-electronics box and a sensing optical fiber cable. This technology can perform measurements that would otherwise be impossible, impractical, or extremely costly to perform.

The concept of distributed sensors was first introduced in the 1980s with the development of Optical Time-domain Reflectometers (OTDR) and their application to the sensor field. It refers to the use of a single optical fiber as a linear continuous sensor providing multiple measurement points spatially continuously distributed over the whole fiber length as depicted in Fig. 2.10. A single optical fiber cable can replace thousands of traditional single-point sensors such as thermocouples or strain gauges, saving complex installation,

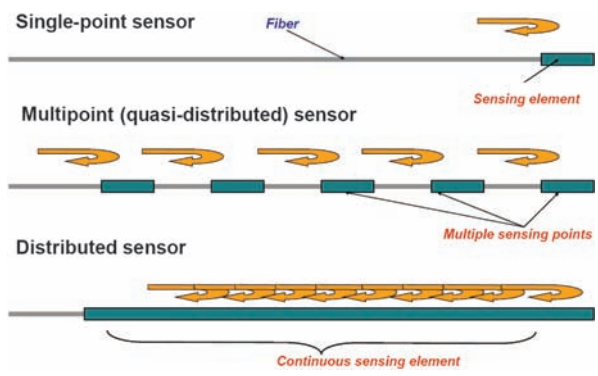

Figure 2.9 Classification of optical fiber sensors according to their topology (Ref 4).

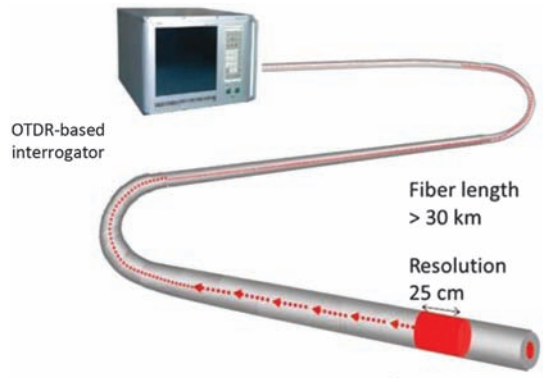

Figure 2.10 Distributed fiber optic sensor.

calibration, and maintenance costs. As a result, temperature and/or strain information is made available through profiles as a function of distance in one shot, providing simultaneous temperature/strain information of thousands of locations with a single instrument.

The geometry of optical fiber makes it an ideal candidate for long-range distributed sensors. Furthermore, the wide range of commercially available fiber cable enables suitable solutions for various monitoring applications, even in the case of extreme environmental conditions.

A distributed fiber optic sensor is capable of performing a multitude of spatial measurements along the entire length. Distributed sensing techniques are based on the recording and analysis of the scattered light at every location along the fiber. Light scattering is associated with inhomogeneities in the propagation medium. Different types of inhomogeneities give rise to different scattering phenomena, ranging from density fluctuation generating Rayleigh scattering to thermally excited acoustic waves (or phonons) and molecular vibrations causing Brillouin and Raman scattering.

References

1. D. A. Krohn, *Fiber Optic Sensors, Fundamentals and Applications*, Third Edition, ISA, Research Triangle Park, NC (2000).
2. Photonic Sensor Consortium, Photonic Sensor Market Survey, Photonic Sensor Consortium, Jan (2013).
3. R. S. Mellberg, "Fiber optic sensors" *SRI International,* Research Report No. 684 (1983).
4. A. Mendez, "Fiber optic distributed pressure sensing and other in-well optical sensors," SPE Applied Technical Workshop, Feb. (2006).
5. A. Mendez and T. Graver, "Overview of fiber optic sensors for NDT applications, IV NDT Pan-American Conference, Oct. (2007).

6. D. A. Krohn, "Fiber optic sensors in industrial applications: an overview," *Proc. ISA* **37**, pp. 1673–1684 (1982).
7. D. A. Krohn, "Fiber optic sensors in industrial applications: an update," *Proc. ISA* **38**, pp. 877–890 (1983).
8. J. Hecht, "Fiber optics turns to sensing," *High Technology*, pp. 49–56 (1983).
9. D. H. McMahon, A. R. Nelson, and W. B. Spillman, "Fiber-optic transducers," *IEEE Spectrum,* pp. 24–29 (December 1981).
10. T. G. Giallorenzi et al., "Optical fiber sensor technology," *IEEE Journal of Quantum Electronics* **Q-E-18**(4), 626–6 (1982).
11. C. M. Davis, "Fiber optic sensors: an overview," *Optical Engineering*, **24**(2), pp. 347–351 (1985) [doi:10.1117/12.7973482].
12. J. H. Brehney, "Fiber optic sensors for aircraft," *Aerospace Engineering*, pp. 12–19 (Sept. 1988).
13. A. D. Kersey, M. A. Davis, H. J. Patrick, M. LeBlanc, K. P. Koo, C. G. Atkins, M. A. Putnam, and E. S. Friebach, "Fiber grating sensors," *Journal of Lightwave Tech*. **1**(8), pp. 1442–1463 (1997**)**.
14. J. P. Dakin, *Distributed Optic Fibre Sensors*, SPIE Critical Review CR44, pp. 377–385 (1992).
15. X. Bao, J. Dkliwago, N. Heron, D. Webb, and D. Jackson, "Experimental and theoretical studies on a distributed temperature sensor based on brillouin scattering," *Journal of Lightwave Technology* **13**(7) pp. 1340–1348 (1995).
16. L. Savage, "Sensing trouble: fiber-optics in civil engineering," *Optics & Photonics News*, pp. 26–33, March (2013).
17. A. D. Kersey, "Multiplexed fiber optic sensors," *Proc. SPIE* **1797**, pp. 61–185 (1995).
18. T. MacDougall and P. Sanders, "Dynamic polarization based fiber optic sensor," Patent Application Publication – US 2009/0290147 A1, Nov. 26, 2009.
19. A. D. Kersey, "Distributed and multiplexed fiber optic sensors," E. Udd and W. B. Spillman, Editors, *Fiber Optic Sensors*, Wiley, New York, p. 277 (2011).
20. M. Ahangrani et. al., "Spontaneous Raman scattering in optical fibers with modulated probe light for distributed temperature Raman remote sensing," *J. Lightwave Technol.* 17, 1379–1391 (1999).
21. Y. T. Cho et. al., "50–km single-ended spontaneous Brillouin based distributed temperature sensor exploiting pulsed based Raman amplification," *Opt. Lett.* **28**, p. 1651 (2005).
22. C.M. Davis, *Selected Papers on Fiber Optic Sensors*, SPIE Press, Bellingham, WA, pp. 12–16 (1995).

Chapter 3
Intensity-Modulated Sensors

3.1 Introduction

Intensity-modulated sensors were defined in Chapter 2 as sensors that detect the variation of the intensity of light associated with the perturbing environment. The general concepts associated with intensity modulation include transmission, reflection, and microbending. However, several other mechanisms that can be used independently (intrinsically) or in conjunction with the three primary concepts include absorption, scattering, fluorescence, polarization, and optical gratings. While intensity-modulated sensors are analog in nature, they have significant usage in digital (on/off) applications for switches and counters.

3.2 Transmissive Concept

The transmissive sensor concept[1,2] is normally associated with the interruption of a light beam in a switch configuration. However, this approach can provide a good analog sensor. Figure 3.1(a) shows the probe configuration for measurement of axial displacement. Figure 3.l(c) gives a curve of output versus distance between the probes. The curve follows a l/r^2 law, where r is distance. A more sensitive transmissive approach employs radial displacement as shown in Fig. 3.l(b). The sensor shows no transmission if the probes are displaced a distance equal to one probe diameter. Approximately the first 20% of the displacement gives a linear output. The curve in Fig. 3.1(c), showing the effects of radial displacement, is for probes with a single fiber, 400-μm diameter.

A modification of the transmissive concept is referred to as frustrated total internal reflection.[4] The two opposing probes have the fibers polished at an angle to the fiber axis, which produces total internal reflection for all propagating modes, as shown in Fig. 3.2. As the fiber ends come close in proximity to one another, energy is coupled. The intensity of light coupled into the receiving fiber is shown in Fig. 3.3. This approach provides the highest sensitivity for a transmissive sensor.

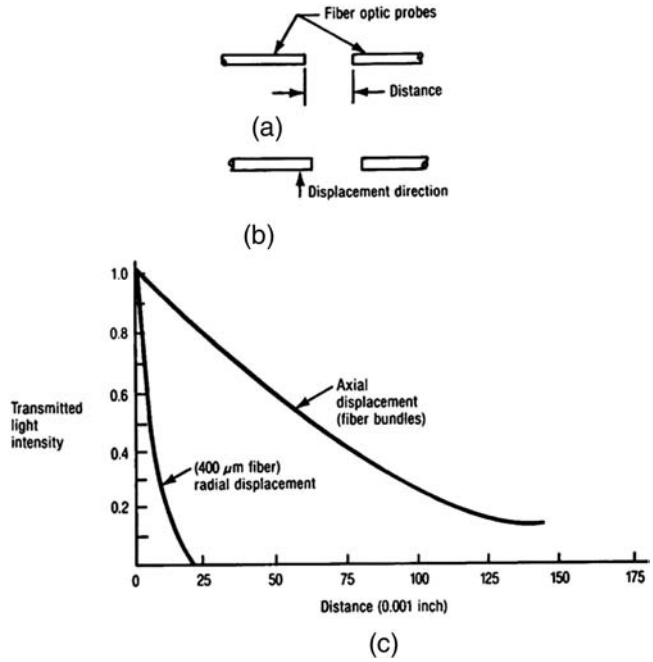

Figure 3.1 Transmissive fiber optic sensor.[3] (a) Axial displacement, (b) radial displacement, (c) output versus distance curve

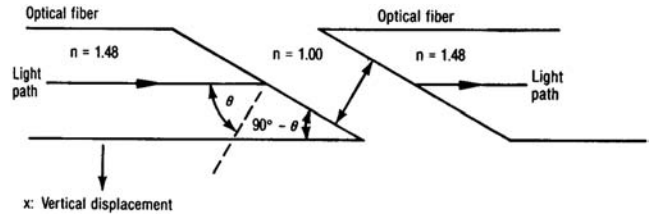

Figure 3.2 Frustrated total internal reflection configuration (reprinted from Ref. 4 with permission).

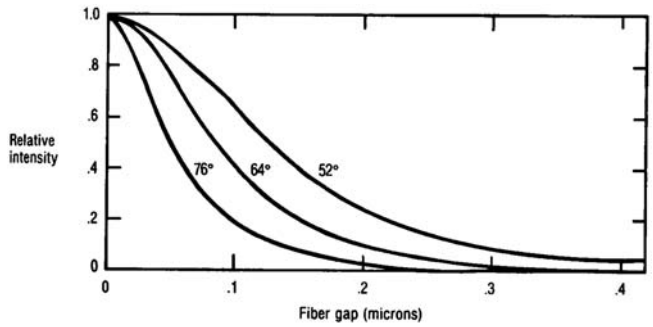

Figure 3.3 Frustrated total internal reflection response curves (reprinted from Ref. 4 with permission).

3.3 Reflective Concept

The reflective concept[5,6] is especially attractive for broad sensor use due to accuracy, simplicity, and potentially low cost. The concept is shown in Fig. 3.4(a). The sensor comprises two bundles of fibers or a pair of single fibers. One bundle of fibers transmits light to a reflecting target, and the other bundle traps reflected light and transmits it to a detector. The intensity of the detected light depends on how far the reflecting target is from the fiber optic probe. Part Figure 3.4(b) shows the detected light intensity versus distance from the target. The linear front slope allows a displacement to be measured with potential accuracy of one millionth of an inch. The accuracy depends on the probe configuration; a hemispherical probe has more dynamic range, but less sensitivity when compared to a random probe (Fig. 3.4). A fiber pair probe

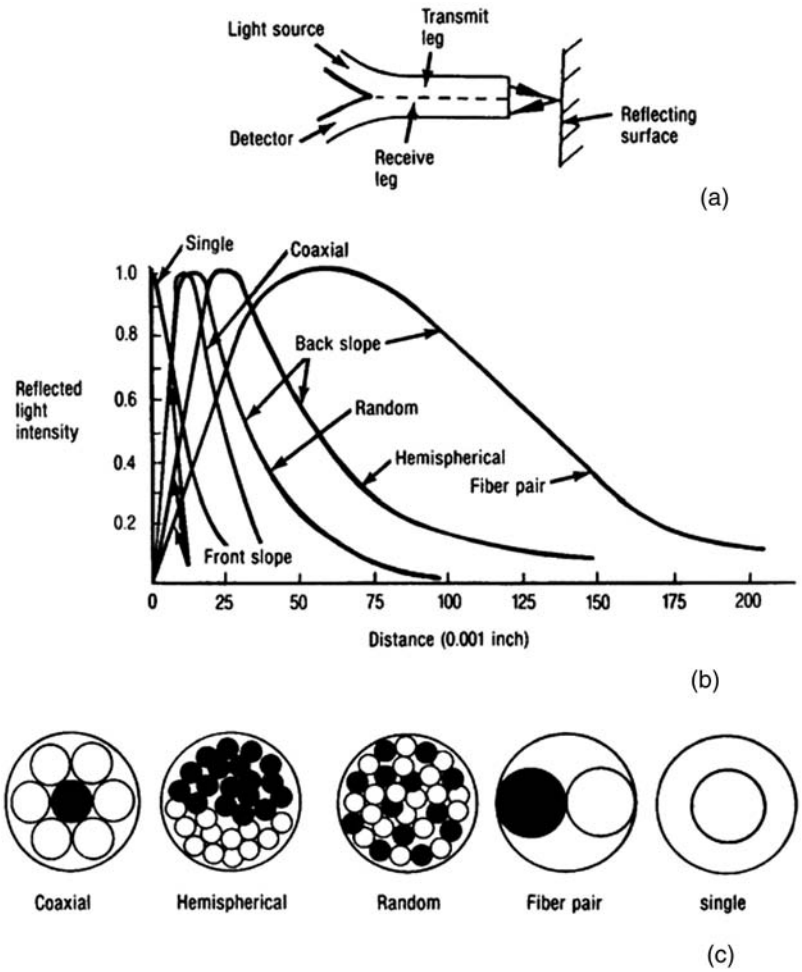

Figure 3.4 Reflective fiber optic sensor response curve for various configurations. (a) Sensor arrangement, (b) output versus distance, (c) probe configuration.

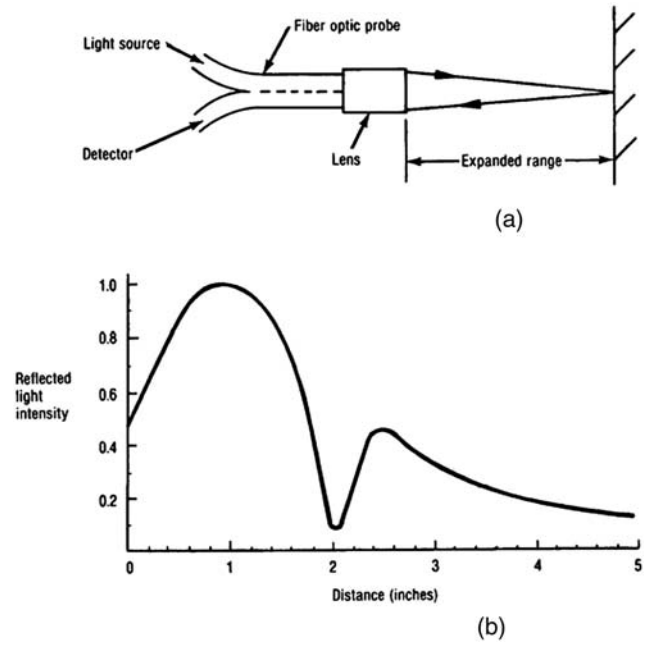

Figure 3.5 Reflective fiber optic sensor with expanded range. (a) Configuration, (b) response curve.

further expands the dynamic range. A fiber pair configuration can increase the response sensitivity similar to a random bundle probe if the plane reflective surface is replaced with a convex reflector.[7] A single fiber used in conjunction with a beam splitter to separate the transmitted and the received beams eliminates the front slope. Depending on the fiber configuration, reflective probes can be tailored for a wide range of applications.

For applications that require a greater dynamic range than possible with any of the fiber configurations, a lens system can be added,[8] as shown in Fig. 3.5(a). Using a lens system in conjunction with a fiber optic probe, the dynamic range can be expanded from 0.2 in to 5 in or more as shown in Fig. 3.5 (b). The detailed mechanism of how the lens extends the sensor range is described in Chapter 10.

3.4 Microbending Concept

Another attractive sensor concept is that of microbending.[9–11] If a fiber is bent, small amounts of light are lost through the wall of the fiber. If a transducer bends the fiber due to a change in some physical property, as shown in 3.6(a), then the amount of received light is related to the value of this physical property. Figure 3.6(b) indicates that as pressure causes the transducer to squeeze together and bend the fiber, the amount of transmitted light decreases with displacement.

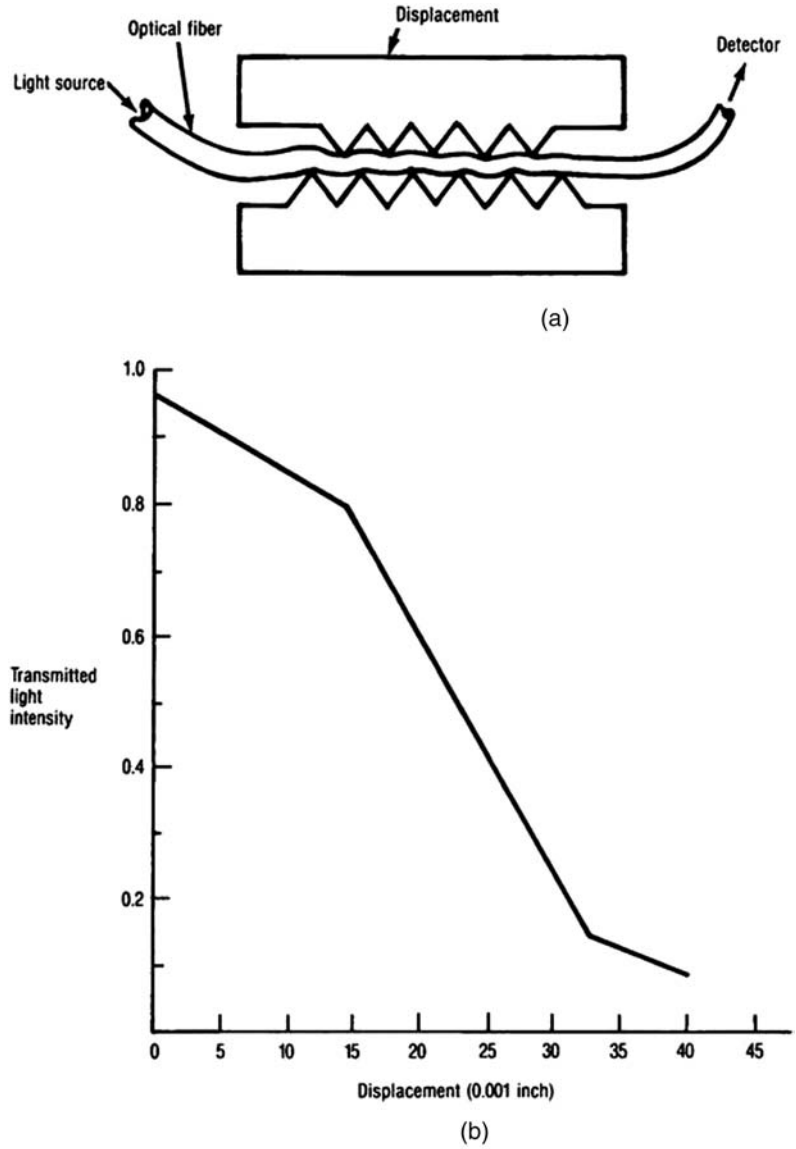

Figure 3.6 Microbending sensor.[3] (a) Sensor arrangement, (b) output versus displacement.

Like reflective sensors, microbending sensors are potentially low cost and accurate. It is also important to note that these sensors have a closed optical path and therefore are immune to dirty environments.

In the response curve of Fig. 3.6(b), the initial nonlinear behavior is due, at least in part, to the rheological behavior of the polymeric protective coatings. The change in slope at high displacement values is due to light depletion. The linear central portion of the curve is the active sensing region.

In general, as the number of bend points increases and/or the spacing between bend points decreases, the sensitivity increases.

3.5 Intrinsic Concept

Intrinsic sensors change the intensity of the returning light from the sensor; however, unlike the transmissive, reflective, and microbending concepts, no movement is required. Intrinsic sensors use the chemistry of the core glass (cladding glass or the plastic coatings) to achieve the sensing activity. The prime mechanisms are absorption, scattering, fluorescence, changes in refractive index, or polarization.

For absorption, doping the core glass results in absorption spectra.[12] Generally, some peaks are temperature sensitive, while others are not. The ratio of intensity at two specified wavelengths provides a temperature sensing function as shown in Fig. 3.7. A similar approach can be considered for scattering.

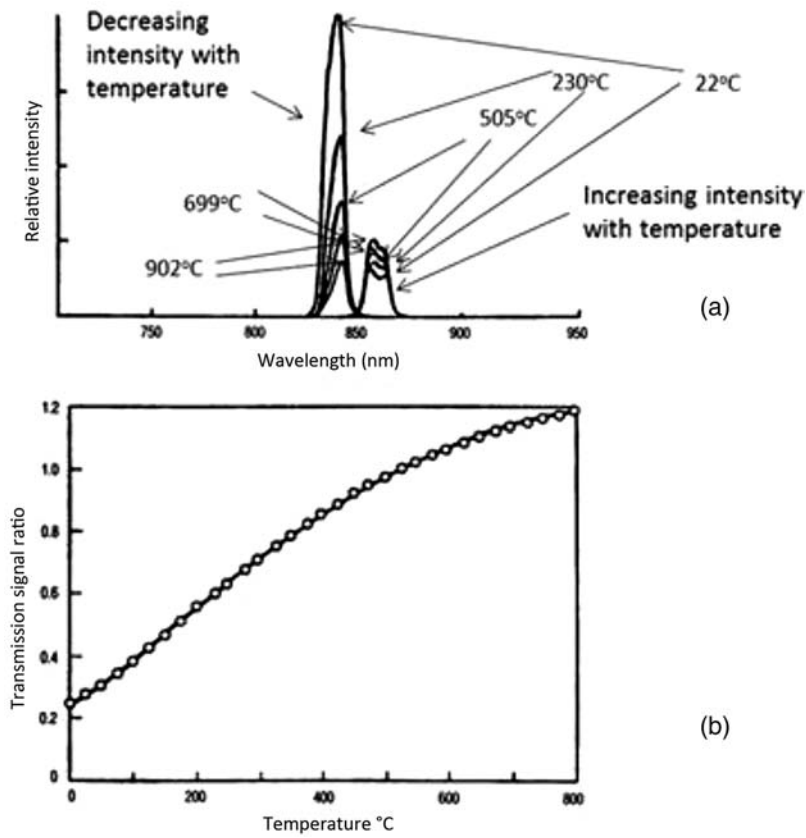

Figure 3.7 Intrinsic temperature sensor using absorption characteristics of the fiber. (a) Transmission through a neodymium doped fiber, (b) response of a neodymium-doped fiber temperature sensor.

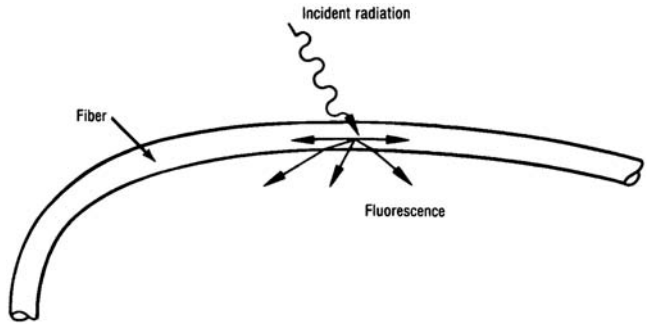

Figure 3.8 Fluorescence stimulated by outside radiation.[16]

Fluorescence can be achieved by doping the glass with various additives. The sensor can function in two modes. A light source can be used to stimulate fluorescence, which is affected by temperature, or the fiber can be stimulated by outside radiation and the fluorescence detected, which is a measure of the level of incident radiation, as shown in Fig. 3.8.

Refractive index changes can vary the amount of received light by effectively changing the numerical aperture of the fiber. Many polymeric coating materials can be made to have index changes with temperature, thus providing a temperature sensor.

Lastly, doping the glass with various rare-earth oxides can make the fiber sensitive to magnetic fields. Such fibers in the presence of magnetic fields rotate the polarized light beam in the fiber, causing a partial extinction and a correlation of light intensity with magnetic field. This concept is referred to as a Faraday rotation, which will be discussed in more detail in Chapter 14.

3.6 Transmission and Reflection with Other Optical Effects

The sensitivity of transmissive sensors can be further enhanced by adding absorption gratings to the fiber face, as shown in Fig. 3.9. To go from

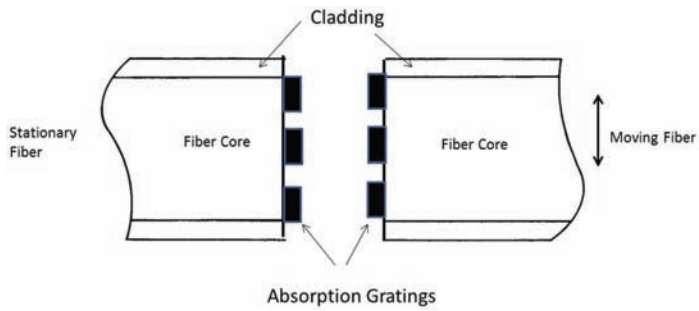

Figure 3.9 Radial displacement sensor with absorption gratings (adapted with permission from Ref. 9).

maximum intensity now requires movement of only one grating spacing instead of one probe diameter; this could increase sensitivity by a factor of five or more.

The grating on the fiber is designed to increase sensitivity for radial displacement. The transmissive sensor can be used for rotational sensing. Consider two cases: Figure 3.10 (case 1) depicts two disks, one fixed and the other able to rotate. Each disk has a grating such that the grating of the two disks can be aligned either in optical line to allow maximum light, in an alignment that allows no light, or in any position in between. Depending on

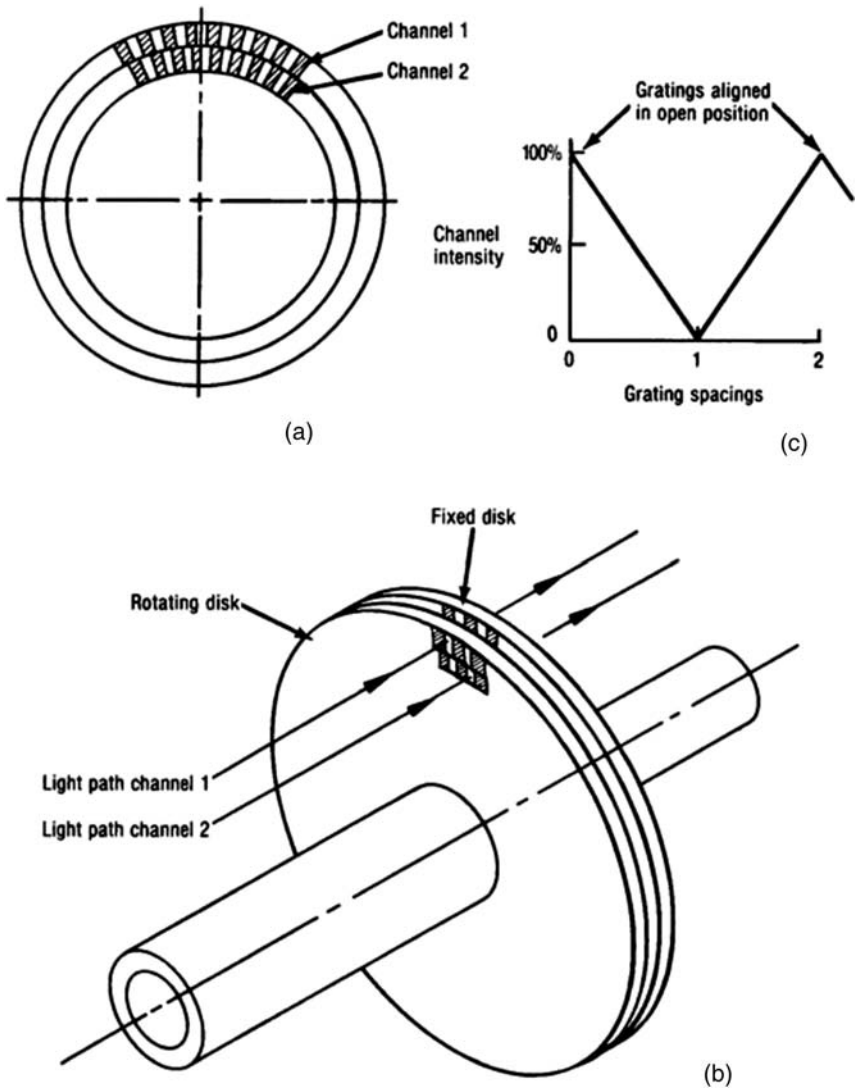

Figure 3.10 Fiber optic rotation sensor.[3] (a) Grating spacing, (b) sensor configuration, and (c) sensor response.

the width of the gratings, the sensor changes intensity from maximum light to zero light in the rotational distance of one grating spacing. The analog signal is linear with the degree of rotation. If two sets of gratings (channels 1 and 2) are used, the direction as well as the magnitude can be determined. Since the signal is repeated for each grating spacing, the analog measurement is limited to small rotations such as might be associated with torque.

In case 2, the gratings are replaced with a fixed and a rotating polarizing lens as shown in Fig. 3.11(a). The transmitted intensity through the polarizing lenses is approximately proportional to $\cos^2\theta$, where θ is the relative rotation, as shown in part Fig. 3.11(b).[13] The linear range for this sensor type is limited.

The transmissive sensor can also be used in conjunction with other optical materials in the light path that alter intensity as a function of environment (see Fig. 3.12). If a material in the light path changes transmission levels

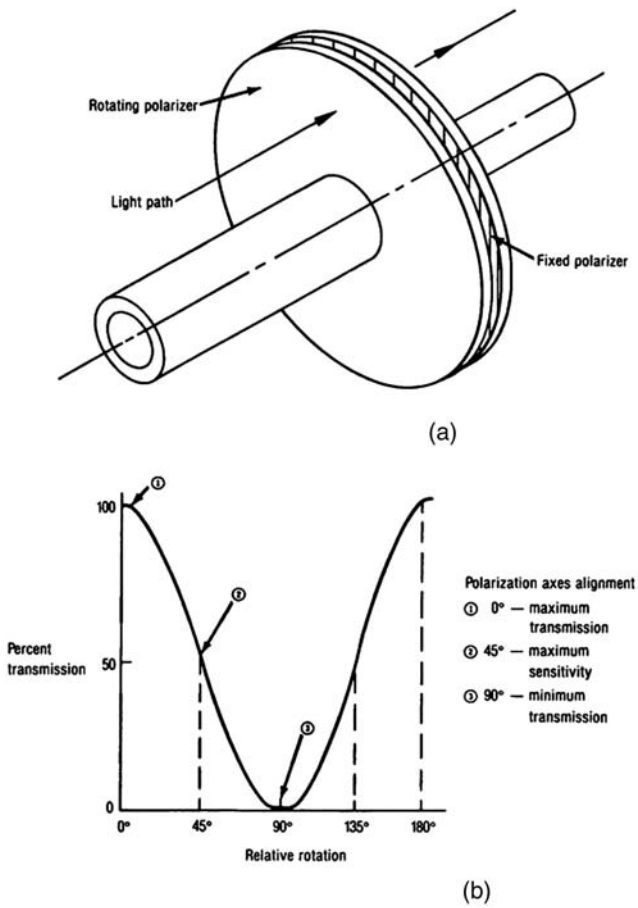

Figure 3.11 Fiber optic rotation sensor using polarization.[3] (a) Sensor configuration, (b) sensor response.

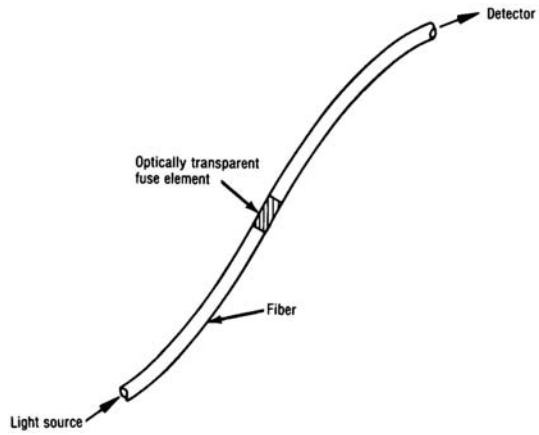

Figure 3.12 Transmissive sensor with optically active material in light path.

abruptly with environmental changes, then a switching function is accomplished. Liquid crystals are materials that can be used for temperature and pressure switching. Analog behavior is observed if the change occurs continuously. A host of materials exhibiting this behavior are available. Examples include the following:

- Photoelastic materials in conjunction with polarized light are pressure sensitive.
- Photochromic material in conjunction with UV light is temperature sensitive.
- Materials with dopants providing strong absorption bands are temperature sensitive.
- Some photoluminescent materials alter transmission in the presence of an electric field.

The list of potential sensing materials is limited only by the imagination of the material scientist.

These active material concepts can be applied to reflective sensors by incorporating the material into the target. An especially attractive reflective-sensor concept involves fluorescence. This concept is also referred to as wavelength modulation since the modulated light has a higher wavelength than the incident light. Figure 3.13 depicts how the sensor works. UV light travels down the fiber optic probe and strikes a target, which fluoresces and reflects back into the receiving fiber.

Often this type of sensor probe uses only a single fiber with transmitted and receiving light rays travelling simultaneously without interfering. The fluorescence is characteristic of the target material. In addition, the intensity of the returning radiation is temperature sensitive. Therefore, this approach has application in both chemical analysis and temperature sensing.

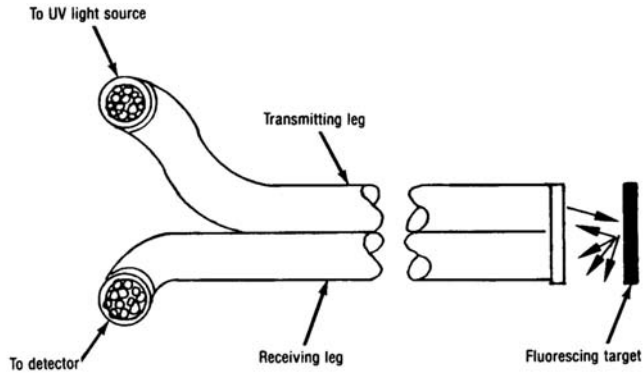

Figure 3.13 Fiber optic fluorescence sensor.[3]

3.7 Speckle Pattern

When light is transmitted in a multimode optical fiber, many modes of light exist with different optical phases. When observed at the end of the fiber, a speckle pattern exists as shown in Fig. 3.14. Mode mixing will cause interference effects that alter the intensity and the form of the speckle pattern due to even very small perturbations to the fiber.[14,15] The fiber is very sensitive to pressure, vibration, and motion changes. Unlike microbending sensors, the fiber does not require an external transducer. Anywhere along the fiber, perturbations can be detected. However, a disadvantage of a speckle pattern sensor is that activation of multiple points makes it difficult to interpret the absolute magnitude of a pressure or vibration disturbance at a given point. As a result, this approach is much better suited to intrusion alarm systems.

3.8 Sources of Error and Compensation Schemes

Analog fiber optic sensors have been used in many industrial and military applications, including displacement, temperature, and pressure sensors.

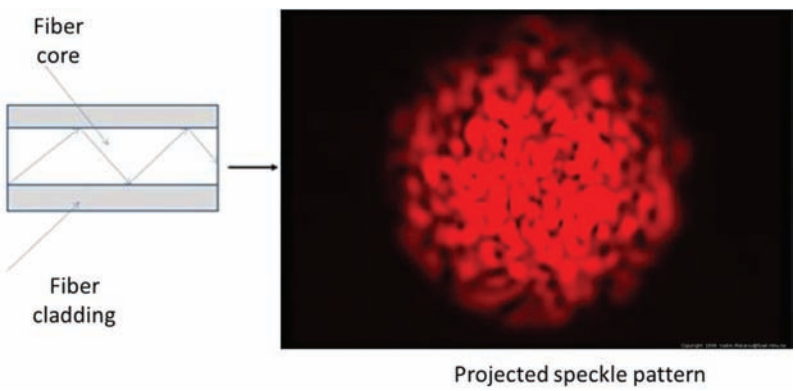

Figure 3.14 Speckle pattern exiting fiber due to modal interference.[16]

Almost all of these sensors use intensity modulation.[17] The major problems include variations in light source intensity (which directly affects the analog sensor output) and microbending in the leads to and from the sensing region.

The light source is typically a light-emitting diode (LED) that varies in intensity by 0.5% per degree centigrade. To resolve this problem, a reference can be used that detects the intensity variations and corrects the LED output, as shown in Fig. 3.15.

In the reflective concept, in addition to light source variations, there are other potential sources of error. Reflectivity of the target can be altered by temperature as well as corrosion or oxidation of the reflecting surface. High pressure can alter the relative position of the transmitting and receiving fibers in relation to the target. To avoid these problems, well-designed packaging is required.[18] Microbending losses in the fiber leads present a problem only if the leads move while the sensor is in operation. Figure 3.16 shows percent transmission of typical optical fibers and the effect of bending. Clearly, the large-core plastic-clad silica fibers (PCS) and the hard polymeric-clad silica fibers are the least sensitive to bending loss and the best suited for sensor leads. Furthermore, the sensitivity of the leads can be reduced if a protective cable construction surrounds the fiber to retard bending loss. Losses in the leads, if not properly controlled, can cause errors in excess of 5%. An interesting point is that as the lead length increases, the light level in the

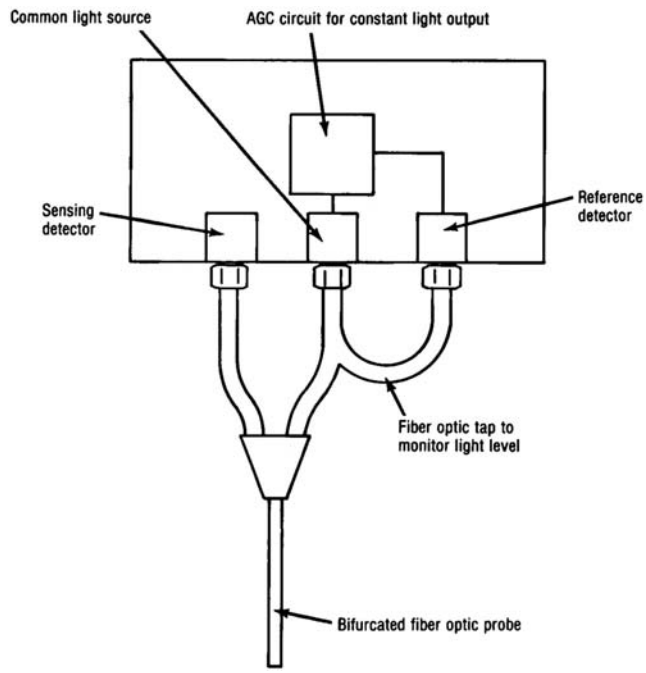

Figure 3.15 Electro-optic configurations to maintain constant light intensity.[3]

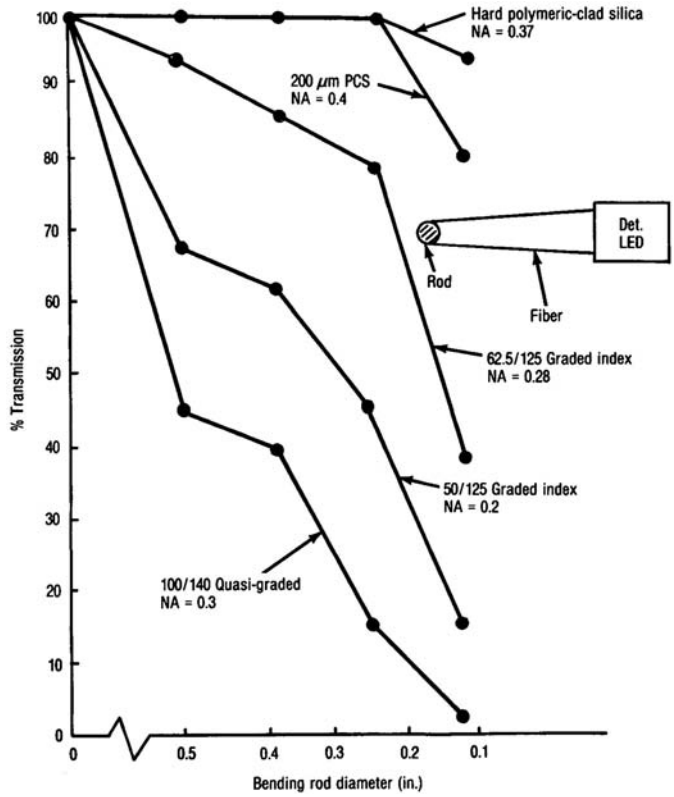

Figure 3.16 Percent transmission versus bending for various optical fibers.[3]

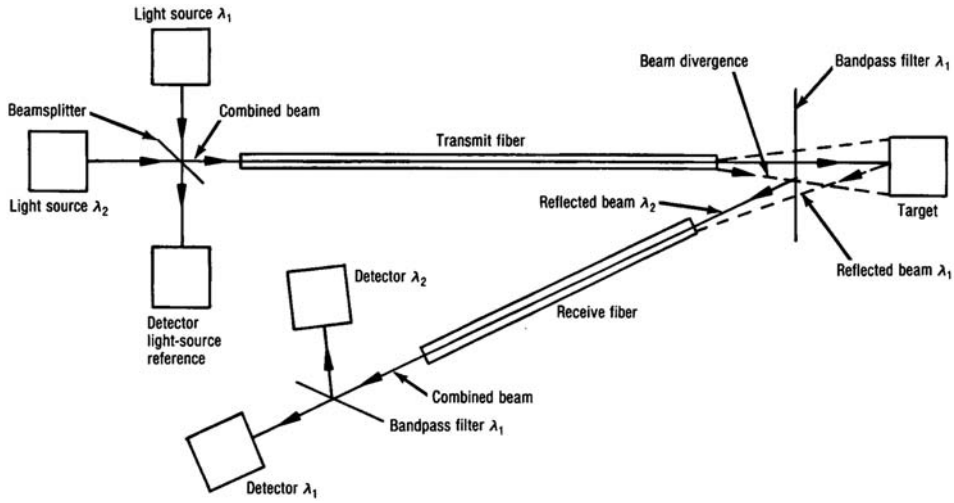

Figure 3.17 Compensated detection system.[19]

sensing system decreases. Analog sensors function best when the leads are 100 m or less. Digital sensors can work well to 1000 m or more.

A detection system that can compensate for variations in light-source intensity and microbending effects that uses a dual-wavelength referencing scheme[19] is depicted in Fig. 3.17. Both light sources are pulsed so that the portion of the split beams λ_1 and λ_2 can be detected and used to compensate the respective sources, similar to that shown in Fig. 3.13. One wavelength λ_1 is used for sensing; the light is transmitted to the target, passes through a band-pass filter, reflects from the target, is collected by the receiving fiber, and is detected. The light beam of wavelength λ_1 has been compensated for light-source intensity. The transmitted beam is modulated by the target and microbending effects. The second wavelength λ_2 is reflected at the band-pass filter, collected by the receiving fiber, and detected. The light beam of wavelength λ_2 has been compensated for light source intensity, and the transmitted beam is a reference not being modulated by the target. Only microbending effects are detected. The difference in intensity of the λ_1 and λ_2 beams eliminates microbending effects, and the result is directly proportional to target modulation effects.

References

1. R. W. Fayfield, "Fiber optics and photoelectric sensing, a good combination," *Instruments and Control Systems*, 45–49 (1982).
2. AMP, "Fiber optics use gains from realistic test method," *AMP Design Digest* **22**, p. 6 (1982).
3. D. A. Krohn, *Fiber Optic Sensors: Fundamentals and Applications*, Third Edition, ISA, Research Triangle Park, NC (2000).
4. W. B. Spillman, Jr. and D. H. McMahon, "Frustrated-total-internal-reflection multimode fiber optic hydrophone," *Appl. Opt.* **19**, 113–117 (1980).
5. C. D. Kissenger and B. Howland, "Fiber optic displacement measuring apparatus," U.S. Patent 3,940,608 (Feb. 24, 1976).
6. A. K. Dejczy, H. C. Primus, and W. A. Herman, "Fiber optic proximity sensor," *NASA Tech. Brief* **4**(3), Item 63, JPL Report NPO-14653/30–4279 (March 1980).
7. A. D. Gaikwad, J. P. Gawande, A. K. Joshi, and R. H. Chile, "An intensity-modulated optical fibre displacement sensor with covex reflector," *International Journal of Advanced Research in Electrical, Electronics and Instrumentation Engineering* **1**(1), 29–35 (2012).
8. D. A. Krohn, "Fiber optic displacement sensor," *Proc. ISA* **39**(1), 331–340 (1984).
9. D. H. McMahon, A. R. Nelson, and W. B. Spillman, Jr., "Fiber optic transducers," *IEEE Spectrum*, pp. 24–29 (December 1981).

10. N. Lagakos, T. Litovitz, P. Macedo, R. Mohr, and R. Meister, "Multimode optical fiber displacement sensor," *Applied Optics* **20**(2), 167–168 (1981).
11. M. Gottlieb and G. B. Brandt, "Measurement of temperature with optical fibers using transmission intensity effects," *Electro-Optics/Laser 79 Conference & Exposition: Proceedings of the Technical Program*, p.100 (Oct 1979).
12. E. Snitzer, W. W. Morey, and W. H. Glenn, "Fiber optic rare earth temperature sensors," First Int. Conf. Optc. Fiber Sensors*, IEEE Conf. Publication* 221, p. 79 (1983).
13. Melles Griot , *Optics Guide 3,* Melles Griot, Irvine, CA, p. 296 (1985).
14. P. S. Lovely, "Multimode Fiber Sensor System with Fiber Coupled to a Detection Fiber by Spacer Means," U.S. Patent 51444689 A (Jul. 1991).
15. C. D. Butler, "Fiber Optic Intruder Alarm," U.S. Patent 4297684 A (Mar. 1979).
16. P. McLaughin, "Old Fashion Security, Cabling Installation and Maintenance," *Fiber Optic Technology Updates* (Feb 2008).
17. D. A. Krohn, "Field experience with fiber optic sensors," *Proc. ISA*, pp. 1051–1061 (1985).
18. E. Pinet, "Pressure measurement with fiber-optic sensors: commercial technologies and applications," *Proc. SPIE* **7753**, 775304 (2011) [doi: 10.1117/12.895536].
19. M. T. Wlodarczyk, "Dual wavelength catheter-type fiber optic pressure sensor," *Proc. SPIE* **1067**, 8–12 (1989) [doi: 10.1117/12.952095].

Chapter 4
Phase-Modulated Sensors

4.1 Introduction

Due to their extreme sensitivity, phase-modulated sensors are the most publicized of all the fiber optic sensors.[1,2] Phase-modulated fiber optic sensors typically involve the use of optical interferometers to measure the change in phase of a single light signal or, more often, the relative phase change between two light waves. To begin a discussion on interference, it is important to first mathematically describe the wave propagation process. The general description of an electromagnetic plane wave propagating in free space is

$$\mathbf{E} = \mathbf{E}_0 e^{\ j(\mathbf{k}\,\mathbf{r}\ \ \omega t)}, \tag{4.1}$$

where $\mathbf{E}$ represents the electric field amplitude, $\mathbf{k}$ = the wave vector, $\mathbf{r}$ = coordinate vector, ω = angular frequency, t = time, and $\mathbf{E}_0 = E_x\hat{\mathbf{x}} + E_y\hat{\mathbf{y}} + E_z\hat{\mathbf{z}}$.

If we consider just a linearly x-polarized plane wave propagating along the z-axis and look at the real portion of the phasor representation:

$$\mathbf{k}\cdot\mathbf{r} \text{ becomes } (2\pi/\lambda)\,z,$$

and

$$\mathbf{E} = E_x \cos\left[\left(\frac{2\pi}{\lambda}\right)z \quad \omega t\right]. \tag{4.2}$$

Since the measurement of the phase modulation is averaged over many values of $\omega t's$, it is acceptable to drop the ωt term, simplifying (4.2) even further:

$$\mathbf{E} = E_x \cos\left[\left(\frac{2\pi}{\lambda}\right)z\right]. \tag{4.3}$$

It is important to point out that this expression describes a plane wave in free space, which implies that the surfaces of constant phase are planes and that they extend to infinity with no change, making this a particularly ideal case. When solving for the electric field component for a wave propagating in a guided medium such as an optical fiber, the boundaries of the core and cladding must be taken into account as well as the noninfinite extension of the

field. The phase fronts of the fields in a single-mode optical fiber (for wavelength operation past cutoff) can be fairly accurately represented by Eq. (4.3); this greatly simplifies the analysis of interferometric behavior in fiber architectures. An additional parameter that must be considered for wave propagation in a medium is the index of refraction, normally represented by n. For this discussion we will consider n as a macroscopic parameter of a charge-free, homogeneous, dielectric material that merely dictates the group velocity of the wave according to the following:

$$v = \frac{c}{n}. \tag{4.4}$$

This leads to modifying Eq. (4.3) to account for properties of the material within which the wave is travelling:

$$\mathbf{E} = E_x \cos\left[\left(\frac{2\pi n}{\lambda}\right) z\right]. \tag{4.5}$$

If we treat the z direction in the fiber as length L we can lump the argument of Eq. 4.5 into the familiar single-phase term

$$\phi = knL, \tag{4.6}$$

$\phi = knL$ leading to a simple expression for the electric field wave:

$$\mathbf{E} = E_x \cos(\phi). \tag{4.7}$$

The intent of Eq. (4.5) is to describe a single linear polarization state. It has been mentioned earlier in the text that multiple polarization states can propagate in the fiber and that typically these states are more generally elliptical and dynamic. Waves of equal polarization states will interfere nonetheless, with the net effect being a reduction in contrast or visibility of the resulting signal.

Generally, phase-modulated sensors employ a coherent laser light source and two separate optical paths or arms. The light is split and injected into each arm. If the environment perturbs one arm relative to the other, a phase shift occurs that can be precisely detected.[3] When these systems are implemented using optical fibers, the two arms typically consist of single-mode fiber. Fiber optic sensors in general are modulated by some physical parameter, which in turn transmits this modulated light signal to a detection system. This detection system will usually include components that are sensitive to wavelength, phase, polarization, or some other property of the optical signal. At the end of this train is a detector that responds to the intensity of the light. This is an important concept to keep in mind throughout the book: with all of the sensor configurations that are possible, the intensity of the light arriving at the detector is always the fundamental measurement.

It can be shown that the time-averaged intensity of Eq. (4.7) is

$$I \propto E_x^2. \tag{4.8}$$

In order to analyze the interference of two waves, one must keep in mind that the resultant electric field is the sum of all the fields present at the spatial point and temporal instance. The intensity resulting from two plane waves [as described in Eq. (4.7)], with equal linear polarization states and field amplitudes, can be found by reverting back to the phasor notation of the wave:

$$\begin{aligned} \mathbf{E}_1 &= Ee^{\,j\phi_1} \\ \mathbf{E}_2 &= Ee^{\,j\phi_2} \\ I &= \mathbf{E}_1\mathbf{E}_1^* + \mathbf{E}_2\mathbf{E}_2^* + \mathbf{E}_1\mathbf{E}_2^* + \mathbf{E}_2\mathbf{E}_1^* \\ I &= 2E^2[1 + \cos(\phi_2 \quad \phi_1)]. \end{aligned} \tag{4.9}$$

Figures 4.1 and 4.2 display the resulting intensity for the cases where (1) the length and refractive index are held constant and the wavelength is changed,

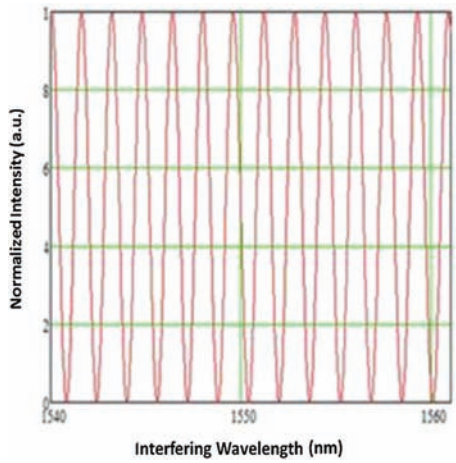

Figure 4.1 Resultant intensity of the interference of two waves as a function of wavelength.

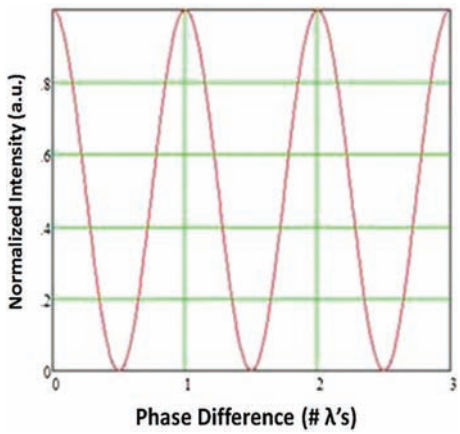

Figure 4.2 Resultant intensity of the interference of two waves.

and (2) the wavelength is held constant but the length L is changed, respectively.

4.2 Interferometers

There are four basic interferometric configurations:[4] the Mach–Zehnder, the Michelson, the Fabry–Pérot, and the Sagnac. The Mach–Zehnder and the Sagnac are the most widely used for hydrophone and gyroscope applications, respectively. However, all four configurations will be discussed in detail in this chapter.

4.2.1 Mach–Zehnder

The Mach–Zehnder (M–Z) interferometer configuration is shown in Fig. 4.3. The laser output beam is split by using a 3 dB fiber-to-fiber coupler, i.e., 50% of the light is injected into the single-mode sensing fiber and 50% into the reference fiber. The light beams are recombined by using a second 3-dB fiber-to-fiber coupler. The combined beam is detected and the phase shift measured.

The phase shift results from changes in the length and the refractive index of the sensing fiber. If the path lengths of the sensing and reference fibers are exactly the same length or differ by an integral number of wavelengths, the recombined beams are exactly in phase, and the beam intensity is at its maximum. However, if the two beams are a ½ wavelength out of phase, the recombined beam is at its minimum value. A modulation of 100% occurs over ½ wavelength of light change in fiber length. This sensitivity allows movements as small as 10^{-13} m to be detected.

4.2.2 Michelson

The Michelson interferometer configuration is shown in Fig. 4.4. The configuration is similar to the Mach–Zehnder approach but uses back reflection caused by the fibers having mirrored ends. The initial coherent laser

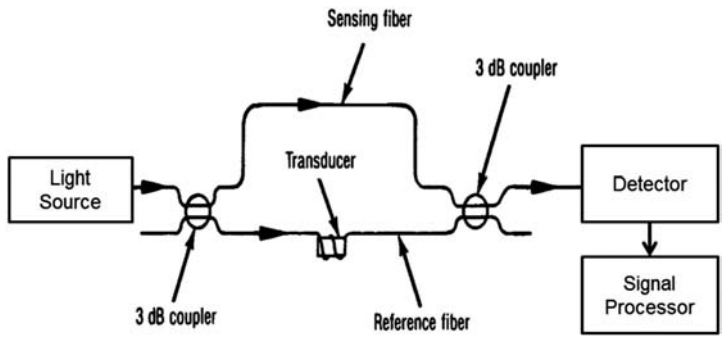

Figure 4.3 Mach–Zehnder interferometer configuration (reprinted from Ref. 4 with permission).

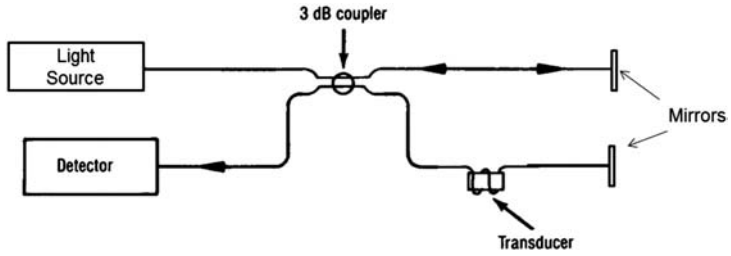

Figure 4.4 Michelson Interferometer configuration (reprinted from Ref. 4 with permission).

beam is split and injected into the sensing fiber by the 3-dB coupler. The reference fiber and the sensing fiber have mirrored ends to reflect the beam back through the two fibers and the 3 dB coupler to a detector. The phase shift is then detected. For the Michelson interferometer, a path length difference of $^1/_4\ \lambda$ in fiber length results in a $^1/_2\ \lambda$ path length change due to the second pass of the reflected beam. The comparison of the Mach–Zehnder and the Michelson interferometers is somewhat analogous to the comparison of transmissive and reflective intensity-modulated sensors. The Michelson approach has the advantage of eliminating one of the 3 dB couplers. However, it has the major disadvantage of the coupler feeding light into both the detector and the laser. Feedback into the laser is a source of noise, especially in high performance systems, and will be discussed in section 4.3.

4.2.3 Fabry–Pérot

The Fabry–Pérot (F–P) interferometer involves the concepts previously discussed but typically does not use a reference fiber. The interference results from successive reflections of the initial beam. The configuration is shown in Fig. 4.5. This multireflection process is unique to the F-P and produces a transfer function much different from that of the other three basic configurations discussed.

DiMarzio[5] provides a thorough derivation of the transmission (and reflection) for a Fabry–Pérot etalon with different reflection coefficients, assuming plane wave propagation:

$$T = \frac{(1 \quad R_1)(1 \quad R_2)}{R_1 R_2 \quad 1} \frac{1}{1 + F\sin^2\left(\frac{2\pi nL}{\lambda}\right)}, \tag{4.10}$$

$$F = \frac{4\sqrt{R_1 R_2}}{R_1 R_2 \quad 1}. \tag{4.11}$$

Figure 4.6 shows the response for both the transmission and reflection from a Fabry–Pérot etalon.

The multiple passes along the fiber magnify the phase difference, which results in extremely high sensitivity. Generally, the Fabry–Pérot sensor has a greater sensitivity compared to the other techniques discussed.

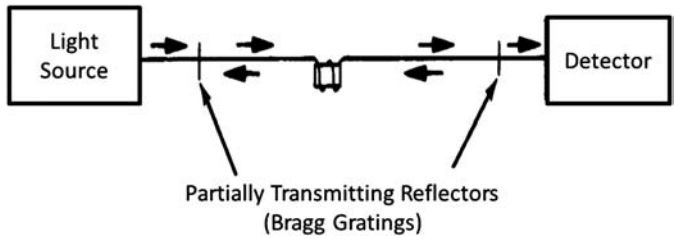

Figure 4.5 Fabry–Pérot interferometer configuration (reprinted from Ref 4 with permission).

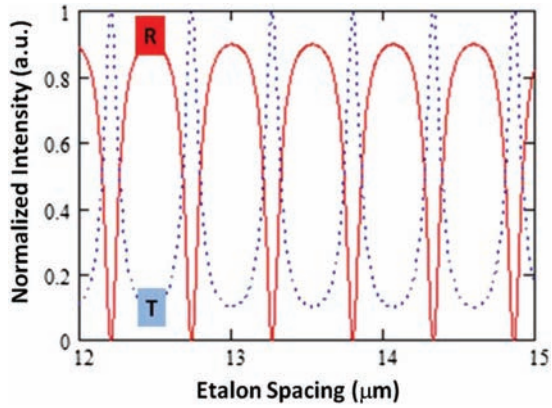

Figure 4.6 Intensity transmission and reflection from a Fabry-Pérot etalon for a wavelength of 1.55 μm.

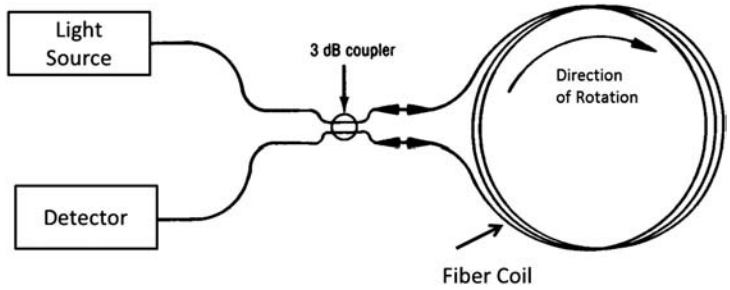

Figure 4.7 Sagnac interferometer configuration (reprinted from Ref. 4 with permission).

4.2.4 Sagnac

The Sagnac interferometer configuration is shown in Fig. 4.7. The Sagnac approach requires that a 3 dB coupler be used to inject light into two ends of a single-mode fiber in a coiled configuration. The injection of light into the fiber is such that light propagates in both clockwise and counterclockwise directions. In this case, both fibers are sensing fibers. While the coil is held stationary, no phase shift occurs since the clockwise and counterclockwise

distances are identical. However, if the coil is rotated in one direction (for instance, clockwise), the light propagation time is shortened for clockwise propagation. On the other hand, the propagation time is longer for the counterclockwise direction since the path is lengthened. The two recombined beams are then out of phase, and a very sensitive rotation measurement is achieved. This approach does not require fiber length and refractive index changes.

4.3 Phase Detection

The phase angle ϕ for a light wave travelling in a fiber defined earlier is repeated here for convenience:

$$\phi = \frac{2\pi L}{\lambda} = \frac{2\pi n_1 L}{\lambda_0}, \tag{4.12}$$

where n_1 is the index of refraction of the fiber core and λ_0 is the wavelength of light in vacuum. If L and λ_0 are in the same units, the phase angle is in radians. As indicated previously, a change in length and/or refractive index will cause a phase change as defined by the following equation:

$$\phi + \Delta\phi = \frac{2\pi}{\lambda_0}\,[n_1 L + n_1 \Delta L + L\Delta n_1]. \tag{4.13}$$

As a simplification, consider a phase change associated with changes in length, as this is the most common application, particularly for the M-Z and Michelson configurations.

Equation 4.12 simplifies to

$$\phi + \Delta\phi = \frac{2\pi}{\lambda_0}\,[n_1 L + n_1 \Delta L]. \tag{4.14}$$

Figure 4.8 shows the phase change associated with an increase in length. Consider the case of the Mach–Zehnder interferometer. It consists of two fibers: a reference fiber and a sensing fiber. If the sensing fiber is unperturbed, then two fibers have the same length L. The outputs of the two fibers interfere constructively and give the maximum intensity output. If the sensing fiber experiences a mechanically or thermally applied strain, the sensing fiber increases in length by ΔL. The intensity output decreases due to destructive interference. The relative phase-shift-versus-intensity curve is shown in Fig. 4.9.

The optical intensity is a function of the relative phase shift for the various interferometric configurations. The Michelson and the Sagnac interferometers are similar in intensity output to the Mach–Zehnder interferometer shown in Fig. 4.10. When the phase shifts are an integral number of wavelengths ($\phi = 0$, 2π, $4\pi\ldots$), the two legs of the interferometer are in phase, providing constructive interference and maximum intensity. The two light beams destructively interfere and have minimum intensity at a phase shift of an

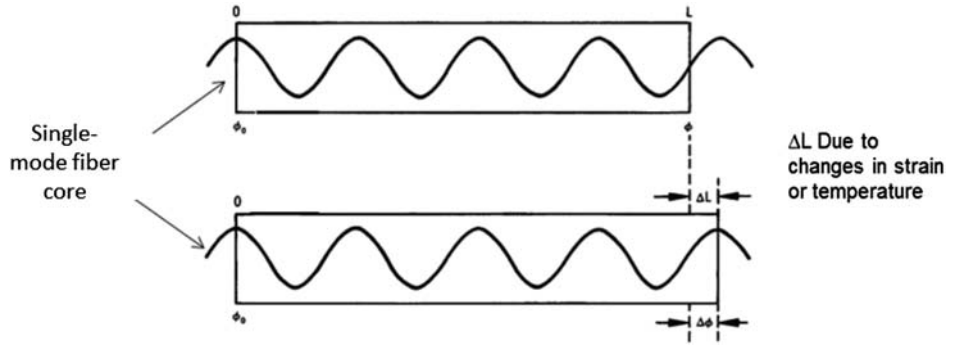

Figure 4.8 Phase change of a light wave through an optical fiber of original length L that has been stretched by a length ΔL (reprinted from Ref. 4 with permission).

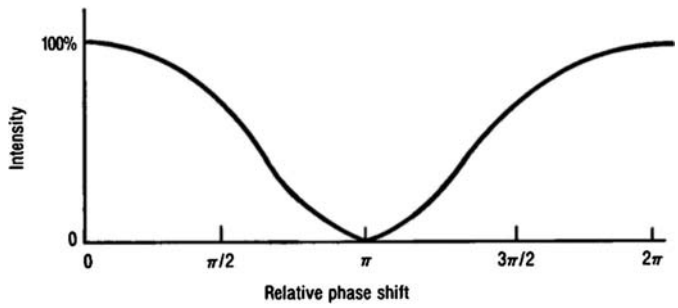

Figure 4.9 Intensity versus relative phase shift (reprinted from Ref. 4 with permission).

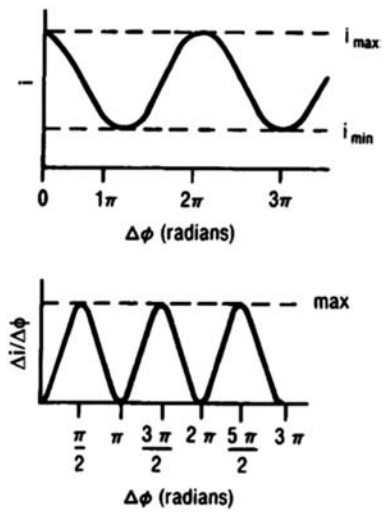

Figure 4.10 Photodetector output current and its derivative resulting from lightwave phase change fiber optic sensor output. Phase sensitivity is a function of the photodetector current i with the change in phase, $\Delta i/\Delta\phi$. Maximum sensitivity occurs when $\Delta\phi$ is multiples of $\pi/2$ (reprinted from Ref. 4 with permission).

integral number of half-wavelengths ($\phi = \pi, 3\pi \ldots$). At the maximum and minimum points, the sensitivity approaches zero. However, in the region of a 1/4 wavelength shift ($\pi/2, 3\pi/2 \ldots$) the rate of change of intensity with phase shift is greatest, providing the highest sensitivity, as shown in Fig. 4.10.

As stated previously, the Fabry–Pérot interferometer is even more sensitive than other interferometric approaches previously disscussed. The intensity versus relative phase-shift curve is shown in Fig. 4.11. The slope of the curve at the inflective points $(\pi/4, 7\pi/4)$ is a measure of the maximum sensitivity, which is twice the value of the other configurations.

As an example of sensitivity, consider the operation of a Mach–Zehnder interferometer at 820 nm using 1 meter of fiber. If the sensor has a resolution of 0.1% and a full-scale change is $\lambda/2$, the displacement sensitivity is $0.001\ [820 \times 10^{9}] = 4.1 \times 10^{10}$ m. If 1 km of fiber is used and experiences the same perturbations, then the fiber would have the same phase shift with l/1000 of the disturbance.

The displacement sensitivity is then 4.1×10^{13} m, approximately what has been reported as the ultimate sensitivity from the various literature sources. The ability to measure displacements at a subatomic level creates a conceptual problem. The sensors are functioning in the world of continuum mechanics, but these displacements are at quantum mechanical levels. It would be difficult to resolve a diaphragm movement, which is l/2000 of the spacing between atoms comprising the material. The conflict is resolved by considering that interferometers do not directly resolve a mechanical target's movement, but measure the difference between two relatively large values, the difference being quite small.

The design improvements for measuring phase over the last decade or so have mostly been directed towards the optical source phase noise and digital demodulation techniques. The refinement of narrow line-width fiber lasers [6] and external cavity semiconductor lasers[7] has provided sources with extremely low phase and intensity noise. These parameters set the noise floor for interferometric measurements. Shown in Fig. 4.12 and 4.13 are phase noise plots for these types of sources.

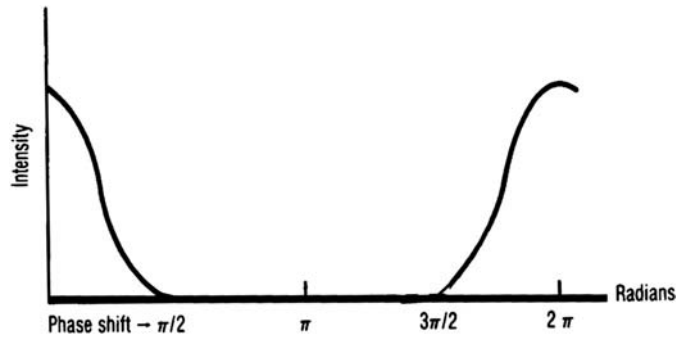

Figure 4.11 Sensitivity versus phase shift (reprinted from Ref. 4 with permission).

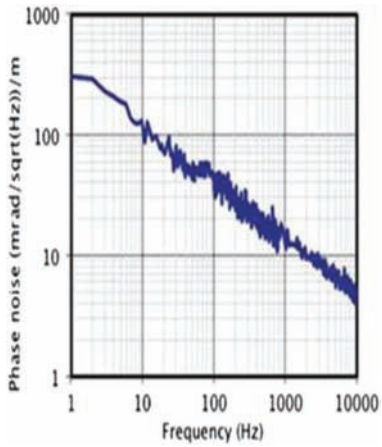

Figure 4.12 Semi-conductor laser phase noise (courtesy of Redfern Integrated Optics).

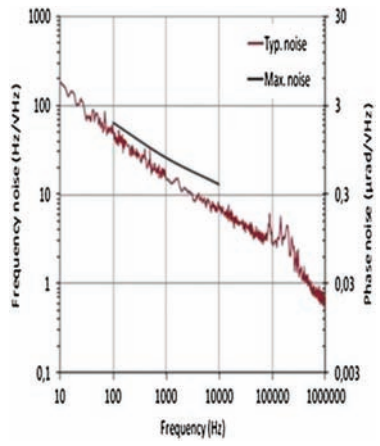

Figure 4.13 Narrow line-width fiber laser phase noise (courtesy of NKT Photonics).

4.4 Detection Schemes

Over the last couple of decades, significant progress has been made toward the demodulation of interferometric signals. In addition to legacy analog techniques,[8] a new class of digital demodulators has been developed.[9] The digital techniques have been applied to multi-channel interrogation, creating the possibility for advanced array-type architectures and signal processing.[12] These array architectures have also lead to the distributed type of sensing systems currently being applied to the measurement acoustic signals [Distributed Acoustic Sensing (DAS)] over lengths of kilometers.[13 15] This distributed sensing application will be covered in more detail in Chapter 18. The Mach–Zehnder interferometer has seen wide application for "point" acoustic sensing, meaning an application where the transducer is designed to

respond to the summation of potentially several signals at a relatively small physical location. As a result, the detection schemes associated with this configuration will be discussed in some detail. Figure 4.14 shows a Mach–Zehnder interferometer using a homodyne detection scheme. The approach converts phase modulation into intensity modulation.

As discussed previously, the highest sensitivity occurs at a phase shift of 90 deg with a minimum at 0 deg. If phase shift drifts from 90 deg toward 0 deg, the sensitivity is significantly degraded and causes a condition known as fading. Using a modulator that shifts the phase to a bias condition of 90 deg creates a condition known as quadrature.

The detection scheme is called homodyne detection. Referring to Fig. 4.14, the laser light is injected equally into the two fibers. The reference fiber and the sensing fiber are clearly marked. The reference arm has a phase shifter to achieve quadrature. The two beams are recombined and detected. The beams are summed, amplified, and fed to a compensation circuit that provides the phase-shift signals. There are several sources of noise in such a configuration, such as phase noise, amplitude noise, and multimode and satellite-mode noise.

Consider phase noise first.[10] The minimum detectable phase shift is a function of the fiber length difference between the two arms of the interferometer. Figure 4.15 is a plot of path length difference versus noise output for various frequencies. As the difference in path length decreases, so does the noise. Figure 4.14 also indicates the minimum detectable phase shift[11]. For the 2-kHz curve, if the two interferometric fibers are matched to within 1 mm, phase shifts of 10^{-6} rad are detectable.

Matching the two legs to within 1 mm is the practical limit due to mechanical and thermal strains. Typical fibers are 100 m or more long. Matching to 1 mm

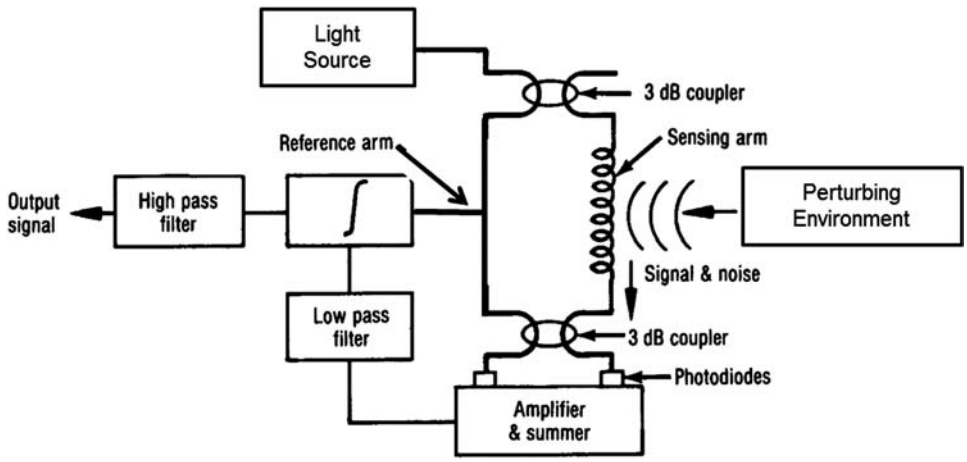

Figure 4.14 A Mach–Zehnder fiber optic interferometer employing phase-locked homodyne detection (reprinted from Ref. 4 with permission).

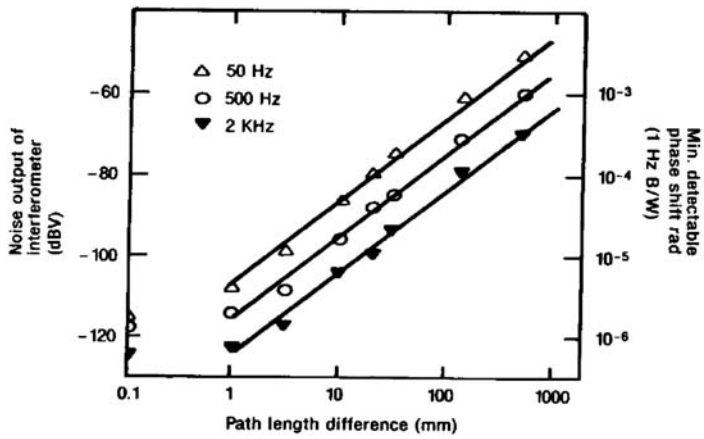

Figure 4.15 Variation of homodyne interferometer output noise as a function of sensing arm path length difference for several output frequencies (courtesy of American Institute of Physics Ref 11).

gives a length accuracy of 0.001%. If the same fibers are matched only to within 1 m (1%), the minimum detectable phase shift increases to 10^{3} radians—three orders of magnitude less sensitive. Phase noise is also due to the laser source, and to a lesser extent, the photodiode response.

Amplitude noise results from fluctuations in the output intensity of the laser source. By using summing techniques in the electronics, the variation can be mathematically eliminated. The technique is called common mode rejection. Using the technique at low frequencies, the minimum detected phase shift is improved by an order of magnitude; at higher frequencies, the advantage is not as pronounced.[4]

Multimode operation in the fiber creates undesirable interference and limits phase shift detection. Back reflections from the fiber–coupler interface cause multimodes to form. The effect of increasing back reflection is shown in Fig. 4.16.

To minimize the effect, Fresnel reflections at the fiber–coupling interfaces have to be reduced. This can be achieved by careful fiber alignment and index-matching fluids at the interface. To eliminate index-matching fluids, fibers can be polished with a slightly convex surface and slight compression applied as two fibers butt together, a technique that nearly eliminates backscatter.

A heterodyne detection scheme is shown in Fig. 4.17. The device employs Bragg modulators. The beam is split at a 3 dB coupler and enters the two Bragg modulators, which shift the wavelength. The frequency of the two modulators is in the range of 50 MHz with a difference between the sensing leg and reference leg of approximately 100 kHz. This frequency shift permits the device to work in the sensitive phase-shift regions without the feedback circuiting required for quadrature. Since the device is less

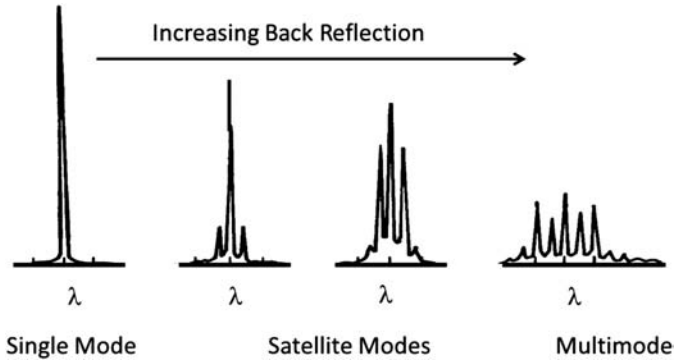

Figure 4.16 Influence of optical feedback on the modal output of a diode laser (reprinted from Ref. 4 with permission).

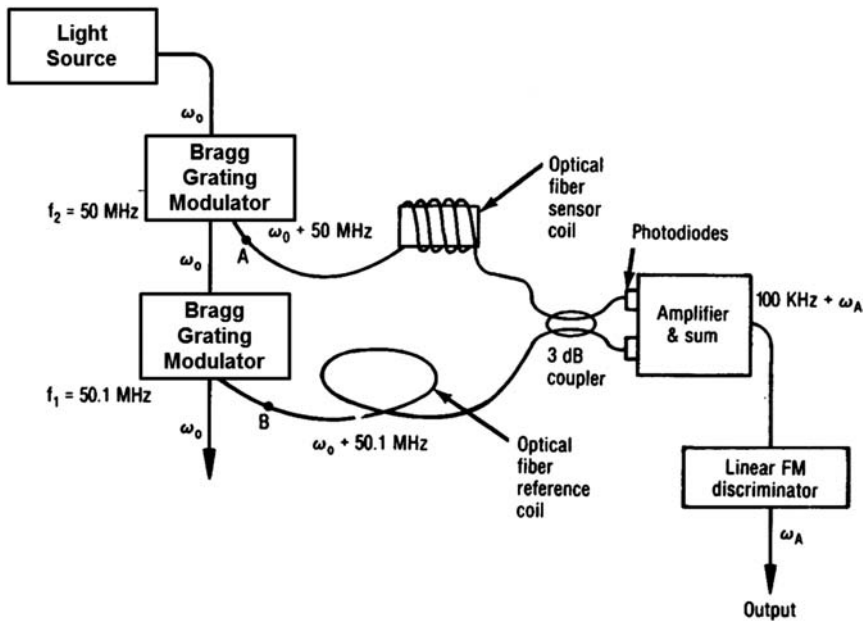

Figure 4.17 An interferometric fiber optic sensor employing heterodyne detection (reprinted from Ref. 4 with permission).

sensitive to low-frequency noise and optical-intensity fluctuations, process circuitry is further simplified.

4.5 Practical Considerations

When constructing fiber interferometers a few practical issues need to be considered. Referring to Eq. (4.9),

$$I = 2E^2 [1 + \cos(\phi_2 \quad \phi_1)]. \tag{4.15}$$

It may appear that the $\Delta\phi$ is a stable, well-behaved parameter. In fact, the phase drift and noise present on both ϕ_1 and ϕ_2 in most cases can be much larger than the actual signal to be measured. As mentioned earlier, during the initial setup of even a simple M–Z or Michelson interferometer, it is important to control the physical lengths of the fibers to nearly 1 mm. If a target $\Delta\phi$ bias level is important to reach, additional adjustment mechanisms are an absolute requirement. Components such as piezo-electric stretchers have been successful in providing knobs for tuning in the bias conditions of interferometers. Other sources of DC drift include temperature gradients along the fiber components: any mechanical disturbance such as acoustic disturbance, vibration, even circulating air can all contribute to short-term drift of the interferometer. With regard to polarization fading, both passive and active approaches have been implemented to help address this problem. More recently, the use of tri-mask polarization diverse receivers has also helped to solve this issue.

The AC noise sources can be divided into either coherent or incoherent, meaning that the disturbance experienced in one fiber is correlated (or uncorrelated) to the disturbance in the other fiber arm. Examples of correlated noise would be amplitude and phase modulation of the optical source, whereas uncorrelated could be microphonic disturbance of the fiber.

Fiber optic interferometers are best used in applications requiring the measurement of AC phenomena. These mechanisms change much faster than the DC drift sources mentioned earlier.

References

1. A. R. Tebo, "Sensing with optical fibers: an emerging technology," *Proc. ISA*, pp. 1655–71 (1982).
2. D. H. McMahon, A. R. Nelson, and W. B. Spillman, "Fiber optic transducers," *IEEE Spectrum,* pp. 24–29 (1981).
3. R. S. Mellberg, "Fiber optic sensors," *SRI International,* Research Report No. 684 (1983).
4. C. M. Davis et al., *Fiber Optic Sensor Technology Handbook,* Dynamic Systems, Reston, Virginia (1982).
5. C. A. DiMarzio, *Optics for Engineers,* CRC Press, New York (2012).
6. Ch. Spiegelberg, J. Geng, Y. Hu, T. Luo, Y. Kaneda, J. Wang, W. Li, M. Brutsch, S. Hocde, M. Chen, J. Babico, K. Barry, W. Eaton, M. Blake, D. Eigen, I. Song, and S. Jiang, "Compact 100 mW fiber laser with 2 kHz linewidth," *Optical Fiber Communication Conference*, PD45 – P1-3 vol. 3 (2003).
7. L. Stolpner, S. Lee, S. Li, A. Mehnert, P. Mols, S. Siala, and J. Bush, "Low noise planar external cavity laser for interferometric fiber optic sensors," *Proc. SPIE* **7004**, 700457 (2008) [doi: 10.1117/12.786226].
8. A. D. Kersey, "Recent progress in interferometric fiber sensor technology," *Proc. SPIE* **1367**, pp. 2–12 (1990) [doi: 10.1117/12.24724].

9. J. Bush, A. Cekorich, and C. K. Kirkendall, "Multichannel interferometric demodulator," *Proc. SPIE* **3180**, 19–29 (1997) [doi:10.1117/12.285601].
10. A. Dandridge, R. Tveten, R. Miles, D. Jackson, and T. Giallorenzi, "Single mode diode laser phase noise," *Applied Physics Letters* **38**, 77 (1980).
11. R. Miles, A. Dandridge, A. Tveten, H. Taylor, and T. Giallorenzi, "Feedback induced line broadening in CW channel-substrate laser diodes," *Applied Physics Letters* **37**, 990 (1980).
12. A. D. Kersey, D. L. Gysling, and F. X. Bostick, "Fiber-optic systems for reservoir monitoring," *World Oil* **10** (1999).
13. D. Gysling, T. Vandeweijer, and A. van der Spek, "Development of a permanent downhole two-phase flow meter," *SRI Multiphase Metering and Pumping Conference*, Houston (2000).
14. T. J. Tayag and R. C. Watson, "Digital demodulation of interferometric signals, modern metrology concerns," Chap. 11 in Modern Metrology Concerns, L. Cocco, Ed., InTech, Rijeka, Croatia (2012).
15. T. J. Kippenberg, A. Schliesser, and M. L. Gorodetsky, "Phase noise measurement of external cavity diode lasers and implications for optomechanical sideband cooling of GHz mechanical modes," New Journal of Physics 15(1), 015019 (2013).

Chapter 5
Wavelength-Modulated Sensors

5.1 Introduction

Wavelength-modulated sensors use changes in wavelength to detect the sensing function. Fluorescence and phosphorescence emit a characteristic wavelength of light if perturbed in the proper way. For instance, a dye in the presence of an analyte can give off a characteristic excitation spectrum. Chapter 15 describes fluorescent sensors for chemical sensing and Chapter 11 for temperature sensing. The emitting spectrum provides a qualitative sensing function, but the intensity of the spectrum (usually ratiometric) is required for qualitative sensing measurements.

Bragg gratings are truly wavelength-modulated sensors.[1,2] The parameter being monitored is a direct function of the wavelength shift associated with the Bragg resonance condition. Once again it is important to mention that the fundamental parameter measured is light intensity. However, the wavelength shift is a direct effect of the associated environmental perturbation and is independent of the light source intensity. Gauge lengths can be as small as 0.01 mm. A distinct advantage of Bragg grating devices is their ability to be used as quasi-distributive sensors. They can be used in wavelength-division multiplexing schemes without additional wavelength-encoding filters.

5.2 Bragg Grating Concept

Figure 5.1 demonstrates the concept of a Bragg grating. The core of the fiber has an index of refraction variation written in the core with intense UV light using a holographic or phase mask approach as shown in Fig. 5.2. The peak change of index (Δn) in the grating region is 10^{-5} to 10^{-3}. The spacing between grating periods is Λ. The length of the grating is typically 1 to 20 mm.

The peak wavelength of the reflection spectrum associated with a particular Bragg grating can be found by first starting with the equation of a mode-coupling resonant condition in an optical fiber:

$$\beta_1 \quad \beta_2 = \frac{2\pi}{\Lambda}, \tag{5.1}$$

where β_n = Mode propagation constant, and Λ = Period of index perturbation. Substituting for β in the case where the energy is coupled to a backward propagating mode:

$$\frac{2\pi n_{\text{eff1}}}{\lambda_B} \quad \frac{2\pi n_{\text{eff2}}}{\lambda_B} = \frac{2\pi}{\Lambda}. \tag{5.2}$$

The Bragg resonant wavelength can be found as follows:

$$\lambda_B = (n_{\text{eff1}} + n_{\text{eff2}})\Lambda, \tag{5.3}$$

where n_{eff} defines the effective index of the mode typically with a value of

$$n_{\text{eff}} = n_{\text{clad}} + 0.6(n_{\text{core}} \quad n_{\text{clad}}), \tag{5.4}$$

where n_{core} and n_{clad} are the material index of refraction values for the fiber core and clad respectively.

In the case of a single-mode fiber where the energy is exchanged between the forward-propagating fundamental mode and the backward-propagating fundamental mode, this reduces to the familiar expression

$$\lambda_B = 2n_{\text{eff}}\Lambda. \tag{5.5}$$

Equation 5.1 holds true for both coupling between forward- and backward-propagating fundamental modes as well as coupling from forward-propagating fundamental mode to higher-order, forward-propagating modes. However, care must be taken to use the correct β and n_{eff} values for this case.

Figure 5.1(a) shows the concept of the periodic perturbation that is responsible for this resonant coupling, along with the resulting transmission and reflection spectra for a typical Bragg grating.

At wavelengths that do not satisfy the Bragg condition, the light passes through the grating essentially unaffected. However, at the Bragg wavelength, the signal is reflected as shown in Fig. 5.1(b). The transmitted signal is shown in Fig. 5.1(c). The intensity of the reflected signal depends on the change in refractive index that comprises the grating and the length of the grating.[2,3]

The gratings described have been based on a uniform profile where both the changes in refractive index and period are uniform. Other profiles can be used to impart unique properties to the gratings. Figure 5.3 shows the uniform, apodized, and chirped profiles. The apodized profile spatially modifies the amplitude of the refraction index change. The chirped profile provides a nonuniform grating period. The apodized grating and chirped gratings can impart unique sensing properties, which will be discussed later in this chapter and in Chapter 12.

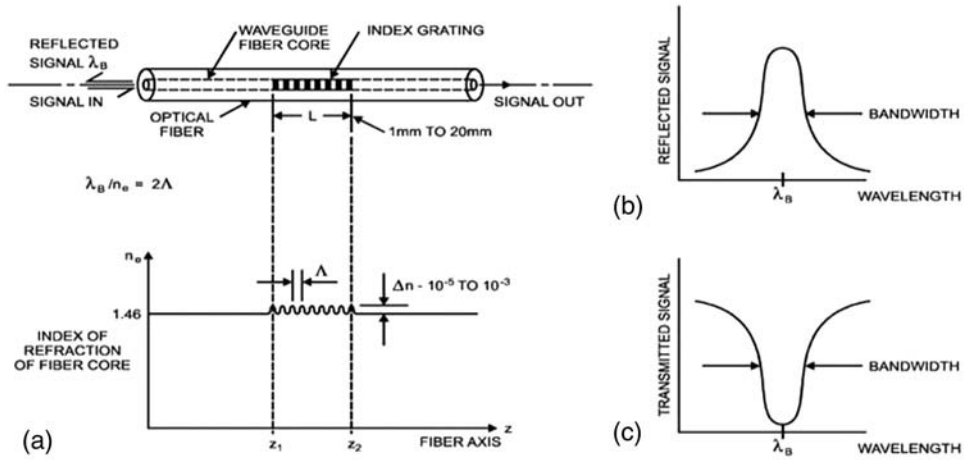

Figure 5.1 Fiber Bragg grating concept. (a) Bragg grating, (b) reflected signal, (c) transmitted signal.

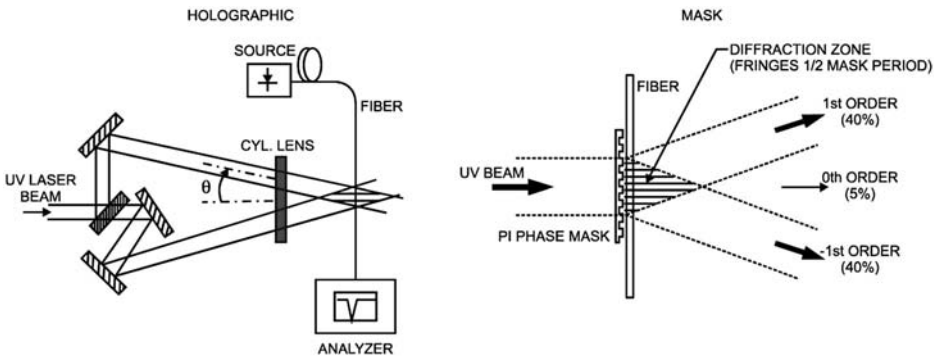

Figure 5.2 Bragg grating fabrication.

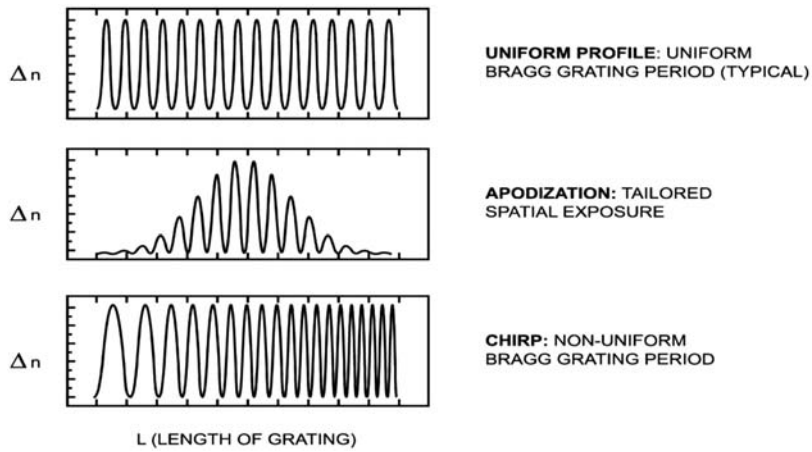

Figure 5.3 Bragg grating: basic definitions.

Figure 5.4 shows a "raised sine" apodization profile. This particular design is used to increase side-lobe suppression, which will aid in the identification of the peak resonant wavelength. This shape maintains a constant DC index term along the length of the grating to help create this effect. Figure 5.5 shows the results of a nonconstant DC term along the length of the grating. As can be seen, depending on the nature of the variation, side-lobes can be created on either the short- or long-wavelength side of the spectral response.

As mentioned earlier, these Bragg gratings can be designed and imprinted into waveguides to create energy transfer from the forward-propagating modes to other higher-order forward-propagating modes. Typically, when this is the case, the term long-period grating is applied as the periods for these structures are on the order of 100 or 1000 times longer than the standard reflective devices. Figure 5.6 shows the principle of operation of a long-period grating. The phase-matching condition that

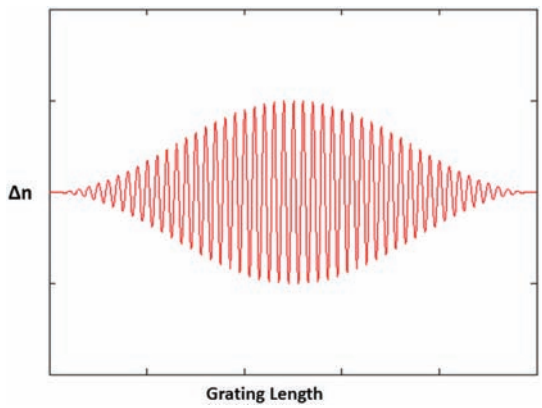

Figure 5.4 Raised sine apodization profile.

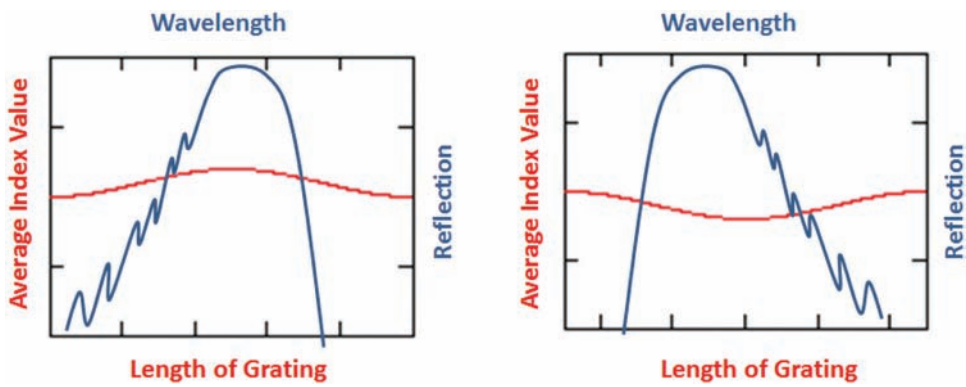

Figure 5.5 Side-lobe peaks as a result of nonconstant average Δn.

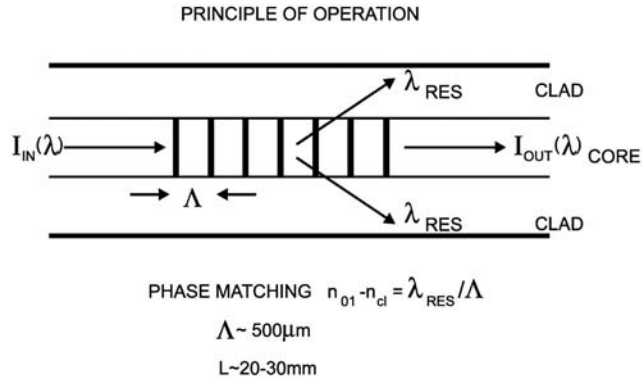

Figure 5.6 Long-period gratings: principle of operation.

allows the core-to-cladding coupling for the long-period case, Eq. 5.3 can be shown to reduce to[4,5]

$$n_{\text{core}} \quad n_{\text{clad}} = \frac{\lambda_{\text{res}}}{\Lambda}. \tag{5.6}$$

This concept has several sensor applications and is especially useful in chemical sensing, where light injected into the cladding can be the basis for a fluorescent sensor. Figure 5.7 illustrates the transmission of a long-period grating. The notch associated with λ_{res} is much broader than for a short-period Bragg grating. This spectral broadening is mainly due to the fact that there are many fewer perturbations or grating periods interacting since the period is so much larger. A simple analogy that explains this is to consider the width of the Fourier transform (FT) of a finite-length sinusoid. The shorter the length or reduction in number of periods causes this spectrum to also broaden as opposed to an infinite sinusoid whose FT is a spike with no spectral width.

Typically, all of these grating structures are thermally annealed after the UV exposure process. Immediately after the exposure process, the Δn created

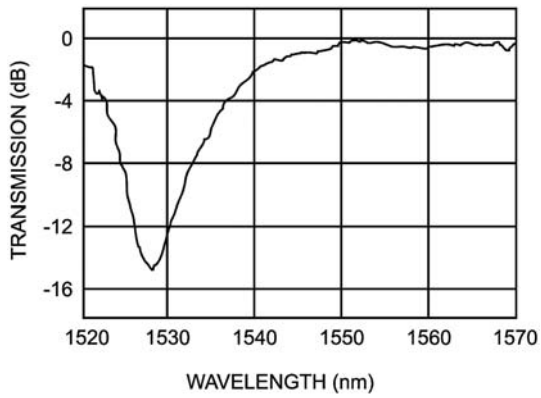

Figure 5.7 Long-period grating transmission.

will begin to decay. In order to accelerate this decay process and create a more stable condition for the index modulation, heat is applied. Depending on the exposure process (especially if a multiple exposure process is used) the annealing process may create a nonuniform decay and dramatically change the reflection and/or the transmission spectrum of the grating. Care must be taken with the recipe to make sure it is tied to the particular exposure process (particularly if hydrogen loading is used) as well as to the targeted operating conditions.

5.3 Bragg Grating Sensors

A Bragg grating sensing system is depicted in Fig. 5.8.[1] The properties of wavelength encoding and low dependence on power intensity of these devices has made them very attractive to the sensor community. A great deal of research has been devoted to create many different configurations and applications. Fundamentally, the vast majority of these sensors are modulated by either strain or temperature. The strain causes a shift in the Bragg wavelength. The magnitude of the shift is a direct function of the strain. A broadband optical source is used, and the system can function in a transmissive or reflective mode. Using a coupler, the return signal can be detected, or the transmission spectrum, also depicting the wavelength shift, can be monitored.

The Bragg grating responds to both strain and temperature.[1] Strain affects the elongation of the fiber, changing the grating spacing. It also causes a refractive index change associated with a Poisson's effect (photoelastic effect) due to dimensional changes in the radial direction. Temperature change causes thermal expansion, which changes the grating spacing. The refractive index itself is temperature dependent. The change in wavelength $\Delta\lambda_B$, associated with both strain and temperature effects, is given by[1]

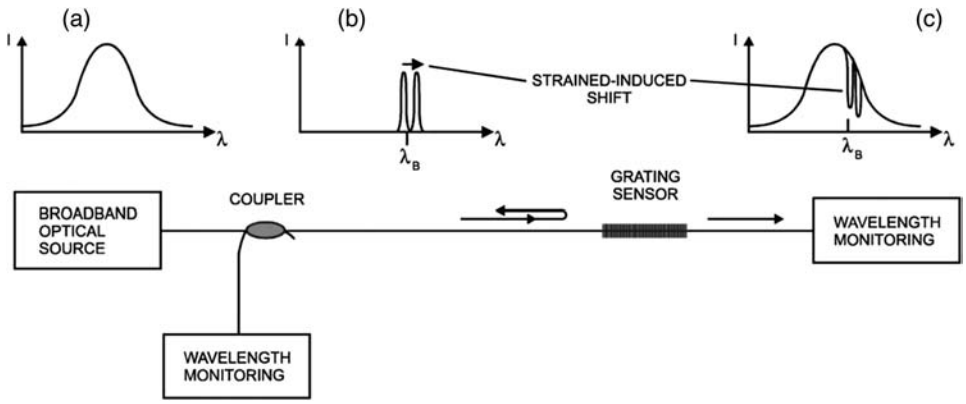

Figure 5.8 Basic Bragg grating-based sensor system with transmissive or reflective detection options (reprinted from Ref. 1 with permission). (a) Input spectrum, (b) reflected spectrum, (c) transmitted signal.

$$\Delta\lambda_B = 2n\Lambda\left[\left\{1 \quad \left[\frac{n^2}{2}\right][P_{12} \quad \nu(P_{11}+P_{12})]\right\}\varepsilon + \left(\alpha + \frac{dn/dT}{n}\right)\Delta T\right], \quad (5.7)$$

where:
Λ = grating spacing,
ε = the applied strain,
P_{11}, P_{12} = the stress optic coefficient,
α = the coefficient of thermal expansion,
ν = Poisson's ratio,
n = the refractive index of the core, and
ΔT = the temperature change.

For silica, the term is

$$\left(\frac{n^2}{2}\right)\left[P_{12} \quad \nu(P_{11}+P_{12})\right] \approx 0.22. \quad (5.8)$$

Therefore, for constant temperature

$$\Delta\lambda_B = 2n\Lambda(0.78)\varepsilon = 1.56n\Lambda\varepsilon. \quad (5.9)$$

Since

$$\lambda_B = 2n\Lambda, \quad (5.10)$$

$$\Delta\lambda_B = 0.78\lambda_B\varepsilon. \quad (5.11)$$

This relationship corresponds to 1 nm of wavelength change for 1000 microstrain at a wavelength of 1500 nm. For the case of zero applied strain, Eq. (5.7) simplifies to

$$\Delta\lambda_B = \left(\alpha + \frac{1}{n}\frac{dn}{dT}\right)\Delta T. \quad (5.12)$$

Since the term $\alpha\Delta T << dn/dT$, the equation further simplifies to:

$$\Delta\lambda_B = 2\Lambda\left(\frac{dn}{dt}\right)\Delta T. \quad (5.13)$$

For silica fibers, the normalized thermal responsivity is

$$\frac{1}{\lambda_B}\frac{\Delta\lambda_B}{\Delta T} = 6.67 \times 10^{-6}/°C. \quad (5.14)$$

At 1500 nm, a change in temperature of 1 °C results in a Bragg wavelength shift ($\Delta\lambda_B$) of 10.2 pm.

Figure 5.9 shows the wavelength curve for both a uniaxial tension load and for a temperature change.[6] From the graphs, the shifts at 1300 nm are predicted from Eqs. (5.9) and (5.14). The curve gets steeper at higher wavelengths. Therefore, sensitivity increases with increasing wavelength.

There are several approaches to temperature discrimination from strain effects in Bragg grating sensors.[7] One approach is to use a reference

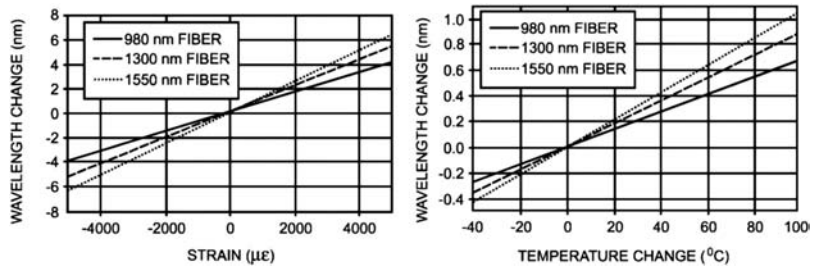

Figure 5.9 Thermal/mechanical response of a Bragg grating sensor.

grating.[1,8,9] A simple approach has the reference grating in thermal contact but isolated from strain effects. While one grating measures temperature and strain, the reference grating measures only temperature. The difference is the result of strain alone. It is often important to have a reference grating experience only temperature effects, with strain effects prevented in the packaging and attachment design. Several approaches use two gratings with different responses to temperature and strain, as defined by[1,7,10]

$$\begin{pmatrix} \Delta\lambda_1 \\ \Delta\lambda_2 \end{pmatrix} = \begin{pmatrix} \varepsilon \\ T \end{pmatrix} \begin{pmatrix} K_{\varepsilon 1} & K_{T1} \\ K_{\varepsilon 2} & K_{T2} \end{pmatrix}, \tag{5.15}$$

where $K_{\varepsilon 1}$ and $K_{\varepsilon 2}$ = the strain response of gratings 1 and 2 respectively, and K_{T1} and K_{T2} = the temperature responses of gratings 1 and 2, respectively.

To achieve different responsivities, Kersey et al.[1] used an approach that varies the cladding diameter between the two gratings. The thinner fiber would have a higher strain response, since for a given load it would experience more elongation and strain. Both gratings experience the same temperature response. An interesting approach was tried by M. G. Xu et al.[10] Two gratings were superimposed upon one another. Since the gratings were collocated, they would experience the same strain and temperature conditions. One grating had a Bragg resonance at 850 nm, while the other had a Bragg resonance at 1300 nm. For strain, the 1300 nm grating had a response that was 6.5% higher. For temperature, the 1300-nm grating had a response that was 9.8% lower. The analysis of the grating-pair response indicated that strain could be resolved to ± 10 micro-strain and temperature to ± 5 °C simultaneously (micro-strain = strain $\times$ 10 ^{6}). Figure 5.10 depicts the configuration used by Xu et al.

A combination of long-period and Bragg gratings has also been used for temperature and strain discrimination.[1,11,12] A schematic representation of a fiber Bragg grating (FBG) and long-period grating (LPG) is shown in Fig. 5.11. The long-period grating is positioned in front of two Bragg gratings and has a resonance centered between the two Bragg gratings. The long-period resonance wavelength is 1306 nm. The Bragg gratings are 1293 nm and 1321 nm, respectively. Long-period gratings can have significantly different responses for temperature and pressure depending on the grating spacing and the core and cladding indices of the fiber.

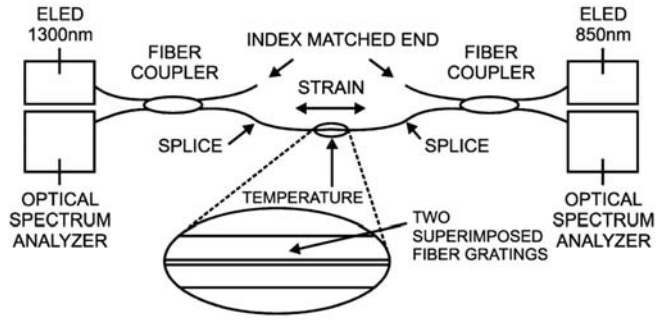

$$\begin{pmatrix} \Delta\lambda_{B1} \\ \Delta\lambda_{B2} \end{pmatrix} = \begin{pmatrix} K_{\varepsilon 1} & K_{T1} \\ K_{\varepsilon 2} & K_{T2} \end{pmatrix} \begin{pmatrix} \Delta\varepsilon \\ \Delta T \end{pmatrix}$$

Figure 5.10 Separation of temperature and strain using dual wavelengths.

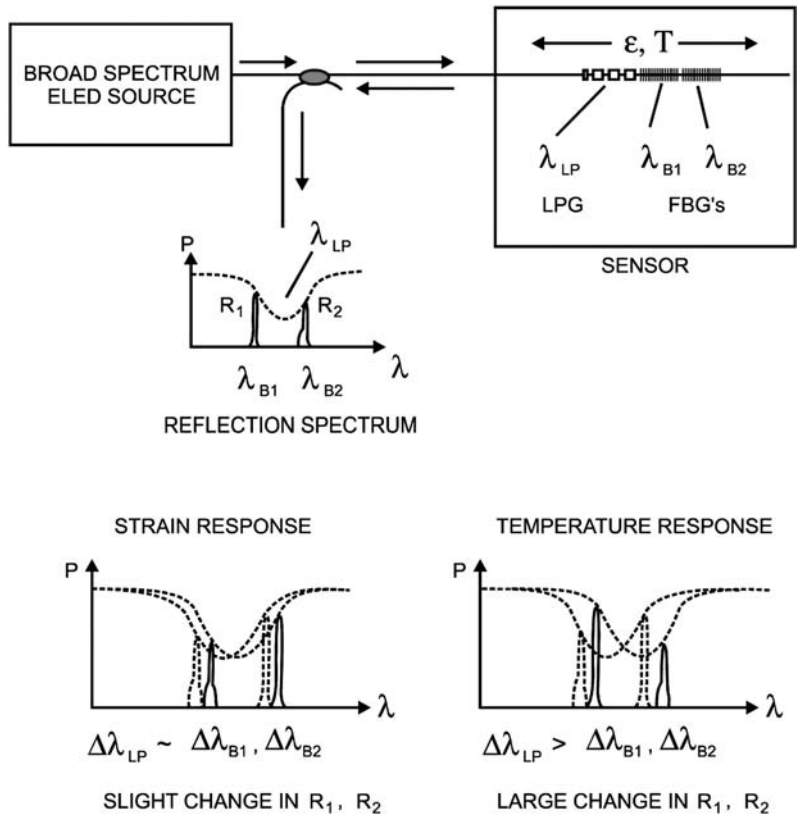

Figure 5.11 Schematic of hybrid FBG/LPG sensor for simultaneous strain and temperature measurements.[1]

For the case shown, the temperature response is much greater than the strain response. An applied strain causes a shift in the Bragg grating with a small shift in the long-period grating. The long-period grating shift modulates the reflected signal of the short-wavelength Bragg grating. The longer-wavelength Bragg grating is unaffected. For a temperature change, the long-period grating experiences a significant wavelength shift. The short-wavelength Bragg grating is not affected, but the longer-wavelength Bragg grating is modulated. Using a ratiometric approach, separation of temperature and strain responses can be achieved. Over a range of 1000 micro-strain and a temperature range of 25 °C, the measured strain and temperature had an accuracy of ±9 micro-strain and ±1.5 °C, respectively.

A practical limitation of using hybrid Bragg gratings and long-period-grating sensors is cost. At this time, long-period gratings are considerably more expensive than standard Bragg gratings. Approaches that combine the two gratings will be costly relative to competing approaches.

Other approaches are also being considered for strain/temperature discrimination. A chirped grating can be used in conjunction with the fiber being tapered in the region of the grating.[1] The taper results in a strain gradient when a higher tension is applied, since the tapered regions experience more strain. As strain is applied, the spectral shift is also accompanied by a line broadening. The effect is shown in Fig. 5.12. The dominant effect of the change of refractive index with temperature is not affected by the taper. Therefore, the spectral shift associated with temperature change does not exhibit the peak broadening effects. In principle, the fact that changes in strain and temperature respond differently should provide means for discrimination.

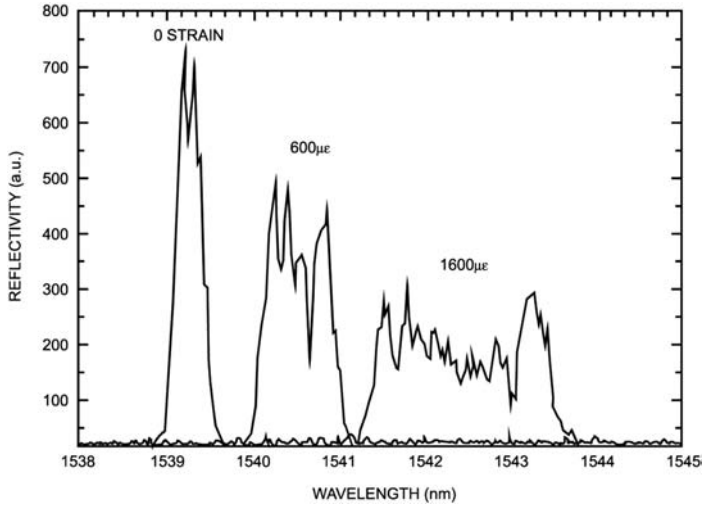

Figure 5.12 Reflectance spectra of chirped grating.[1]

5.4 Distributed Sensing

Bragg grating-based sensors are well suited for distributed sensing, which implies that multiple sensing points can be distributed along a single fiber.[19] The approaches to multiplexing will be discussed in the next section, but the concept is shown in Fig. 5.13.

Distributed Bragg grating sensors use two basic interrogation schemes.[18] The first is time-division multiplexing (TDM). In this case, multiple sensors are written into one length of fiber. All of the gratings function at the same wavelength. By using optical time-domain detection reflectometry (OTDR), the time and relative response for a pulse to return from a specific Bragg grating identifies both the spatial location of the grating as well as the magnitude of the change being applied, which is a measure of the parameter that is causing a perturbation such as strain or temperature. The approach generally uses low-reflection gratings to maximize the grating count allowed on a single fiber. A Bragg grating can be designed to have a range of reflectivities (less than 20% to greater than 90%). Depending on the distributed system architecture, the reflectivity must be chosen to optimize resolution and channel count. For example, if the inline gratings are working at the same wavelength, there must be sufficient transmitted light for distant sensing points to function. The gratings must have some reasonable separation, typically one meter, so one grating can be distinguished from another, although smaller spacing resolution is possible.

The second approach is based on wavelength-division multiplexing (WDM). Since Bragg gratings are designed to function at specific wavelengths, they are inherently compatible with the WDM approach. Interrogators can use a broadband light source and a tunable filter detection system, or a tunable light source and a broadband detection system. The swept laser source has high power relative to other sources and therefore can support a higher sensor count. One issue is that each grating sensor element requires a wavelength range of

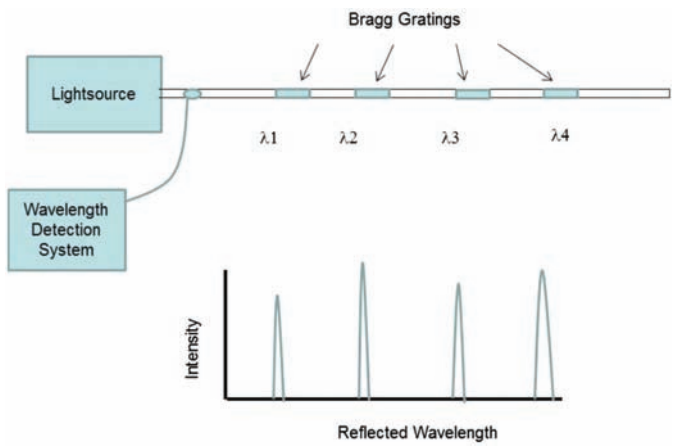

Figure 5.13 Distributed fiber optic sensing concept based on Bragg gratings.

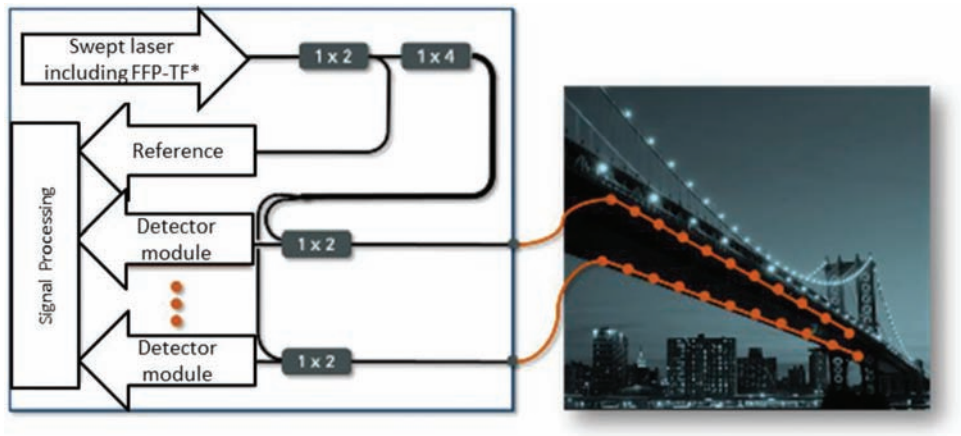

Figure 5.14 High-capacity WDM distributed sensing system (Ref. 22) (*Fiber Fabry-Pérot – tunable filter).

2 to 3 nm. The spectral range of the light source is the limitation to total sensor element count. The scan frequency of the detection system determines the application capability of the interrogator. For scan rates in the 1- to 10-Hz range, the interrogator is limited to static monitoring conditions such as measuring strain in a structural member. For scan rates approaching 1 kHz, the interrogator can monitor dynamic conditions such as vibration or vibration signature changes in a structural member.[21]

A high-capacity WDM distributed sensing system is shown in Fig. 5.14. Current systems, due to their high power, can extend to tens of kilometers. They can expand to 64 channels and, due to the wide tuning range, up to 100 sensors per fiber.

5.5 Wavelength Detection Schemes

The systems that measure the peak wavelength change of Bragg gratings can be divided broadly into two types. The first uses a broadband source and some type of dynamic wavelength filter on the receiver side, while the second employs some type of tunable source with a static detector. In conjunction with both of these methods, two common key components are a stable wavelength reference for absolute measurements and a peak detection algorithm. Error and noise sources created from distorted grating reflection spectrums, as well as tuning components, must all be smoothed out and somehow allow for a very precise peak determination. Tunable filters such as scanning fiber Fabry–Pérot and scanning Michelson interferometers have been employed on the detector side and, most recently, tunable semiconductor or fiber ring lasers on the source side. When choosing a detection system, one must also consider the polarization dependence of the grating and additional interference effects from highly coherent sources.

The optical spectrums of these two methods are shown in Fig. 5.15. It is important to note here the bandwidth of the interrogating filter versus that of the tunable laser. Again, depending on the application, one will have advantages over the other.

These types of interrogation methods will produce a time series that will then need to be processed through some peak detection algorithm, which will also have as an input the wavelength reference. Typical wavelength references that have been used include acetylene gas cells and ultrastabilized Bragg gratings.

The wavelength shift in a Bragg grating has also been measured using interferometric detection schemes.[1,13,14] This technique is especially useful to measure weak Bragg grating resonance shifts. The schematic configuration is shown in Fig. 5.16. Light from the grating passes through an interferometer

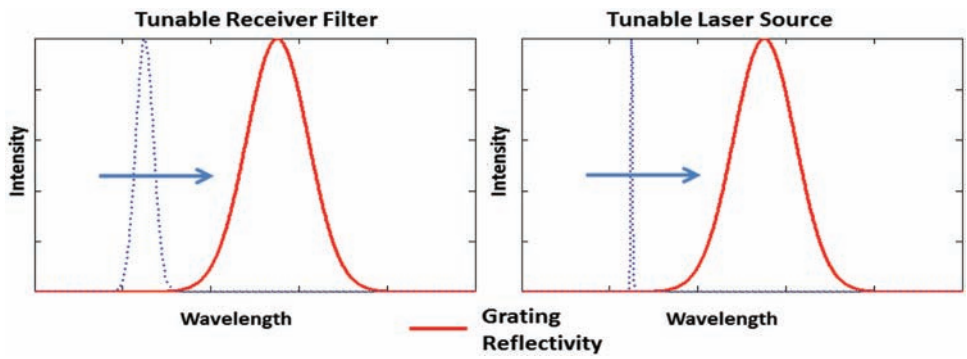

Figure 5.15 Peak wavelength detection methods.

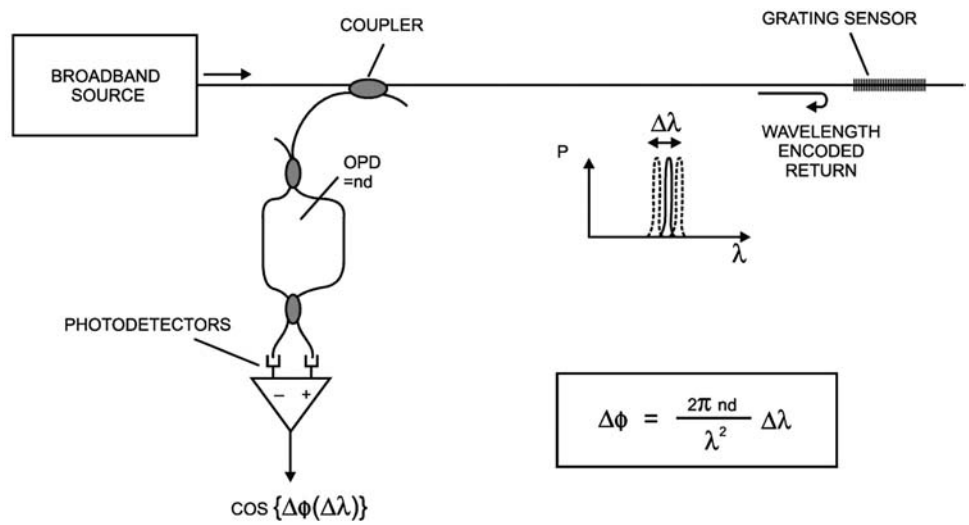

Figure 5.16 Interferometric detection system for FBG sensors.[1]

with unequal path lengths and exhibits a phase shift associated with the grating wavelength shift, given as[1]

$$\Delta\phi = \frac{2\pi nd}{\lambda^2}\Delta\lambda. \tag{5.16}$$

The optical path difference is *nd*. From a functional standpoint, the sensitivity is a function of the path difference, which must be less than the coherence length of the reflected light from the grating. Typically, the optical path difference will be approximately 1 cm for a 1 cm grating operating at a wavelength of 1.3 μm.

The sensitivity can be greatly enhanced if the Bragg grating sensor concept is expanded to a Bragg grating laser sensor.[1,15] The concept is shown in Fig. 5.17. The two gratings are of matched Bragg wavelength to create a laser cavity within the fiber itself.[16] To achieve the lasing action, the fiber must be doped with a rare-earth metal such as erbium.[17] The fiber Bragg grating laser sensor functions in a manner analogous to a Bragg grating sensor. Changes in the cavity length associated with strain and temperature cause a change in the laser-wavelength output. Compared to a Bragg grating sensor, the coherence length of a Bragg grating laser sensor is orders of magnitude greater. Therefore, an optional path difference of 100 m or more can be used in unbalanced interferometric detection schemes.

As an example, if a Bragg grating laser sensor and a Bragg grating sensor had the same $\Delta\lambda$ for a given perturbation, the effect of the optical path difference (100 m versus 1 cm) increases the sensitivity of the laser sensor by four orders of magnitude.

The use of these concepts in distributive sensing will be discussed in Chapter 17.

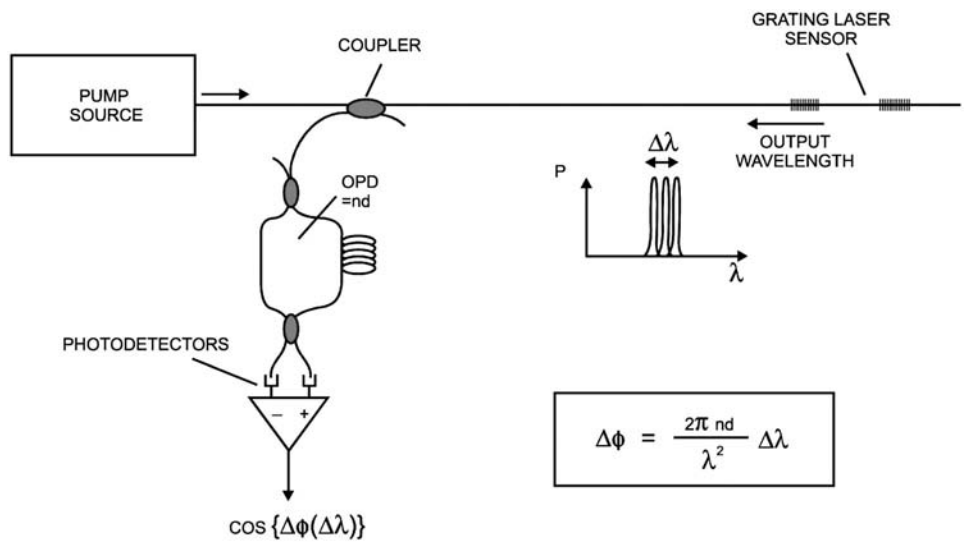

Figure 5.17 Basic fiber Bragg grating laser sensors with interferometric detection.[1]

5.7 Harsh Environments

As applications for sensors expand, environmental requirements become a limiting factor. Many energy applications require the fiber-based sensors to function at temperatures approaching 300 °C in a hydrogen-rich environment. Combustion monitoring requires operation at 800 °C. Many advances in fiber technology over the last several years allow sensors to withstand these harsh requirements. Bragg grating packaging has also experienced similar advancements using innovative packing to allow strain and temperature sensors to be functional over a broad range of environmentally difficult applications.[20] As an example of these advancements, Bragg grating sensors have been used to monitor temperature and pressure in explosive environments where the pressure exceeded 1 million pounds per square inch and the temperature exceeded 400 °C in a 25-msec timeframe.[23]

References

1. A. D. Kersey, M. A. Davis, H. J. Patrick, M. LeBlanc, K. P. Koo, C. G. Atkins, M. A. Putnam, and E. S. Friebach, "Fiber grating sensors," *Journal of Lightwave Tech.* **1**(8), 1442–1463 (1997).
2. W. W. Morey, G. Meltz, and W. H. Glenn, "Fiber optic and laser sensors VII: fiber Bragg grating sensors," *Proc. SPIE* **1169**, 98–107 (1989) [doi: 10.1117/12.963022].
3. C. M. Ragdale, P. C. J. Reid, and I. Bennion, "Fiber grating devices," *Proc. SPIE* **1171**, 148–152 (1989) [doi: 10.1117/12.963147].
4. V. Bhatica and A. M. Vengsarkar, "Optical fiber long-period grating sensors," *Opt. Letter* **21**, 692–694 (1996).
5. A. M. Vangsarkar, J. R. Pedrazzani, J. B. Judkins, P. J. Lemaire, N.S. Bergano, and C. R. Davidson, "Long period fiber gratings based gain equalizers," *Opt. Letters* **21**, 336–338 (1996).
6. 3M, "Fiber Bragg grating application note: the mechanical and optical reliability of fiber Bragg gratings," (February 1996).
7. J. D. Jones, "Review of fiber sensor techniques for temperature strain discrimination," 12th annual conference in Optical Fiber Sensors, 36–39 (1997).
8. H. Singh and J. Sirkis, "Simultaneous measurement of strain and temperature using optical fiber sensors: two novel approached," *Proc. OFSII* (1996).
9. L. A. Ferriera, A. B. Ribeiro, J. L. Santos, and F. Farchi, *IEEE Photon Tech Letters* **8**, 1519 (1996).
10. M. G. Xu, J. L. Archambault, L. Reekie, and J. P. Dakin, "Discrimination between strain and temperature effects using dual wavelength fiber grating sensors," *Elect. Lett.* **30**, 1085 (1994).

11. H. J. Patrick, G. M. Williams, A. D. Kersey, J. R. Pedrazzani, and A.M. Vengsarkor, "Hybrid fiber grating/long period grating sensors," *IEEE Photon. Technol. Letters* **8**, 1223–1225 (1996).
12. V. Bhatia, D. K. Campbell, T. D. D'Alberto, G. A. Ten Eyck, D. Sherr, K. A. Murphy, and R. O. Claus, "Standard optical fiber long period gratings with reduced temperature sensitivity for strain and refractive index sensing," *Tech. Digest Conf. Opt. Fiber Communication*, Dallas, Texas, pp. 346–347 (1997).
13. A. D. Kersey, "Multiplexed fiber optic sensors," *Proc. SPIE* **1797**, 161–185 (1992) [doi: 10.1117/12.141286].
14. A. D. Kersey, T. A. Benkoff, and W. W. Morey, "High resolutions fiber Bragg grating based strain sensor with interferometric wavelength shift detection," *Electronic Letters* **28**, 236 (1992).
15. K. P. Koo and A. D. Kersey, "Bragg grating based laser sensor system with interferometric interrogation and wavelength division multiplexing," *Journal of Lightwave Tech.* **13**, 1243 (1995).
16. W. W. Morey, G. A. Ball, and G. Meltz, "Photo Induced Bragg gratings in optical fiber," *Optics and Photonics News* **5**(2), 8–13 (1994).
17. V. Mizrachi, D. S. D. Giovanni, R. M. Atkins, S. G. Grubb, Y. K. Park, and J. M. P. Delavaux, "Stable single-mode erbium fiber grating laser for digital communication," *Journal of Lightwave Tech.* **11**(12), 2021–2025 (1993).
18. S. H. Yu, D. J. Richardson, and B. Y. Kim, "Interrogation of fiber grating sensor arrays with a wavelength laser," *Optics Letters* **23**(11), 843–845, (1998).
19. C. Baldwin, J. Niemczuk, J. Kiddy, and T. Salter, "Review of fiber optic accelerometers," *IMAC XXIII Conference & Exposition on Structural Dynamics* (2005).
20. V. Wnuk, A. Mendez, S. Ferguson, and T. Graver, "Process for mounting and packaging of fiber bragg grating strain sensors for use in harsh environmental applications," *Proc. SPIE* **5758** 46, (2005) [doi: 10.1117/12.601971].
21. A. Cusano, A. Cutolo, J. Nasser, M. Giordano, and A. Calabro, "Dynamic strain measurements by fibre bragg grating sensor," *Eurosensors XVI*, Prague, Czech Republic, Vol. 110, pp. 276–281 (2004).
22. Micron Optics, inc. "Technology Lighting the Way for Discovery," www.micronoptics.com (2013).
23. E. Udd and J. Benterou, "Improvements to high-speed monitoring of events in extreme environments using Bragg grating sensors," *Proc. SPIE* **8370**, 83700L (2012) [doi: 10.1117/12.915726].

Chapter 6
Scattering-Based Sensors

6.1 Absorption and Transmission Loss in Optical Fibers

The light-guiding properties and transmission distance range capability of optical fibers are affected by the waveguide and materials properties (both intrinsic and extrinsic) from which the fibers are made. Silica glass fibers have an intrinsic optical absorption loss that is the result of the interplay of several mechanisms such as UV and IR absorption, Rayleigh scattering, as well as absorption by impurities and metal ions. Typically, the absorptions introduced by these mechanisms intersect each other producing a sort of V-shaped optical transmission spectrum. Figure 6.1 illustrates the optical transmission spectrum for a silica glass fiber, where it can be appreciated that the short-wavelength absorption tail is the result of the UV absorption, while the bottom attenuation is limited by the Rayleigh scattering, and the long wavelength tail is the result of the IR absorption. A minimum absorption wavelength region exists for which maximum transmission distance in a fiber can be achieved. This low-attenuation point occurs around 1.55 μm and has a value of ~0.15 dB/km. Historically, light sources emitting in the 850 nm and 1310 nm windows were first used in fiber optic communication systems and, to date, some fiber sensing systems still operate at those wavelengths. However, most current fiber optic communication and sensing systems operate in the C-band window—for communications band—spanning from 1528 nm to 1561 nm.

Among the multiple factors contributing to the optical loss in a fiber are: absorption from water (OH^- ions) and transition metal impurities; scattering produced by inhomogeneities and density irregularities in the fiber's core glass; core-cladding boundary irregularities, micro- and macrobending losses; as well as joint and coupling losses. These loss mechanisms are illustrated in Fig. 6.2, and at each point in the fiber they reduce the amount of energy traveling forward by light lost by radiation or back reflected in the opposite direction—more on this point will be discussed in the next section.

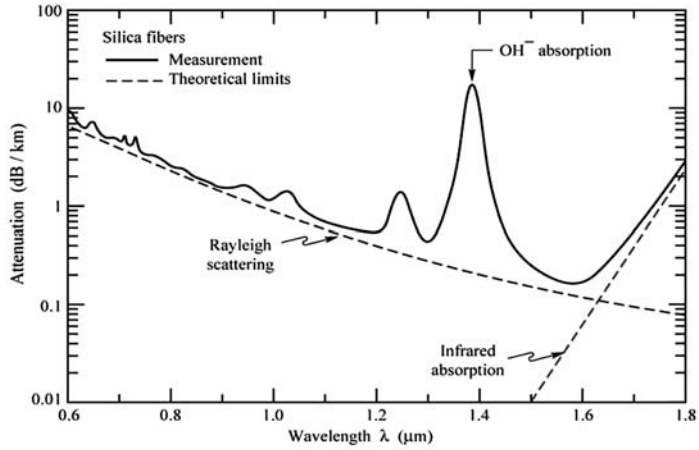

Figure 6.1 Transmission spectrum of a silica glass fiber.

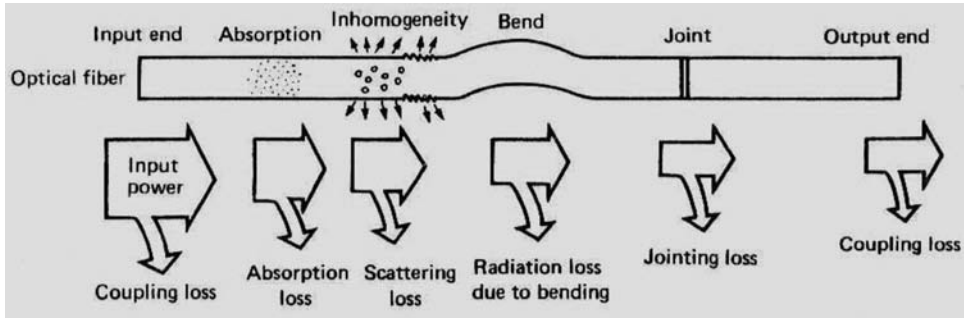

Figure 6.2 Causes of loss in an optical fiber.

The combined loss effects result in transmission attenuation in the fiber. This attenuation causes an exponential decay of the optical power (light intensity) along the fiber, as illustrated in Fig. 6.3 and can be expressed as

$$P(z) = P_o e^{-\alpha_T z}, \tag{6.1}$$

where

$P(z)$ is the optical power at a distance z from the fiber's input,
P_o is the coupled input power into the fiber,
α_T is the attenuation coefficient, and

$$\alpha_T = \alpha_{absorption} + \alpha_{scattering} + \alpha_{bending} + \text{waveguide losses}. \tag{6.2}$$

6.2 Optical Time-Domain Reflectometry (OTDR)

As discussed in the previous section, microscopic density fluctuations—variations in refractive index—and inhomogeneities in the fiber's core glass

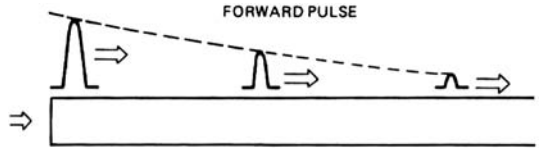

Figure 6.3 Attenuation of an optical pulse along an optical fiber.

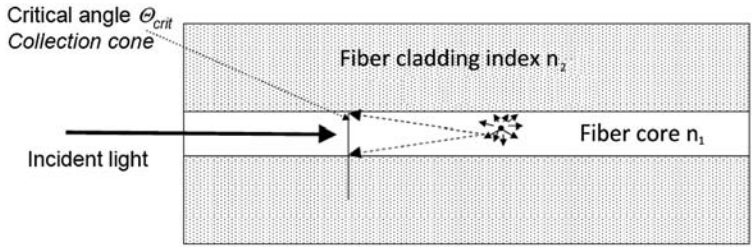

Figure 6.4 Back reflection of Rayleigh light scattering in an optical fiber.

act as scattering centers that refract light in nearly an isotropic way (all directions) from the scattering site. This is known as Rayleigh scattering. A portion of this scattered light is reflected back and effectively captured within the fiber's acceptance cone and guided back to the original light source as shown in Fig. 6.4. The amount of collected backscatter power/unit length (dl) is given by[9]

$$P_{\text{backscatter}} = P_{\text{input}}\alpha_{\text{scattering}}dl(\text{NA})^2/4n_c^2, \tag{6.3}$$

where $\alpha_{\text{scattering}}$ is the Rayleigh backscattering loss coefficient, which at 1.55 μm is on the order of 2.5×10^{-5} (1/m) and depends on wavelength as $1/\lambda^4$, hence the spectral decay proportional to λ^4 observed in fiber attenuation plots. Because of the limited amount of back-reflected light effectively coupled and guided back inside the fiber and the high loss coefficient, the power of a back-reflected Rayleigh scattered light pulse is 40 to 60 dB down in intensity compared to the launched pulse.

The optical time-domain reflectometer (OTDR) is a practical and powerful fiber optic test and measurement instrument developed for telecommunication applications and dating back to 1976[2] that relies on the detection of back-reflected Rayleigh scattering signals to measure the attenuation profiles of long-haul fiber optic links. In an OTDR (see Fig. 6.5), an optical pulse is launched in the fiber, and a photodetector measures the amount of light which is backscattered as the pulse propagates down the fiber. The detected signal, the so-called Rayleigh signature, displays an exponential decay with a distance that is directly related to the linear attenuation of the fiber as the light pulse travels down and back along the fiber. This is a distributed process, since at each position along the fiber there are scattering centers that will produce back-reflected radiation signals.

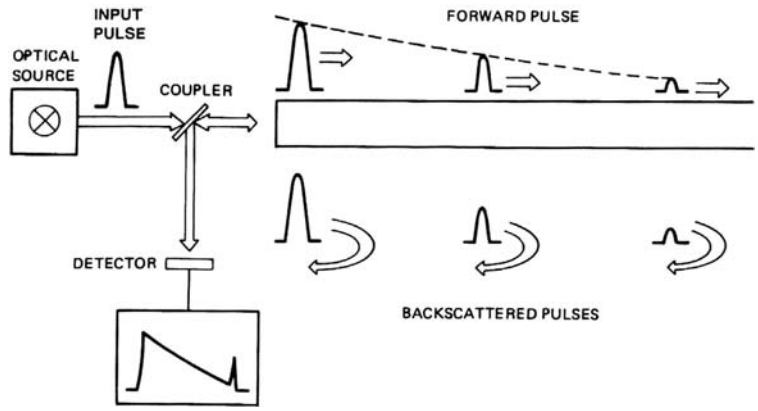

Figure 6.5 Optical time-domain reflectometry operating principle (adapted from Ref. 2 with permission).

Because of the low scattered-light intensity, high-power, short-duration pulses from suitable laser sources are required. The magnitude of the detected power is proportional to the product of the light pulse's duration times its peak intensity. This results in one of the fundamental trade-offs in an OTDR system: dynamic range (the longer the pulse duration, the greater the signal strength) and spatial resolution (the smaller the pulse width, the finer the spatial distances that can be determined). In addition, OTDR systems must rely also on high-sensitivity detectors such as avalanche photodetectors (APDs), and signal-averaging techniques are necessary to detect the low-level reflected signals.

A full trace of the reflected light intensity can be generated by placing a photodetector at the input of the fiber, where the combination of multiple back-reflected pulses will form a continuous envelope. This envelope will display the characteristic fiber attenuation and particular loss sources present along the fiber. An OTDR trace (Fig. 6.6) basically displays the average received optical power from a collection of back-reflected pulses on the vertical axis—this represents a measure of the fiber's power throughput along

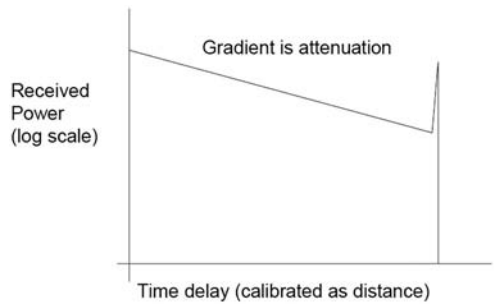

Figure 6.6 Idealized trace of an OTDR reflected signature.

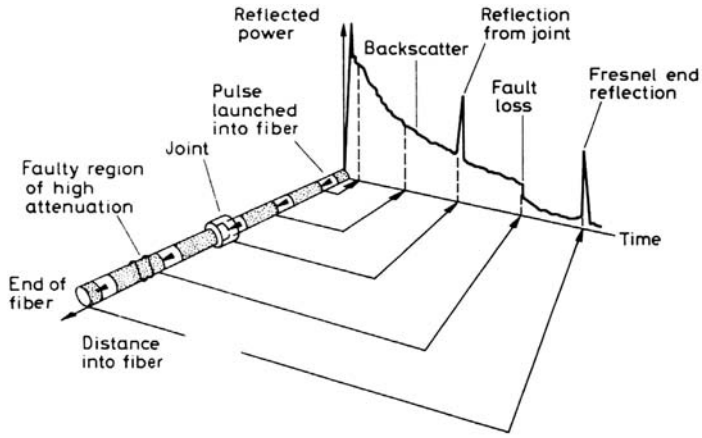

Figure 6.7 An OTDR trace illustrating the various fiber loss and faults that can be detected (adapted from Ref. 4 with permission).

its length—and the time delay, which is calibrated to represent distance, along the fiber, as the horizontal axis.

As illustrated in Fig. 6.7, in addition to information on fiber losses, OTDR profiles are very useful to localize breaks, to identify and locate fiber faults, to evaluate splices and connectors, and, in general, to assess the overall quality of a fiber link. The trace slope represents the fiber's attenuation factor, while any fault that produces a back-reflected signal will result in a spike or increase in intensity over the ODTR trace profile.

A powerful aspect of OTDR is its capability to locate events along a fiber with a high degree of spatial resolution. Localization and position quantification with an OTDR instrument is possible thanks to the time-of-flight of the coupled light pulses. Each injected probing light pulse travels along the fiber with a speed c/n_c, where c is the speed of light (in vacuum it is 3×10^8 m/s) and n_c is the fiber's core refractive index. By gate timing the launch of a pulse to its arrival, as depicted in Fig. 6.8, the pulse travel time τ is converted to the traveled distance L, by the basic relation

$$L = \frac{c\tau}{2n_c}. \tag{6.4}$$

Assuming an average core index of ~1.5, the time delay τ per meter in a typical silica fiber would be 5 nsec. Therefore, the total travel time to scan 1 m of fiber is 10 nsec. Hence, an OTDR system with an input light pulse of 10-nsec width duration can achieve a spatial resolution of at least 1 m. The spatial resolution of an OTDR is the smallest distance between two scattering sites that can be resolved by the instrument and is typically associated with the launched light pulse width:

$$\Delta_{Z\min} = \frac{c\tau_{pw}}{2n_c}, \tag{6.6}$$

where τ_{pw} is the OTDR's light source coupled-pulse width.

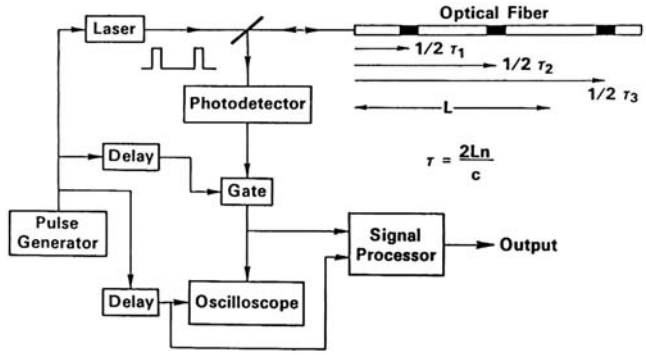

Figure 6.8 Diagram depicting typical timing circuitry of an OTDR and the relationship between distance and travel time for the coupled light pulses.

As depicted in Fig. 6.9, the total number N of resolvable points with the same spatial resolution over the entire length L of interest is given by

$$N = \frac{L}{dl}. \tag{6.6}$$

To avoid overlapping of subsequent pulses before a complete fiber length L is completely interrogated by a traveling pulse, the coupled input pulses must be separated in time by at least twice the pulse width and have a specific pulse rate. For instance, to scan a 10-km-long fiber, the time between pulses must be >100 μs, for a pulse rate <10 kHz.

The overall performance of an OTDR measuring instrument is determined by a number of different operating parameters such as light pulse intensity and duration, pulse repetition rate, receiver sensitivity and bandwidth, saturation level, linearity, crosstalk, and others.

There are a number of variant configurations of OTDR systems[5–8] that differ by either the type of backscattered signal employed (Rayleigh, Raman,

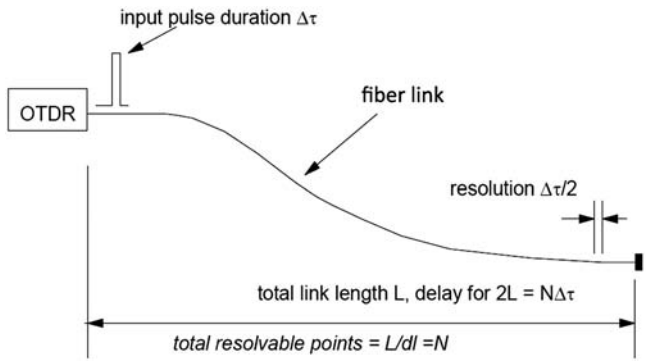

Figure 6.9 The spatial resolution and distance range are dictated by the input light pulse duration and its repetition rate.

or Brillouin), the modulation technique (either time or frequency domain), or the detection scheme (direct detection analog, photon counting or coherent). The basic OTDR technique is based on a time-domain, single-pulse approach that has the same configuration as described earlier and illustrated in Figs. 6.5 and 6.8. In contrast, in an optical frequency-domain reflectometer (OFDR), the distance information is determined from the frequency distribution of the returned backscatter signal, not its temporal travel time. This typically involves the use of a chirped, radio-frequency (RF)-modulated source.

6.3 Light-Scattering Mechanisms

When a monochromatic light wave having a wavelength λ_0 travels through a transparent medium such as glass, most of the energy propagates forward, experiencing a loss from the medium's attenuation. However, a small portion of the light undergoes scattering, which is the dispersal of a light beam into a multitude of other beams radiated in a range of directions as a result of the physical interaction between the light's photons and the matter of the transmitting medium. Figure 6.10 pictorially illustrates the interaction between traveling photons and the molecules in a transmitting medium that give rise to scattering. There are several scattering mechanisms that operate in glasses,[9] known as Rayleigh, Mie, Raman, and Brillouin scattering. Rayleigh scattering occurs when photons collide with inhomogeneities in the guiding medium; such inhomogeneities can include voids, density variations, impurities, composition fluctuations, structural variations, and other micro- and nanoscopic variations divergent from the average of the surrounding medium. Raman scattering occurs when traveling photons interact with thermally excited molecular vibrations; Brillouin scattering is the result of traveling photons interacting with bulk molecular vibrations.

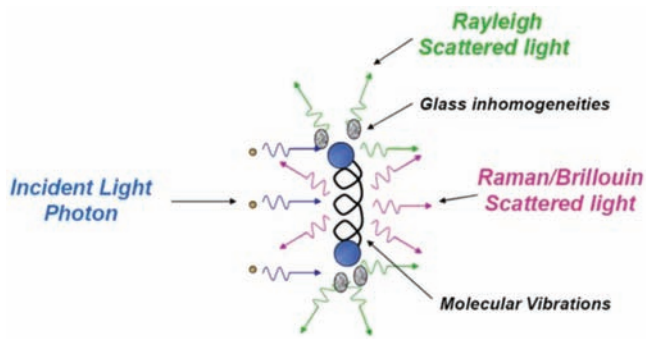

Figure 6.10 Pictorial representation of scattering mechanisms (elastic and inelastic). Rayleigh scattering is caused by index variations. There is no energy transfer, which defines an elastic collision. Raman/Brillouin scattering is caused by molecular vibrations. There is an exchange of energy which defines an inelastic collision.

It should be noted that any incident wavelength will produce the above-described scattering effects, but its effects could be stronger or weaker depending on the given scattering effect and its intrinsic wavelength dependence. Furthermore, scattering effects can be further classified as either spontaneous or stimulated. Spontaneous scattering refers to a linear process where the interaction between the light's photons and the scattering centers are not perturbed by the incident light wave. Conversely, when the optical intensity of the traveling light wave increases above a certain level (threshold), the excess light energy modifies the scattering properties of the medium resulting in a stronger and more efficient scattering process, or stimulated scattering. The critical threshold of optical powers above which stimulated scattering processes can take place has been evaluated[1] for both single-mode and multimode fibers at a wavelength of 1 μm and are summarized in Table 6.1.

6.3.1 Elastic versus inelastic scattering

Given the dual nature of light, where in some instances light photons can be considered particles and in others radiation waves, when discussing some of the scattering-process physics it helps to think of the incoming light as particles. In this case, the light particles—or photons—will collide with either the medium's inhomogeneities described earlier or the medium's molecular lattice. The process of Rayleigh scattering is said to be elastic because the incoming photon is reflected back in a different direction without an energy transfer, thus preserving its original wavelength (remember that the photon energy is expressed as $E = h\nu = hc/\lambda$, where ν is the photon's frequency and h is Planck's constant).

When the incident photons interact with the molecules in the medium in such a way that energy is either gained or lost from the collision, the wavelength of the scattered photons shifts. Such scattering processes are said to be inelastic. Raman and Brillouin scattering are both inelastic scattering processes involving three wave interactions of the incident wave, the scattered wave, and thermally excited molecular vibrations within the material (glass). These molecular vibrations (lattice vibrations) are also known as phonons. Raman scattering is driven by optical phonons, which are thermally driven and result in excited molecular vibrations where neighboring atoms are moving almost 180 deg out of phase. Brillouin scattering is produced by

Table 6.1 Threshold power levels needed to attain stimulated Raman and Brillouin scattering.

λ = 1 μm	Threshold power (mW)	Core diam (μm)	Fiber type
Raman Scattering	3.3	10	Single mode
	150	50	Multimode
Brillouin Scattering	9.8	10	Single mode
	440	50	Multimode

acoustic phonons resulting from acoustic waves traveling within the material and making neighboring atoms move almost in phase. Since phonon density is temperature dependent, inelastic scattering processes such as Raman and Brillouin are intrinsically sensitive to temperature changes and thus suitable as sensing mechanisms for distributed temperature sensing devices. A summary of the characteristics of elastic versus inelastic scattering in terms of collisions of particles follows:

- Elastic
  - Rayleigh scattering
    - No energy is lost
    - Emitted λ is equal to pump λ
- Inelastic
  - Raman scattering and Brillouin scattering
    - There is an exchange of energy, which results in a change in λ
  - Stokes
    - Energy is absorbed from the interaction
    - Longer λ emission
  - Anti-Stokes
    - Energy is gained from interaction
    - Shorter λ emission

6.3.2 Stokes and anti-Stokes scattering components

Because incident photons in an inelastic collision process can gain and lose energy, scattered photons will have different wavelengths and, depending on whether they are up- or downshifted, they are known as either Stokes and anti-Stokes components, respectively. A loss of energy corresponds to a Stokes-type scattering, where the scattered photon is downshifted in frequency (longer wavelength). Conversely, a gain of energy from the collision results in a frequency-upshifted scattered photon (shorter wavelength) or anti-Stokes component.

The observed frequency shifts are characteristic for a given material and correspond to its specific molecular vibrational and rotational energy levels (quanta). Hence, the Stokes and anti-Stokes components can be best understood in terms of an energy diagram as depicted in Fig. 6.11. As an incident photon collides with the molecules of glass in the medium, its energy is absorbed, and a photon is emitted from this virtual state to a ground energy level. The emitted photon is a Stokes emission with a frequency ν_s, where

$$\nu_s = \nu_i \quad \nu, \tag{6.7}$$

where ν is the frequency corresponding to the energy level at which the respective scatterer (stokes or anti-stokes) is located with respect to the incident photon as depicted in Fig. 6.11. Anti-Stokes scattered photons absorb energy and are emitted from higher energy levels (other than the actual

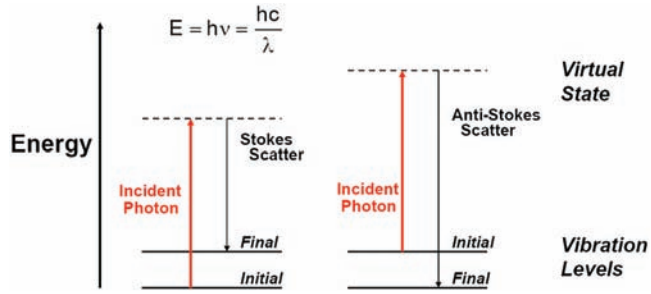

Figure 6.11 Energy-level representations for the emission of Stokes and anti-Stokes scattering components.

ground state), hence their intensity is temperature dependent. Their emission frequency ν_a is given by

$$\nu_a = \nu_i + \nu. \tag{6.8}$$

Commonly, Stokes and anti-Stokes components will result in a group of emission lines corresponding to different energy levels of the material. However, in the case of glass, being an amorphous material without a specific crystalline structure, the lines are broader becoming emission bands as opposed to distinct emission lines observed in gases, liquids, and crystalline materials.

6.3.3 Scattering emission spectrum

The overall scattered light that can be observed reflected back from an optical fiber is the result of the superposition of one or more of the scattering processes described earlier. Figure 6.12 shows the spectra of scattered light. The contributions from Rayleigh, Raman, and Brillouin effects can clearly be

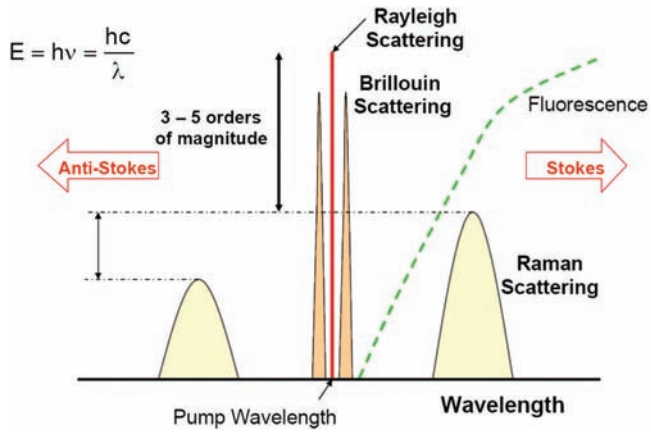

Figure 6.12 Pictorial representation of the scattering emission spectrum in a silica fiber.

observed. The Rayleigh component—as an elastic scattering—displays no wavelength shift and occurs at the same wavelength as the incident light wave. The Brillouin components are an order of magnitude less in intensity, have narrow emission lines (tens of megahertz of linewdith) and are separated by about 11 GHz (for a 1550-nm incident pump beam). In contrast, the Raman scattering components are three to five orders of magnitude smaller in intensity than the Brillouin components and separated from the Rayleigh components by about 13 THz with broader lines (~6 THz). The Stokes and anti-Stokes components can clearly be appreciated.

6.4 Rayleigh Scattering

Rayleigh scattering is the dispersal of an incident light beam caused by random inhomogeneities that manifests as microscopic refractive index variations—such as density variations, compositional variations, impurities, and other irregularities—frozen in the glass during the cooling of an optical fiber as it is being drawn, as depicted in Fig. 6.13. Rayleigh scattering is an elastic scattering process since there is no energy exchange and no frequency shift; the scattering centers are stationary, frozen into the material structure and, thus, the scattered photons have the same wavelength as the incident light wave.

A fundamental requirement of Rayleigh scattering is that the scattering centers must have a physical size much smaller than the wavelength of the incident beam (approximately one-tenth that of the incident λ). In this case, the particle is electrically small, and the phase shift across it is small, so it does not introduce any additional effects such as polarizibility or induced molecular vibrations.

Rayleigh scattering disperses light in all directions from the scattering center with a radiation pattern similar to that of an electric dipole (see Fig. 6.14). The intensity of scattered light I is given by Rayleigh's formula:

$$I = I_0 \frac{8\pi^4 N\alpha^2}{\lambda^4 R^2}(1 + \cos^2\theta), \tag{6.9}$$

where I_0 is the incident light intensity, N is the number of scatterers, α is the polarizibility, and R is the distance from the scatterer. Notice the dependence

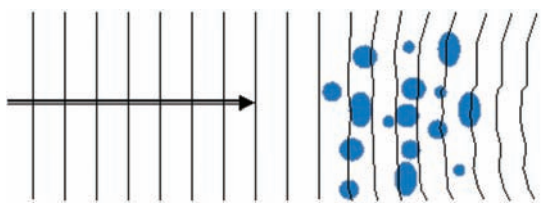

Figure 6.13 Inhomogeneities in a glass fiber produce refractive index variations that act as scattering centers for Rayleigh scattering.

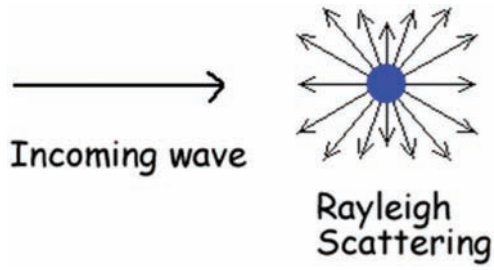

Figure 6.14 Dispersal of light produced by Rayleigh scattering.

of its strength with $1/\lambda^4$. Rayleigh scattering is stronger at shorter wavelengths. This is the same mechanism responsible for the sky being the color blue: Rayleigh scattering from water molecules in the air. Notice that the scattered light intensity is also a function of the scattering angle, being one-half of the value at right angles.

In a germanium-doped silica fiber, the Rayleigh scattering attenuation coefficient α_{rs} can be approximated by the following expression:[10]

$$\alpha_{rs} = \frac{(0.76 + 0.51 * \Delta n)}{\lambda^4} \quad [\text{dB/Km}]. \tag{6.10}$$

If the scattering particle is on the same order of magnitude in size as the wavelength, then Mie scattering occurs. The mechanism is similar to Rayleigh scattering, but the radiation pattern is different, as shown in Fig. 6.15, with Mie scattering displaying a more pronounced forward energy and radiation lobe pattern. Rayleigh and Mie scattering are not different mechanisms, they are simply distinct models approximating the scattering process applicable at different wavelengths. For instance, Fig. 6.16 shows the regimes where Rayleigh and Mie scattering dominate as a function of the ratio of a particle's diameter to wavelength.

Although Rayleigh scattering is relatively insensitive to temperature, it can still be used as a distributed sensing technique; although, in this approach, it would not be possible to distinguish whether changes in scattering signals are due to fiber loss effects or temperature changes.

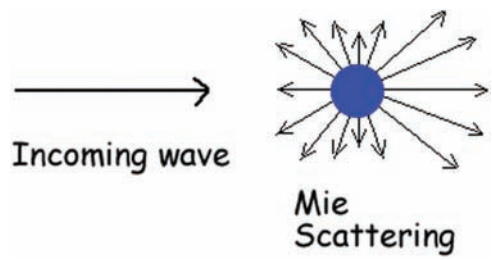

Figure 6.15 Radiation pattern from Mie scattering.

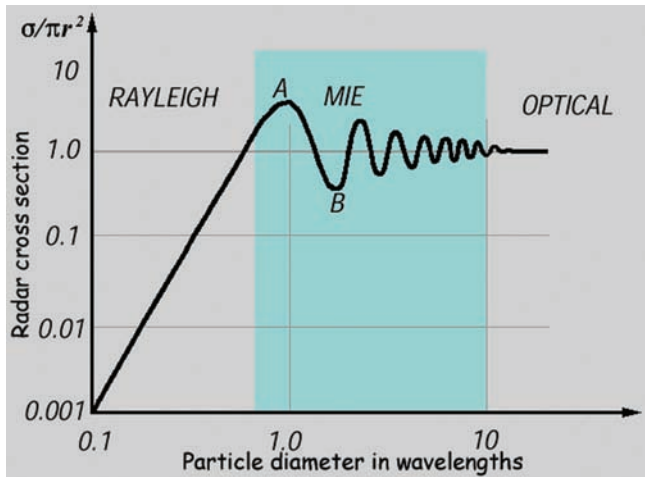

Figure 6.16 Relationship between particle size and regime for Rayleigh and Mie scattering.

6.5 Raman Scattering

Spontaneous Raman scattering is an inelastic process resulting from the interaction of the incident light beam with thermally excited vibrational modes of the glass molecules. Raman scattering radiates scattered photons that have been shifted to wavelengths that are longer and shorter than that of the incident wavelength λ_0, as illustrated in Fig. 6.17. This process simultaneously undergoes a transition between two vibrational states, thus producing an up- and downshifted scattered photon, known as the Stokes and anti-Stokes components, respectively.

Raman scattering can be viewed as an electron transition process (as depicted in Fig. 6.11) in which an incident photon is absorbed and produces a transition from a vibrational-rotational level of the ground state to a virtual (time-dependent) excited state, followed by a transition back down to a level adjacent to the starting level. Since the vibrational levels of the ground state are populated according to Boltzmann's law, the electronic populations at higher levels increase as the temperature rises. Therefore, the anti-Stokes components, which experience an energy gain, are particularly sensitive to temperature, with an intensity change on the order of $\sim$0.8 %/K, and thus are used as the detection mechanism in distributed fiber sensing systems. At high temperatures the molecular vibrations are highly excited, and the Raman sidebands are of equal intensity. Conversely, at very cold temperatures, the bands practically disappear. Hence, temperature sensing via Raman scattering has intrinsic limitations on both the upper and lower temperature range. However, the temperature range of most industrial applications is within the physical limits of the Raman scattering effect.

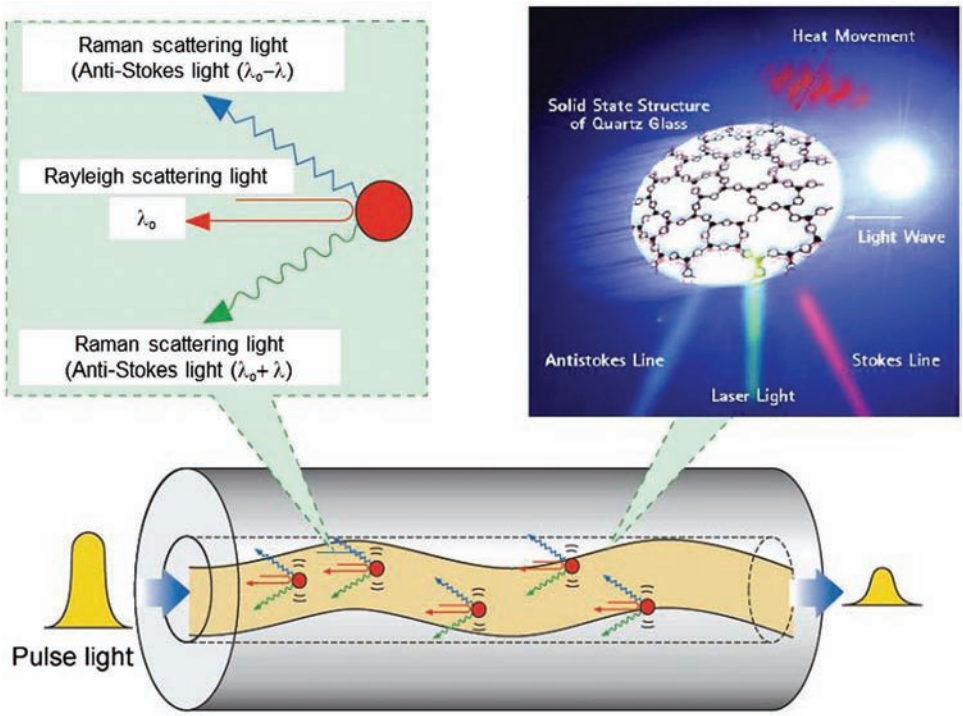

Figure 6.17 Raman scattering process in a silica glass fiber (source: LIOS).

Typically, Raman scattering produces an emission in both the forward and backward direction with a spectrum consisting of many lines many hundreds of wavenumbers away from the central Rayleigh scattering peak. However, in silica glass, being an amorphous material, the lines broaden, becoming uniform bands 200 cm^{-1} (~15 THz) wide, centered around 440 cm^{-1}, as depicted in Fig. 6.18. Any pump wavelength can be used to produce Raman scattering, although the signal strength decreases with increasing wavelength. The intensity

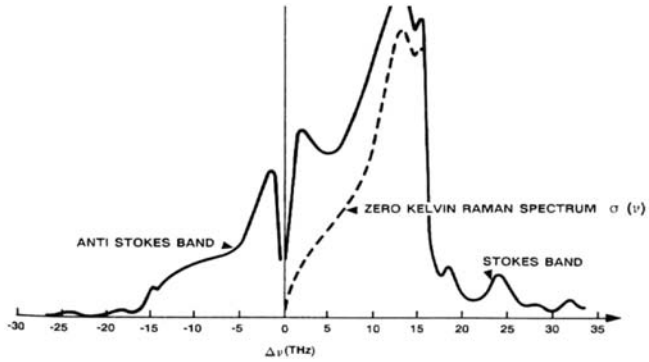

Figure 6.18 Raman scattering spectrum in silica glass.[2]

of the Raman scattering I_R, as mentioned earlier, is at least three orders of magnitude less than that of Rayleigh scattering, and is expressed as

$$I_R = \frac{I_0 N_0 \sigma_R}{(\lambda_i \pm \lambda)^4}, \tag{6.11}$$

where I_0 is the intensity of the incident light, λ_i is the incident beam wavelength, N_0 is the population of the starting ground level (equal to N_g, the ground level population for the Stokes line, and $N_0 = N_g\, e^{\nu/kT}$ for the anti-Stokes component), and σ_R is the Raman cross section for silica glass.

6.6 Brillouin Scattering

Spontaneous Brillouin scattering is an inelastic interaction process between the photons of an incident light beam and the density (index) variations induced by a pressure wave produced by a traveling acoustic wave within the glass material (Fig. 6.19). This acoustic wave is set off by thermally induced molecular vibrations in the structural lattice. Because the pressure variations are periodic, the induced refractive index fluctuations act as a Bragg grating structure, reflecting light in a given direction and of a given wavelength, as represented in Fig. 6.20. Furthermore, a Doppler frequency shift is induced between the incident beam and the scattered ones because of the relative movement and difference in propagation velocity between the light beams and the traveling acoustic wave. In other words, the scattered light beams are reflected back from a forward-moving grating. This optical grating is formed inside the fiber's core as a result of density changes in the glass induced by the non-uniform pressure profile associated with the acoustic wave traveling inside the fiber. Diffraction from a retreating acoustic wave produces a downshifted scattered beam or Stokes component. Conversely, a refracted beam from an approaching acoustic wave produces an upshifted scattered wave or anti-Stokes component. The Doppler-frequency shift is maximum in the backward direction and zero in the forward direction. The frequency shift ν_B depends on the acoustic velocity V_A in the glass and is expressed as

$$\nu_B = \frac{2nV_A}{\lambda}. \tag{6.12}$$

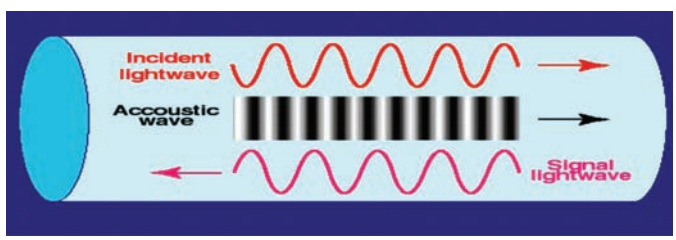

Figure 6.19 Basic Brillouin scattering mechanism. A traveling acoustic wave inside a glass fiber produces a pressure wave that in turn induces a periodic refractive index change from which incident light is reflected (source: Omnisens).

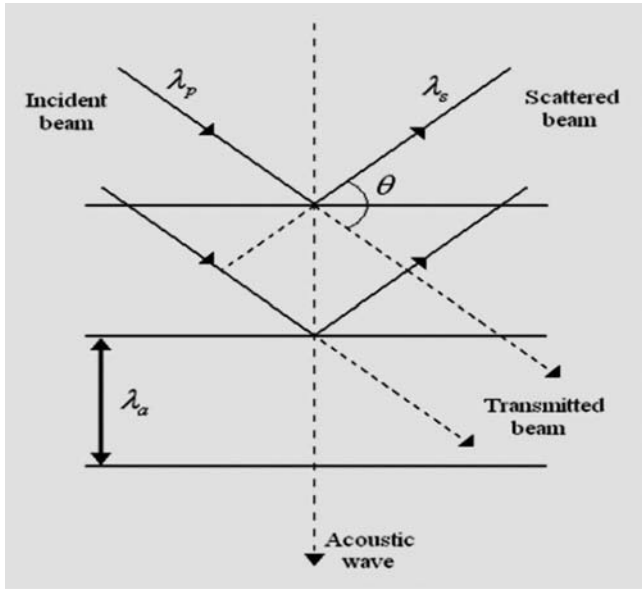

Figure 6.20 Graphical representation of the reflective Bragg grating structure produced by an acoustic traveling wave in a Brillouin scattering process. Here, λ_p is the pump wavelength (incident beam), and λ_s is the Stokes-component wavelength.

The acoustic velocity V_A (nominally 5945 m/s at room temperature) and the refractive index n are both a function of temperature and strain, and thus allow for the intrinsic capability of Brillouin scattering to perform distributed temperature and/or strain measurements by measuring the spectral shifts on the stokes and anti-Stokes Brillouin scattering spectra.

As seen in Fig. 6.12, the Brillouin scattering spectrum consists of very narrow ($\sim$100 MHz) Stokes and anti-Stokes spectral lines, shifted by only a few tens of gigahertz from the incident-light wavelength.

6.6.1 Stimulated Brillouin scattering

The previously described process represents the spontaneous form of Brillouin scattering. A stimulated version also exists that has practically the same mechanisms but a slightly different inducing cause. Stimulated Brillouin scattering (SBS) is produced by an intense incident optical signal, one that has an optical power above the spontaneous Brillouin threshold. This intense light wave has a very strong, intrinsically electromagnetic field, which, by itself, causes mechanical vibrations in the fiber's glass molecules, inducing a periodic index Bragg grating just as was the case in the spontaneous Brillouin scattering mechanism. The effect is nonlinear and requires a long interaction length and a light source with a narrow linewidth (long coherence length).

6.7 Distributed Fiber Sensing and Scattering Effects

As described earlier, distributed fiber optic sensing techniques are based on the recording and analysis of scattered light at every location along an optical fiber. Different types of light scattering are produced by different mechanisms—from density fluctuations that generate Rayleigh scattering, to thermally excited acoustic waves (or phonons) and molecular vibrations that cause Brillouin and Raman scattering. Figure 6.21 shows the full spectrum of the scattered light from a monochromatic light of wavelength λ_0 propagating in an optical fiber. By definition, the upshifted components (in the wavelength domain) are called Stokes components, and the downshifted components are called anti-Stokes components. From these spectra, it can clearly be appreciated that Rayleigh scattering has no strong dependence on temperature or strain and its emission wavelength matches that of the incident wavelength, given that it is an elastic scattering process. However, Rayleigh scattering is strongly dependent on the imperfections and losses along a fiber. Raman scattering possesses both Stokes and anti-Stokes components since it is an inelastic scattering process, whereby its anti-Stokes component is strongly temperature dependent, with its intensity increasing with temperature but with no apparent strain sensitivity. In contrast, Brillouin scattering is characterized by much narrower but stronger scattering emission lines that shift in wavelength in direct proportion to external temperature and/or strain changes. This, in a nutshell, is the key essence of fiber optic distributed-sensing techniques and the respective uses of each scattering effect for sensing purposes are summarized in Table 6.2.

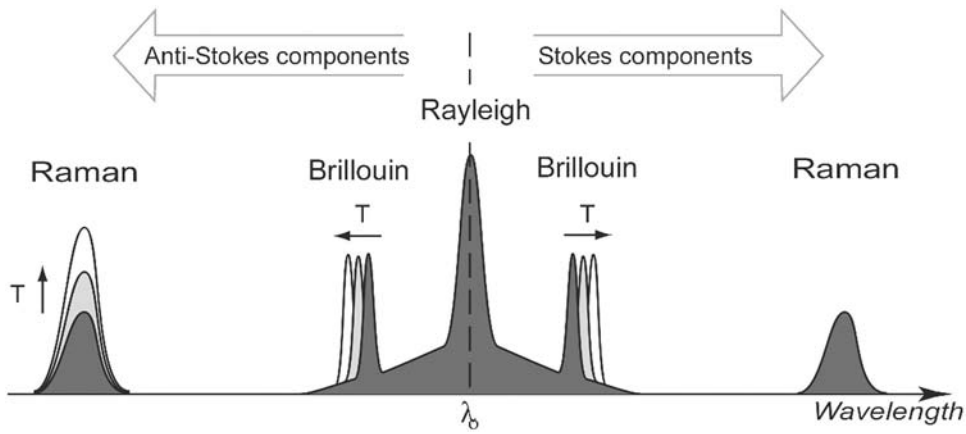

Figure 6.21 Full scattering spectra from silica glass fiber illustrating the specific scattering emission for Rayleigh, Raman, and Brillouin scattering (source: Omnisens).

Table 6.2 Temperature and strain sensitivities for different scattering effects in optical fibers.

	Effect	Pump relative position	Temp sensitivity	Strain sensitivity
Rayleigh	Molecular scatter	Incident	Weak	Weak
Raman	Molecular vibration	26 THz separation	Strong anti Stokes (intensity)	Weak
Brillouin	Acoustic wave	22 GHz separation	Strong (wavelength)	Strong (wavelength)

References

1. R. H. Stolen, S. E. Miller, and A. G. Chynoweth, *Optical Fiber Communications*, Academic Press, New York, p. 147 (1979).
2. M. K. Barnoski and S. M. Jensen, "Fiber waveguides: a novel technique for investigating attenuation characteristics," *Appl. Opt.* **15**, 2112–2115 (1976).
3. CSELT, *Optical Fibre Communication*, McGraw-Hill Education (1980).
4. G. D. Pitt et al., "Optical fibre sensors," *IEE Proceedings*, vol. 132, pt. J, no. 4 (1985).
5. S. D. Personick, "Photon probe—an optical time-domain reflectometer," *Bell Sys. Tech. J.* **50**(3), 355–366 (1977).
6. W. Eichoff, and R. Ulrich, "Optical frequency domain reflectometry in single-mode fiber," *Appl. Phys. Lett.* **39**, 693 (1981).
7. R. I. MacDonald, "Frequency domain optical reflectometer," *Appl. Opt.* **20**, 1840 (1981).
8. J. K. Everard, "Novel signal processing techniques for enhanced OTDR sensors," *Proc. SPIE* **798**, 42 (1987) [doi: 10.1117/12.941083].
9. R. D. Maurer, "Light scattering by glasses," *J. Chem. Phys.* **25**, 1206 (1956).
10. T. Izawa and S. Sudo, *Optical Fibers: Material and Fabrication*, KTK Scientific Publications, Tokyo, Japan, p. 35 (1987).
11. http://hyperphysics.phy-astr.gsu.edu/hbase/hph.html.

Chapter 7
Polarization-Based Sensors

7.1 Introduction

As discussed in Chapter 1, the propagating modes of a single-mode optical fiber can be expressed as a combination of linearly polarized (LP) modes with the fundamental mode designated as the LP_{01}. Also highlighted was the concept of describing the light energy as a combination of two degenerate modes possessing orthogonal linear polarizations. The polarization evolution of light in an optical fiber has been studied quite extensively. Typical eigenmode analysis can be applied, and, in most cases, linear polarization states are used as the basis vectors. However, it is important to note that any two orthogonal basis vectors are sufficient to completely describe all polarization states in the waveguide. In fact, as will be discussed later in this chapter, for Faraday rotation it is more mathematically convenient to use circular states (left and right) as the basis vectors to describe the process.

Polarization-based fiber optic sensors typically involve an extrinsic birefringent component to perform the actual polarization modulation. Intrinsic types of sensors include Faraday rotation and some Bragg gratings, which are written in polarizing-maintaining (PM) type fibers. Other components required for the system including polarizers and analyzers can also be implemented in fiber and are described in further detail in Section 7.2.

The sensitivity of optical components to polarization has been known and studied for a very long time. Most of the effects studied manifest themselves as operations on linear coordinate systems. Again, these are systems that possess linear eigenvectors. Detailed in Fig. 7.1 is a general component in a linear right-handed coordinate system. The angle of the light vector θ is defined as being positive when measured from the vertical coordinate y as observed while looking into the light source.

7.2 Analysis of Birefringent Optical Systems

Jones calculus provides a simple and insightful tool to analyze birefringent systems for cases where the light source can be considered coherent throughout

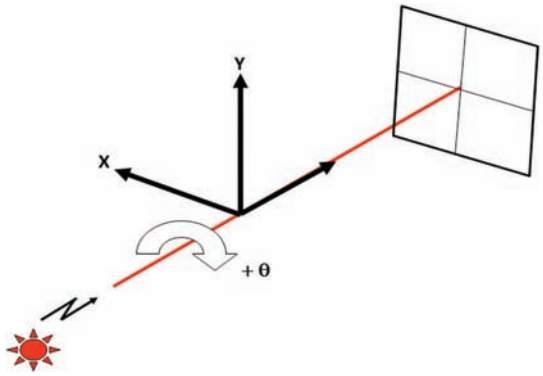

Figure 7.1 General layout of a birefringent optical system.

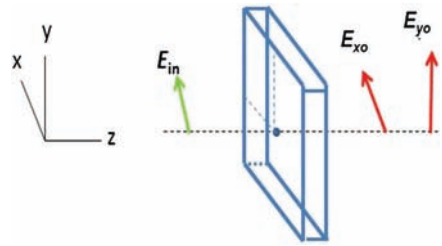

Figure 7.2 Optical propagation through a linear birefringent medium.

the system. Thorough descriptions of this particular method are found in Refs. 1 and 2. Also, it is worth mentioning that the Poincaré sphere provides still an additional method to look at polarization evolution through a birefringent medium.

The simple base case of a linear birefringent isotropic element, where linearly polarized light is injected at a 45-deg angle relative to the birefringent axes, is shown in Fig. 7.2. Using Jones calculus matrix representation, the intensity output at the x and y axes can be calculated as follows:

$$\begin{pmatrix} E_{x0o} \\ E_{y0o} \end{pmatrix} = \begin{pmatrix} \frac{\sqrt{2}}{2} & \frac{\sqrt{2}}{2} \\ \frac{\sqrt{2}}{2} & \frac{\sqrt{2}}{2} \end{pmatrix} \begin{pmatrix} e^{\frac{j\delta}{2}} & 0 \\ 0 & e^{\frac{j\delta}{2}} \end{pmatrix} \begin{pmatrix} \frac{\sqrt{2}}{2} & \frac{\sqrt{2}}{2} \\ \frac{\sqrt{2}}{2} & \frac{\sqrt{2}}{2} \end{pmatrix} \begin{pmatrix} 1 \\ 0 \end{pmatrix}, \quad (7.1)$$

where

$$\delta = \frac{2^*\pi}{\lambda^*}(n_x \quad n_y),$$

and the birefringence of the material is

$$B = n_x \quad n_{\mathrm{y.}} \quad (7.2)$$

By positioning a linear polarizer at either the x or y axis, the corresponding curves in Fig. 7.3 are obtained.

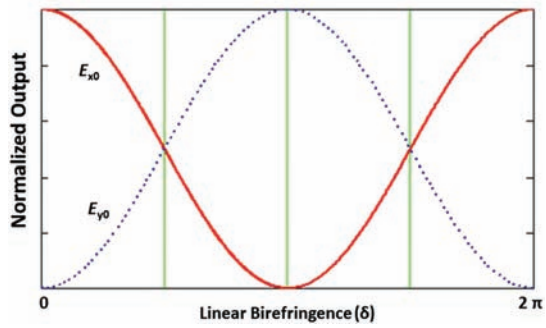

Figure 7.3 Output of a linear birefringent element.

Again, it is important to note that the fundamental measurement is the intensity of the light signal transmitted through this system. In effect, the retardance modulation is transferred to an intensity modulation. The implementation of this type of sensor configuration with fiber typically involves an extrinsic birefringent component. These components include photoelastic materials and electro-optic crystals, for example.[3,4] Figure 7.3 can be thought of as a static or DC case of birefringence modulation. In the case of an electro-optic crystal, the sensor is usually designed to measure an AC signal. By adding a quarter-wave plate to the components laid out in Fig. 7.4, a sensor can be configured that is biased at 50% power, and the AC signal rides on top of this DC bias. This output is similar to that of a Faraday rotator-based sensor, which has the net effect of rotating a linear polarization in response to an applied magnetic field along the direction of light propagation.

The time-varying signal of this type of setup is shown in Fig. 7.5. Looking closely at the two curves, it can be seen that they are 180 deg out of phase. Depending on the application, it is sometimes extremely important to provide time-replicated signals that are in phase with the physical process being monitored. In these cases, care must be taken to align the output analyzer with the correct axis.

As mentioned previously, the polarizer/analyzer component can also be supplied via optical fiber. Single-mode fibers using a depressed inner cladding design[5] have been successfully demonstrated to provide >40 dB of extinction ratio with ~5 m of fiber. This particular fiber is constructed with an elliptical layer, providing ease of splicing to standard germanium-doped fibers. This

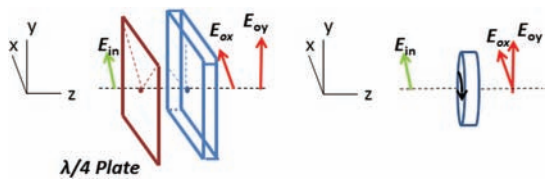

Figure 7.4 Configurations for time-varying measurements.

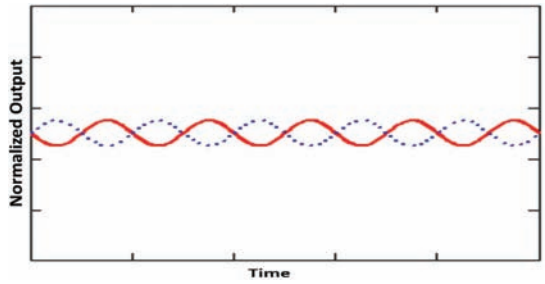

Figure 7.5 Output signal of a time-varying applied birefringence.

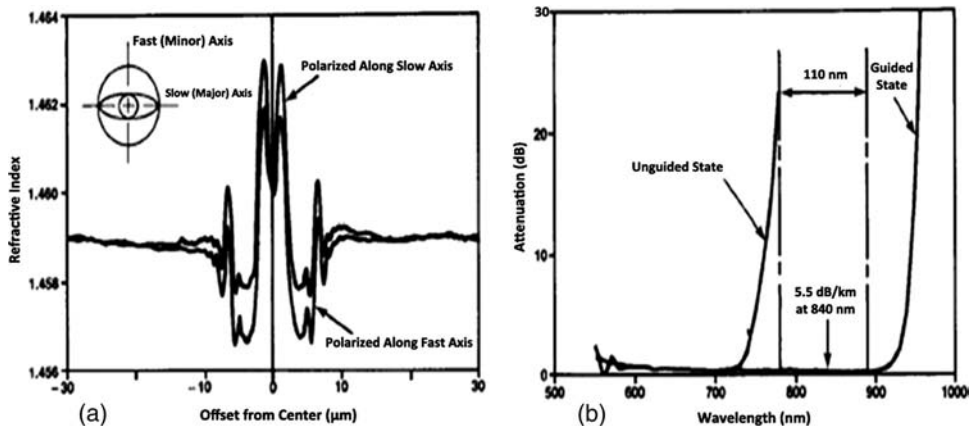

Figure 7.6 (a) Index profile of polarizing fiber and (b) corresponding attenuation curve for both polarizations.

allows practical implementation in sensing systems and ease of packaging. The details of this fiber structure are shown in Fig 7.6.

In addition to the polarizer/analyzer function, optical fiber-based retarders have also been used as part of optical fiber sensing systems.[6] These components can provide a means for performing much of the sensor signal processing in the optical domain. This alleviates the complexity of the associated mechanical and/or electronic components. An example of this type of component is shown in Fig. 7.7.

7.3 Birefringent Effects in Bragg Gratings

An important property of Bragg gratings that is sometimes overlooked is the dependence of the grating reflection spectrum on the polarization state of the light used to interrogate the sensor. As noted in Chapter 5, the equation for the peak reflection wavelength from a Bragg grating is:

$$\lambda_B = 2n_{\text{eff}}\Lambda. \tag{7.3}$$

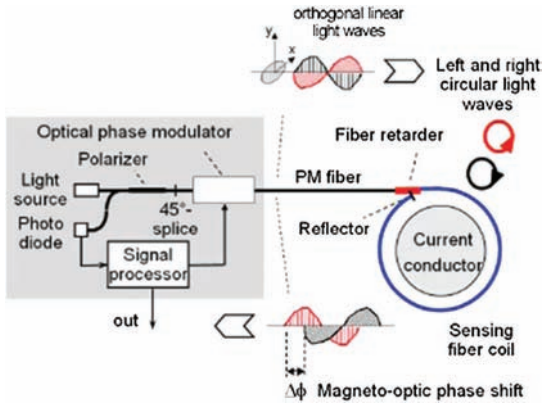

Figure 7.7 Optical fiber-based retarder.[6]

This can be extended to provide peak wavelength information for a Bragg grating in a linear birefringent medium. Here the peak reflection wavelengths for each axis are

$$\lambda_{Bx} = 2n_{\text{eff}x}\Lambda, \tag{7.4}$$

and

$$\lambda_{By} = 2n_{\text{eff}y}\Lambda, \tag{7.5}$$

where x and y designate birefringent axes in the x and y directions, respectively. Most fiber waveguides possess enough asymmetry to create some level of birefringence. In addition, fabrication processes for imprinting Bragg gratings can add to this birefringence. For gratings exposed into PM fibers, the peak wavelength spread is significant and on the order of ~200–500 pm. However for standard low-birefringent fibers, this peak wavelength difference is on the order of ~2–5 pm.

The reflection spectrum of the Bragg grating for both polarization states is diagrammed in Fig 7.8. The plot clearly shows the error that can be expected

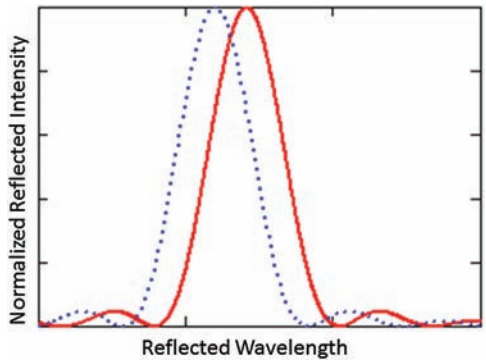

Figure 7.8 Peak wavelength difference due to birefringent Bragg grating.

if the grating is interrogated with light polarized in a particular axis. In most sensor applications, the peak wavelength is directly related to the parameter being measured, so any error in this calculation translates directly to an error in the overall measurement. Typical interrogation systems will use a depolarized source to average out this error between the two axes. When this is done, the peak detection is more consistent and stable, with any offsets being addressed in calibration.

7.4 Application Examples

Several commercial sensing systems have been produced that utilize polarization-modulation techniques for performing measurements of physical phenomena. Figures 7.9 and 7.10 show this technology in practice. The first system is a fiber optic voltage sensor that utilizes an electro-optic (E-O) crystal. An electric field applied to the E-O crystal in the correct orientation will modulate the birefringence of the crystal. This E-field sensor can easily be configured to measure voltage.

The second example utilizes the Pockels effect in a BGO (bismuth germanium oxide) crystal. Care is taken here to configure the sensor to

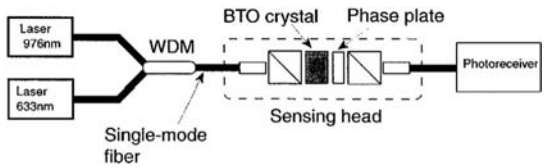

Figure 7.9 Fiber optic voltage sensor.[7]

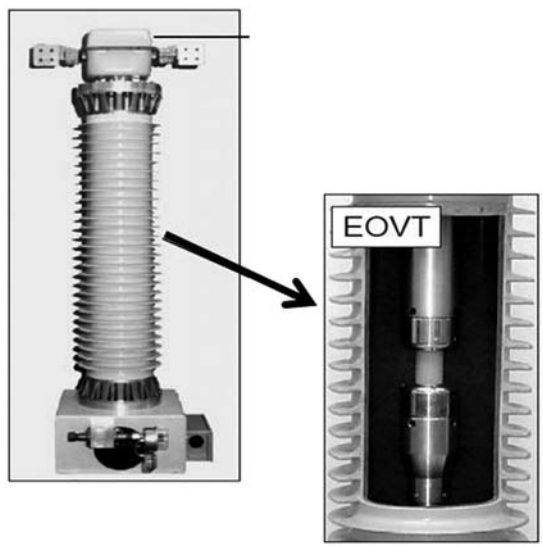

Figure 7.10 Commercial voltage sensing system (image courtesy of ABB).[8]

perform the actual line integral of the electric field to calculate voltage. This technique and architecture reduce any effects from ambient electric fields.

Another interesting architecture has been presented by Enokihara et al.[7] This is diagrammed in Fig. 7.11 and shows the principle of polarization-rotated reflections to add some noise and error rejection to these measurements.

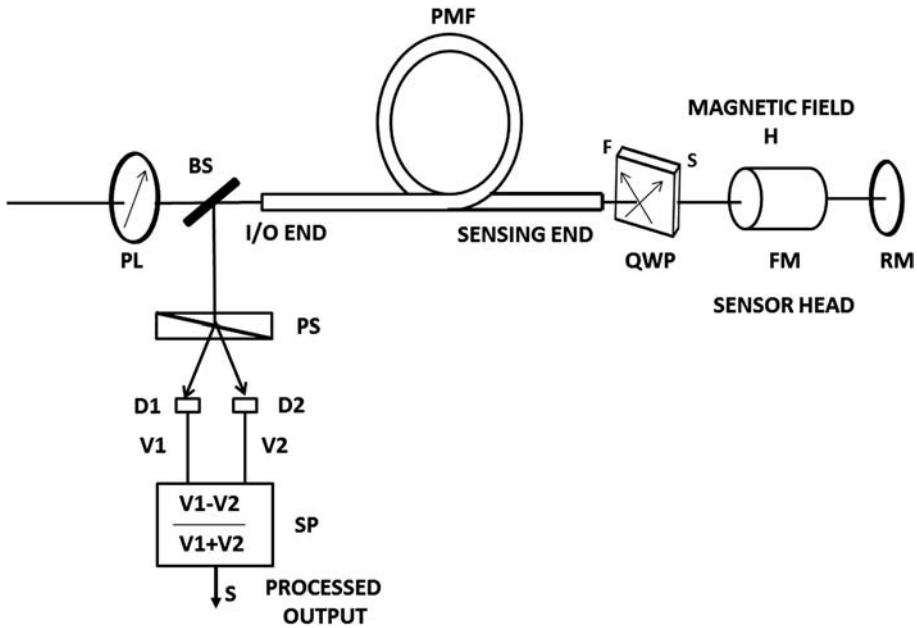

Figure 7.11 Polarization-rotated reflections.

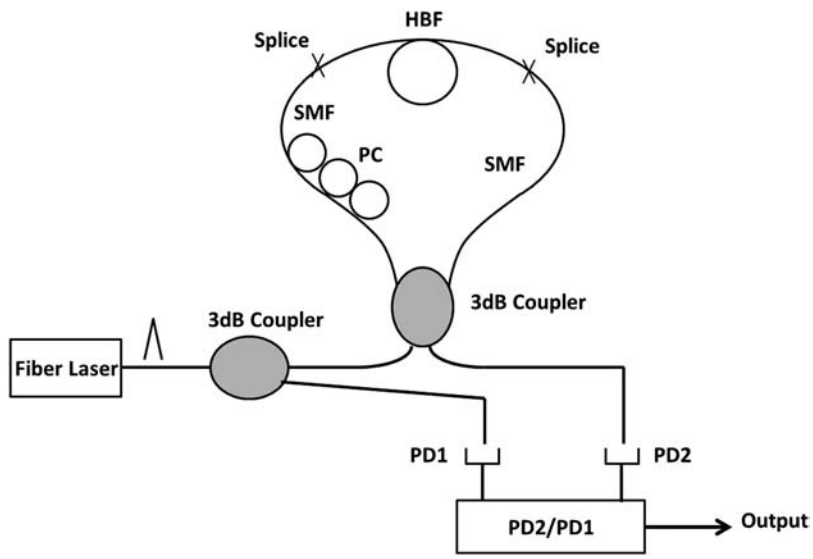

Figure 7.12 High birefringence optical fiber loop mirror.[10]

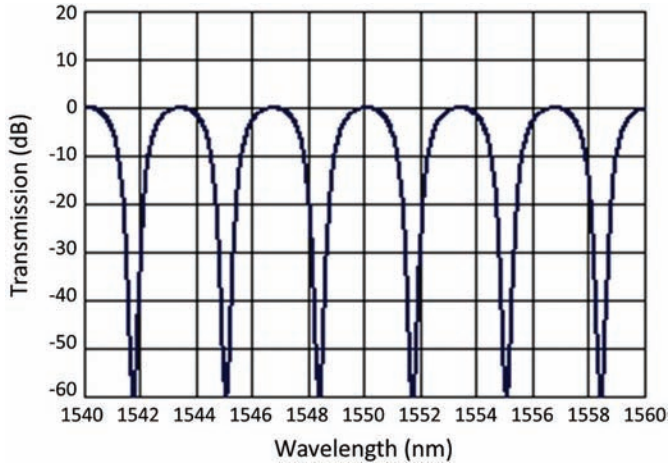

Figure 7.13 High-birefringence optical fiber loop mirror signal output.[10]

The sensing system shown in Fig. 7.12 is a unique example of a polarization-based sensor since it can also be considered to have properties similar to an interferometric sensor. In this setup the response of the system is composed of the interference of two counter-rotating beams in the fiber loop. The fiber loop contains portions of high-birefringence fiber that can be spliced in and in some cases multiple pieces are included and rotated relative to one another. The system response is shown in Fig. 7.13. As can be seen, the filter response is wavelength dependent. By applying strain or temperature, for example, to the high-birefringence section of the loop, this response is modulated and can be then used to measure these parameters.

References

1. A. Yariv and P. Yeh, *Optical Waves in Crystals*, John Wiley and Sons, New York, (1983).
2. C. R. Jones, "A new calculus for the treatment of optical systems," *JOSA* **31**, 488–493 (1941).
3. G. A. Sanders, J. N. Blake, A. H. Rose, F. Rahmatian, C. Herdman, "Commercialization of fiber-optic current and voltage sensors at NxtPhase," *Optical Fiber Sensors Conference Technical Digest*, *Ofs* **15**, 31–34 (2002).
4. W. B. Spillman, Jr., "Multi-mode fiber optic pressure sensor based on the photo-elastic effect," *Optics Letters* **7**, 388 (1982).
5. M. J. Messerly, J. R. Onstott, and R. C. Mikkelson, "A broad-band single polarization optical fiber," *Journal of Lightwave Technology* **9**(7), 817–820 (1991).

6. M. Lenner et al., "Characterization of fiber wave retarders for interferometric fiber optic current sensors," *IEEE Avionics, Fiber-Optics and Photonics Technology Conference*, 49–50 (2011).
7. V. N. Filippov, A. N. Starodumov, V. P. Minkovich, and Y. O. Barmenkov, "Optically controlled fiber voltage sensor," *IEEE Photonics Technology Letters* **12**(7), 870–872 (2000).
8. K. Bohnert, P. Gabus, and H. Brandle, "Fiber optic current and voltage sensors for high-voltage substations," *16th International Conference on Optical Fiber Sensors*, 752–754 (2003).
9. A. Enokihara, M. Izutsu, and T. Sueta, "Optical fiber sensors using the method of polarization-rotated reflection," *Journal of Lightwave Technology* **5**(11), 1584–1590 (1987).
10. Y. Liu, B. Liu, X. Feng, W. Zhang, G. Zhou, S. Yuan, G. Kai, and X. Dong, "High birefringence fiber loop mirrors and their applications as sensors," *Applied Optics* **44**(12), 2382–2390 (2005).

Chapter 8
Digital Switches and Counters

8.1 Introduction

All intensity-modulated fiber optic sensors are analog in nature, but they have a broad usage potential in digital applications. Until recently, they were used as absence/presence sensors, i.e., is the object there or not? Digital applications have now expanded to pressure, temperature, and liquid-level switches. Photoelectric sensors have been used for many years in absence/presence applications. Since fiber optic sensors are almost always more expensive than photoelectric sensors, the driving force for using fiber optics is generally due to environmental considerations. Fiber optic sensors, due to their small mass, are less susceptible to vibration. Fiber optic devices are immune to electromagnetic interference and radio frequency interference and, therefore, are free from electrical noise problems. They also are explosion proof. Their small size makes them easy to install, and conduit and shielding are generally not necessary. Figure 8.1 shows illustrations of photoelectric and fiber optic sensors for comparison.

8.2 Scan Modes

The two basic scan modes are through-scan and reflective scanning. Through-scan uses fibers in an opposed transmissive mode, as shown in Fig. 8.2. The transmitting fiber optic bundle is opposed by the receiving bundle. If an object interrupts the light path, the object is detected. The bundles can be replaced by large-core single fibers, but bundles provide more light and a larger scan area than single fibers. Therefore, the choice of bundle versus single fiber depends on the application. The through-scan approach provides for the maximum collection of light; therefore, it is the most effective technique in dirty environments and for long distances between the sensor and the object. It is especially well suited for detecting opaque objects, but sufficient light may penetrate translucent objects to prevent detection.

Reflective scanning uses fiber optic probes that are bifurcated, i.e., the transmit and receive legs are separate at the electro-optic interface and have a

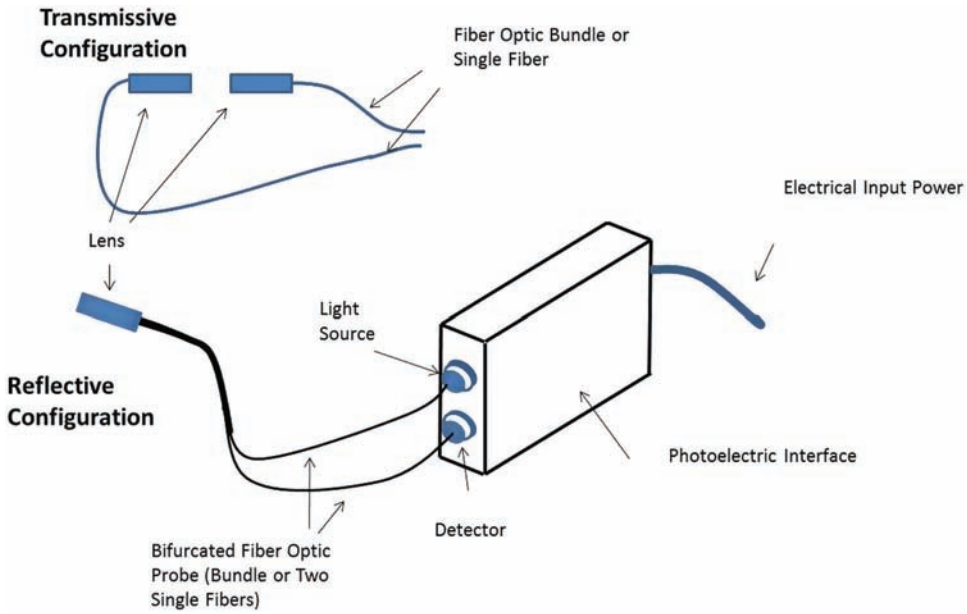

Figure 8.1 Photoelectric and fiber optic sensors[1] (courtesy of Micro Switch^{TM}).

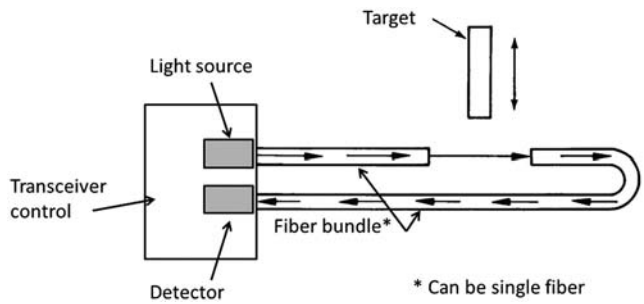

Figure 8.2 Through-scan mode. The fiber bundle can also be a single fiber.

common leg near the target. Light is transmitted to the target through the transmitting portion of the common leg, reflected from the target, and returned to the photodetector via the receive portion of the common bundle. An object is detected when it interrupts the light path between the target and the probe. The technique works well for object detection in which surface reflectivity is poor. If a highly reflective object breaks the light beam, there may be sufficient reflected light collected by the receiving leg to generate a false signal. Reflective scanning is characterized by the target reflectivity, i.e., retro-reflective, diffuse, and specular.

A retro-reflective fiber optic sensor is shown in Fig. 8.3. The retro-reflecting target is highly efficient in reflecting light back along the same light path as the incident beam. The reflection phenomenon is independent

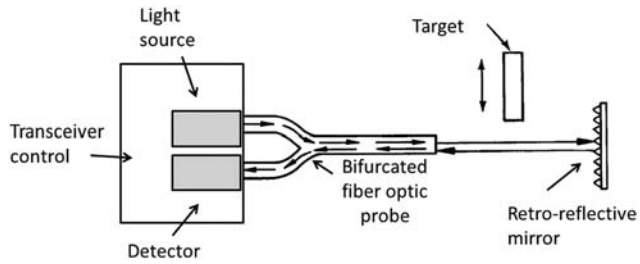

Figure 8.3 Retro-reflective fiber optic sensor.

of the angle at which the light initially hits the retro-reflector. Figure 8.4 shows the topography of retro-reflective surfaces that allow for high reflection efficiency. The reflectors use either spherical balls or three-corner cubes.

The three-corner cube also has the unique property of being a polarizing retarder. In essence, if polarizing filters with their axes at 90 deg to each other are placed at the receiving and transmitting ends of the probe, the plane of polarization is effectively rotated 90 deg. Only light reflected from the three-corner cube can pass through the receiving polarizing filter. All other light is rejected. This feature eliminates false signals from highly reflective objects, as discussed earlier.[2,3]

Diffuse scanning occurs for targets with relatively rough surfaces. The initial incident light beam is scattered in numerous directions with the received light level being low. In this case, the reflecting target is the object to be detected, as shown in Fig. 8.5. The primary application is in proximity sensing. A potential problem can occur if the background has a high reflectivity relative to the target material. In such cases, false triggering is likely.

Specular targets are the third application of reflective scanning. The surface is characterized as being smooth and shiny or mirror-like. The angle of incidence equals the angle of reflection, as shown in Fig. 8.6.

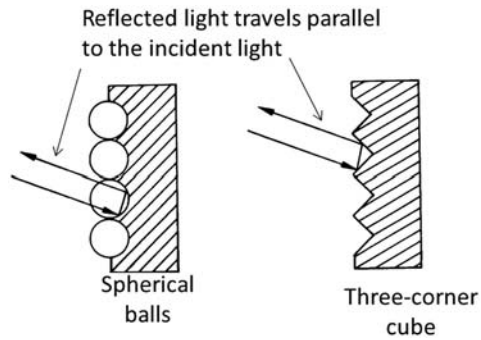

Figure 8.4 Retro-reflective surface topographies.

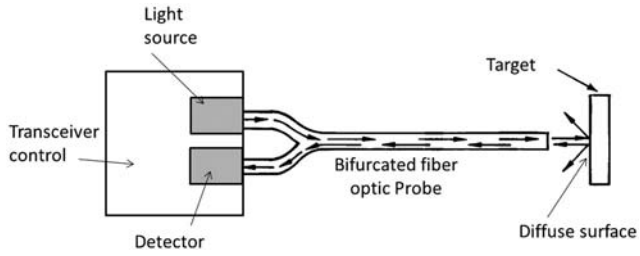

Figure 8.5 Reflective fiber optic diffuse scanning.

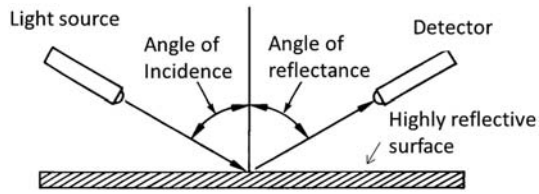

Figure 8.6 Specular scanning.

For distances that are small (usually less than 1 cm), bifurcated probes can be used. However, for larger distances between the target and the probe or for large angles of incidence, the transmit and receive legs require separation, as would be the case for a transmissive through-scan mode. This technique is especially useful in differentiating between highly reflective surfaces and dull areas.

8.3 Excess Gain

Excess gain is one of the parameters used to characterize absence/presence sensors.[2 4] It is defined as the ratio of light intensity hitting the detection system to the light intensity required to activate the detection system. Therefore, a ratio of 1:1 is just sufficient to operate the system. Generally, an excess gain is specified to handle degradation of the system caused by airborne contamination, dirty optics, potential misalignment, surface reflectivity changes, etc. Typical excess gain curves for the four modes discussed (through-scan, retroreflective, diffuse, and specular) are shown in Figs. 8.7–8.10, respectively. The data in tables 8.l and 8.2 have been worked out to show a relative level of excess gain requirements for photoelectric sensors.

8.4 Contrast

The use of absence/presence sensors requires that the sensor be able to differentiate between two different light levels. Contrast is defined as the ratio of the level of detected light in the light condition to the level of detected light in

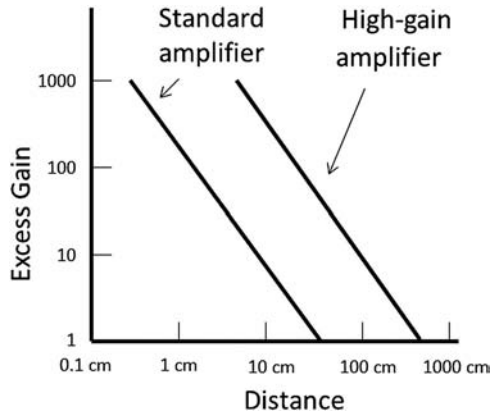

Figure 8.7 Excess gain in through-scan mode.

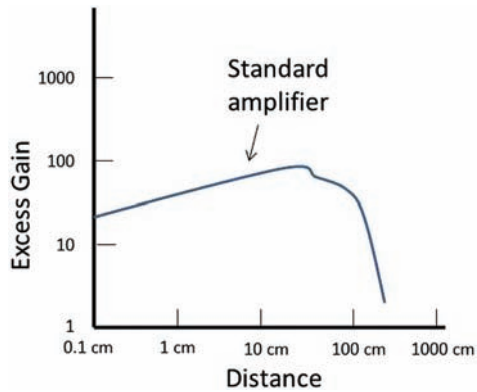

Figure 8.8 Excess gain in retro-reflective scan mode.

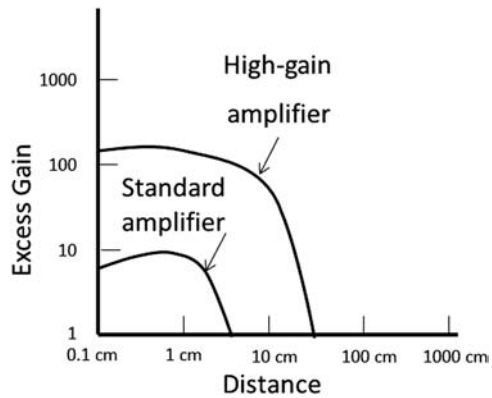

Figure 8.9 Excess gain in diffuse scan mode. The range is based on 90% reflectance with a test card.

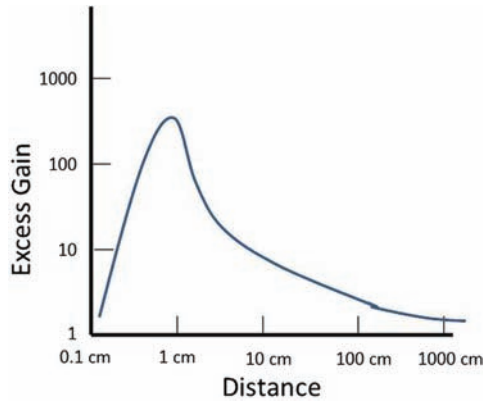

Figure 8.10 Excess gain in specular scan mode.

Table 8.1 Excess gain required for various operating environments.[4]

Minimum excess gain required	Operating environment
1.5×	Clean air; no dirt buildup on lenses or reflectors.
5×	Slightly dirty: slight buildup of dust, dirt, lint, moisture, oil film, etc., on lenses or reflectors; lenses cleaned regularly.
10×	Moderately dirty: obvious contamination of lenses or reflectors, but not obscured; lenses cleaned occasionally or when necessary.
50×	Very dirty: heavy contamination of lenses; heavy fog, mist, dust, smoke, or oil film; minimal cleaning of lenses.

Table 8.2 Relative reflectivity chart.[4]

Material	Reflectivity	Excess Gain Required
Kodak white test card	90%	1
White paper	80%	1.1
Newspaper (with print)	55%	1.6
Tissue paper: 2 ply	47%	1.9
Tissue paper: 1 ply	35%	2.6
Masking tape	75%	1.2
Kraft paper, cardboard	70%	1.3
Dimension lumber (pine, dry, clean)	75%	1.2
Rough wood pallet (clean)	20%	4.5
Beer foam	70%	1.3
*Clear plastic bottle	40%	2.3
*Translucent (brown) plastic bottle	60%	1.5
*Opaque white plastic	87%	1.0
*Opaque black plastic (nylon)	14%	6.4
Black neoprene	4%	22.5
Black foam carpet backing	2%	45
Black rubber tire wall	1.5%	60
*Natural aluminum, unfinished	140%	0.6
*Natural aluminum, straightlined	105%	0.9
*Black anodized aluminum, unfinished	115%	0.8
*Black anodized aluminum, straightlined	50%	1.8
*Stainless steel, microfinished	400%	0.2
*Stainless steel, brushed	120%	0.8

*For materials with highly reflective surfaces, the reflectivity figure represents the maximum light return with the scanner beam exactly perpendicular to the material surface.

the dark condition. Generally, if the contrast ratio is less than 3:1, the contrast is considered poor, and care must be exercised in choosing a detection scheme. Above a ratio of 3:1 contrast does not normally present a problem. A common problem mentioned previously is a highly reflective object interrupting the light beam in a diffuse scanning mode. False triggering can be expected. To eliminate this problem, the reflection target can be replaced with a retro-reflective material, or through-scanning can be used. The retro-refractive target increases the contrast ratio so that the signal from the interruption of the light path by a highly reflective object still is way below the detected signal from the target. Using a through-scan mode eliminates the possibility of detecting reflected light. Another potential problem is a transparent or translucent object breaking the light beam in a retro-reflective mode or a through-scan mode. Sufficient light may pass through the object that a false signal will occur. In this case, the diffuse reflective mode may be best.

8.5 Beam Diameter

A second characterization parameter is the beam diameter, which is defined by the locus of points at which the excess gain equals 1. It defines the off-axis distance at which the system will still operate. The highest energy is on or near the axis of the transmitting leg, with the transmitted energy falling off as the distance parallel to the axis or perpendicular to the axis increases (see Fig. 8.11).

The effective beam diameter is the portion of the beam diameter that reaches the receiver. For a through-scan configuration, Fig. 8.12 defines the effective beam. Figure 8.13 defines the effective beam for a reflective scan.

8.6 Electro-Optic Interface

The electro-optic interface is a transceiver that contains the light source, drive circuitry, photodetector, and amplification circuitry. Most interfaces use an LED as the light source. The interfaces are divided into two basic categories: modulated and non-modulated.[5]

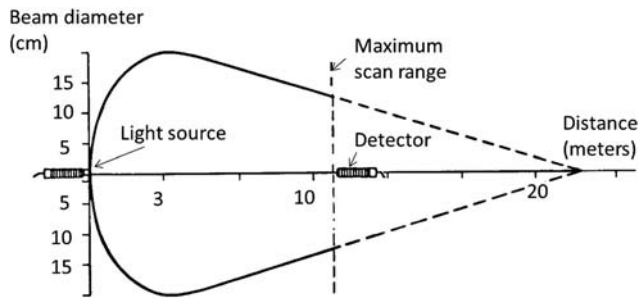

Figure 8.11 Beam diameter.

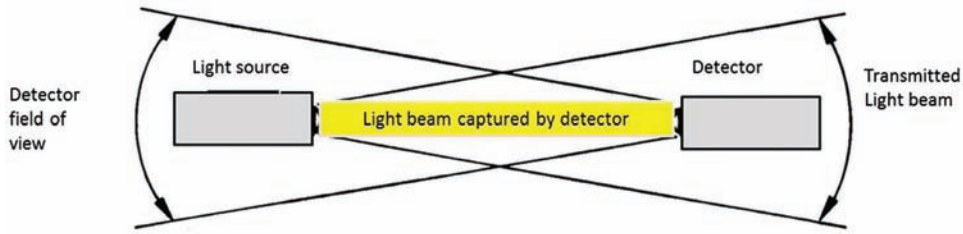

Figure 8.12 Effective beam diameter: through-scan configuration.

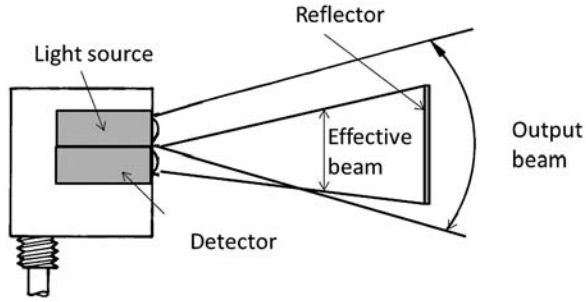

Figure 8.13 Effective beam diameter: reflective configuration.

Non-modulated units use a constant output level. They are capable of receiving high data rates as might be required in a high-speed tachometer, but they are susceptible to false triggering due to ambient light being detected. Modulated systems pulse the LED at a relatively high frequency (typically several kilohertz). The detection system is designed only to receive signals at this pulse rate. Therefore, ambient light signals are eliminated in the detection scheme.

One major disadvantage of LED light sources is their inability to be used in sensing color. Light-emitting diodes transmit over a very narrow wavelength. Infrared (IR) light-emitting diodes, in particular, are unable to be used to distinguish color. Therefore, for sensing applications in which color discrimination is required, broad-spectrum light sources must be used.

Figure 8.14 shows a typical modulated electro-optic interface.[6] The scanning mode is through-scan. The scanning block shows the oscillator, which pulses the LED light source, the receiver, and the amplification circuitry. The demodulator filters out unwanted light signals. The logic module drives the interface output. The output signal can be altered in time so that specific operations can be controlled.[7] The output can trigger on light or dark operate mode, i.e., when the detector sees light or dark. On-delay logic (off-delay logic) allows a predetermined time after detection before the power is switched on or off. If the detection signal ceases during the delay period, the power will not be switched. On-delay logic is useful in detecting jams because

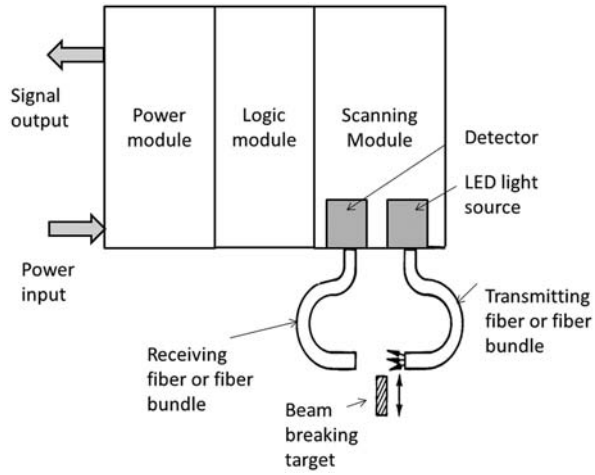

Figure 8.14 Typical modulated electro-optic interface.

triggering will not occur with normal object flow but only with delays in flow associated with jams.

One-shot logic provides an output for a defined time if a detection signal is observed. It is useful for triggering a process operation as the leading or trailing edge passes. It can also be used for overspeed or underspeed detection. Counters are used to count the number of beam breaks. If used in conjunction with a one-shot, the counter will trigger after a detectable event.

8.7 Applications

Most widespread applications are for absence/presence sensors.[8] Figure 8.15 illustrates a series of applications, such as the monitoring of product movement in a production line shown in parts (a) and (d). The sensors can count objects as well as determine if there is a jam. Generally, as the environment becomes more severe, fiber optic sensors are favored over conventional photoelectric sensors. Figure 8.15(b) shows fiber optic sensors in a web detection scheme. The sensor can monitor for tears and other defects, in addition to precisely monitoring the web edge. Fiber optics have been used successfully in ejected part detection, vibrating feeder-bowl control, and part-in mold detection. Because of their sensitive nature and ability to detect small targets, fiber optic sensors have been used for thread detection as well as for the detection of other small objects [Fig. 8.15(c)]. Targets as small as 25 μm can be detected.

Advances in the manufacturing of circuit boards require pick-and-place machines to operate very precisely at high speeds. Surface-mount components are loaded onto a template and guided into the correct position. To function, pick-and-place machines require leading-edge detection, which is facilitated with fiber optic detection systems.[9]

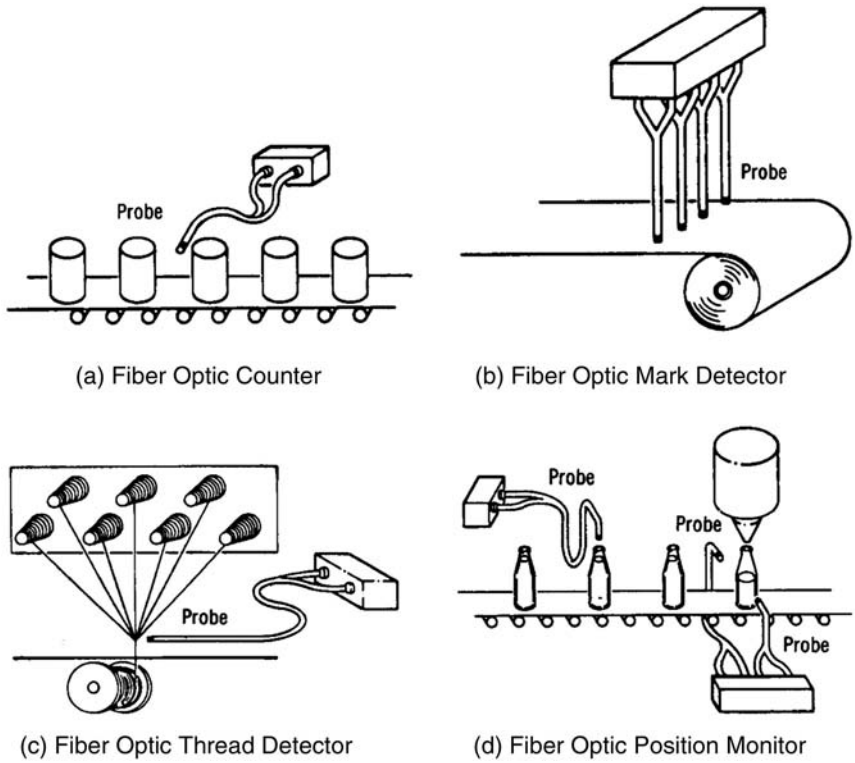

Figure 8.15 Switch and counter applications.

Fiber optic absence/presence sensors have been used extensively as tachometers. A typical tachometer is shown in Fig. 8.16. The device uses a bifurcated fiber optic probe with a reflective or absorption strip, which is used as the target, to provide a pulse train corresponding to rotation rate. In many applications where rotation rate determination is required, access is quite difficult. The use of fiber optics generally eliminates this problem.

Fiber optic tachometers have also been used in motor-speed control. Figure 8.17 depicts a schematic representation of a speed-control system. A specific application of a fiber optic tachometer is shown in Fig. 8.18. The flywheel in the watt-hour meter is rotating 50 revolutions for the movement of one unit on the least-significant dial indicator. The flywheel (rotating disk) has

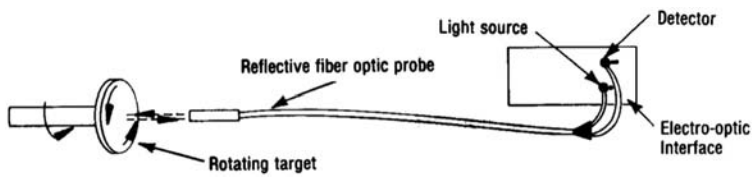

Figure 8.16 Fiber optic tachometer.

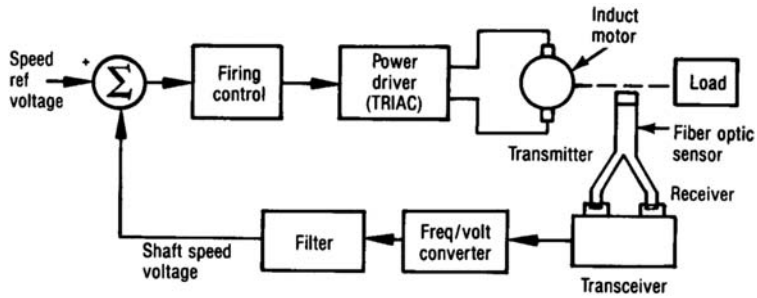

Figure 8.17 Fiber optic speed-control system.

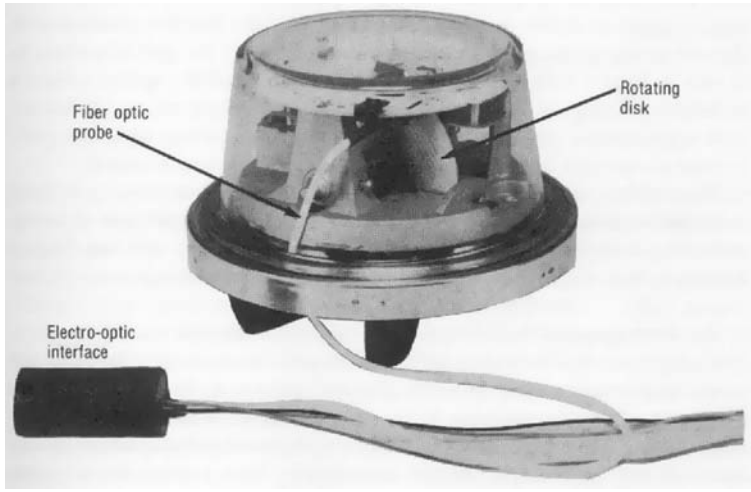

Figure 8.18 Fiber optic tachometer used in a watt-hour meter.

a black absorption strip for encoding purposes. The environment that the sensor must withstand is surprisingly severe, and this dictates the use of fiber optics. The sensor/encoder cannot be defeated by direct or indirect sunlight or by manual tampering. The relative humidity often approaches 100%, and the lensing effect of the glass housing in direct sunlight can result in temperatures exceeding 150 °C.

Another application that often requires fiber optic absence/presence sensors is hot object detection. In this case, if the object is warmer than the incandescent temperature, the object itself provides the light source. Therefore, only the receive probe in a through-scan configuration is needed. Conventional bundle or single-fiber probes are limited to about 300 °C because polymeric protective coatings cannot withstand higher temperatures. Advanced packaging is available too, and can extend the temperature range to 480 °C.[9] Special adapters, such as quartz rod extenders, are often required when temperature requirements extend beyond 800 °C. These act as a large

fiber optic to handle the heat. The stiff, large, quartz rods do not require protective coatings.

As mentioned previously, there is a large potential switch application in the machine tool area. Sensors can be used to gauge parts or determine if the cutting tool is present. In almost all situations, a high volume of liquid coolant or airborne contamination flows in the vicinity of the cutting tool. The coolant and the debris can foul the optics by essentially blinding the optical probe.[10,11]

Commercial systems have addressed this problem. The probes can be kept clean even in the presence of high volumes of coolant by using an air-wipe concept as shown in Fig. 8.19. With a slight positive pressure over the end of the probe, coolant and debris are kept off of the optical surface, as shown in Fig. 8.20. The system is further enhanced if a spoiler causes a turbulent swirling airflow, which improves the cleaning action. In normal field applications, most of the machinery that uses cutting tools has compressed air sources in close proximity so that installation is simple.

Widespread use of digital fiber optic switches and counters has been limited due to functionality. Most applications have been limited to absence/presence sensors, since these are the simplest sensors to develop and use. Digital sensing is now expanding to liquid level, temperature, and pressure (see Fig. 8.21).[10]

For the expanded digital sensor, the target provides the sensing function. If a target can be fabricated such that its position or state relative to the probe end is a function of some physical parameter to be sensed, then physical

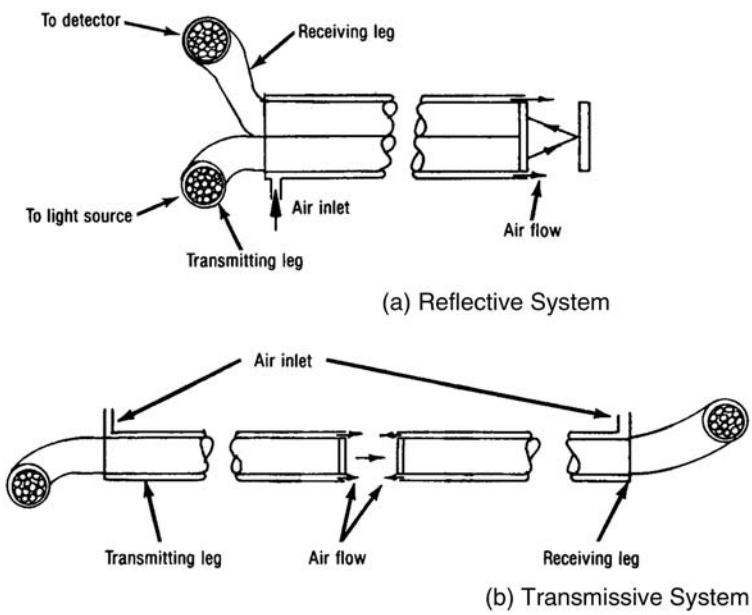

Figure 8.19 Fiber optic sensors with air wipes.

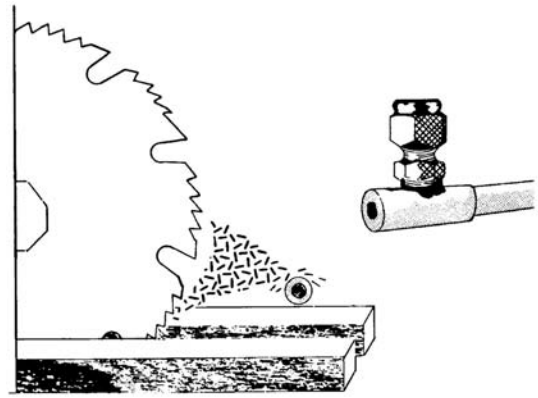

Figure 8.20 Air wipe for dirty environments (courtesy of EOTec Corporation).

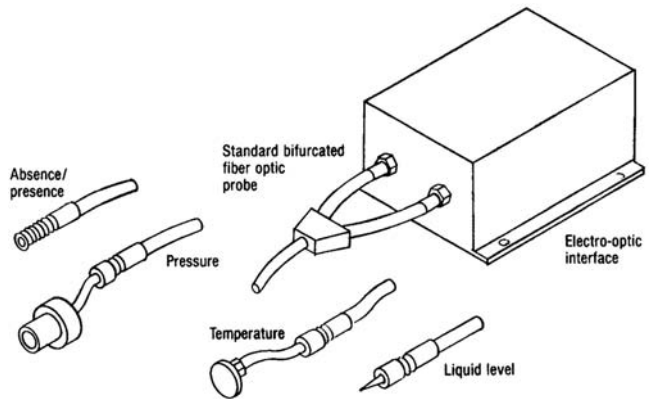

Figure 8.21 Expanded sensor functionality.

property sensors can be fabricated. All of the sensors shown in Fig. 8.21 use a reflective technique.

Consider a reflective bimetal element as one such target. As the surrounding area reaches its set point temperature, the element moves abruptly. The distance between the probe and target shown in Fig. 8.22 changes correspondingly, affecting the amount of light reflected back to the probe, which provides the basis for switching. Pressure sensing via fiber optics is provided by a method analogous to bimetal temperature element sensing. A flexible pressure-sensitive diaphragm with a reflective inner surface varies its distance from the fiber optic probe tip in response to a pressure input, as shown in Fig. 8.23. Using a snap diaphragm, a pressure set point is achieved.

Level sensors are categorized as switches for high/low level and leak detection or as magnitude sensors for actual liquid level. Fiber optic devices have found more applications in the former category.

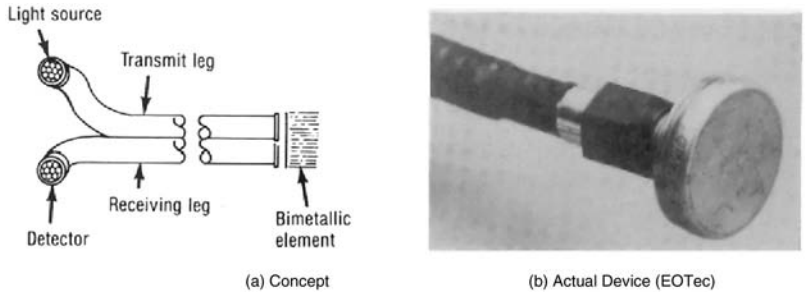

Figure 8.22 Fiber optic temperature switch.

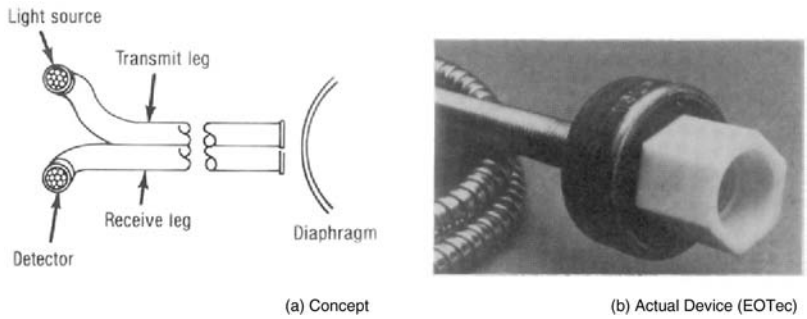

Figure 8.23 Fiber optic pressure switch.

Liquid level is one of the prime process-control parameters, especially in the petrochemical and chemical industries. The explosive nature of many of the processes makes fiber optics especially desirable. Leak detection and fuel level are required in many military applications. The immunity to electromagnetic interference (EMI) and radio-frequency interference (RFI) is the driving force for fiber optic usage in these applications.

An approach to liquid-level sensing uses the concept of total internal reflection, which is affected by changes in the index of refraction of the media surrounding the transmitting core. Commercial fiber optic sensors are available to determine the absence or presence of a liquid using total internal reflection approaches.[12]

An example of a sensor using refractive-index change to detect the presence of a liquid functions by transmitting light to a prism, typically quartz (refractive index = 1.46). In the medium of air (refractive index = l.0), the prism acts as a fiber optic, with the air being the cladding. The prism tip is shaped to promote back reflection, which is detected. In the presence of a liquid, which has a higher index of refraction than air, much of the light is not totally internally reflected, but is passed into the liquid. Figure 8.24 shows the concept graphically.[13] Figure 8.25 shows a prism at the end of a fiber optic probe, with the transmission and receiving legs being low-loss optical fibers that have remotability.[14]

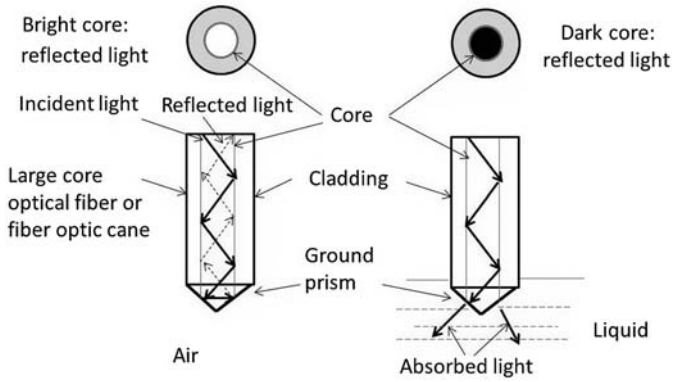

Figure 8.24 Refractive-index change in a liquid level sensor.

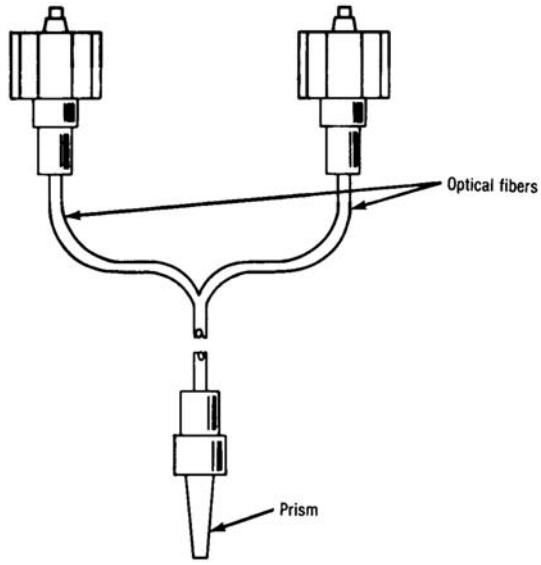

Figure 8.25 Optical fibers used to remote a prism-type refractive-index change liquid-level sensor.

Sensors of this type are point sensors. They are ideal for high/low monitoring as well as leak detection. A very small amount of liquid is required for switching. To achieve multilevel sensing, several sensors of various lengths can be ganged together. Using a similar principle, a fiber can be inserted in a U configuration with the cladding removed.[15] The refractive index change associated with liquid immersion causes light leakage, as shown in Fig. 8.26.

The sensors described so far are used in a digital mode to determine the absence or presence of liquid. However, since the sensor is analog in nature and provides an output that is a function of the refractive index of the liquid,

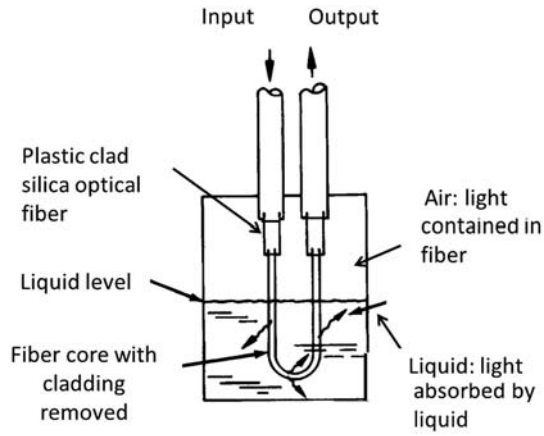

Figure 8.26 Refractive-index change liquid-level sensors in U configuration.

Table 8.3 Output for various liquids using fiber optic/prism refractive-index change sensor.

Medium	Relative Output
Air	1.00
Water	0.11
Isopropyl alcohol	0.07
Gasoline	0.03
Milk	0.20

the sensor can discriminate between liquids. The outputs for various liquids and air are given in Table 8.3.

An example application of such a sensor is in leak detection in a tank farm. The sensor threshold can be set so that water does not trigger the sensor, but gasoline gives an alarm condition.

With the exception of the liquid-level switch, the devices used for physical property sensors, which were discussed in the previous examples, are optomechanical in nature.[16,17] Intrinsic fiber optic physical property switches are also possible. These devices do not require the use of a mechanical transducer. A multitude of materials will change their optical properties with environmental changes and can interact with a transmissive or reflective fiber optic system. Currently, most devices are experimental, but a few concepts are worth mentioning. For example, polymeric materials can abruptly change transmission and/or reflectivity at rather precise temperatures and can function as the basis for a temperature switch. In addition, liquid crystals are sensitive to temperature and pressure with abrupt transmission changes and potentially can function as temperature or pressure switches. Any material that undergoes a physical change of state at a given temperature, pressure, or chemical level is a potential switch component.

References

1. Anonymous, "MicroSwitch," MP Series Catalog (1984).
2. W. E. Damuck, Jr., "A comparison of photoelectric and fiber optic sensors," *Proc. ISA* **39**, 303–12 (1984).
3. D. A. Krohn, *Fiber Optic Sensors: Fundamentals and Applications*, 3rd Edition, Instrument Society of America, Research Triangle Park, NC (2000).
4. Anonymous, *Photoelectric Control and Reference Manual*, Banner Engineering (1983).
5. R. W. Fayfield, "Fiber optics and photoelectric sensing, a good combination," *Instrumentation and Control* **55**, 45–49 (1982).
6. Veeder Root, *Photoelectric Sensors - Specification Requirements* (1983).
7. J. Streckenbach, "A short course in photoelectronic sensors (Part II)," *Sensors* **7**, 48–53 (1990).
8. D. A. Krohn, "Fiber optic sensors in industrial applications: an update," *Proc. ISA* **38**, 877–90 (1983).
9. Anonymous, "Products and applications," www.bannerengineering.com (2013).
10. D. A. Krohn, "Fiber optic sensors," *IEEE Solid-State Sensors Workshop* (1986).
11. D. A. Krohn, "Field experience with fiber optic sensors," *Proc. ISA* **40**, 1051–61 (1985).
12. Anonymous, "Fiber optics and liquid level sensors," www.honeywell.com/sensing, (2013).
13. J. Rakucewicz, "Fiber optic methods of level sensing sensors," *Sensors*, 5–12 (1986).
14. R. S. John, "Fiber Optic Liquid Level and flow Sensor System," U.S. Patent 4,320,394 (1982).
15. S. Dokas, "Active components in fiber optic sensors," *Sensors*, 20–34 (1987).
16. Anonymous, *Fiber Optic Sensors: A Complete Reference Manual*, EOTec (1986).
17. R. F. Coulombe, "Fiber optic sensors–catching up with the 1980s," *Sensors* **1**(12), 5–8 (1984).

Chapter 9
Displacement Sensors

9.1 Introduction

Fiber optic displacement sensors are multipurpose devices that find uses in a broad range of industrial, automotive, aerospace, military, and medical applications. Optical-fiber-based displacement sensors are attractive because of their EM and RF immunity, i.e., their capability to operate in extreme environments—from cryogenic to elevated temperatures—under vacuum or in the presence of strong vibrations. For such reasons, these devices are commonly used in aeronautic and aerospace applications, nuclear power plants, and robotic systems, and for civil engineering and geotechnical measurements, and many other harsh or hazardous location type applications.

In general, such sensors are most typically used as devices to measure and/or monitor relative movement (displacement). However, they can also be utilized as sensors for position, thickness, concentricity, alignment, proximity, rotation, torque, etc. Furthermore, depending on their design and configuration, they can perform their measurement via direct contact or non-contact.

Several different techniques are commonly used in the design of fiber optic displacement sensors. Among the most common are the following:

- Reflective technology
- Microbending technology
- Modulating technology
- Fabry–Pérot technology
- Fiber Bragg grating technology

Next, we shall review each one of the types and provide more details on their design features and characteristics.

9.2 Reflective Technology

The basic concept of a reflective sensor is shown in Fig. 9.1. The sensor is composed of two fiber optic legs (bundles or single fiber). One leg transmits light to a reflecting target, and the other leg traps reflected light and transmits

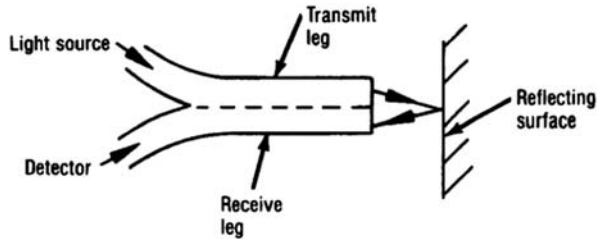

Figure 9.1 Reflective fiber optic sensor.

it to a detector. The intensity of the detected light depends on how far the reflecting target is from the fiber optic probe. The basic response curve is shown in Fig. 9.2.[1 5] The curve shows a maximum with a steep linear front slope and a back slope that follows a $1/R^2$ dependence, where R is the distance between the tip of the fiber optic probe and the reflecting surface.

The curve is easily understood if the geometric optics are considered. Light exits the transmitting fibers in a solid cone defined by the numerical aperture. The spot size hitting the target is given by (assuming the fiber is small in relation to R)

$$D = 2R\tan\theta, \tag{9.1}$$

where θ is the half-angle between the normal to the fiber exit surface and the exit divergence cone (numerical aperture), and D is the spot diameter.

Since the angle of reflection equals the angle of incidence, the spot size that impinges back on the fiber optic probe after reflection is twice the size of the spot that hits the target initially. As the distance from the reflecting surface increases, the area of the spot increases in a manner directly proportional to R^2 (see Fig. 9.3). The amount of detected light is inversely proportional to the spot area or $1/R^2$, since the receiving fiber is fixed in size and less of the fiber

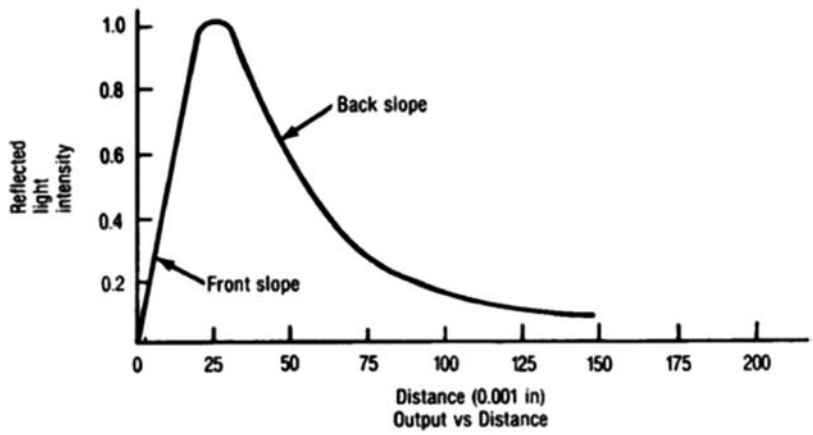

Figure 9.2 Reflective fiber optic sensor response curve.

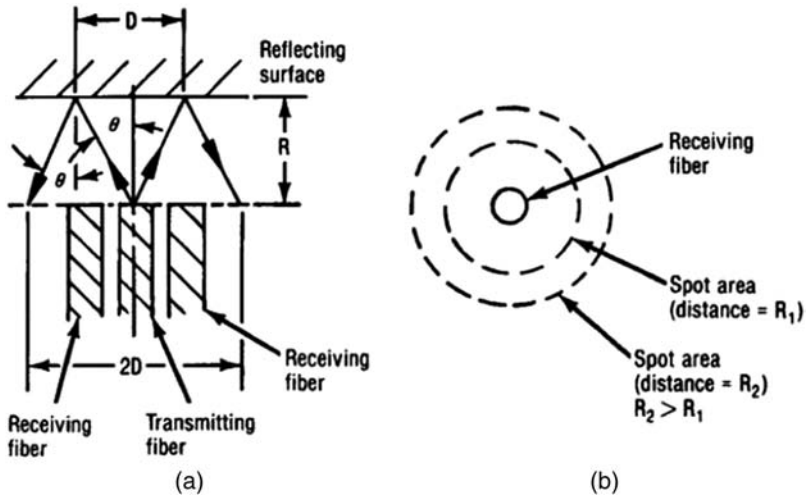

Figure 9.3 Back slope considerations. (a) Fiber target geometry and (b) reflected spot area.

face intersects the returning light as it expands with distance. As the probe tip comes closer to the reflecting target, a position is reached at which the reflected light rays are not coupled into a receiving fiber. At the onset of this occurrence (position 2), a maximum forms, which drops to zero as the reflecting surface contacts the probe, as shown in Fig. 9.4.

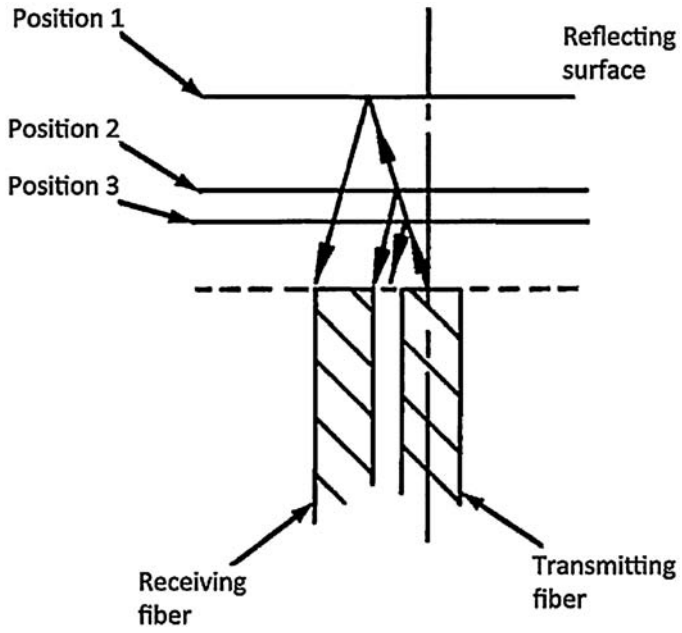

Figure 9.4 Front slope considerations.

It is clear from an explanation of how the curves are generated that the output (transfer function of the displacement sensor itself) can be tailored to have specific displacement sensitivities and operating ranges by using various optical configurations of different light sources, fiber types, fiber bundle shapes and sizes, as well as different arrangements of the transmitting and receiving fiber bundles, as shown in Fig. 9.5(b). For example, the random configuration has, on the average, the closest transmit fiber to receive fiber spacing. Therefore, at closer target distances, it would have higher sensitivity, and lower sensitivity at longer distances. The fiber pair probe has the largest transmit fiber to receive fiber spacing (center-to-center) and, therefore, is the least sensitive at close target distances. It should be noted that in a single-fiber configuration the front slope disappears, because when the reflecting surface is approached, light continues to be reflected into the same fiber, which is functioning in both transmit and receive modes. This is true even to the point of contact. The front slope also disappears if a fiber optic lens (SELFOC® Nippon Sheet Glass) is added to the probe, since the lens prevents the probe tip from coming close enough to generate the front slope. The output of a fiber-pair probe with a SELFOC lens is shown in Fig. 9.6. A SELFOC [or graded-index (GRIN)] lens is a fiber optic, self-focusing lens.

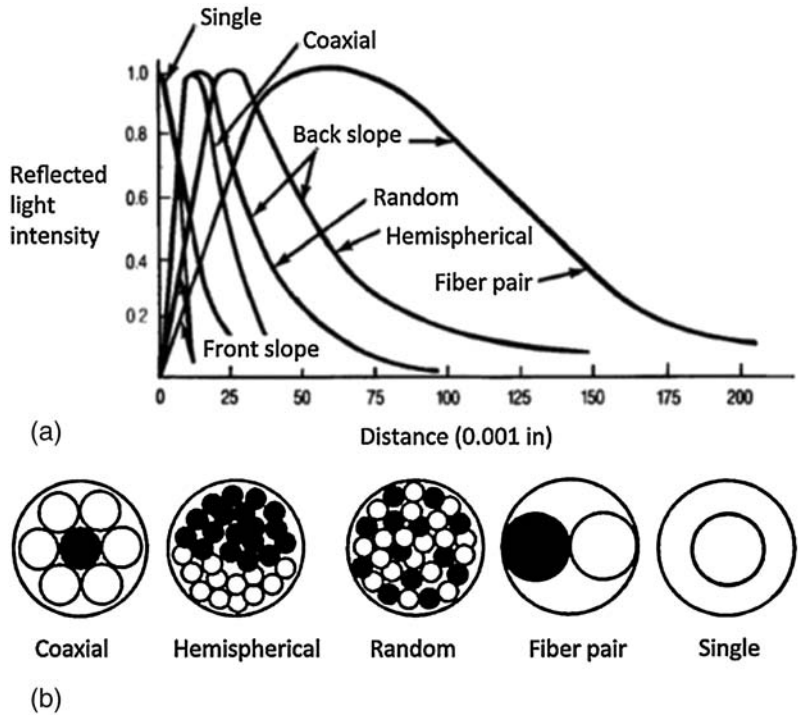

Figure 9.5 (a) Reflective fiber optic sensor response curves for (b) various bundle configurations.

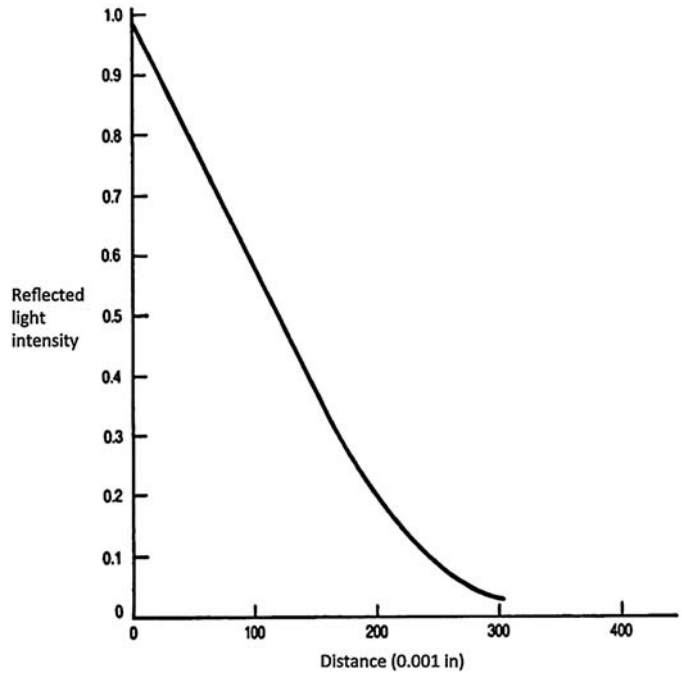

Figure 9.6 Response curve for fiber pair with a SELFOC lens.

The fiber's numerical aperture is a critical parameter in the response of the sensor to distance. If the fibers composing a bundle have an increasing numerical aperture, the dynamic range of the sensor is decreased while the sensor sensitivity is increased. Consider that as the numerical aperture is increased, the positions in Fig. 9.4 move closer to the target. This effect applies to both multiple- and single-fiber probes.[6]

Dual probes provide a means for increased sensitivity. Consider the arrangement in Fig. 9.7.[7] The probe distances are set so that the reflected intensity is the same for probe A in the front slope and probe B in the back slope. As the target moves closer, the detected intensity for probe A decreases while the detected intensity for probe B increases.

The difference between the two readings provides a larger output than either probe used singly and, therefore, increased sensitivity. In addition, displacement direction information is obtained as well as magnitude. A similar effect can be obtained if the probes are equidistant from the target but on opposite sides, as shown in Fig. 9.8. Depending on whether the probes are both set on the front or the back slope, if the target moves in either direction, the measured displacement of one probe will increase while the other decreases. The graph in the lower portion of Fig. 9.8 shows the differential output (output of probe A minus output of probe B) for the probes positioned on the front slope.

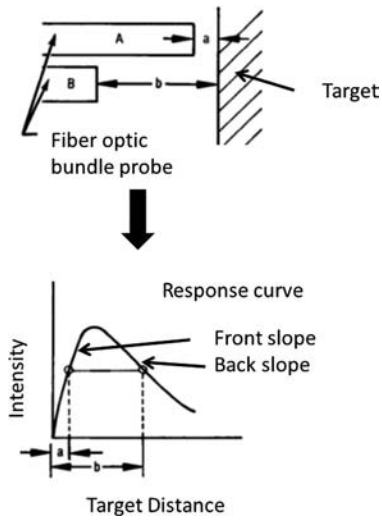

Figure 9.7 Dual reflective probes on the same side of the target.

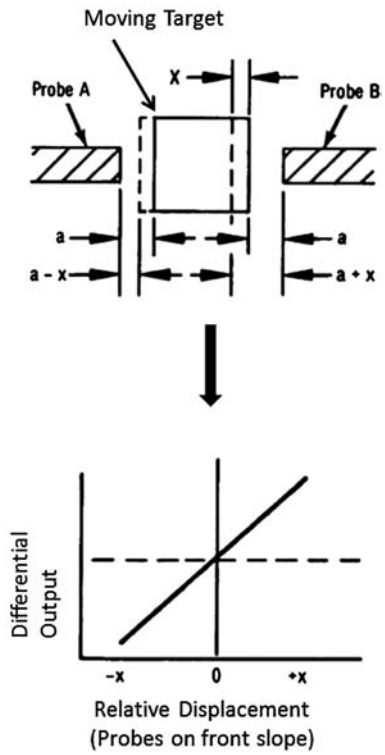

Figure 9.8 Dual probes on opposite sides of the target.

The major disadvantage of the sensors described is the limited dynamic range. While sensitivities approaching 1 μin. are possible, the dynamic range is limited to about 0.2 in. Many applications require that the sensor be used at a much greater distance (up to several inches) from the reflecting target. Using a lens system in conjunction with a fiber optic probe, the dynamic range can be expanded to 5 or more inches,[1,2] although the sensitivity will be correspondingly reduced. Figure 9.9 gives the response curve for various focal length settings using a random probe. With the exception of the curve for an infinite focal length, the curve now has two maxima. The explanation for the trough at the focal length is straightforward. The object is in exact focus at that point, and light from a particular fiber has a very small spot size and reflects back on itself; therefore, the detected intensity is minimized. As the object moves in and out of focus, the defocused spot couples more reflected energy into an adjacent receiving fiber, increasing the level of detected light. The highest sensitivity is on the front slope of the trough. The sensitivity and dynamic range can be adjusted by changing the focal length of the lens. In essence, it is possible to be 3 in. from the surface and detect movement to an accuracy of 0.001 in. over a dynamic range of 1 in. using a 3-in. focal length lens.

There are some difficulties with reflective fiber optic displacement sensors. The best performance is obtained with specularly reflective surfaces and objects, characterized by finely ground, lapped, mirrored, or polished surfaces that reflect the rays with greater intensity and uniformity. Furthermore, perpendicularity is also critical, and angular deviations should be kept to a minimum, since the sensor integrates distance data with changes in reflectivity and angularity of the target. In an effort to characterize the behavior, a microfinish comparator was used in which lapped surfaces were prepared by cutting tools of varying coarseness.

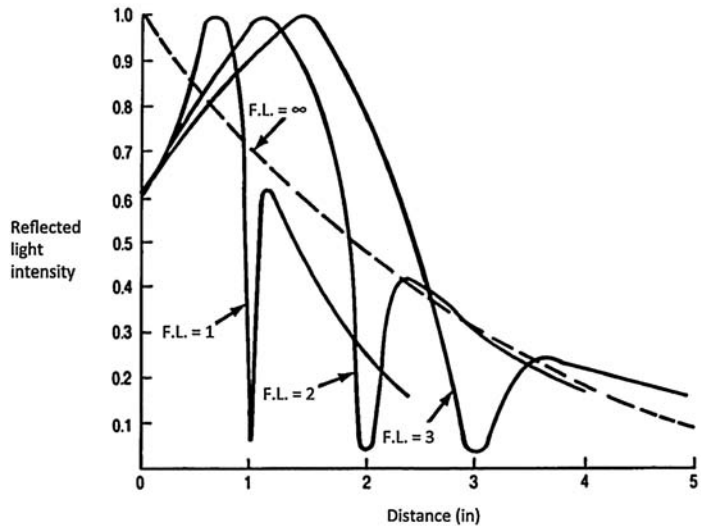

Figure 9.9 Response curves for a reflective sensor coupled with a lens system for various focal lengths (F.L).

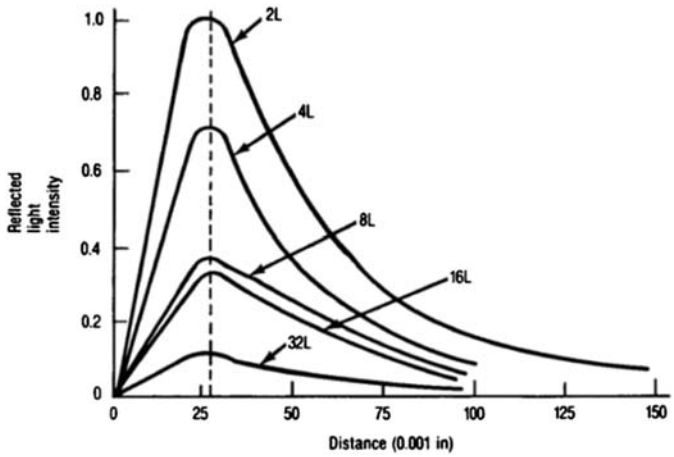

Figure 9.10 Effect of target reflectivity changes.

A $2L$ surface is nearly specular. The diffuse nature of the surfaces increases from $4L$ to $8L$ to $16L$, with $32L$ being the most diffuse. A plot of reflected light intensity versus distance for different surfaces is given in Fig. 9.10. As the surface becomes rougher, the reflected light intensity drops substantially. However, the general shape of the curve remains constant with the maximum fixed at a given distance. If the same target is always being used in an application and the surface remains clean, the reflectivity variations are eliminated. On the other hand, if different surfaces are being measured, a reference probe will be required to compensate for the reflectivity variations.

The sensor is also sensitive to rotation of the reflecting target, as shown in Fig. 9.11. The errors appear to be small ($\pm 3\%$) for rotations of ± 5 deg about the normal. Decreases in light intensity become quite pronounced at large angles.

A major advantage of a reflective fiber optic sensor is that contact is not required for measurement. There are applications, however, in which surface reflectivity can change due to contamination, so that a closed system is required. Using an optical version of a linear voltage displacement transformer (LVDT), contact of the part to be measured is required by the mechanical plunger, but all other problems are eliminated. The optical sensing occurs in a closed environment in which the sensor, through reflections at the mirror, tracks the movement of the plunger (Fig. 9.12).

These reflective displacement sensors can also be operated under liquids. The response of the sensor under a given fluid is different from that in air, but the general response will be similar, except that it will have a shifted peak and different slopes for its sensitivities. The sensor would need to be tested and calibrated for operation under a given fluid.

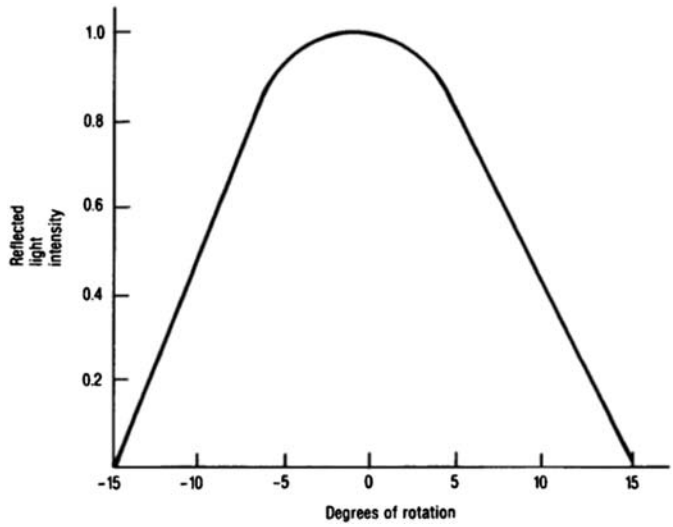

Figure 9.11 Effect of target angularity.

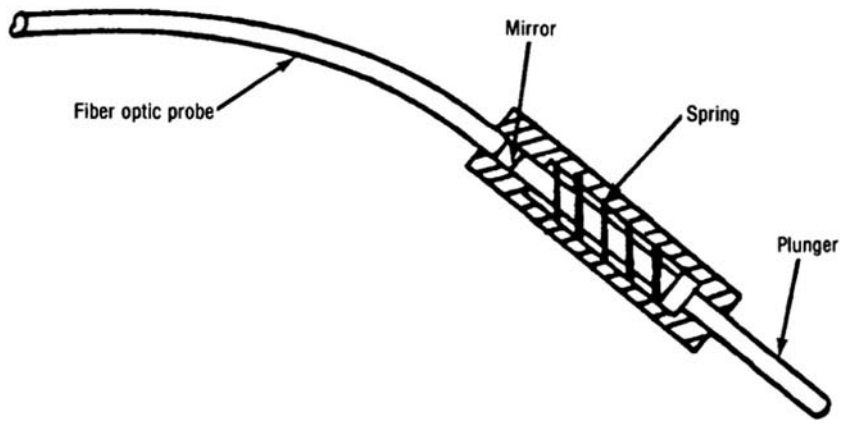

Figure 9.12 Optical version of an LVDT.

Similarly, the expected operating temperature range varies and will dictate the type of materials that the sensor metal tips, adhesives, and specific fiber types would need to be, as well as the protective cable jackets.

9.3 Microbending Technology

All optical fibers will radiate energy when bent.[8] The energy distribution in a bent fiber is shown in Fig. 9.13. Theoretically, the energy field in the cladding extends to infinity. Therefore, at some radiation distance X_r, the energy is

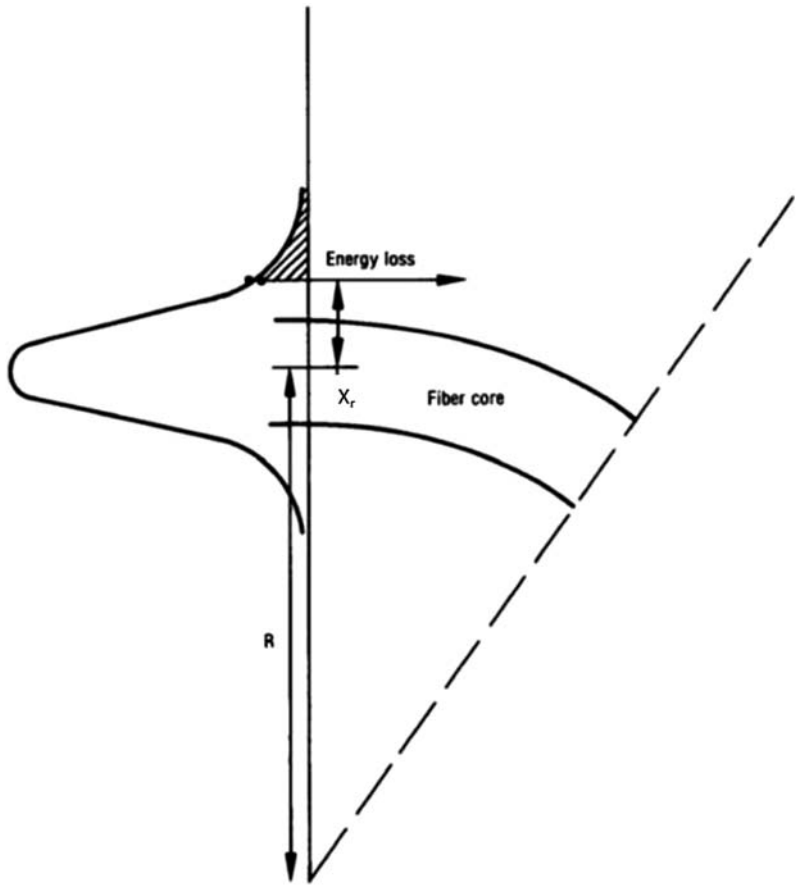

Figure 9.13 Energy distribution in a bent fiber.

implied to propagate at a velocity greater than the speed of light due to the longer travel path. Since this is not possible, the waveguide effect ceases. Subsequently, the energy is lost to radiation.

The effect of microbending is shown in Fig. 9.14.[9] As the perturbing bend points contact the fiber, energy is lost.

The parameters that influence microbending loss include fiber numerical aperture, core size, core-to-cladding ratio, and periodicity of fiber deformation. When a periodic microbend is introduced, mode coupling occurs between modes with longitudinal propagation constants β and β_1.[10–12] Therefore,

$$\beta \quad \beta_1 = \frac{2\pi}{\Lambda} \tag{9.2}$$

where Λ is the wavelength of periodic bending. The difference in propagation constant for adjacent modes is given by

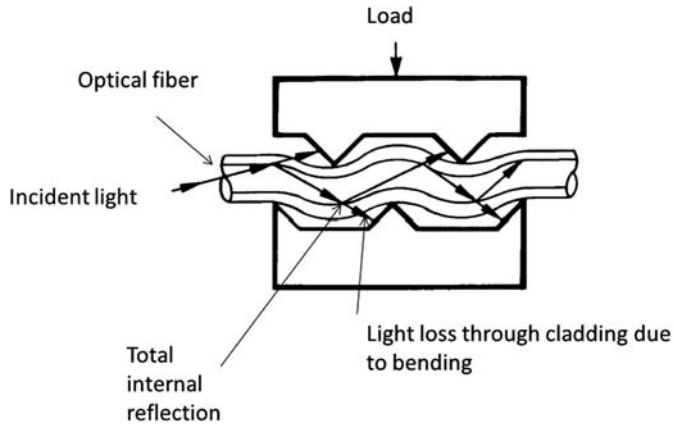

Figure 9.14 Light leakage as a result of microbending.

$$\beta_{m+1} \quad \beta_m = \frac{2.83 \text{ NA } (m)}{an_1(M)}, \tag{9.3}$$

where NA is the numerical aperture, n_1 is the core refractive index, a is the core radius, m is the modal group label, and M is the number of modal groups. Equating Eqs. 9.2 and 9.3 and solving for Λ gives:

$$\Lambda = \frac{an_1(M)}{1.414 \text{ NA}(m)}. \tag{9.4}$$

Higher-order modes M are coupled with a small Λ, and lower-order modes m are coupled with a large Λ.

Microbending transducers are based on coupling core modes to radiated modes. The greatest sensitivity occurs when the highest-order core modes are made to radiate. This situation can be mathematically approximated when $M = m$. Therefore, Eq. 9.4 is reduced to

$$\Lambda = \frac{an_1}{1.44 \text{ NA}}. \tag{9.5}$$

As the numerical aperture increases, the periodic perturbation spacing must decrease for maximum sensitivity. As core size decreases, the spacing must also decrease. Generally, high-NA fibers or small-core fibers guide light more strongly and require more severe bending to lose light than low-NA fibers. For a given fiber diameter, increases in the core-to-cladding ratio increase microbending sensitivity, since, for a given displacement, the large core will have more bending and, therefore, more light leakage.

It has been shown that light loss is strongly dependent on the microbending periodic perturbation Λ. As this period approaches the magnitude of the ray period of light propagating in the fiber, a strong resonance is possible with the light loss showing a maximum.[13] Figure 9.15

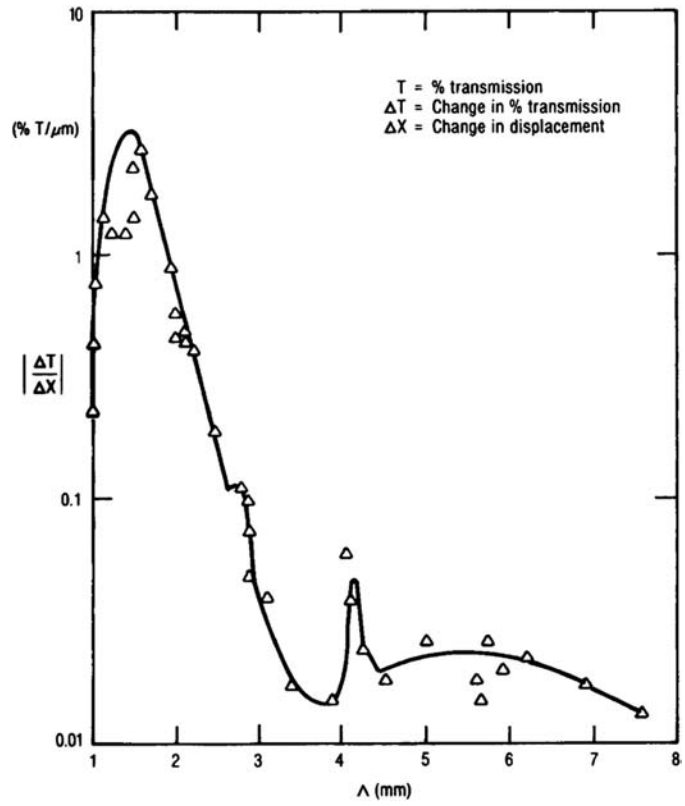

Figure 9.15 Displacement sensitivity versus Λ (courtesy of IEEE, © 1982).

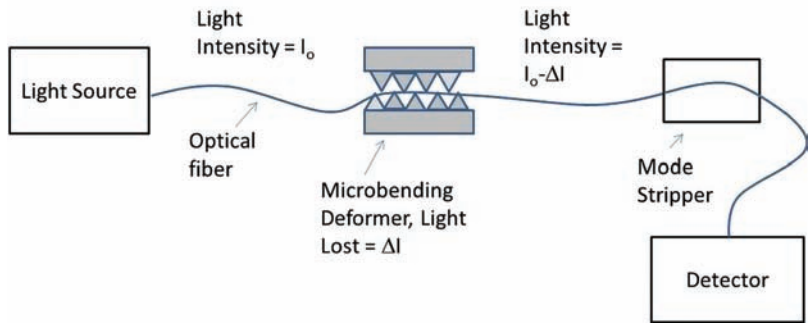

Figure 9.16 Typical bright-field microbending sensor configuration.

plots the change in transmission relative to the change in displacement, $\Delta T/\Delta X$ versus Λ. The data was obtained with a step-index fiber under conditions of constant load using the fixture in Fig. 9.16. The primary peak corresponds to the periodicity that couples the highest-order modes to radiant modes. As the period increases, the sensitivity decreases, corresponding to the difficulty associated with coupling low-order modes.

The length of a fiber in a microbending sensor configuration affects sensitivity. It has been demonstrated[14] that as the fiber increases in length, the sensitivity decreases. This observation can be explained by the fact that as the fiber length increases, higher-order modes are lost even without a microbending perturbation. Upon microbending, the high-sensitivity leaky modes are already depleted, and microbending sensitivity is diminished. The length dependence will be a factor in distributive sensors in which the sensing fiber can be quite long.

Coatings play a critical role in microbending. Coatings that allow cladding modes to be reradiated back into the core minimize light loss and decrease sensitivity for a fiber of a specific length. However, the length over which the sensor can function is increased. As an example, silicone coatings have considerably more reradiated modes than UV elastomers and are much less sensitive to microbending. Absorbing coatings that prevent reradiated modes provide high sensitivity to microbending.

Microbending sensors can be divided into two categories:[15] bright field and dark field. Bright-field sensors measure the light level transmitted in the fiber, the change being associated with microbending losses. A typical bright-field configuration is shown in Fig. 9.16. Dark-field sensors measure the light lost through the fiber cladding. Dark-field configurations are shown in Figs. 9.17 and 9.18.

Using the system depicted in Fig. 9.16, light was injected into the fibers at different angles. The microbending fixture was under constant load.

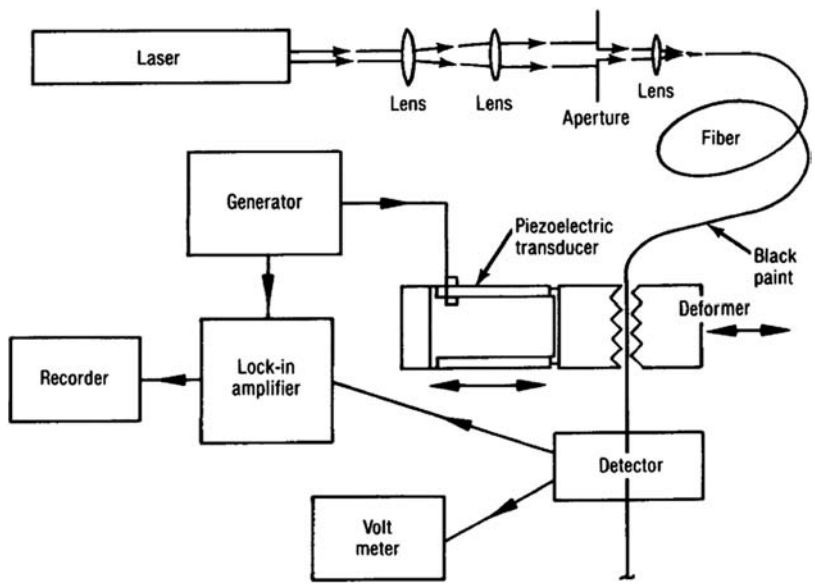

Figure 9.17 Experimental setup for studying displacement microbending sensor (courtesy of the Optical Society of America).[10]

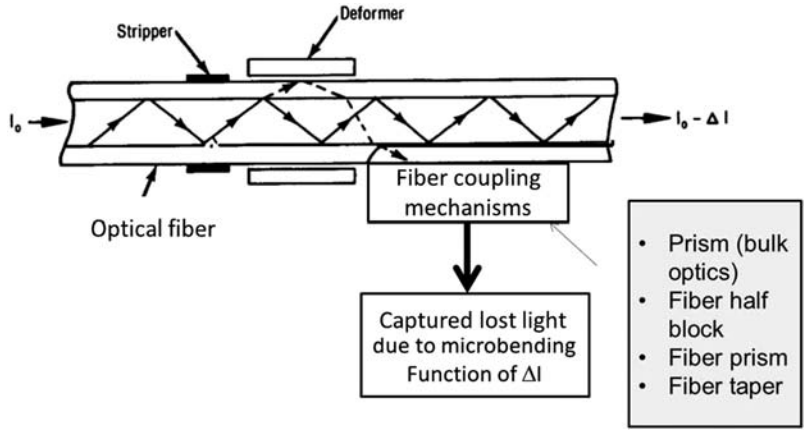

Figure 9.18 A dark-field microbend intensity-type fiber optic sensor.

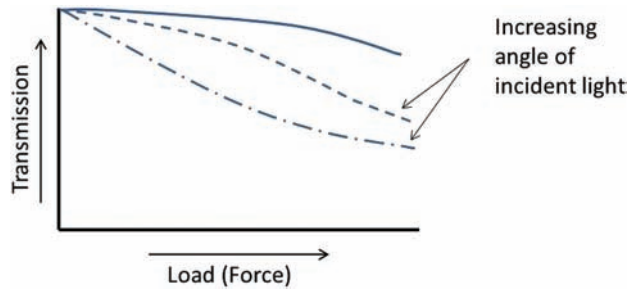

Figure 9.19 Microbending loss versus angle of incident light.

Therefore, the fiber microbending is constant. It is clear that the higher incident angle light, which corresponds to higher-order modes, resulted in greater microbending loss, as shown in Fig. 9.19.[16]

One major potential application for microbending sensors is displacement measurement. Figure 9.20(b) shows transmission versus displacement using the bright-field mode. As discussed in Chapter 3, the response curve has three distinct regions. In the first region, the compliant coating absorbs the initial displacement movement, and the fiber bending is partially limited. The small bending level results in only the leakiest modes radiating. The second region gives a linear response over about 60% of the transmission range. This region is normally used for sensing. As the displacement further increases, light depletion in the higher-order modes occurs, and sensor sensitivity is greatly reduced.

It is anticipated that in the dark-field mode the collection efficiency is greatly reduced. Therefore, the response curve is similar in shape, but the mirror image is reduced by some light-collection efficiency scale factor, as shown in Fig. 9.21.

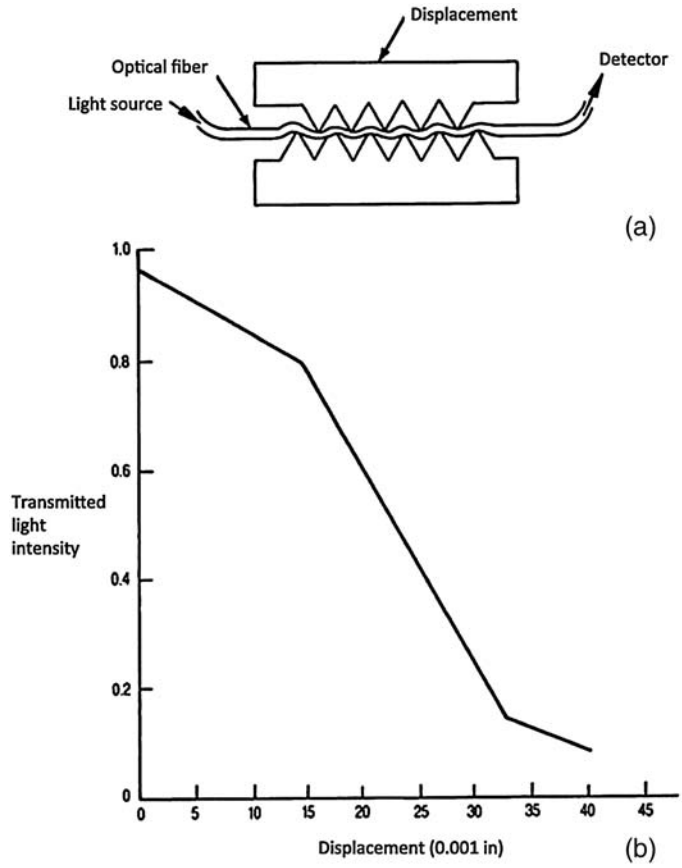

Figure 9.20 (a) Microbending-sensor arrangement transmission versus (b) displacement (bright-field microbending).

A major consideration in microbending sensors is stability. Most fibers are coated with a polymeric material as a protective mechanical buffer. It has been observed that such coatings can flow under heavy loads and/or increased temperature. As a result, accuracies are limited to no better than 1% with potential hysteresis problems. Advances in the use of metallized coatings may reduce this problem.

Microbending sensitivity is a function of several fiber parameters, including numerical aperture, core size, core-to-cladding ratio, length, coating, reradiation, and coating rheological behavior. Figure 9.22 shows the light loss versus bending for several commercial fibers. In general, high-NA fibers with silicone or hard polymerical (fluorinated) coatings exhibit the lowest sensitivity and are ideal for leads to and from the point of sensing. Lower-NA fibers coated with UV elastomers show high microbending sensitivity. While the data in Fig. 9.22 is for macrobending effects (large bend diameter), the observation is pertinent to microbending.

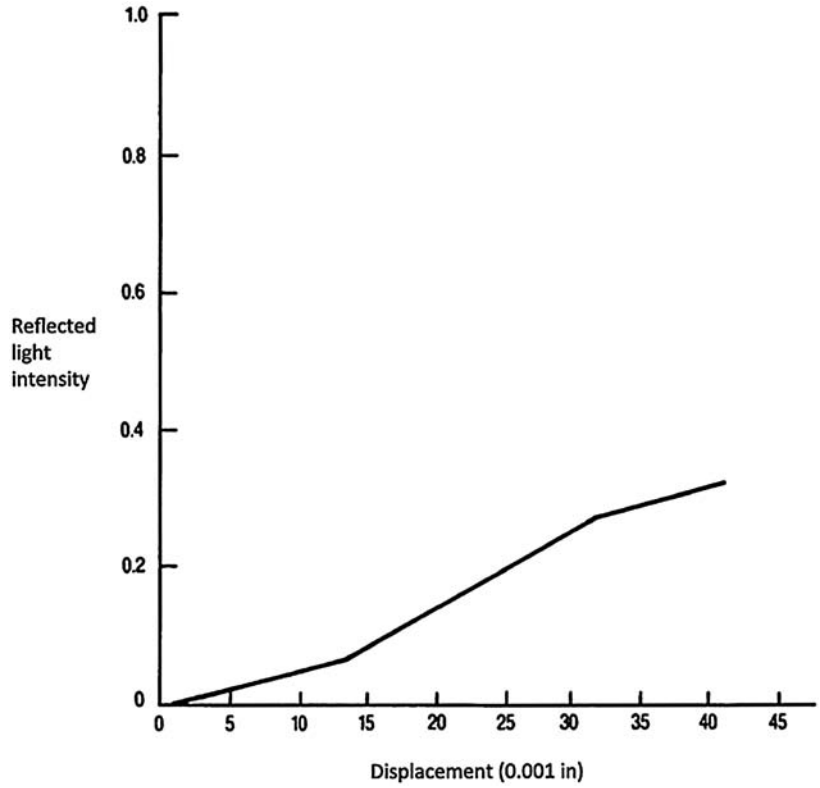

Figure 9.21 Transmission versus displacement (dark-field microbending).

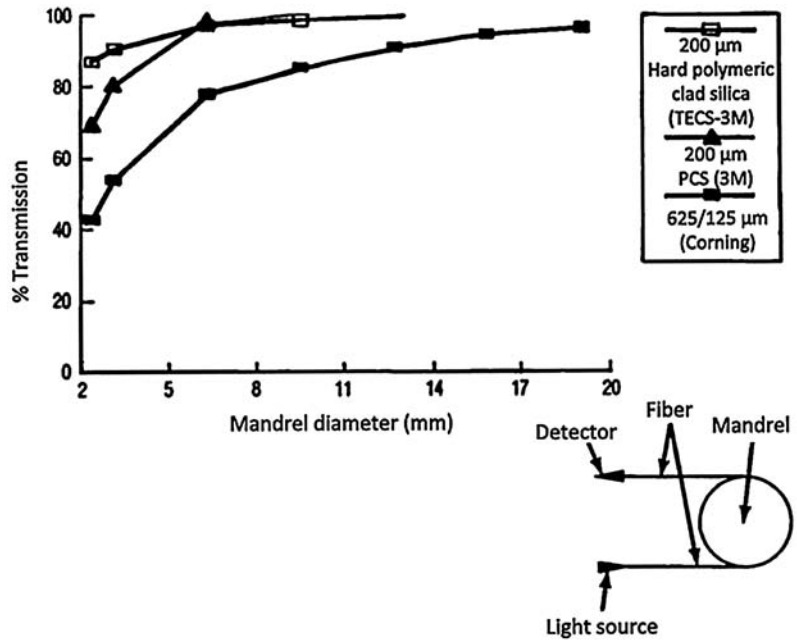

Figure 9.22 Bending loss for various commercial optical fibers.

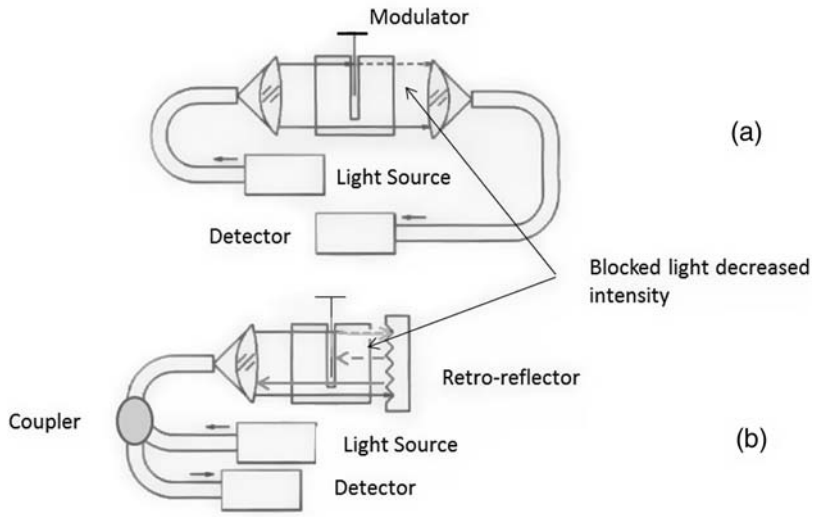

Figure 9.23 Schematic of a modulating type of fiber displacement sensor. (a) Transmissive mode and (b) reflective mode.

9.4 Modulating Technology

As shown in Fig. 9.23, modulating displacement sensors perform their function by modulating the intensity of the light via a movable device that is connected to the object thats displacement is to be monitored. The modulating device can be a shutter, a neutral-density or interference filter, a reticle, or something similar. The device can operate either in transmission or reflection mode. A practical problem with such devices is the optical coupling, which may require lenses as well as precision alignment of the components to ensure adequate light throughput.

9.5 Fabry–Pérot Technology

Fiber Fabry–Pérot interferometers have also been exploited as transducer elements to develop fiber displacement sensors. [17] Most commonly, a thin film Fizeau interferometer (TFFI) or a precision, tapered glass wedge are used as the sensing element. The TFFI or glass wedge act as a spatially varying Fabry–Pérot cavity, whereby the cavity gap separation varies along its length, which coincides with the axial direction of displacement (or position) measurement. Perpendicular to this cavity is a multimode fiber optic tip, which couples light in and out of the variable cavity as it travels past the tip. Figure 9.24 shows a photo of an actual commercial device. These displacement sensors can have travel strokes of up to 30 mm with a resolution of approximately 1 μm.

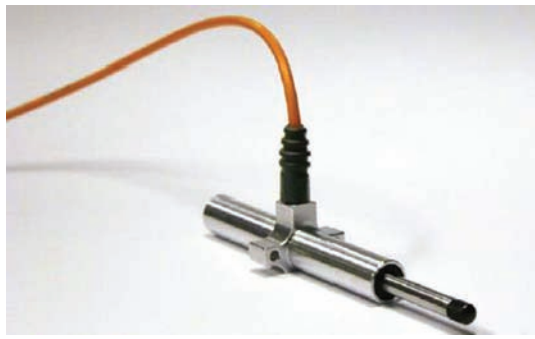

Figure 9.24 Aspect of a commercial Fabry–Pérot fiber optic displacement sensor (courtesy of Opsens).

9.6 Bragg Grating Technologies

Bragg gratings can be used as displacement sensors by measuring the strain induced in the grating along its axial direction,[18–20] thus producing a wavelength shift that is proportional to the applied displacement (or position). For a typical silica fiber, 1% strain is within the proof-test level. For a 1-m fiber, the strain level corresponds to 1 cm of displacement. The practical limit is about 2% strain or a 2-cm displacement limit. To scale this up to measure displacements on the order of several centimeters, while shortening the length of measuring fiber needed, designers have resorted to the use of spring-loaded mechanisms.

For instance, Fig. 9.25 shows a schematic of a FBG-based displacement sensor that uses a spring-loaded sliding rod. One end of the fiber grating is fixed to the body of the sensor, which will also serve as the anchoring or reference point of the device. The other fiber end is connected to a spring via a metal wire that is itself connected to a sliding rod that will ultimately be connected to an external point or the object under measurement. The effective force—and thus the strain—seen by the FBG element is adjusted by

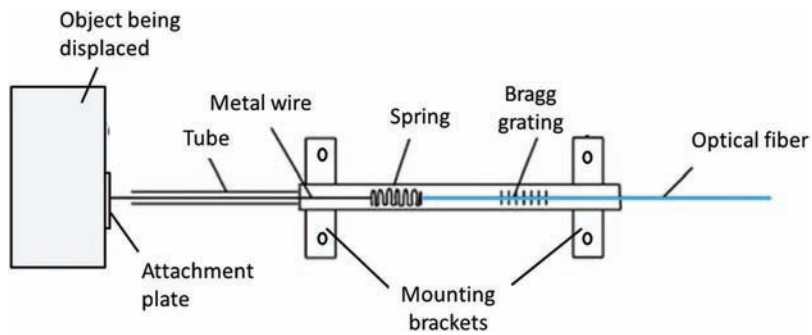

Figure 9.25 A schematic of a FBG-based displacement sensor that uses a spring-loaded sliding rod.

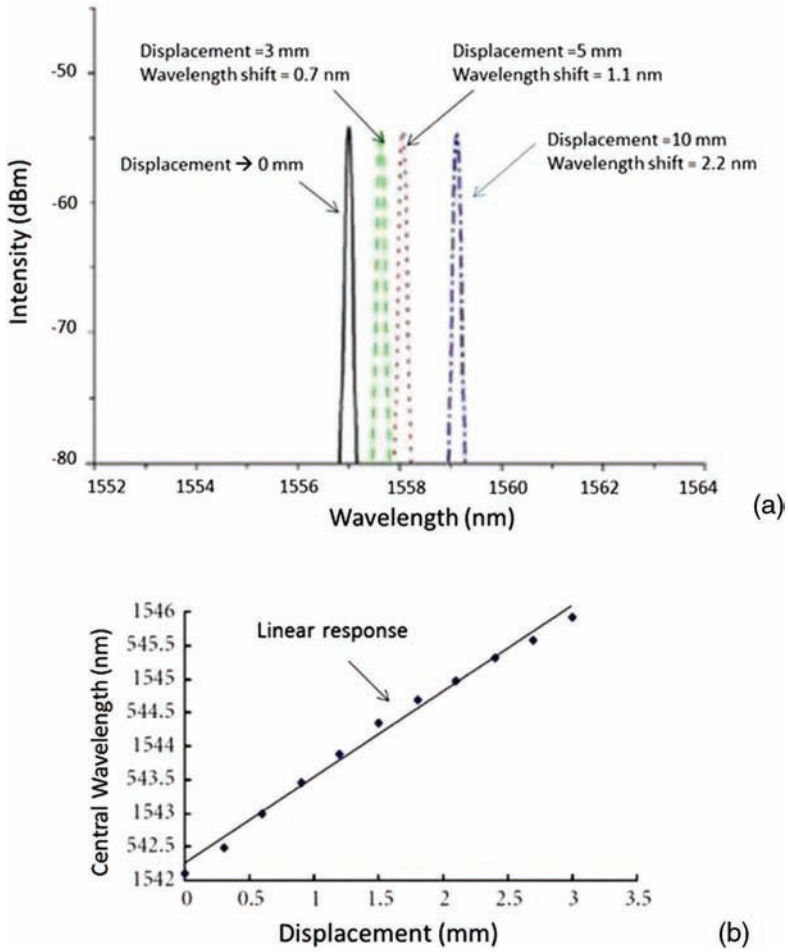

Figure 9.26 (a) Spectral shift response and (b) wavelength versus displacement sensitivity curve for the sensor in Fig. 9.25.

the spring constant. As the sliding rod moves out, it strains the FBG, resulting in a spectral shift of its peak wavelength toward longer wavelengths. The device is very linear and repeatable, and can operate in uni- or bi-directional modes as shown in Fig. 9.26. Typically, such displacement sensors have a stroke travel of <10 cm, with a resolution of 0.05% full scale. To correct for possible temperature effects, a second grating is connected in series and isolated from any mechanical strain.

For larger displacement range measuring capability, other mechanical artifacts are used. For example, instead of connecting the fiber grating to a spring-loaded rod, it is strained by a rotating cam and roller mechanism that rotates in proportion to the length of a flexible steel wire being pulled. Such cable displacement sensors have displacement ranges on the order of 50 cm to 100 cm.

9.7 Applications

Fiber optic displacement sensors are commonly used in applications where there is a harsh environment, or an intrinsically safe sensor is needed, and/or the available space is too small for a conventional sensor to be fitted. These devices are used in the measurement of displacement, position, or vibration. Some of the most common applications are: in the modal analysis of computer disks and disk drive mechanisms; surface finish analysis; edge detection of films, tapes, and webs; defect detection of thin films and layers; defect detection of bearings and shafts; turbine blade tip clearance; cryogenic pump monitoring; and many others.

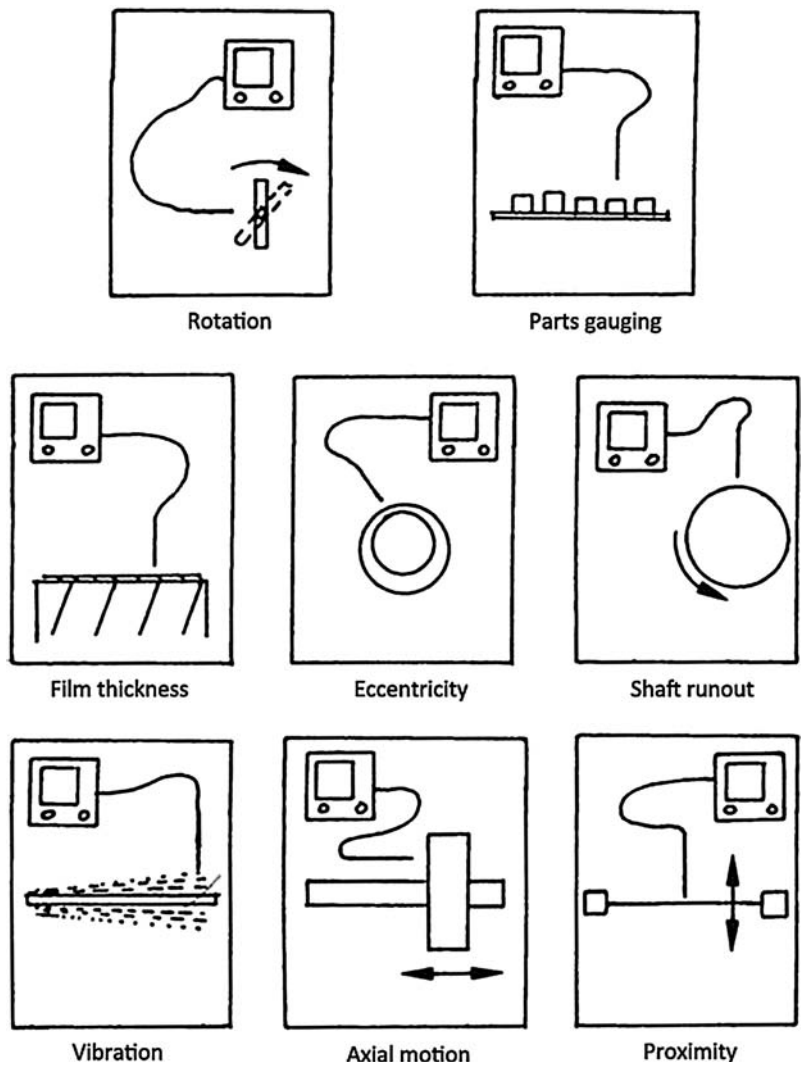

Figure 9.27 Displacement sensor applications.

As single-point sensors, reflective or microbending displacement/position sensors have a wide range of applications. Figure 9.27 shows several applications using a reflective sensor. Measurement of axial motion, proximity, eccentricity, and shaft runout are straightforward displacement applications. Vibration measurement normally requires a high-speed electro-optic interface to record the vibration "signature."

Film thickness measurement is somewhat more complex in that the reflective return signal from a target is perturbed by the presence of a film. The change in signal associated with the film can be correlated with its thickness. Parts gauging uses the analog displacement nature of the sensor output to discriminate high/low objects. The last application shown is for rotation. As indicated previously, displacement sensors are sensitive to

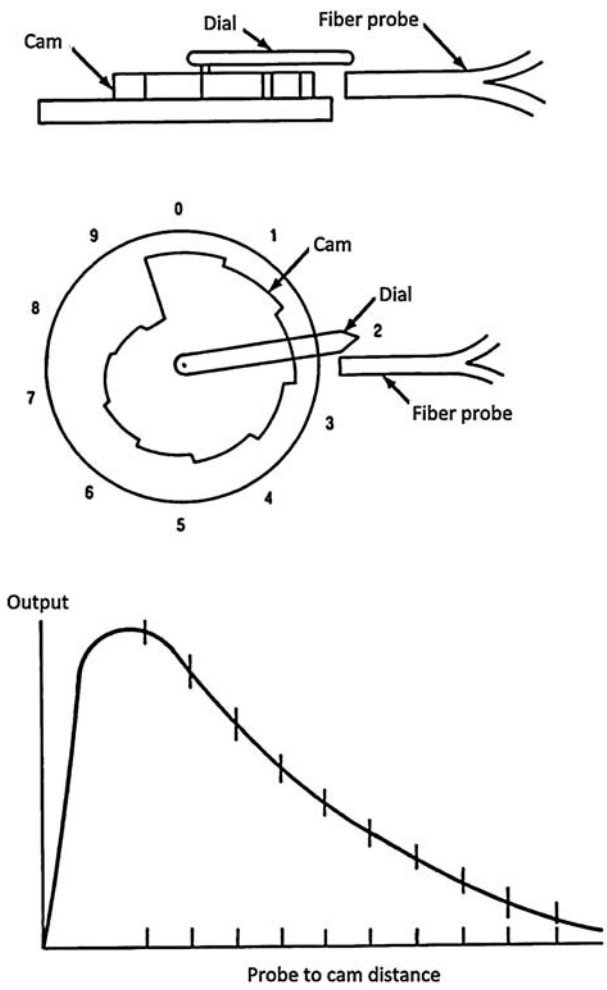

Figure 9.28 Dial encoder configuration.

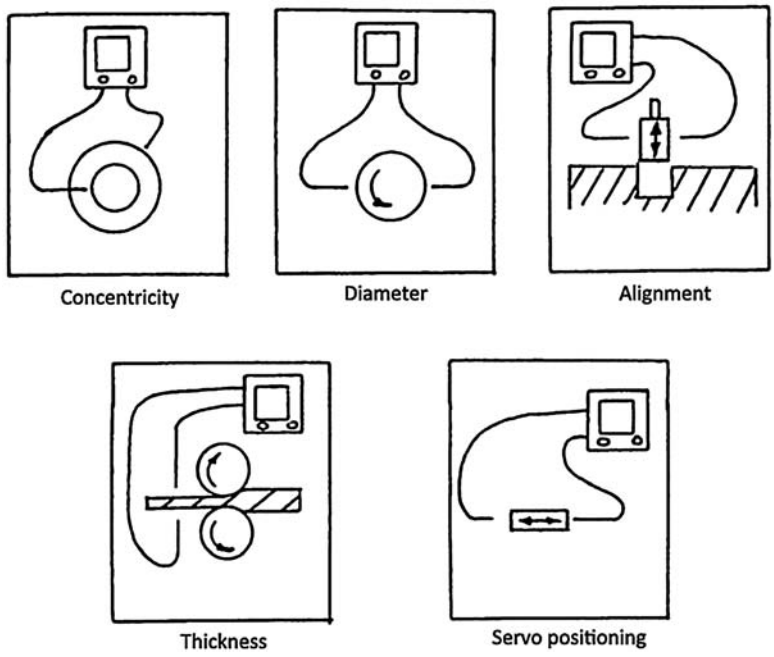

Figure 9.29 Typical applications of dual probes.

rotation since the rotation causes the average target-to-probe distance to change, as well as the angle of reflectance.

Another application is for dial encoding.[21] A specially fabricated cam is placed on a shaft that supports a meter dial, as shown in Fig. 9.28. The cam increases the distance between the fiber optic probe and the reflective target in a step-wise sequence of 10 distinct distances. Each step corresponds to a digit on the 0–9 dial indicator. The linear portion of the back slope is used.

As mentioned previously, dual probes provide for greater sensitivity as well as directionality. Figure 9.29 depicts dual-probe applications that include measurement of concentricity, diameter, alignment, thickness, and servo positioning. Consider the servo-positioning application. Movement to the left or right at a given distance corresponds to specific values for each probe. If the magnitude registered for one probe does not correspond to the calibrated magnitude registered for the other probe, a difficulty such as misalignment, uneven wear, or contamination could be signaled.

A rotational shaft with limited movement used in the measurement of torque is monitored by dual reflective fiber optic probes, as shown in Fig. 9.30, and by dual microbending sensors, as shown in Fig. 9.31. In both cases, the shaft rotates an eccentric cam, causing displacement proportional to torque. Both sensors monitor magnitude and direction.

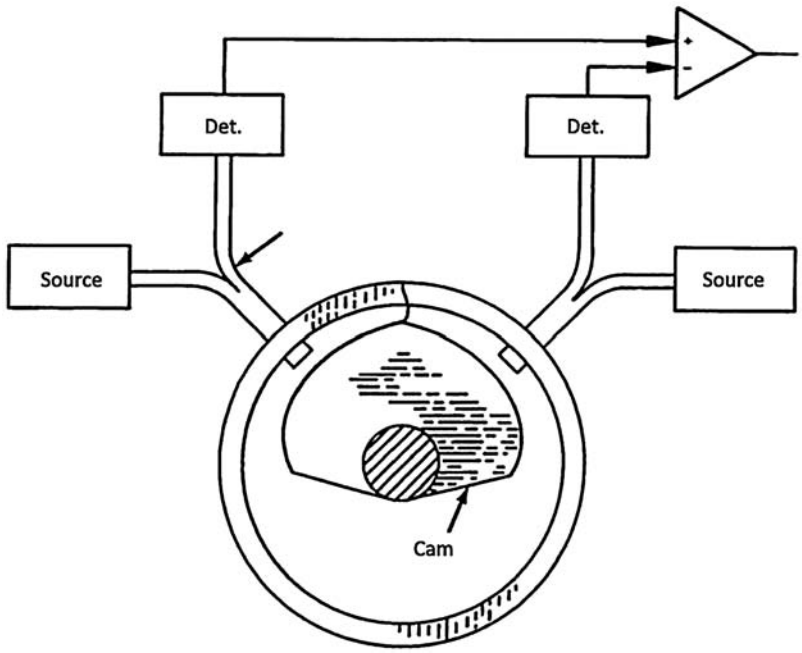

Figure 9.30 Torque sensor using dual reflective sensors.

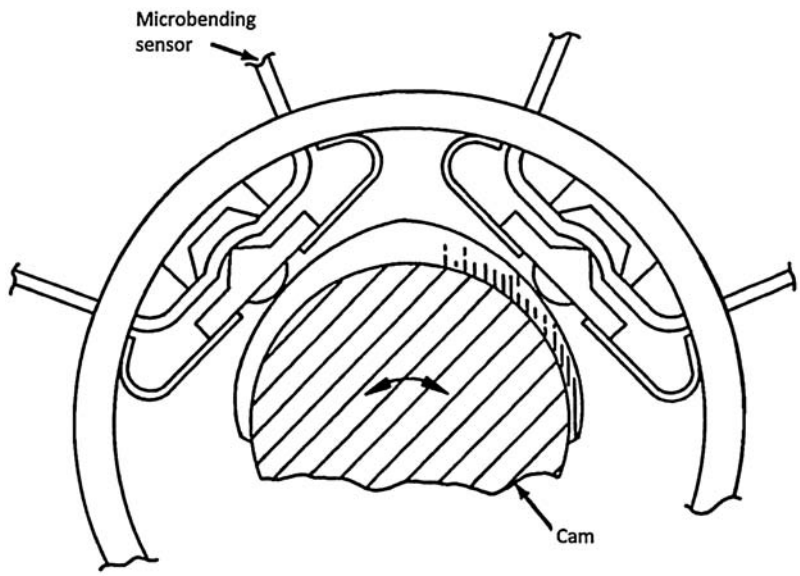

Figure 9.31 Torque sensor using dual microbending sensors.

Finally, displacement can also be measured in digital format using fiber optics. The sensor requires a gray code card and a transmission-interrupt sensor for each bit of required accuracy. Typically, five or more transmissive sensors are required. The sensor concept eliminates intensity errors associated with analog sensors, but it is generally more bulky, more costly, and problematic in dirty environments.

References

1. D. A. Krohn, "Fiber optic displacement sensors," *Proc. ISA* **39**, 331–40 (1984).
2. C. D. Kissinger and B. Howland, "Fiber optic displacement measuring apparatus," U.S. Patent 3,940,608 (Feb. 24, 1976).
3. A. K. Bejczy, H. C. Primus, and W. A. Herman, "Fiber optic proximity sensor," *NASA Tech. Brief* (1980).
4. C. Kissinger, "Fiber-optic lever displacement sensors and automated reflections compensation improvements," FOC/LAN 83, Atlantic City, pp. 300–304 (1987).
5. C. Kissinger, "Fiber-optic lever displacement sensors: principles, implements, and applications," *Proc. ISA* **87**, 251–1261 (1987).
6. A. R. Perlin, "Single optical fiber transducers," *Inter-Optic* **89**, Tokyo, Japan (1989).
7. M. M. Rasmay, G. A. Hockman, and K. C. Kao, "Propagation in optical fiber waveguides," *Electrical Communication* **50**(3), 162–169 (1975).
8. D. A. Krohn, "Fiber optic sensors: a technology overview," *Innovations*, 11–13 (1982).
9. R. F. Coulombe, "Fiber optic sensors–catching up with the 1980s," *Sensors* **1**(12), 5–10 (1984).
10. N. Lugakos, W. S. Trott, T. R. Hickman, J. H. Cole, and J. Bucaro, "Microbend fiber optic sensor as extended hydrophone," *IEEE J. Quantum Electronics* **QE-18**(10), 1633–1638 (1982).
11. I. G. Giallorenzi et al., "Optical fiber sensor technology," *IEEE J. Quantum Electronics* **QE-18**(4), 665 (1982).
12. D. Marcuse, "Microbending losses of single-mode, step-index and multimode, parabolic-index fibers," *Bell System Technical Journal* **55**(7), 937–955 (1976).
13. F. De Formal, J. Arnaud, and P. Facq, "Microbending effects on monomode light propagation in multimode fiber," *JOSA* **73**(5), 661–668 (1983).
14. N. Lagakos and J. A. Bucam, "Fiber-optic sensor," *Applied Optics* **26**, 2171–2180 (1987).
15. N. Lagakos, T. Litovitz, P. Macedo, R. Mohr, and R. Meister, "Multimode optic fiber displacement sensor," *Applied Optics* **20**(2), 167–168 (1981).

16. J. N. Fields, C. K. Asawa, O. G. Ramer, and M. K. Barnoski, "Fiber optic pressure sensor," *J. Acoust. Soc. Amer.* **67**, 816–818 (1980).
17. G. Duplain, C. Belleville, S. Bussière, and P. A. Bélanger, "Absolute fiber-optic linear position and displacement sensor," *12th International Conference on Optical Fiber Sensors* **16**, OTuD5 (1997).
18. K.-C. Chuang and C.-C. Ma, "Pointwise fiber Bragg grating displacement sensor system for dynamic measurements," *Appl. Opt.* **47**, 3561–3567 (2008).
19. Y. Zou, X. Dong, G. Lin, and R,. Adhami, "Wide range FBG displacement sensor based on twin-core fiber filter," *J. Lightwave Technol.* **30**, 337–343 (2012).
20. J. Wang, Q.-m. Sui, Z.-f. Wang, J. Chang, G.-d. Peng, et al. "Development and application of subminiature multipoint FBG displacement sensor," *Proc. SPIE* **8351**, 835139 (2012) [doi: 10.1117/12.915976].
21. D. A. Krohn, L. A. Buffone, and E. I. Vinarub, "Fiber optic dial encoder," U.S. Patent 4,500,870 (1985).

Chapter 10
Strain Sensors

Several techniques have been developed for measuring strain using fiber optic sensors. The three most widely used approaches include Bragg gratings, interferometric configurations, and Rayleigh scattering.

10.1 Bragg Grating Strain Sensors

Fiber Bragg grating optical strain sensors provide many advantages over conventional electrical systems, as has been discussed previously. They are well-suited for applications requiring long-range capabilities in terms of distance, as well as applications requiring long spans of time without degradation. Furthermore, these sensors are suitable for harsh environmental conditions due their immunity to lightning and resistance to corrosion.[1]

Fiber Bragg grating (FBG) sensors can be used as point sensors or distributed sensing systems. For applications that cover large areas, multiple FBG sensors can be integrated into a single optical fiber. The system configurations can be simplified using only a single cable and single interrogator to monitor a large number of sensing points. This results in a reduction in cabling maintenance and installation processes, and provides cost-effective monitoring solutions. Due to the fact that FBG optical sensing uses wavelength rather than amplitude modulation, these sensing systems can reach very long distances (more than 10 km) without the need for signal conditioning.[2]

Fiber optic Bragg gratings are well suited for strain measurement. They are compatible with a wide array of materials including composites, enabling them to play a key role in smart structures. Depending on the design, Bragg grating interrogators can monitor 20 sensing points and potentially up to 100 sensing points on a single fiber.[1]

Fiber optic Bragg gratings were discussed in detail in Chapter 5. But as a quick review, the FBG is a series of localized changes in the refractive index of the glass fiber that creates the grating effect. The optical fiber is connected to a light source, which typically transmits light in a wavelength band of about 40 nm (a broader spectrum of light is sometimes used). When the light

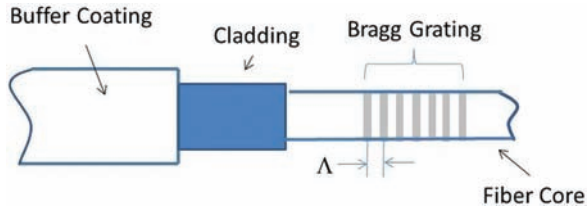

Figure 10.1 Fiber Bragg grating strain measurement concept. The grating spacing is a function of the applied strain (reprinted from Ref. 2).

encounters the FBG strain sensor, a specific wavelength is reflected based on the properties of the gratings, while the rest of the light in the transmission band passes through the grating. As the FBG expands or contracts due to strain, so does the gap between these gratings, as depicted in Fig. 10.1 and Fig 10.2, thereby changing the reflected wavelength of light. The reflected

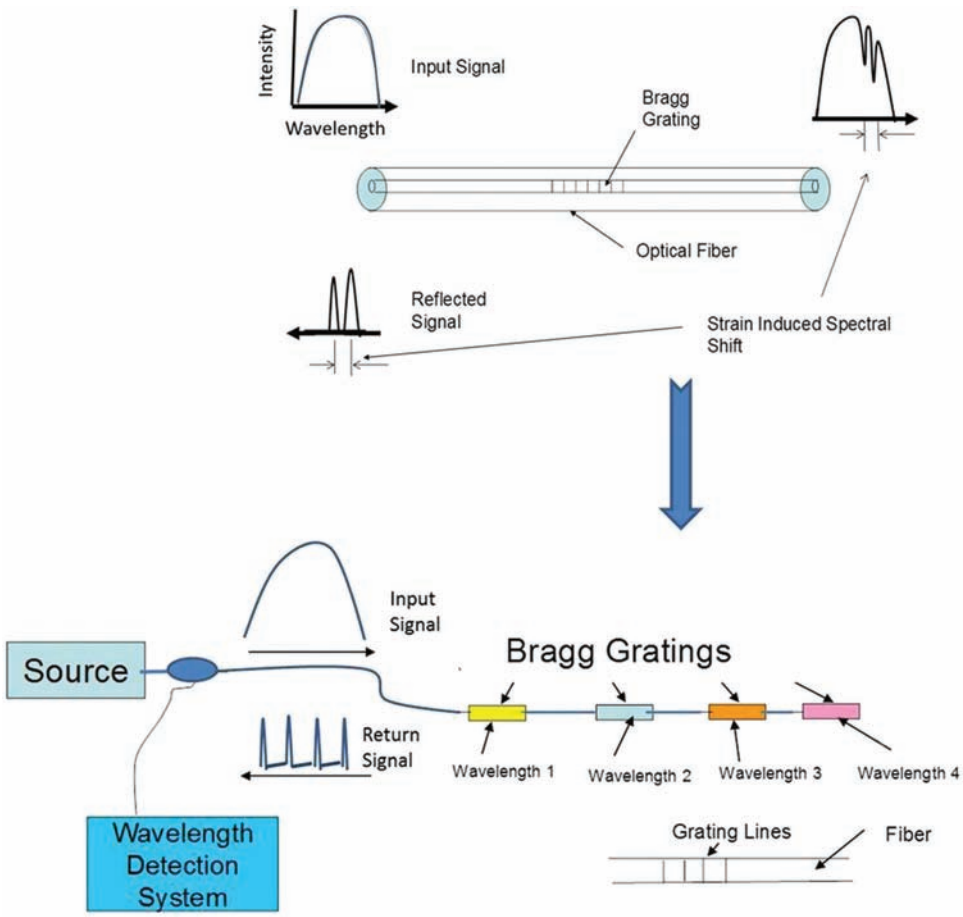

Figure 10.2 Basic Bragg grating-based sensor system (reprinted from Ref. 3).

light is then measured, and the change in wavelength can be converted to a strain value.[2]

A Bragg grating sensing system is depicted in Fig. 10.2.[3] The Bragg grating responds to both strain and temperature.[3] Strain effects the elongation of the fiber, changing the grating spacing. It also causes a refractive index change associated with Poisson's effect (photoelastic effect) due to dimensional changes in the radial direction. Temperature change causes thermal expansion, which changes the grating spacing. The refractive index itself is temperature dependent. The change in wavelength $\Delta\lambda_B$ associated with both strain and temperature effects is given by[3]

$$\Delta\lambda_B = 2n\Lambda\left[\left\{1 \quad \left[\frac{n^2}{2}\right][P_{12} \quad \nu(P_{11}+P_{12})]\right\}\varepsilon + \left(\alpha + \frac{dn/dT}{n}\right)\Delta T\right], \quad (10.1)$$

where

Λ = grating spacing
ε = the applied strain,
P_{11}, P_{12} = the stress optic coefficient,
α = the coefficient of thermal expansion,
ν = Poisson's ratio,
n = the refractive index of the core, and
ΔT = the temperature change.

For silica, the term is

$$\left(\frac{n^2}{2}\right)[P_{12} \quad \nu(P_{11}+P_{12})] \approx 0.22. \quad (10.2)$$

Therefore, for constant temperature ($\Delta T = 0$),

$$\Delta\lambda_B = 1.56n\Lambda\varepsilon, \quad (10.3)$$

where the spacing between grating periods is Λ.

Errors due to temperature are a problem for Bragg grating strain sensors since constant-temperature environments seldom occur in real-world monitoring. Several approaches can be used to separate temperature from strain effects in Bragg grating sensors.[4] One approach is to use a reference grating.[1,5] A simple approach has the reference grating in thermal contact but isolated from strain effects. While one grating measures temperature and strain, the reference grating measures only temperature. The difference is the result of strain alone. Since it is not always possible to mount a Bragg grating that measures only temperature in close proximity to the Bragg grating measuring strain, alternative approaches use two gratings with different responses to temperature and strain, so that errors associated with temperature can be compensated.[6] Athermal (temperature independent) packaging schemes are another approach to minimize the effects of temperature change.[7,8] For a typical Bragg grating functioning in the 1550-nm range, the wavelength shift associated with temperature is typically 10 pm/°C. If the package design is

made from materials that have different coefficients of expansion that compensate for the temperature shift, errors can be drastically reduced to much less than 1 pm/°C. The grating wavelength is plotted versus temperature in Fig. 10.3 for a standard grating and for an athermally packaged grating. For applications that require accuracy less than 1 pm, a combination of athermal packaging and compensation may be required.

Figure 10.4 shows two Bragg grating sensors and how they are packaged. As discussed previously, one sensor can be used to measure both strain and temperature effects. The other Bragg grating measures only temperature changes and provides temperature compensation.

To attach the FBG to the structure that is being monitored, the proper adhesive has to be chosen to meet both the mechanical and environmental requirements.[9] Preparing the mounting surface and protecting the fiber from damage are critical considerations. The connecting cables must be sufficiently rugged to suit the application.

Bragg gratings are inherently self-referencing.[9] As a result, long-term static strain testing is very easy to accomplish with FBGs, due to their ability to have a starting point. Each Bragg grating has an associated zero-strain wavelength. However, when it is attached to a structure, this will cause some strain in the grating. After the FBG is attached to the structure, it is allowed to

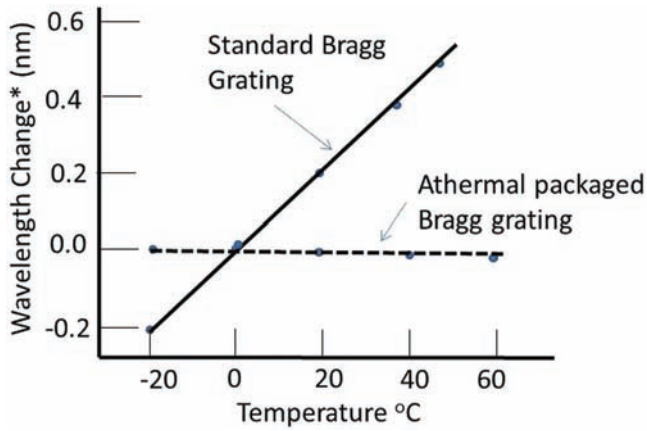

Figure 10.3 Grating wavelength versus temperature for standard and athermally packaged grating. The initial Bragg grating wavelength is 1550 nm.[7]

Figure 10.4 Two FBG optical strain gages from Micron Optics Inc. that can be bonded or welded onto the structure under test.[2]

come to a steady state, which establishes the starting point. During the test, the reflective wavelength of the fiber Bragg grating is monitored and compared to the initial wavelength that was measured. The change in wavelength provides a measurement of time-dependent stress on the structure. The self-referencing capability allows the instrumentation (interrogator) to be mobile without being dedicated to a specific system. As a result, in an application such as monitoring multiple bridges, an interrogator is not required for every bridge but can be shared with different locations, which results in a significant cost savings.

Dynamic strain sensing can be used for low-frequency phenomena, such as earthquakes, earth tremors, the ebb and flow of tides, and wind. FBGs can be attached to structures, buildings, or piers and monitored for the vibrations during these naturally occurring events. Dynamic-strain monitoring (under 100 Hz) can be used to monitor traffic flow on a bridge or vibration in a machine and can give an indication of vibration signature changes that could indicate the onset of failure and enable preventive maintenance.[9]

Interrogators use either a tunable laser or a broadband source to cover the wavelength spectrum, typically the C-band. The broadband source has a lower intensity than the laser, but can potentially cover a wider spectrum. The tunable laser has higher intensity and sweeps through the bandwidth range. Table 10.1 shows the specifications for several commercial interrogators. Most of the interrogators work in an expanded C-band range. However, interrogators are available that cover the S-band and L-band range. The number of sensors can vary depending on design, but all commercial units can monitor at least 16 gratings. The accuracy is ± 2 pm. The scan frequency can cover both static and dynamic strain applications. The dynamic range allows

Table 10.1 Specifications for commercially available interrogators.

Parameter	Company A	Company B	Company C	Company D
Wavelength Range	S band (1460 1530 nm), C band (1530 1565 nm), L band (1565 1625 nm)	1510 1590 nm	1510 1590 nm	1520 1570 nm
Resolution	0.15 pm @100 Hz		1 pm	0.25 pm
Maximum Sensors	16 per fiber per wavelength range (48)*	80 (160)*	16	100
Repeatability	±1 pm	±1 pm	±1 pm	
Accuracy	±2 pm	±2 pm	±2 pm	±1 pm
Scan Frequency	0 5000 Hz**	1 500 Hz	1 500 Hz	5 Hz
Dynamic Range	85 dB	25 dB	25 dB	60 dB
Optical Power	3 dBm			
Max. Output Current	1 mV			
Power Consumption	12 W (150 W 500 kHz option)	35 W	35 W	150 W
Package	Portable Rack mountable available	Portable or Rack Mount	Portable	Portable

* Expanded wavelength range.

** All sensors sample simultaneously.

Bragg grating sensors with reflectivities less than 1% to be measured accurately.[1]

Bragg grating sensors can be individually interrogated as a single point sensor and multiplexed to enable multipoint distributive sensing, where multiple sensing points are on a single optical fiber. Due to the wavelength-encoded nature of the signals in optical FBGs, transmission or bending losses in the fiber are not a problem since the measurement is not based on intensity. Since Bragg grating sensors are at specific points along the fiber, these systems are referred to as quasi-distributed sensors.[9]

Since each grating is written at a unique wavelength, these systems are inherently wavelength-division multiplexed (WDM). As an example, in the C-band each Bragg grating has a distinct operating wavelength region. It is important to provide sufficient wavelength spacing between the gratings to prevent overlap. WDM systems are limited in sensor count to the operating spectrum and the spectral width of each sensor, typically 16 sensors in the C-band. Figure 10.5 shows the interrogation scheme of several Bragg gratings using wavelength-division multiplexing in the reflection mode. In real time, the specific Bragg wavelength shifts of each FBG can be determined. A broadband source is used. The return can be analyzed by several techniques, including, for example, using a Fabry–Pérot tunable filter.[9]

WDM interrogators that use a fast-sweeping laser as a light source instead of a broadband source have advantages. These advantages are longer range (due to higher power) and greater sensor capacity (due to the wider wavelength windows of 50 to 100 nm).

The number of sensors that can be interrogated can be significantly increased using time-division multiplexing (TDM) techniques in combination with WDM. A TDM/WDM scheme is illustrated in Fig. 10.6. This approach has the ability to simultaneously interrogate multiple fibers, each with 12 to 16 sensors.

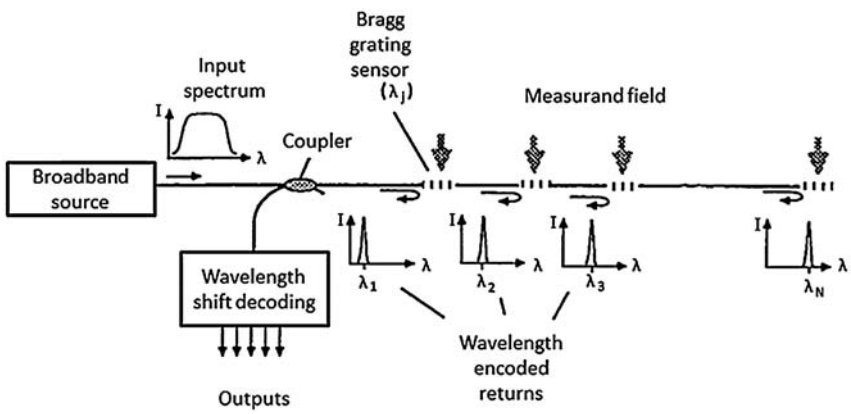

Figure 10.5 Distributed WDM Bragg grating sensing system.[9]

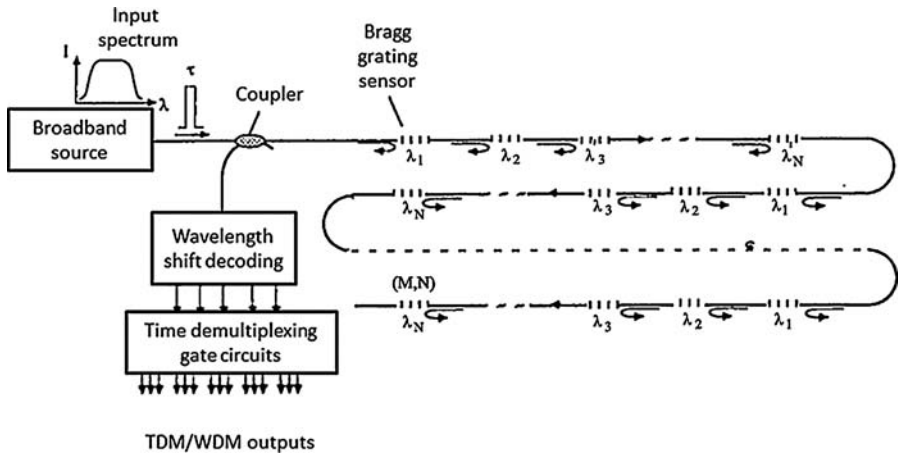

Figure 10.6 TDM/WDM Bragg grating sensing system.[9]

In TDM systems, the reflections from the FBGs at every point in the array will return to the detector at increasingly later times, depending on the distance from the detector. The detector is synchronized and time-gated, to allow selective interrogation of a given FBG array in time for a given wavelength window.

This TDM/WDM configuration approach can interrogate up to 160 different FBGs by scanning multiple arrays with 12 to 16 gratings each. The system uses a tunable Fabry–Pérot filter as the wavelength selector. A drawback of this type of implementation is the limited spacial resolution. Therefore, FBGs can be spaced no closer than 1 m.[9]

There are other limitations to the TDM technique.[9] Cross-talk is problematic. There are two sources for cross-talk: multiple reflections and spectral shadowing. Multiple-reflection cross-talk is caused by the delay introduced into an upstream reflected light signal that has undergone multiple reflections along its path and has overlapped in time with the reflected signal of a downstream grating. The effect is a direct function of the grating's reflectivity and can be minimized using low-reflectivity gratings ($<5\%$). The use of low-reflectivity gratings with high sensitivity detection is critical for large-sensor-count sensing systems.

Cross-talk from spectral shadowing is the distortion introduced in the reflected spectrum of a downstream grating. This distortion is due to the double pass of the incoming light through an upstream grating. Many of the cross-talk problems can be eliminated by staggering the grating arrays to avoid spectrum overlaps, using arrays that branch off instead of serial arrays, or adding delay lines to increase the time interval between gratings.

There are several design considerations and issues. Bragg grating sensors should be used in a tensile mode. Therefore, the gratings must be prestressed so that any compressive stresses that occur during installation are compensated

for with a positive net initial tensile stress.[10] Attachment of the fiber to the surface being measured presents some engineering challenges. The fiber has multiple interfaces. The first interface in the fiber is its single or dual coating. The second is the attachment of the coated fiber to the test surface. If delamination occurs at any of the interfaces, the strain measurement is compromised. It may be necessary to remove the coating or use a thin hard coating such as polyimide on the fiber. The coatings and epoxy used for attachment have viscoelastic properties that may allow movement over time under load and cause the measured strain to creep, giving misleading values. Proper selection and evaluation of materials is important to minimize potential errors.[11]

In a recent application for monitoring strain on an offshore drilling platform, careful attention was paid to the choice of packaging and bonding materials to allow the best Bragg grating strain sensor performance in a saltfog environment. The results were approximately 3.53-pm/microstrain accuracy with a linearity of greater than 99%.[12]

10.2 Interferometric Strain Sensors

Fiber optic interferometric strain sensors are based on phase changes of light propagating in an optical fiber. The phase change results from strains that change the length of the fiber that forms the interferometric cavity. This approach provides very high sensitivity.[13] There are several types of interferometric sensors, but the two most widely used in strain measurements are Fabry–Pérot and Mach–Zehnder.

Figure 10.7 shows two potential approaches to building a Fabry–Pérot interferometer. The device has two parallel reflective surfaces that can be created either by having an air gap between two fibers (extrinsic) or by inserting Bragg grating mirrors in a fiber (intrinsic). Interference occurs with the superposition of multiple reflective beams off of the parallel surfaces. This concept is often referred to as an etalon. The phase difference is given by[13]

$$\Delta\phi = \frac{2\pi(n2L)}{\lambda}, \tag{10.4}$$

where λ is the wavelength of incident light, n is the refractive index of the cavity material, and L is the length of the cavity. When the etalon is attached

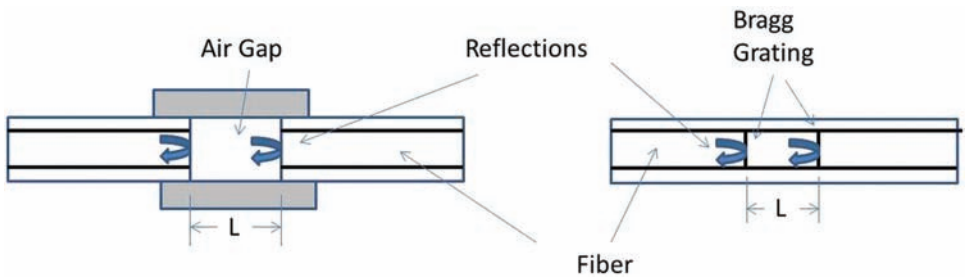

Figure 10.7 Fabry–Pérot interferometric sensor concepts.[13]

to a surface under strain, the change in the cavity length creates a phase change that is a function of the surface strain. Fabry–Pérot interferometric sensors have demonstrated less than 50-pm displacement resolution with a 2-nm/m strain resolution.[14]

Figure 10.8 shows the major elements of a Mach–Zehnder interferometer. The incident light is split into two paths: the sensing arm and the reference arm. When the sensing arm is under stress (strain), the fiber is stretched and the interference between the sensing arm and the reference arm is manifested as phase shift. The change in length associated with the measured strain is related to the phase shift $\Delta\Phi$, which is defined as[16]

$$\Delta\Phi = kLn\left(\frac{\Delta L}{L} + \frac{\Delta n}{n}\right), \tag{10.5}$$

and because $\Delta L/L$ is the strain ε,

$$\Delta\Phi = kLn\left(\varepsilon + \frac{\Delta n}{n}\right), \tag{10.6}$$

where L is the fiber length, k is the wave number, and n is the refractive index. For constant temperature applications, the refractive-index change is small, simplifying the phase–strain relationship. However, when the temperature is not constant, compensation is required for temperature effects.

Mach–Zehnder interferometric sensors can potentially achieve a strain resolution of 1 nm/m (10^{-6} microstrain).[15] In practical applications, the resolution is <0.01 microstrain with a long-term accuracy of $<1\%$. Interferometric sensors can be used in distributed multisensor configurations shown in Fig. 10.9. Position resolution on the order of 1 m in 10-km length can be achieved. Also, interferometric sensors can monitor dynamic strain up to about 2 kHz.[15]

Various scattering phenomena can be used in conjunction with a Mach–Zehnder interferometric configuration. Both Brillouin and Rayleigh scattering are sensitive to both temperature and strain. The limiting factor is the very low intensity of back-reflected light. However, Rayleigh backscattering is significantly higher in intensity than Brillouin scattering and, as such, can provide superior spatial resolution, especially in long distance distributed sensing applications. Instead of OTDR, Rayleigh scattering can use *coherent* optical frequency domain reflectometry (c-OFDR) (shown in Fig. 10.10[17]),

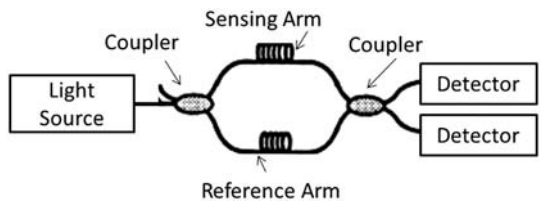

Figure 10.8 Mach-Zehnder interferometer.[15]

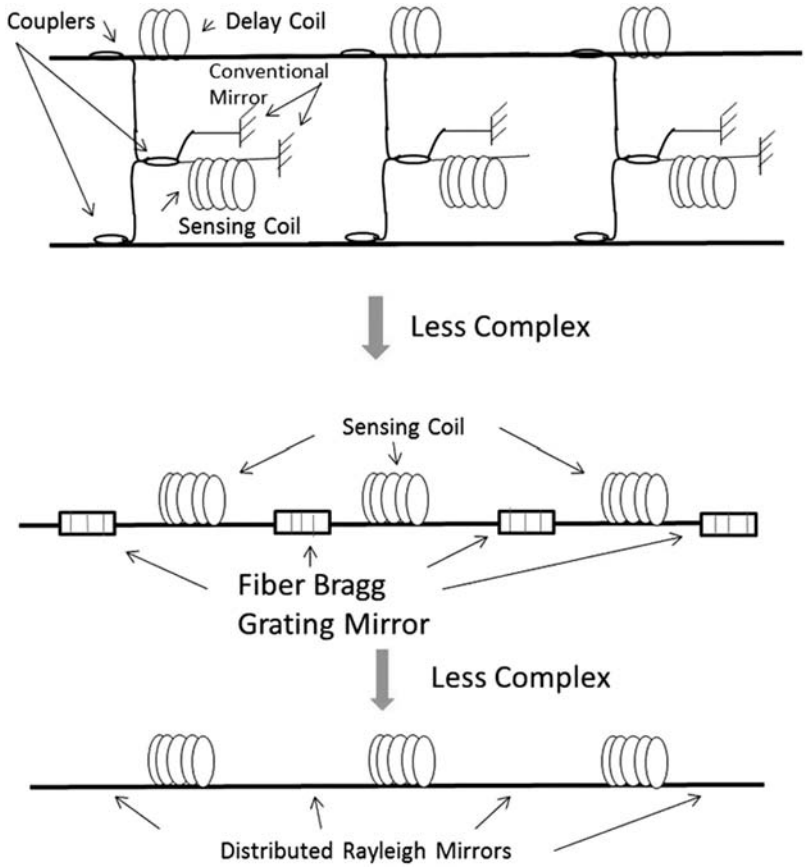

Figure 10.9 Distributed interferometric sensor configurations (reprinted from Ref. 15 with permission).

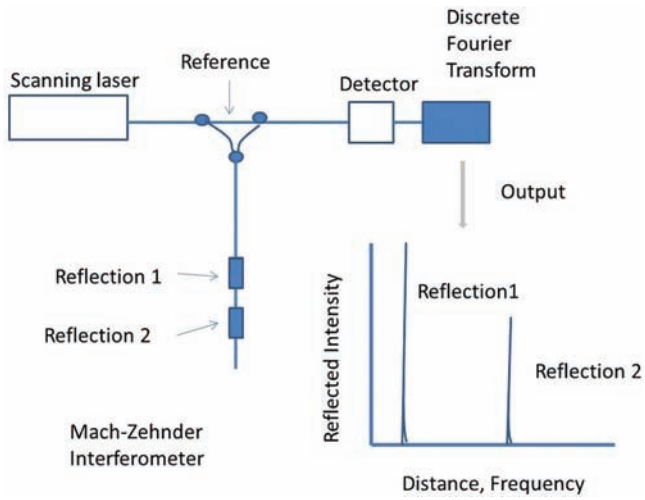

Figure 10.10 Mach–Zehnder interferometer based on Rayleigh scattering.[17]

which provides significantly higher resolution. Changing the frequency of the input wavelength generates a periodic signal in which the frequency corresponds to the location of the scattering point along the fiber. The frequency of the interference signal increases as the distance increases. The intensity of the frequency response is a function of changes in strain or temperature. Spatial resolutions of 1 mm on fiber lengths of 70 m are possible. This approach allows a measurement range of 10,000 microstrain, accuracy of 2 microstrain with an acquisition rate of up to 100 Hz.[18] In comparison, Brillouin-based strain sensors can resolve strain to approximately 10 microstrain with an acquisition rate of 1 Hz.[19]

Interferometric sensors have similar issues to Bragg grating sensors in terms of attachment to a surface to be monitored. The sensors must be packaged to be athermal or be temperature compensated. The proper attachment procedure and materials need to be designed so that the sensor is actually measuring strain associated with the target surface without viscoelastic or delamination errors.

Distributed acoustic sensing (DAS) is not a classic strain sensor but can be used to characterize vibration signature. It uses Rayleigh scattering. The interrogator launches a high-frequency light pulse into the single-mode fiber and analyses the backscattered light. The acoustic energy associated with the perturbation to the fiber is unique and can be used to identify events such as traffic flow on a bridge structure. In DAS, the entire fiber is the sensor such that the fiber can sense a perturbation anywhere along its length. The event location can be located to within 1 m over a 50-km distance.[21]

10.3 Applications

Fiber optic sensors have been used for a wide range of structural monitoring applications ranging from tunnels, dams, and bridges to offshore drilling platforms.[10 12,21] The objective is to monitor static strain and dynamic strain to identify the need for preventive maintenance and provide warning of

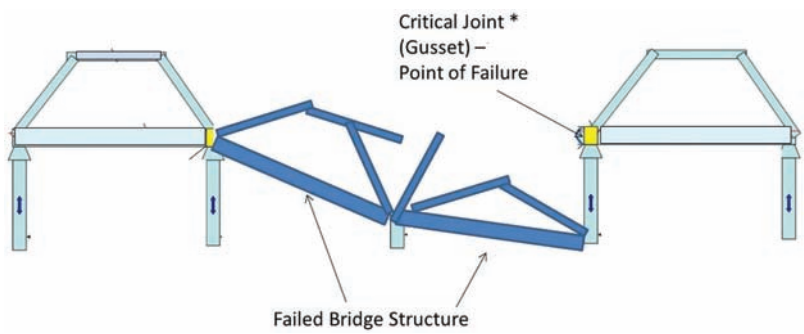

Figure 10.11 Catastrophic bridge failure.

the potential of catastrophic failure. Figure 10.11 shows the devastation associated with a bridge failure analogous to the 2007 bridge failure in Minneapolis, MN.[21]

One approach to structural safety in general and bridge safety in particular is to use a combination of static and dynamic strain sensors to monitor the structure.[21] Figure 10.12 shows the concept for a bridge. Once the sensors are installed, a baseline sensor response is documented. The deterioration of the structure will be manifested in changes in both static strain and dynamic strain (referred to as vibration signature). As an example, it may be very difficult to see an internal crack in a critical load member. However, the crack can act as a damper and alter the load member's vibrational signature, which is changing over time as the crack grows.

In the bridge structure of Fig. 10.12, the sensors are usually in a distributed configuration with multiple sensors using a common interrogator. The most common fiber optic sensor technology used for this type of application is Bragg grating, which can monitor both static and dynamic strain. However, interferometric senor technology can provide vibration sensor technology over a wide dynamic range. Figure 10.13 indicates the dynamic strain change for a Bragg grating as a function of time as a truck moves over a bridge span. The replacement bridge in Minneapolis is instrumented with a fiber optic sensing system.

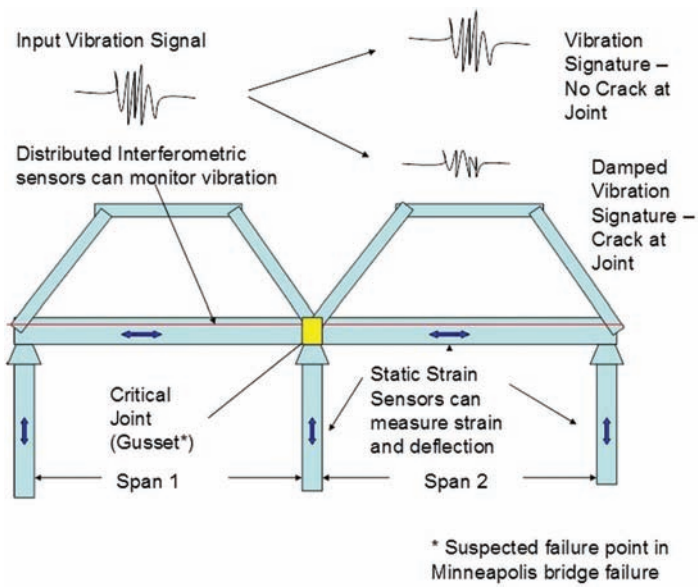

Figure 10.12 Conceptual use of static and dynamic strain monitoring in a bridge application.[21]

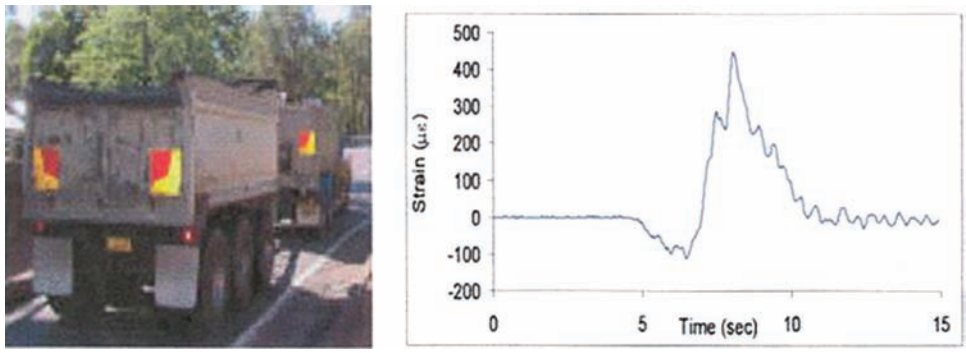

Figure 10.13 Strain change with time associated with Bridge Traffic[22] (courtesy of Micron Optics).

References

1. M. Kreuzer, "Strain measurement with fiber Bragg grating sensors," www.hbm.com (2006).
2. National Instuments Corp., "FBG Optical Sensing: A New Alternative for Challenging Strain Measurements" National Instruments, www.ni.com April, 2011.
3. A. D. Kersey, M. A. Davis, H. J. Patrick, M. LeBlanc, K. P. Koo, C. G. Atkins, M. A. Putnam, and E. S. Friebach, "Fiber grating sensors," *Journal of Lightwave Tech*. **1**(8), 1442–1463 (1997).
4. J. D. Jones, "Review of fiber sensor techniques for temperature strain discrimination," *12th Annual Conference on Optical Fiber Sensors*, 36–39 (1997).
5. L. A. Ferriera, A. B. Ribeiro, J. L. Santos, and F. Farc "Simultaneous measurement of displacement and temperature using a low finesse cavity and a fiber Bragg grating," *IEEE Photon Tech Letters* **8**, 1519 (1996).
6. M. G. Xu, J. L. Archambault, L. Reekie, and J. P. Dakin, "Discrimination between strain and temperature effects using dual wavelength fiber grating sensors," *Elect. Lett.* **30**, 1085 (1994).
7. AOS GmbH, "Athermalisation for FBG's" www.aos-fiber.com (2009).
8. Y. Lo, "Packaging a fiber Bragg grating with metal coating for an athermal design," *Journal of Lightwave Technology* **21**(5), (2003).
9. Micron Optics, Inc., "Optical fiber sensor guide: fundamentals and applications," www.micronoptics.com (2005).
10. I.-W. Wu et al., "FBG bending gauge on bridges: an effort towards standardization of bridge structural health monitoring," *Proc. SPIE* **6595**, 65952Y (2007) [doi: 10.1117/122.725918].

11. W. R. Habel, "Standards and guidelines: Could they enhance user confidence in fibre sensor technology?" *Proc. SPIE* **6619**, 661906 (2007) [10.1117/12.738336].
12. T. Wang, et al., "Fiber Bragg grating strain sensors for marine monitoring," *Photonic Sensors*, **3**(3), 267–271, (2013).
13. B. H. Lee et al., "Interferometric fiber optic sensors," *Sensors*, 2467–2486 (2012).
14. M. Schmidt, B. Werther, N. Furstenau, M. Matthias, and T. Melz, "Fiber optic extrinsic Fabry–Pérot interferometric strain sensor with < 50 pm displacement resolution using three wavelength digital phase demodulation," *Optics Express* **8**(8), 474–480 (2001).
15. J. Cole, C. Kirkendall, G. Cogdell, and T. Giallorenzi, "Twenty-five years of interferometric fiber optic acoustic sensors at the naval research laboratory," *Washington Academy of Sciences* (2004).
16. D. A. Krohn, *Fiber Optic Sensors: Fundamentals and Applications*, 3rd Edition, Instrument Society of America, Research Triangle Park, NC, p. 152 (2000).
17. D. Samic, "Distributed fibre optic temperature and strain measurement with extremely high spatial resolution," *Photonik International* (2012).
18. Luna, "Fiber Optic Sensing," www.lunainc.com (2013).
19. Silixa Ltd, "Intelligent distributed acoustic sensor" www.silixa.com (2011).
20. "Minneapolis Bridge Collapse," *New York Times*, August 2, 2007.
21. D. A. Krohn, "Photonic sensor application in transportation security," *Proc. SPIE* **6758**, 675802 (2007) [doi: 10.1117/12.737316].
22. T. Graver, D. Inaudi, and J. Doormink, "Growing market acceptance for fiber optic solutions in civil structures," *Proc. SPIE* **5589**, 44–55 (2004) [doi: 10.1117/12.580455].

Chapter 11
Temperature Sensors

11.1 Introduction

One of the most frequently measured physical parameters is temperature. Often times, temperature changes can be an indicator of physical changes occurring in other parameters of interest. Furthermore, since temperature is an interfering parameter in the measurement of other physical variables, it also becomes necessary to measure temperature to correct any temperature-induced effects that could lead to measurement errors of other measurements such as strain, pressure, displacement, etc. In addition, several other considerations drive the need for the utilization of fiber optic temperature sensors instead of conventional ones [such as thermistors, thermocouples, resistance temperature detectors (RTDs), or similar]. Thermometers are often required to operate in the presence of strong electromagnetic fields, while in contact with human patients, or to be interrogated over long distances. Sensors with metallic leads will experience eddy currents in such environments, which will create both noise and the potential for heating of the sensor, which in turn causes inaccuracy in the temperature measurement. In medical applications, it is imperative to offer electrical isolation and to be able to function in conjunction with magnetic resonance imaging (MRI) and computed tomography (CT) scan-type equipment. Fiber optic temperature sensors, which do not use metallic transducers to perform their conversion, allow for minimized heat dissipation by conduction and provide quick response. Since they are less perturbing to the environment, they have the potential for extreme accuracy.[1]

Several fiber optic sensing concepts have been exploited to develop thermometers as well as to perform temperature measurements based on reflectance, microbending, fluorescence, absorbance, and blackbody radiation, as well as intensity-, phase- or wavelength-modulated approaches.[2–5] In addition, a unique temperature-sensing capability of the optical fiber is to perform truly distributed temperature sensing along its length through the use of Raman and Brillouin scattering effects. In the sections to follow, a review will be made of the most common fiber optic temperature sensing techniques.

11.2 Reflectance and Absorbance Sensors

As described in Chapter 7, reflective sensors can very accurately determine position. This property can be also exploited to measure temperature. Figure 11.l depicts a bimetallic element attached as a transducer to a bifurcated, reflective, fiber optic probe. The bimetallic element can be designed to provide a snap action at a specific threshold temperature, at which point it moves abruptly relative to the probe tip, thus resulting in a switching action at a set temperature point. The element can also be designed to move continuously and provide movement proportional to temperature in an analog mode.

A response curve for a simple, analog, bimetallic element is shown in Fig. 11.2.[6] An actual sensor is shown in Fig. 11.3. Figure 11.4 shows another approach using differential thermal expansion. The two targets (alumina and silica), which have substantially different material thermal expansions, reflect

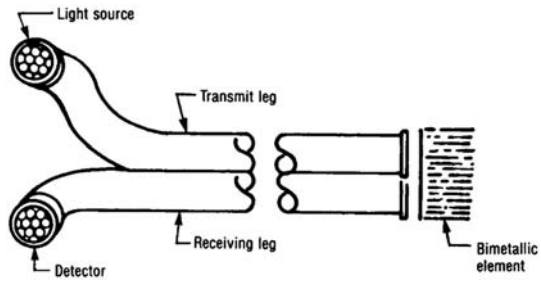

Figure 11.1 Reflective fiber optic temperature sensor using a bimetallic transducer.

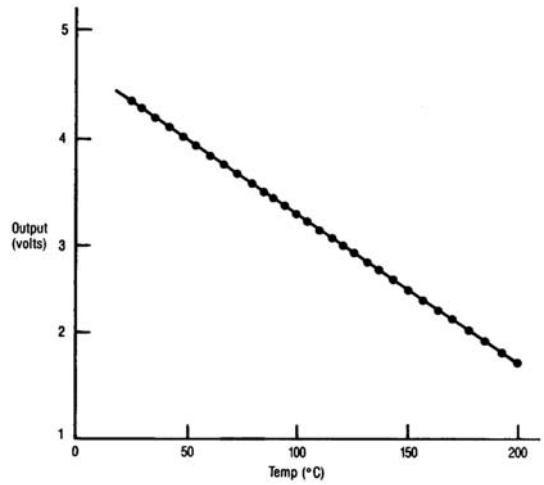

Figure 11.2 Response curve for a reflective fiber optic temperature sensor using a bimetallic transducer.

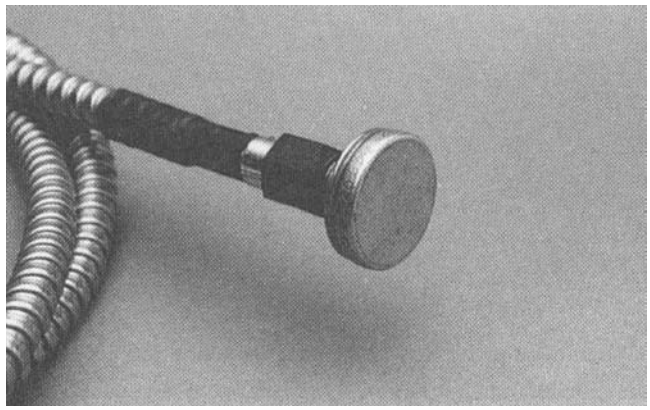

Figure 11.3 Actual reflective fiber optic temperature sensor using a bimetallic transducer.

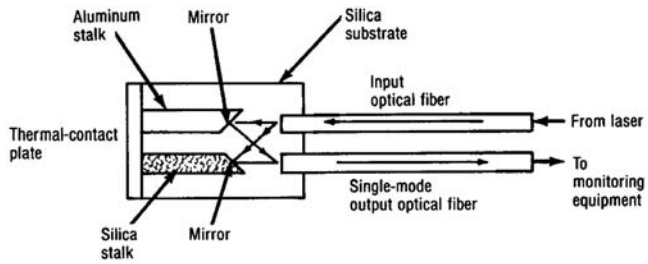

Figure 11.4 Reflective fiber optic temperature sensor using differential thermal expansion.

light into the output optical fiber. As the targets move relative to each other as a function of temperature, interference fringes are created, and the fringes are counted. The concept provides a digital indication of temperature using reflectance.[7]

As previously mentioned, active sensing materials can be placed in the optical path of a reflective probe to provide an enhanced sensing function. A wide variety of materials can be used for temperature sensing, including liquid crystals, birefringent materials, semiconductor materials, materials that fluoresce, and thermochromic substances that can change spectral response as a function of temperature.

For example, Scheggi et al.[8] demonstrated a biomedical temperature sensor based on the use of a thermochromic solution of cobalt (II) salt dissolved in isopropyl alcohol (85%) and water (15%). The solution was kept in a small reservoir on the tip of a multimode fiber. As shown in Fig. 11.5, the solution displays a strong optical absorbance at around 660 nm, while it is optically stable below 500 nm and above 750 nm. Hence, a spectral ratiometric measurement can be performed by taking light reflectance readings at 660 nm and 840 nm.

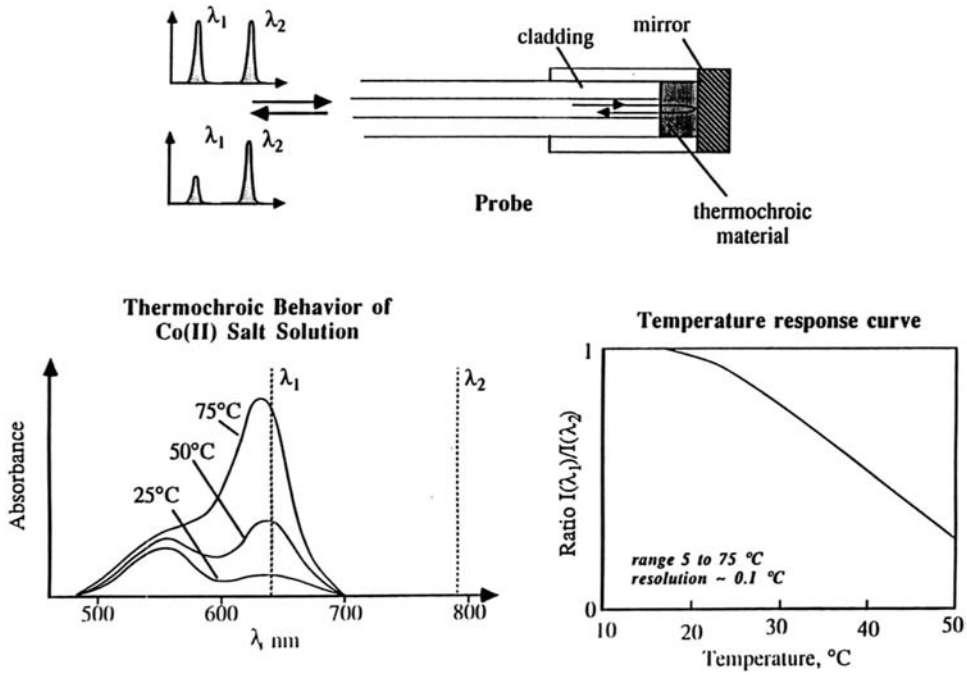

Figure 11.5 Reflective fiber optic thermochromic temperature sensor [after (Ref. 1)].

Other suitable materials are liquid crystals that exhibit color changes and/or reflectivity changes at a fixed wavelength due to temperature changes. The sensor mechanism is quite simple. Light passes through the input fiber and is reflected from the liquid crystal. The reflected light is detected, the intensity of which is a function of temperature. The working range is quite limited, 35 °C to 50 °C, but accuracies as good as 0.1 °C have been reported.[1] Figure 11.6 shows a reflective temperature sensor that uses a birefringent crystal. Birefringent crystals are optically transparent crystalline materials in which the indices of refraction are different for the orthogonally polarized light waves. The light is carried to the crystal by a transmitting fiber and passes through a polarizer prior to passing through the crystal. The light is reflected from a mirror and passes back through the crystal, polarizer, and receiving fiber to the detector.

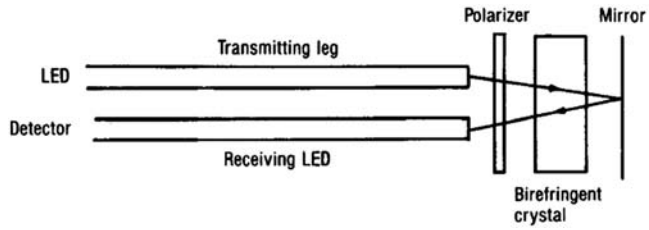

Figure 11.6 Reflective fiber optic temperature sensor using a birefringent crystal.

There are other optical materials in which the index of refraction, and therefore the birefringence, is a strong function of temperature. The net change in birefringence alters the intensity of received light, which is proportional to temperature; thus, a temperature sensor can be devised. For example, sapphire displays a temperature-dependent birefringence that can be exploited as a polarimetric temperature sensor.[9]

Another popular approach with commercial success is intensity based and relies on the use of a thin semiconductor sliver as a target.[10,11] Temperature measurement is based on the fact that band edge absorption of infrared light in crystals and semiconductor materials such as GaAs is temperature dependent. As the temperature increases, the edge band moves toward longer wavelengths and can be exploited to act as a temperature-dependent spectral mirror. Figure 11.7 depicts the sensor configuration. These sensors have accuracies of $\pm 0.3\,^{\circ}\mathrm{C}$ and temperature ranges from -40 to $+250\,^{\circ}\mathrm{C}$.

Another reflective concept is spectral modulation.[12–14] The configuration is shown in Fig. 11.8. The sensing-target element acts as a spectral mirror, changing the spectral reflectance over the light source bandwidth. One example of such material could be so-called color glass filters. The bandwidth of the light source is sufficiently broad that the sensing element can resolve the wavelength into discrete components. The ratio of two of the discrete component wavelengths varies in a manner proportional to the perturbing environment—in this case, temperature. The target for a temperature sensor comprises a material with a high refractive-index change with temperature. Light is transmitted through the target to a stationary reflector and back through the target material.

Unlike a bimetallic diaphragm, there is no movement; the path length, and hence the spectral response, changes due to index change. The target material is typically 1 to 2 wavelengths deep. The small size of the sensor allows it to

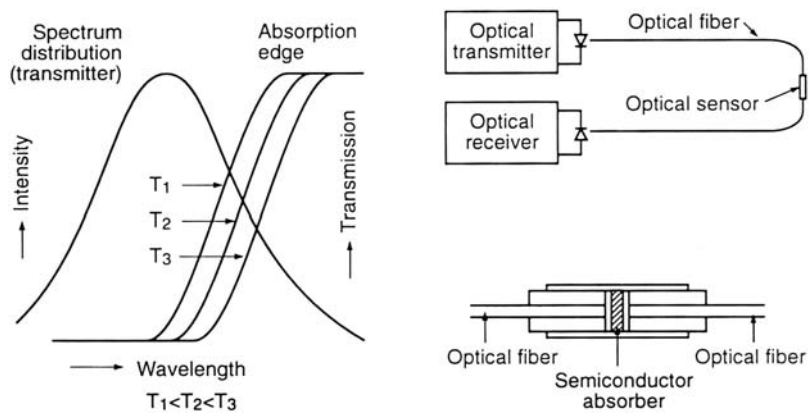

Figure 11.7 Reflective temperature probe in which a semiconductor crystal is hermetically sealed inside a glass capillary tube (from Ref. 11).

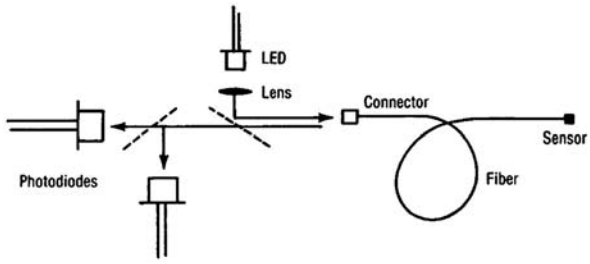

Figure 11.8 Schematic representation of a reflective fiber optic sensor using spectral modulation.

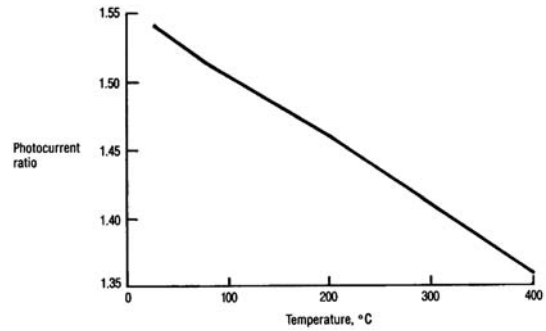

Figure 11.9 Ratiometric signal for typical temperature sensor using spectral modulation.

respond quite rapidly to dynamic temperature changes. The ratiometric signal versus temperature is shown for the sensor in Fig. 11.9. The upper limit of the sensor is dictated by the fiber coatings. The resolution is approximately 1 °C over a linear range of 400 °C.

Another embodiment of a spectrally modulated temperature sensor makes use of dielectric, multilayer, thin film filters deposited on the tips of single-mode or multimode fibers.[14] The thin films change their spectral response as a function of temperature, producing an intensity back-reflection that decreases with temperature. As described earlier, to make the device insensitive to light variations and source aging effects, two distinct wavelengths are used—one being immune from the temperature effects.

11.3 Fluorescence Sensors

The reflective concept can be expanded to include fluorescent targets.[15–20] In this configuration, the target does not reflect an incoming light signal but, rather, absorbs an incident UV light excitation pulse that produces a fluorescent response in a sensitive compound that emits visible radiation. The sensor uses a single fiber made of pure quartz to maximize the transmission of input UV light. The sensor tip is shown in Fig. 11.10.

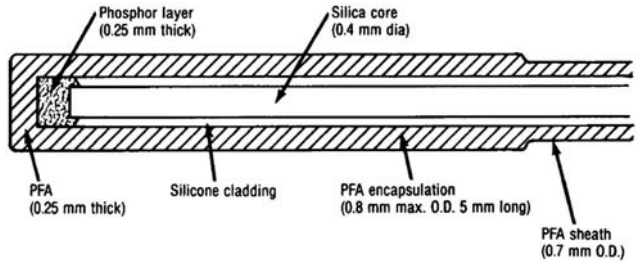

Figure 11.10 Sensor tip (highly enlarged) for a fluorescence sensor (PFA is the fluoropolymer perfluoroalkoxy) (reprinted from Ref. 15 with permission).

The fiber tip is coated with a phosphor layer and encapsulated. The sensor system is shown in Fig. 11.11. An ultraviolet lamp is the light source. The UV light excites the phosphor (magnesium fluorogermanate activated with tetravalent manganese) with light pulses on the fiber-end tip, producing a fluorescence response that results in visible light radiating back into the optical fiber. Since the incoming and outgoing light beams are of different wavelength, no interference takes place. The decay rate of the fluorescent light is proportional to the temperature of the phosphor tip. This sensor can be used over a temperature range of -200 to $+400\,^{\circ}C$.

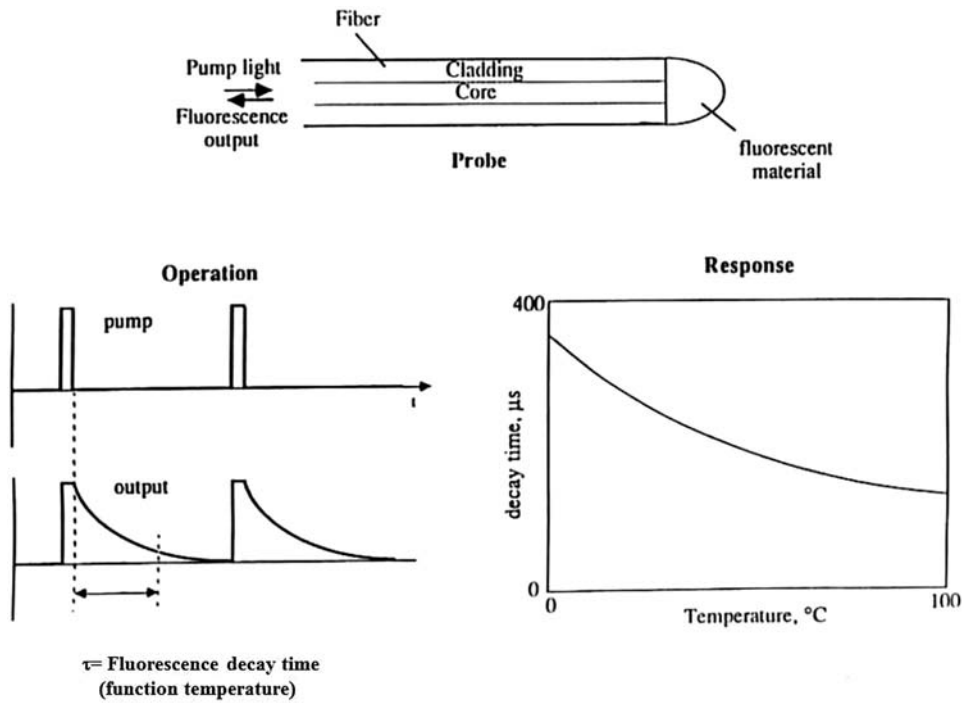

Figure 11.11 Schematic representation of the fluorescence temperature sensor system.

In another approach, the relative intensities of two sharp fluorescent emission lines that are given off when the phosphor is excited by UV radiation are measured. The lines vary with temperature. As a result, their intensity ratio is a measurement of temperature.

A rare-earth phosphor that has been used successfully in such a fluorescent sensor is europium activated gadolinium oxysulfide.[15] The excitation spectrum and emission spectrum are shown in Fig. 11.12. The emission lines are temperature dependent and are denoted by L, M, or H (low, medium, or high temperature), which defines the temperature range in which the lines quench or fade. The intensity ratio of lines marked *a* and *c* has been used to determine temperature. The operating range of the sensor is from 50 °C to above 250 °C. Over this broad temperature range, the accuracy is on the order of 1 °C. Over a much narrower temperature range, the accuracy approaches 0.1 °C. An important feature of this sensing concept is that the measured temperature is a direct function of phosphor temperature and is independent of variations caused by the light source, microbending in the leads, and connector-related intensity variations.

Fluorescence temperature sensors are especially useful for surface temperature measurement.[20] They have distinct advantages in that they have low thermal mass and fast response. Conventional temperature measurement techniques often alter the surface temperature by changing its thermal mass or by providing conductivity paths via the sensor leads. However, the use of a UV pulsed source can be bothersome in some applications. Fluorescence temperature sensors can have an accuracy of ±0.1 °C with response time as little as 25 ms for small (10-mm-diameter) sensors.

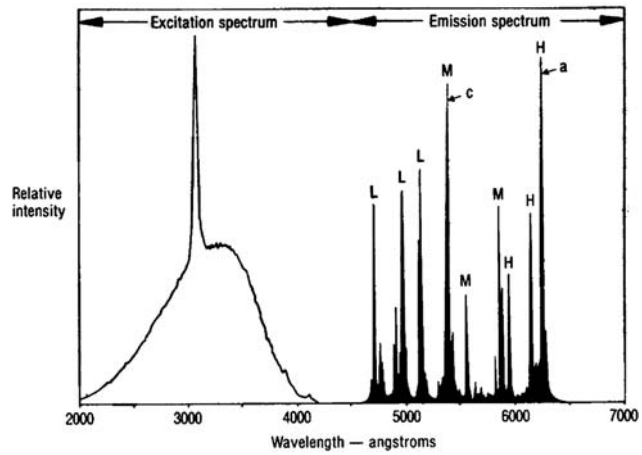

Figure 11.12 Excitation and emission spectrum for a fluorescence fiber optic temperature sensor (reprinted from Ref. 15 with permission).

11.4 Microbending Sensors

Microbending can be used as a temperature monitor in two different schemes.[21] The sensor can function by a change in the refractive index difference or by a change in the radius of bending with temperature. As described in Chapter 3, the microbending loss is a function of the difference Δn between the refractive index of the core and that of the cladding. For a given degree of bending, as Δn becomes smaller, the fiber becomes more lossy and leaks more light when the fiber is being bent. The temperature effects are pronounced on polymer-clad glass fibers, where the temperature dependence of the refractive index for the polymeric coating is significantly larger than for the glass core. Therefore, such fibers are sensor candidates. Glass-clad glass fibers can also exhibit such behavior. Gottlieb, Brandt, and Butler[21] have characterized several commercial glass combinations in which the indices of refraction cross over at a given temperature, as shown in Fig. 11.13. These fibers have the potential to act as temperature switches at the crossover point.

The change in bend radius with temperature can easily provide a sensing function by using a bending mechanism device with a high thermal expansion. The dependence of bending loss on radius of curvature is shown in Fig. 11.14 for several fibers.[21] It is clearly shown that relatively small radius changes can significantly increase loss. If a continuous multipoint

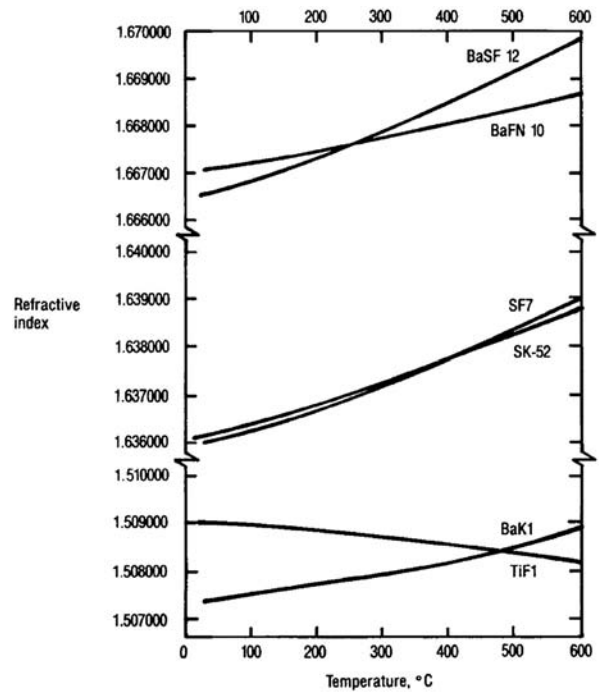

Figure 11.13 Crossover of refractive index of several pairs of fiber glasses. The codes refer to Schott glass designations for various commercial glasses.[21]

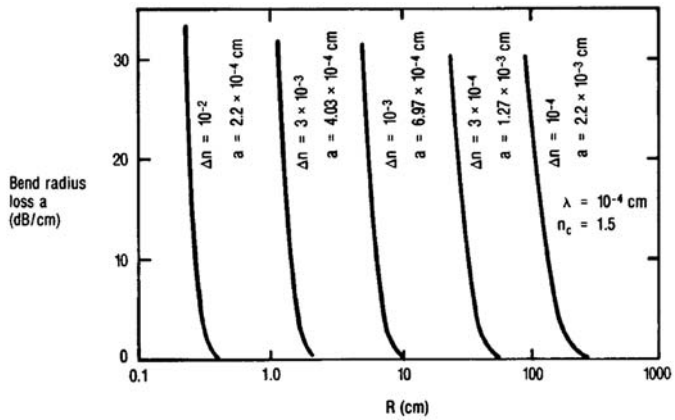

Figure 11.14 Dependence of bending loss on radius for several fibers (From [21]).

sensor is being designed, the parameters of the fiber and microbending transducer must be chosen so that one hot spot does not shut off the entire fiber. Figure 11.15 shows various configurations of a microbending temperature sensor. In fig. 11.15(a), the fiber is wrapped around a pipe that can expand or contract; the sensor is monitoring the pipe in a continuous manner. In Fig. 11.15(b), the configuration shows a point monitor where only the specific sensing point has sufficient thermal movement to affect the sensor. The configuration of Fig. 11.15(c) is similar to a strain gauge; if a microbending-sensitive fiber is bonded to a high thermal expansion material in the configuration shown, lateral expansion or contraction will change the curvature of the fiber.

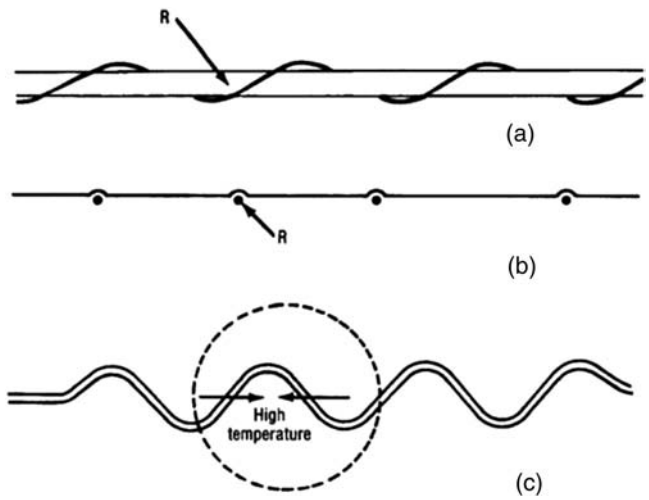

Figure 11.15 Several configurations for a bend loss temperature monitor. (a) Continuous monitor, (b) point monitor, (c) variable radius monitor (reprinted from Ref. 21 with permission).

11.5 Blackbody Radiation

Blackbody fiber optic temperature sensors are based on the fact that infrared radiation is emitted when a material is heated.[2,3,22] The intensity and wavelength of the radiation is a function of the temperature and is commonly referred to as blackbody radiation. The wavelength of radiation is also a function of temperature. At low temperatures (<100 °C) the wavelength of transmission is above 4 μm, so most conventional fibers are not effective. Typically, pure silica fibers have a transmission cutoff near 2 μm. At higher temperatures, the wavelength requirement for sensing drops into the operational range of silica fiber.

The most advanced temperature sensors using this approach have optical fibers made of sapphire. A typical configuration is shown in Fig. 11.16.[2] The tip of the fiber is coated with a thin film of a noble metal to form a blackbody cavity. The sensor has an operational measurement range of 500 °C to 2000 °C. The response time is potentially several orders of magnitude faster than that of a conventional thermocouple.

11.6 Doped Fibers

An intrinsic sensor is defined as one in which the sensing function takes place in the fiber itself (core, cladding, or coating), and the intensity of light transmitted in the fiber is proportional to the perturbing environment. An intrinsic sensor for temperature involves the phenomenon of absorption. It has been found that rare-earth materials such as neodymium (Nd), erbium (Er) and europium (Eu), when added to a conventional glass, result in absorption spectra with temperature-sensitive properties.[23–26] Two wavelengths were found with unique temperature behavior for Nd-doped fibers.[23]

As shown in Fig. 11.17, at 840 μm the absorption decreases with temperature; at 860 μm the reverse is true up to 500 °C. The intensity of

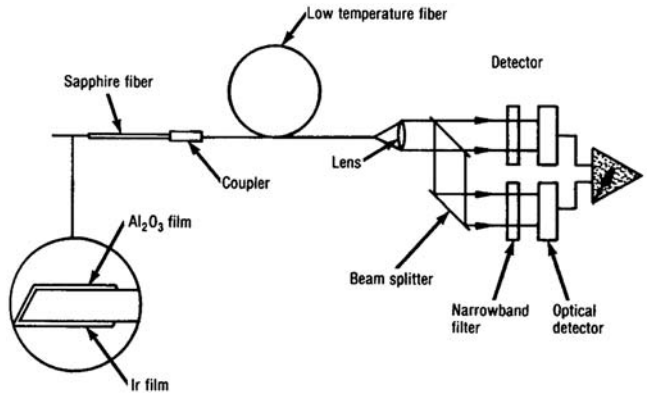

Figure 11.16 Blackbody temperature sensor configuration.

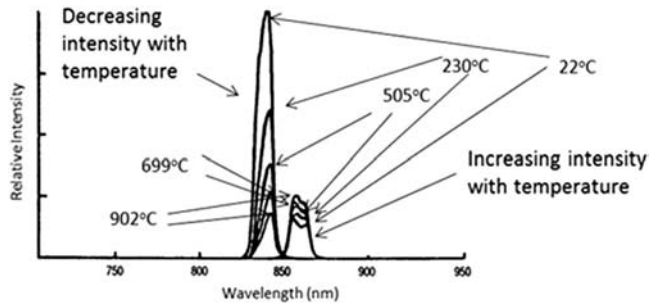

Figure 11.17 Temperature sensitivity absorption spectra for a neodymium-doped glass fiber (Adapted from [25]).

each of the two wavelengths is determined, and the ratio provides a measure of temperature, as shown in Fig. 11.18. The operational range of the sensor is about 0 to 800 °C. A schematic of the sensor system is shown in Fig. 11.19.

Additional research work on rare-earth-doped fibers has shown that their fluorescence lifetime is temperature sensitive and therefore has the potential of a temperature sensor with a broad operating range.[26] Figures 11.20 and 11.21 show fluorescence lifetime versus temperature for Nd-doped fiber and for Er-doped fiber with various erbium concentrations, respectively. The fluorescence spectrum is achieved by pumping the rare-earth-doped fibers with a laser diode. The fluorescence lifetime is sufficiently short (10 μs or less), so it can be used for real-time temperature sensing. While the Er-doped fiber sensor has the potential to operate at higher temperatures, the Nd-doped fiber sensor has better performance and is functional over the range of −190 °C to +750 °C.

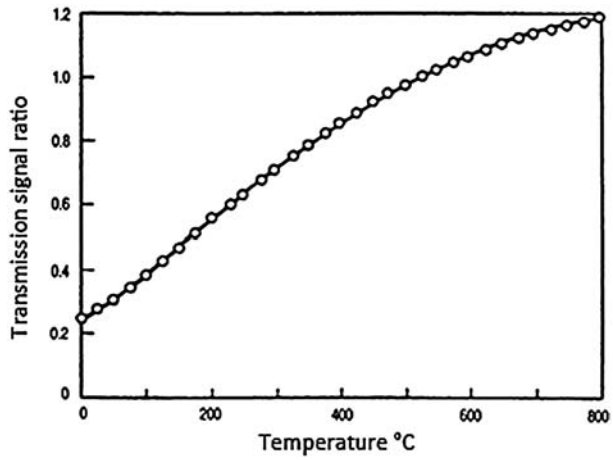

Figure 11.18 Temperature response curve for neodymium-doped glass fiber. (Adapted from [25]).

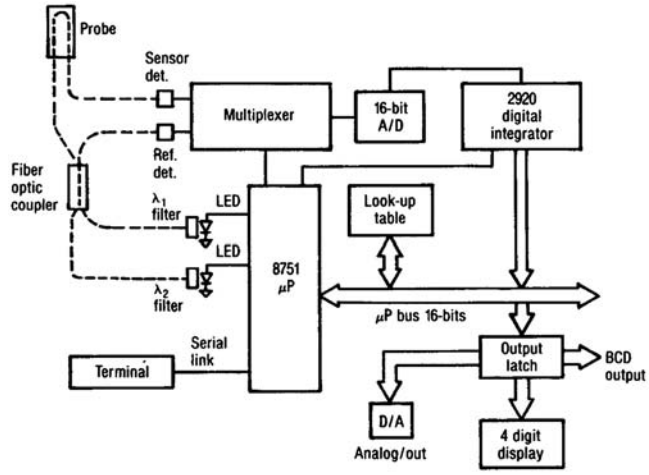

Figure 11.19 Sensor system schematic (courtesy of IEEE, © 1983).[23]

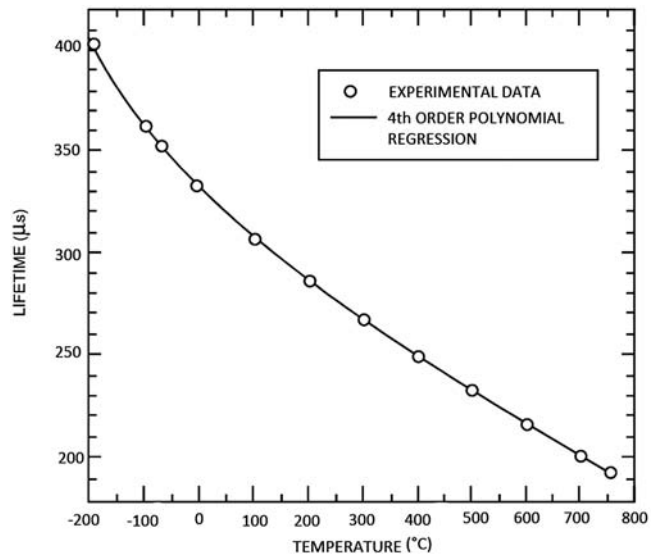

Figure 11.20 Experimental results of the thermal characteristics of the Nd^{3+}-doped fiber.[26]

11.7 Interferometric Sensors

As was discussed in Chapter 4, interferometric sensors are sensitive to both changes in length and refractive index. Their operation depends on the change in phase of the injected light signal as a function of temperature. The temperature phase shift itself depends on both changes to the refractive index of the fiber as well as to changes in its length from thermal expansion. Both effects act simultaneously and combine to cause a net change in the optical

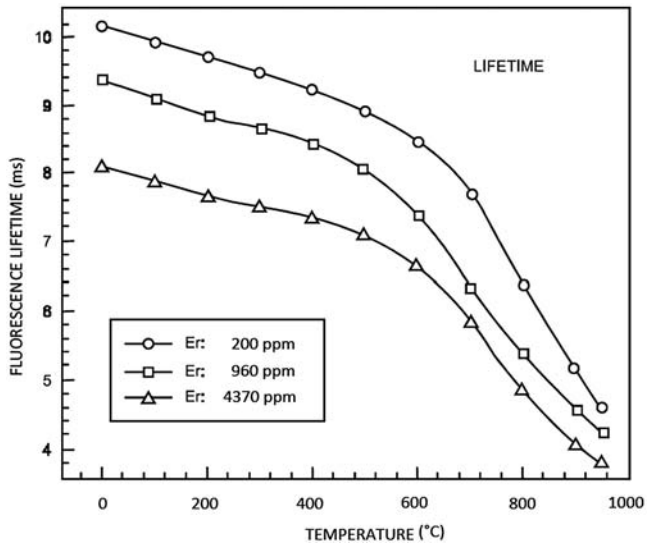

Figure 11.21 Fluorescence lifetimes of Er-doped fibers as a function of temperature.[26]

path length of the light traveling in the fiber. This technique offers extremely high temperature sensitivity, down to 0.005 °C.

For an interferometric temperature sensor, the phase shift as a function of temperature $\Delta\phi/\Delta T$ is given by[27]

$$\frac{\Delta\phi}{\Delta T} = \frac{2\pi L}{\lambda}\frac{n\Delta L}{L\Delta T} + \frac{\Delta n}{\Delta T}, \tag{11.1}$$

where L is fiber length, and n is refractive index. For high-silica-content fibers, the $\Delta n/\Delta T$ term dominates, since the length is relatively insensitive to temperature due to the low coefficient of expansion of silica. The sensitivity of this approach was calculated to detect temperatures as low as 10^{-8} °C. Generally, such high sensitivities are unnecessary, and less expensive techniques will be used. However, this clearly exemplifies the intrinsic capabilities and high sensitivity benefits offered by interferometric approaches.

The phase differential can be implemented using a single fiber, in which case either a shallow or long Fabry–Pérot cavity will be used, whereby several back-reflecting waves will be generated from each of the two mirrors that define the cavity and that will interfere with one another, producing a single- or multifringe response. Alternatively, the interferometer can be formed using two separate fiber arms—one exposed to temperature and the other isolated and used as a reference—in one of the standard configurations such as Mach–Zehnder or Michelson.

A single-fiber interferometric approach is shown in Fig. 11.22.[28] The fiber tip has two reflecting surfaces. One is on the inside surface of the fiber end, and the other is the attached mirror. Both reflected beams travel back through the single fiber. The two beams interfere with the reflected light intensity,

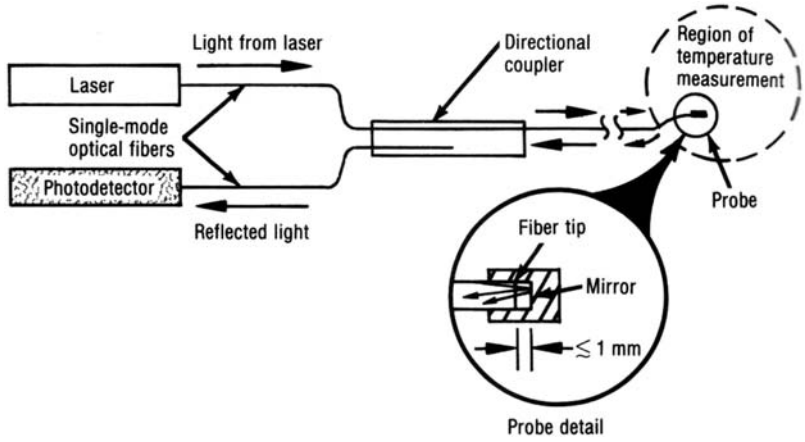

Figure 11.22 Temperature sensor using a single-fiber, Fabry–Pérot cavity interferometer.

being a function of the interference. The interference is, in turn, a function of the gap distance between the fiber-end face and the mirror. The gap is proportional to the differential thermal expansion of the fiber relative to the mirror (mount). In another similar embodiment of this approach, a 1.5-mm-long Fabry–Pérot cavity is defined in a single-mode fiber by mirrors formed with a fusion-splicing technique.[29] The sensor has a temperature sensing capability from –200 to + 1050 °C.

Low-coherence interferometry[30] has also been used to achieve high-temperature sensitivity and broad dynamic range. The approach referred to uses a fiber Fabry–Pérot interferometer (FFPI) as the sensor with a phase modulator, which is a fiber Mach–Zehnder interferometer (FMZI). Figure 11.23

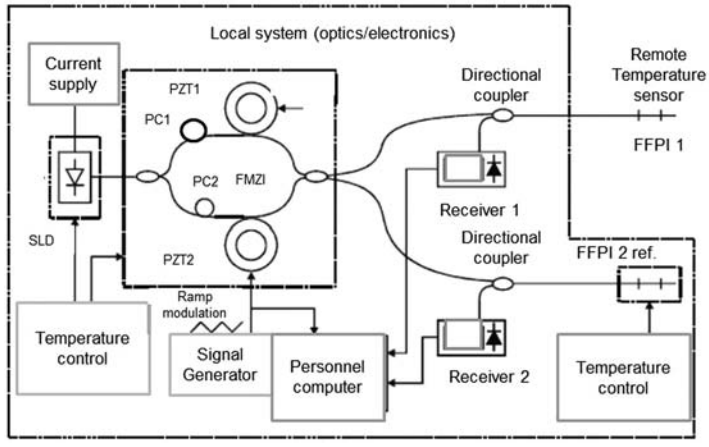

Figure 11.23 Temperature sensor using low-coherence interferometry.[30] (PZT: Photo-electric transducer, PC: Polarization controller, OPD: Optical path length difference, FMZI: Fiber Mach-Zehnder interferometer, FFPI: Fiber Fabry-Pérot interferometer).

shows a schematic representation of the sensing system. The maximum fringe pattern occurs when the optical path difference of the FMZI equals the round-trip optical length of the FFPI. A 1-mm-long FFPI in the schematic discussed above has shown sensitivity of 0.1 °C and a dynamic range of 700 °C.

11.8 Fiber Bragg Grating Sensors

Optical FBGs have also been exploited as effective fiber thermometers and temperature-sensing devices. The fundamental principle is that the peak Bragg wavelength of an FBG shifts to longer wavelengths as the temperature increases, and towards shorter wavelengths when the temperature decreases. The response is linear, and its temperature sensitivity coefficient is a function of the operating wavelength and the material's properties of the fiber in which the FBG is inscribed.

As discussed in Chapter 5, the Bragg wavelength λ_B at which light is reflected is given by

$$\lambda_B = 2\Lambda n, \tag{11.2}$$

where Λ is the period of index modulation, and n is the refractive index of the fiber core. The change in Bragg wavelength associated with temperature change can be expressed as[31,32]

$$\Delta\lambda_B = \lambda_B\left(\alpha + \frac{dn}{dT/n}\right)\Delta T, \tag{11.3}$$

or

$$\Delta\lambda_B = \lambda_B(\alpha + \xi)\Delta T, \tag{11.4}$$

where α is the coefficient of expansion, ξ is the thermo-optic coefficient of the fiber, and ΔT is the temperature change.

The dominant term is the refractive index change with temperature, which is 12 times greater than the change associated with thermal expansion. Using Eq. (11.4), the fractional wavelength shift per °C is 6.7×10^{-6}/°C for silica fiber up to 150 °C. Above 150 °C, this value increases to about 9.6×10^{-6}/°C at 400 °C.

Figure 11.24 shows a plot of Bragg wavelength versus temperature. While the response of a Bragg grating to temperature is shown to about 800 °C, the prolonged use of Bragg grating temperature sensors is limited to temperatures <400 °C, otherwise, the grating itself is gradually erased due to the annealing of the index change produced through the photosensitivity effects used in the first place to inscribe the grating. For example, Fig. 11.25 shows that heating the grating at temperatures above 400 °C begins to decrease reflectivity. Superimposed in Fig. 11.25 are the transmission curves for the grating at various annealing temperatures. As the temperature increases, reflectivity decreases, and the peak of the reflectivity broadens. For operation at elevated temperatures (up to 1000 °C), special fiber gratings are needed such as those

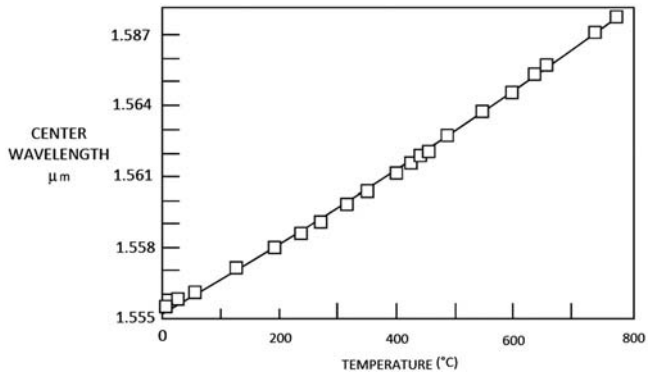

Figure 11.24 Bragg wavelength shift versus temperature.[32]

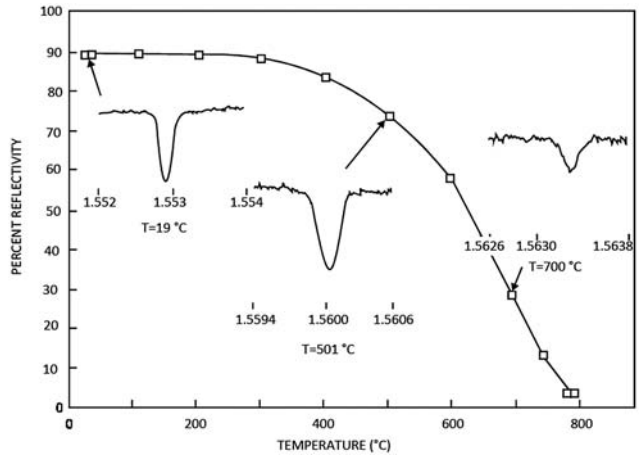

Figure 11.25 Thermal annealing of fiber Bragg gratings.[32]

formed by regeneration techniques and IR femtosecond laser writing techniques.[33,34] Such FBGs are resistant to high temperatures and able to operate indefinitely at elevated temperatures without risk of losing their reflectivity.

To date, FBG temperature sensors are extremely popular and are commercially available in a variety of styles and packaging configurations to meet the needs of different applications, and can be of small size as shown in Fig. 11.26. The one key consideration is to ensure that the portion of the fiber where the FBG is present is mechanically isolated and free to move so that the grating itself responds only to temperature changes and does not introduce any reading errors from strain- or pressure-induced effects that could affect the peak wavelength shift.

The Bragg grating concept is characterized by a rapid response to temperature changes. The temperature range in which the sensor can function

Figure 11.26 Photograph of a fiber Bragg grating temperature sensor (photo courtesy of Micron Optics Inc.).

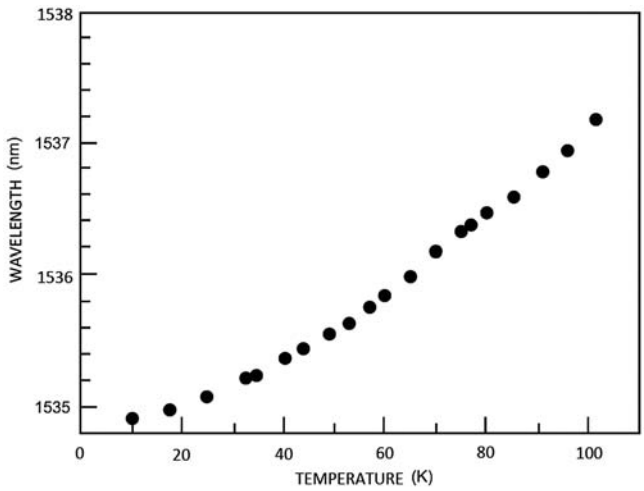

Figure 11.27 Wavelength shift of a grating at cryogenic temperatures.[35]

in a stable manner is at cryogenic levels to about 400 °C. Figure 11.27 shows a plot for temperature response in the 0–100 K range. Bragg grating temperature sensors have the potential to be used in temperature measurements associated with superconducting devices, which require electromagnetic interference (EMI) isolation at liquid helium temperatures.[35]

11.9 Distributed Temperature Sensing (DTS)

In the early 1980s, Raman scattering was first proposed for temperature sensing applications,[36] as it was demonstrated that the magnitude of the anti-Stokes Raman scattering component is highly temperature sensitive, whereas the Stokes component is not. The Raman scattering DTS method is based on the measurement of the ratio of the anti-Stokes to Stokes backscatter intensity components as a function of time (distance); this provides a distributed temperature profile along the fiber, as depicted in Fig. 11.28. To date, the technique has been used extensively in various applications and industries, and several commercial DTS instruments are available.

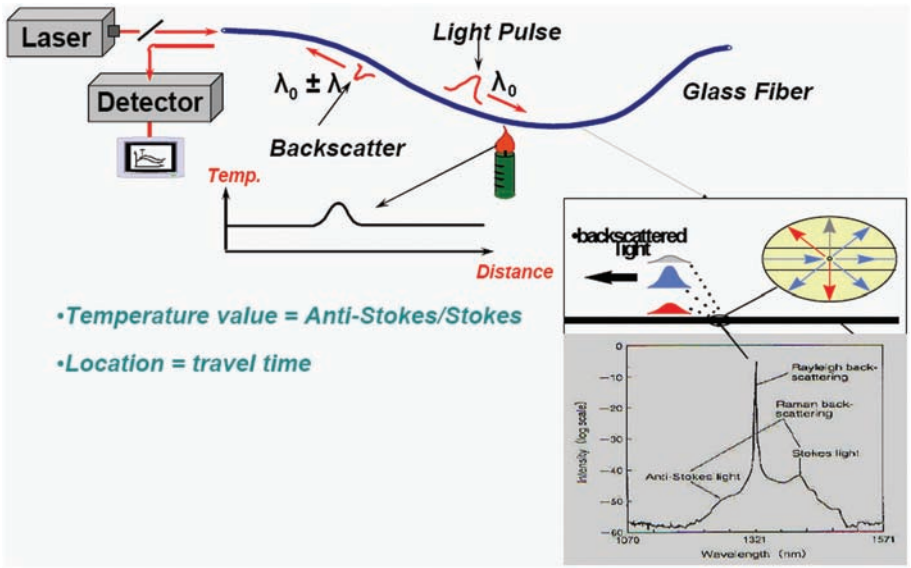

Figure 11.28 Operating principle of Raman scattering distributed temperature sensing (DTS).

The intensity of the Raman scattering I_R is expressed as[37]

$$I_R = \frac{I_o N_o \sigma_R}{(\lambda_i \pm \lambda)^4}, \tag{11.5}$$

where I_o is the intensity of the incident light, λ_i is the incident beam wavelength, N_o is the population of the starting ground level (equal to N_g, the ground level population for the Stokes line, and $N_o = N_g\, e^{\nu/kT}$ for the anti-Stokes component), and σ_R is the Raman cross section for silica glass. The Stokes and anti-Stokes intensity expressions become

$$I_S = \frac{I_o N_g \sigma_R}{(\lambda_i + \lambda)^4}, \tag{11.6}$$

and

$$I_{AS} = \frac{I_o N_g e^{\nu/kT} \sigma_R}{(\lambda_i \quad \lambda)^4}, \tag{11.7}$$

respectively.

The anti-Stokes component is highly sensitive to temperature due to its intrinsic dependence on the absorption of energy from phonons, which is a Boltzmann-driven process with its energy population driven by temperature. Figure 11.29 is a graph of the relative intensity of the anti-Stokes component power versus temperature.

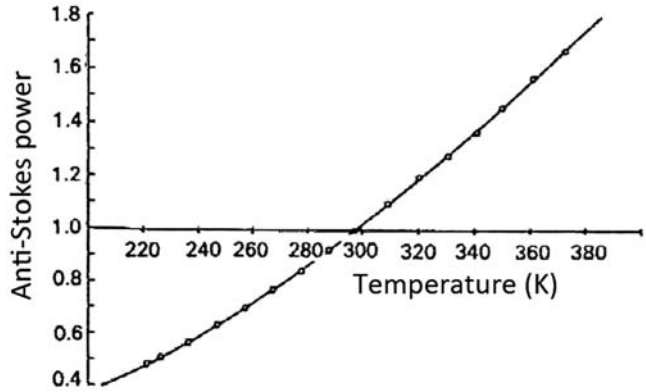

Figure 11.29 Temperature dependence of the Raman anti-Stokes component.[36]

The ratio R of the anti-Stokes to Stokes components is given by

$$R(T) = \frac{I_{AS}}{I_S} = \left(\frac{\lambda_s}{\lambda_a}\right) e^{(hc\Delta\nu/kT)}. \tag{11.8}$$

This ratio is practically independent of the material (cancelling most of the common fiber effects for both scattering components—within a certain spectral range) and depends only on temperature. Thus, a Raman DTS measurement provides an absolute indication of the temperature distribution in the medium, irrespective of the received light intensity, launch conditions, or fiber geometry of material composition. Furthermore, by taking the ratio of the Raman backscatter components, the temperature measurement itself is self-referencing.

To determine the absolute temperature value from this ratiometric measurement of the backscattering signals, Raman DTS systems utilize a reference fiber coil inside their electronics or, alternatively, a calibration run is performed by placing a test fiber coil in a controlled temperature bath. This coil is kept at a constant known temperature, say θ, which produces a backscatter ratio $R(\theta)$. Then, any unknown measured temperature T can be calculated from a re-arrangement of Eq. 11.8 as follows:

$$T = \left\{\frac{1}{\theta} \quad \frac{k}{hcv} \ln\left[\frac{R(T)}{R(\theta)}\right]\right\}^{1}, \tag{11.9}$$

where R(T) is the uncalibrated Raman backscattering ratio and $R(\theta)$ is the ratio from the fiber reference coil at the known temperature θ.

Current commercial Raman DTS systems are well established, functional, and effective devices displaying a very low cross-sensitivity to other parameters, such as pressure or strain. Their main disadvantage is the weak backscatter signal that requires long averaging times and the use of pulsed lasers to achieve adequate returned signal intensity.

The basic setup of a Raman DTS comprises a pulsed laser source that injects a high intensity light pulse into a fiber (typically multimode, but single-mode fiber are used for long-range systems) that acts as the sensing element. Raman backscattered light travels back to the fiber's input where it is coupled out via a splitter into a pair of photodetectors fitted with thin optical filters to select the specific peaks of the Stokes and anti-Stokes spectral components. The photodetectors convert the optical intensity into electrical signals, and the ratio of anti-Stokes/Stokes intensity is obtained. It should be noted that, because of the small intensity of the backscattering signals, signal averaging and integration must be done over a certain time interval in order to obtain a reasonable signal strength and adequate signal-to-noise ratio in the system. The anti-Stokes/Stokes intensity ratio is converted into temperature units by the use of a calibration factor that takes into consideration the fiber characteristics and the particular set-up configuration. Distance information is calculated using the OTDR principle by the specific travel time of each pulse received from the pulse train coupled into the fiber. The data is processed and displayed in graphical form to show a plot of temperature magnitude versus distance. Figure 11.30 illustrates an example of a Raman DTS measurement setup. A portion of the fiber under test is kept in an ice-water bath, while another fiber loop is placed inside hot water. The bottom trace shows the overall temperature profile for the entire fiber length, with the regions of cold and hot temperatures corresponding to the ice and hot water baths, respectively.

Most commercial Raman DTS systems operate using the OTDR configuration, although there is at least one system that operates using the OFDR technique. Each manufacturer uses a different type of laser source (either a laser diode or fiber laser) in their system, operating in one of several wavelength ranges: 900 nm, 1060 nm, 1310 nm, or 1550 nm. In general, most systems are designed for use with multimode optical fibers in order to take advantage of their large numerical aperture (the large acceptance cone of the fiber increases the amount of

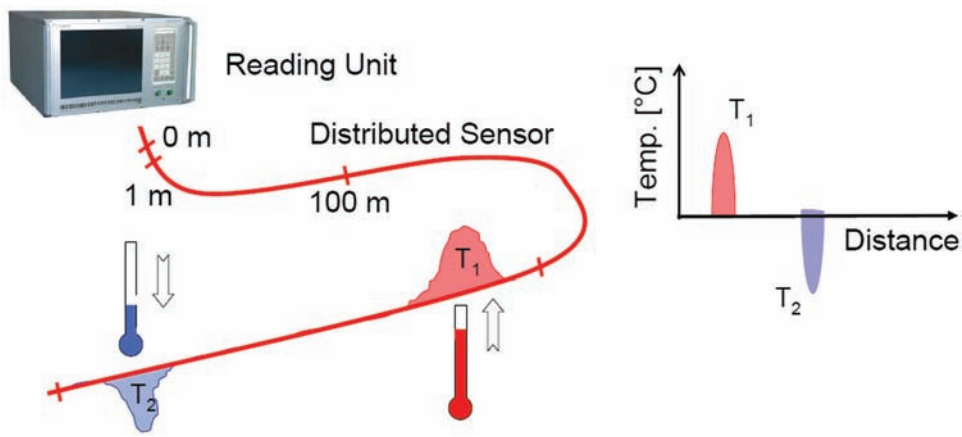

Figure 11.30 Illustration of the Raman DTS measurement (courtesy of Omnisens).

backscattered light that is guided, i.e., useable for sensing purposes) and to accommodate the low intensity of the spontaneous Raman backscatter light. However, the high attenuation of multimode fibers limits the spatial range of Raman DTS to a few kilometers. Hence, some Raman DTS systems are available that operate with single-mode fibers and have range capabilities in excess of 10 km.

A most powerful and unique feature of Raman DTS systems is their capability to perform continuous, distributed measurements of temperature over long distances (tens of kilometers) providing both absolute-temperature and distance-localization information. Raman DTS readings provide a temperature-versus-distance profile of the thermal distribution along a specific test specimen or process onto which the sensing fiber optic cable has been attached. In essence, Raman DTS operates in reflection, such that the electronics remotely interrogates the backscatter light along one or more separate fibers. The continuous temperature profile is composed from hundreds to thousands of measurement points provided by the train of optical pulses launched into the system. Such a multitude of scanning light pulses provides the technique with the capability to measure temperature at meter intervals along the sensing fiber. This approach is simpler and more effective than installing a large quantity of conventional temperature sensors such as thermocouples or RTDs; the cost, installation effort, and wiring requirements would make this approach extremely cumbersome, impractical, and cost prohibitive.

Furthermore, by comparing temperature profiles over time, it is possible to determine the dynamics of any specific process or event of interest, such as the oil flow dynamics in a reservoir or the thermal insulation changes caused by wax buildup in an oil pipeline.

Among the many advantages that Raman DTS offers are the following:

- Distributed temperature measurement over multi-kilometer distances,
- Distance localization of temperature events with 1-m spatial resolution,
- Temperature measurement in the −190 °C to +500 °C range,
- Remote interrogation,
- Immunity to electromagnetic interference,
- Intrinsically safe operation in hazardous or explosive environment locations,
- Simple use and installation,
- Ability to interrogate multiple fibers and set-up measurement zones,
- Capability to measure and compare temperature profiles taken at different times, and
- Possibility to perform real-time temperature measurements and setup alarms.

11.10 Applications

The range of applications of temperature sensors is quite broad, from monitoring relatively low-temperature biological processes to monitoring high-temperature engine parts and furnaces. Several concepts have had great

commercial success and broad use, such as the GaAs reflective sensor, the fluorescent sensor, FBG thermometers, and Raman-scattering distributed sensing systems.

Bimetallic sensors are available in a range from 50 °C to 300 °C. Their potential for use lies in applications such as engine control, air compressors, and industrial processing equipment. Such sensors can be made rugged to withstand shock and vibration. Generally, they are large relative to the fiber and intrinsic sensors, and as a result, have limited dynamic response.

The fluorescence sensor has no metallic components and can be put into an extremely small package. It is especially useful in applications requiring electrical immunity or isolation. The high accuracy (0.1 °C) and small size have made the sensor concept ideal for biological and physiological applications. Hyperthermia, one such area, is a potential cancer therapy requiring local tissue heating using an RF field. The fluorescent sensor has been successfully used in such applications.

Any relatively low-temperature (less than 250 °C) processes using RF heating (such as wood processing and revulcanization of rubber) are potential candidates for this sensor type. The technique is also useful in diagnostic instrumentation associated with high-voltage equipment. The detection of localized heating can often predict the onset of equipment malfunction.

Thermometers based on GaAs etalon devices have been used extensively in biomedical and electric transformer hot spot detecting applications. Similarly, FBG-based temperature sensors are very common and used in a broad variety of applications, primarily for civil infrastructure monitoring.

The blackbody sensor concept has a range of 500–2000 °C. Due to its small size and extremely fast response time, it has applications in many high-temperature processes such as characterizing the heat flow in a gas turbine engine.

The intrinsic concept (such as the approach using absorption) provides a sensing mechanism that can detect hot spots. If such an intrinsically sensing fiber were used in electric motor or transformer windings, it could provide an overheat alarm. It also has potential in distributive temperature sensors, which will be discussed in Chapter 18.

References

1. K. A. Wickersheim and R. B. Alves, "Recent advances in optical temperature measurement," *Industrial Research and Development*, 11–19 (1979).
2. J. J. Dils, "Optical fiber thermometry," *J. Applied Phys.* **84**, 1198 (1973).
3. M. Gottlieb and G. B. Brandt, "Fiber optic temperature sensor based on internally generated thermal radiation," *Applied Optics* **20**(19), 3408–3414 (1981).

4. M. Gottlieb and G. B. Brandt, "Measurement of temperature with optical fibers using transmission intensity effects," *Proc. International Fiber Optics and Communications Conference* **1**, 31–37 (1981).
5. J. C. Anderson, J. Davis, and A. C. Lamb, "Fiber optic temperature/pressure sensor system," U.S. Patent 4,703,174 (1987).
6. D. A. Krohn, "Fiber optic sensors in industrial applications: an update," *Proc. ISA*, 877–890 (1983).
7. Anonymous, "Multipurpose photonic transducers," *NASA Tech. Briefs*, 520–521 (1984).
8. A. M. Scheggi, M. Bacci, M. Brenci, G. Conforti, R. Falcial, and A. G. Mignani, "Thermometry by optical fibers and a thermochromic transducer," *Opt. Eng.* **26**(6), 534–537 (1987) [doi: 10.1117/12.7974111].
9. A. Wang, P. Zhang, R. G. May, K. A. Murphy, and R. O. Claus, "Sapphire fiber-based polarimetric optical sensor for high-temperature applications," *Proc. SPIE* **2191**, 13–22 (1994) [doi: 10.1117/12.173942].
10. G. Beheim, K. Fristch, and D. J. Anthan, "Fibre-optic temperature sensor using a spectrum-modulating etalon," *Proc. SPIE* **0838**, 238 (1987) [doi: 10.1117/12.942513].
11. K. Kyuma, S. Tai, T. Sawada, and M. Nunonshita, "Fiber-optic instrument for temperature measurement," *IEEE J. Quant. Elect*. **QE-18**, 676 (1982).
12. E. W. Saaski, J. C. Hartl, and G. L. Mitchell, "A fiber optic sensing system based on spectral modulation," *Proc. ISA*, 1177–1184 (1986).
13. E. P. Yazbak, "New developments in temperature measurements," *Control* **7**, 36–40 (1987).
14. A. Wang and K. A. Murphy, "Optical-fiber temperature sensor based on differential spectral reflectivity," *Smart Materials and Structures* **1**(1), 5–7 (1992).
15. K. A. Wickersheim and R. V. Alves, "Fluoroptic thermometry: a new RF-immune technology," in *Biomedical Thermology*, M. Cautherie and E. Albert, Eds., Alan R. Liss, Inc., New York, 547–554 (1982).
16. R. V. Alves, J. Christol, M. Sun, and K. A. Wickersheim, "Fluoroptic thermometry: temperature sensing using optical fibers," *Proc. ISA*, 925–931 (1983).
17. K. Wickersheim and M. Sun, "Phosphors and fiber optics remove doubt from difficult temperature measurements," *Research and Development*, 114–119 (1985).
18. K. Wickersheim and M. Sun, "Fiberoptic thermometry and its applications," *J. Microwave Power* **22**(2), 85–94 (1987).
19. K. T. V. Grattan and Z. Y. Zhang, *Fiber Optic Fluorescence Thermometry*, Chapman & Hall, Suffolk, England (1995).

20. W. Kolbeck, "Fiber optic thermometry for difficult surface temperature measurements," *Sensors* **7**, 17–24 (September 1990).
21. M. Gottlieb, G. B. Brandt, and J. Butler, "Measurement of temperature with optical fibers," *ISA Transactions* **19**(4), 55–63 (1980).
22. R. R. Dils and M. P. More, "Optical fiber thermometer measurements in automotive engineers," *Proc. ISA*, 307–322 (1986).
23. E. Snitzer, W. W. Morey, and W. H. Glenn, "Fiber optic rare earth temperature sensors," *Proc. Optical Fiber Sensors Conference*, 79–82 (1983).
24. K. T. V. Grattan and A. W. Palmer, "Simple neodymium rod fiber optic temperature sensor," *Technical Digest OFC/OFS Conference*, p. 142 (1985).
25. M. C. Farries and M. E. Fermann, "Temperature sensing by thermally-induced absorption in a neodymium doped optical fibre," *Proc. SPIE* **798**, 115–120 (1987) [doi: 10.1117/12.941094].
26. Z. Y. Zhong, K. T. V. Grattan, A. W. Palmer, T. Sun, and B. T. Meggitt, "Rare earth doped fiber optic sensors for high temperature measurements up to 1100 °C," *Proc. 12th International Conference on Fiber Optic Sensors*, 556–559 (1997).
27. T. G. Giallorenzi, J. A. Bucaro, A. Dandridge, G. H. Sigel, J. H. Cole, and S. C. Rashleigh, "Optical fiber sensor technology," *IEEE J. Quant. Elec.*, **QE-18**(4), 626–665 (1982).
28. J. M. Maram, "Fiber optic temperature sensor," *NASA Tech Briefs*, 74 (1987).
29. C. E. Lee, R. A. Atkins, and H. F. Taylor, "Performance of a fiber optic temperature sensor from –200 to 1050 °C," *Opt. Lett.* **13**(11), 1038–1040 (1988).
30. H. S. Choi and H. F. Taylor, "High performance fiber optic temperature sensor using low coherence interferometry," *Proc. 12th International Conference on Fiber Optic Sensors*, 570–573 (1997).
31. W. W. Morey, G. Meltz, and W. H. Glenn, "Fiber optic Bragg grating sensors," *Proc. SPIE* **1169**, 98–107 (1989) [doi: 10.1117/12.963022].
32. W. W. Morey, "Development of fiber Bragg grating sensors for utility applications," *Electric Power Research Institute*, Report TR-105190 (1998).
33. E. Lindner, J. Canning, C. Chojetzki, S. Brückner, M. Becker, M. Rothhardt, and H. Bartelt, "Thermal regenerated type IIa fiber Bragg gratings for ultra-high temperature operation," *Optics Communications*, **284**(1), 183–185 (2010).
34. S. Mihailov, "Fiber Bragg grating sensors for harsh environments," *Sensors* **12**, 1898–1918 (2012).

35. T. Mizunami and S. Gupta, T. Shimomura, "Fiber optic cryogenic temperature sensor down to 10K," *Proc. 12th International Conference on Optical Fiber Sensors*, 548–551 (1997).

36. A. H. Hartog and D. N. Payne, "Remote measurement of temperature distribution using an optical fiber," *Proc. ECOC*, 215–220 (1982).

37. R. D. Maurer, "Light scattering by glasses," *J. Chem. Phys.* **25**, 1206 (1956).

Chapter 12
Pressure Sensors

12.1 Introduction

The basic advantages of fiber optic sensors such as immunity to EMI, compact size, and fast response hold true as well for fiber optic sensors applied to the measurement of pressure. Over the years, pressure sensing has included a wide variety of technologies and application areas. The product spectrum ranges from low-cost measurements, such as tire-pressure monitors, to space shuttle applications. The discussion here will be limited to devices that incorporate fiber optic technologies to perform pressure measurement. The application sectors for fiber optic pressure sensors can mainly be divided into segments based on pressure range, temperature range, and frequency response. The basic operating principles of optical modulation for sensing applications have been addressed earlier in the text and will not be repeated here.

In regards to the fiber optic-based designs, the main applications have been directed toward the following: low-pressure, *in situ*, biomedical, high-frequency equipment monitoring, and high pressure oil/gas reservoir monitoring.[1 22] In addition, as is similar to most fiber optic sensing research areas, there have been many other niche ideas that have been designed and built for a multitude of specialized requirements.

The designs that have found the most widespread application have been those based on either FBG technology or Fabry–Pérot architectures. Other approaches such as microbending are described in detail in Chapter 9 of Ref. 23. Applications of fiber optic sensors in the high-pressure oil and gas reservoir monitoring market have seen the most commercial penetration.[18,20] The unconventional sector of this market is characterized by temperatures approaching 300 °C, while conventional offshore installations are subjected to temperatures of 150 °C and below. The maximum pressure for these applications are approximately 1000 and 15,000 psi respectively.

From a commercial standpoint, a reliable, long-term, pressure-monitoring device can bring substantial value to a producing field, which then justifies the investment in this state-of-the-art measurement system. The application of

reservoir monitoring is characterized by very slow-changing pressures. Update rates on the order of one minute or more are quite acceptable. The important value comes from being able to monitor the pressure of the reservoir from its immediate turn on far into its later life. In order to do this effectively, the sensor must maintain a high level of stability, as recalibration is typically not an option. These measurements provide valuable information on the depletion of the reservoir and how best to optimize the production and yield of its resources. For example, a 1% improvement on a 10,000 barrels/day well is equivalent to an annual savings of ~$3.5 million (in 2013 dollars). This is somewhat of an extreme case, but it can be seen from this example that the right monitoring equipment combined with competent reservoir management can be well worth the investment.

Distributed acoustic sensing (DAS) based on coherent Rayleigh backscatter, as well as incoherent Rayleigh and Brillouin scattering have also been implemented in pressure sensing architectures.

12.2 Conventional and Specialized

Figure 12.1 shows the inner workings of a state-of-the-art, conventional-technology-based pressure gauge. This particular device is a quartz resonator, in which a quartz crystal is assembled as part of a resonating electrical circuit. When the device is exposed to pressure, its resonant frequency changes, and the change can be detected by the associated circuitry. This response can then be transmitted digitally via an electric transmission line to a remotely located processor or interrogator. These types of sensors provide high accuracy and fine resolution at a very fast update rate (on the order of <1 sec). In addition, they possess very good long-term stability, especially at temperatures below 125 °C.

Figure 12.1 Quartz resonant gauge courtesy of Quartzdyne Inc.

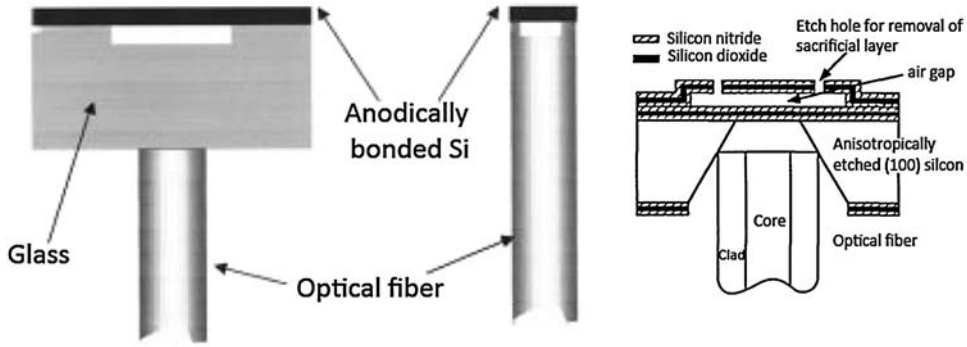

Figure 12.2 Specialized low-pressure fiber optic sensors (reprinted from Ref. 7 with permission).

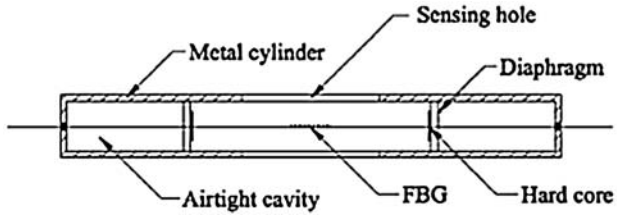

Figure 12.3 Ultrathin FBG pressure gauge (reprinted from Ref. 17 with permission).

As with most electronic devices, there are always challenges with the ability of circuit materials to handle elevated temperature exposure. A typical failure mode for such devices usually involves the inability of solder joints to survive the exposure to temperatures above 125 °C. The fact that these devices also require power at the sensor head to function (active) can be a drawback in certain applications.

In addition to the conventional sensor just described, many low-pressure and specialized sensors have been developed for assorted applications.[1 23] A few of these are shown in Figs. 12.2 and 12.3.[7,16,17]

A majority of these sensors involve the fabrication of a membrane on the end of the optical fiber in order to create a F-P cavity. As can be seen in these diagrams, the membranes are not much bigger than the size of the fiber tip, indicating their fragility and target low-pressure level. There have also been devices fabricated using the combination of specialized fibers and gratings. These have included optical fibers with very small diameters (<125 μm) to enhance the conversion of pressure to strain as well as the use of photonic crystal and microstructured waveguides. Many of these sensors have been developed to fit into very small areas or are made to be ultrasensitive in order to measure very small pressures (15 psi). Early on, photoelastic materials were configured into polarization modulation architectures and used to measure pressure as well. Another specialized

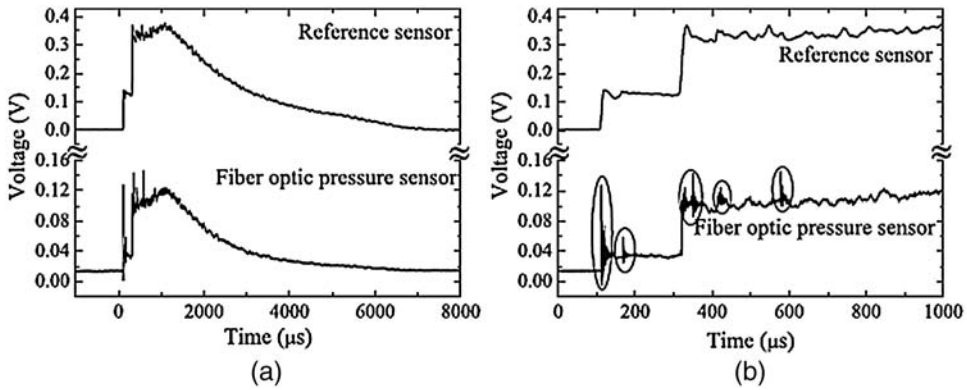

Figure 12.4 Fast-response fiber optic pressure gauge.

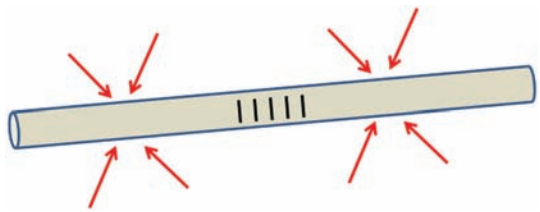

Figure 12.5 Infinitely long fiber containing Bragg grating exposed to hydrostatic pressure.

application is that of high frequency pressure measurement,[22] which is characterized by pressure changes on the order of tens of milliseconds. These sensors typically are applied to the measurement of either combustive or explosive events. The response of such a sensor is shown in Fig. 12.4. When using wavelength-encoded sensors such as F-P or FBG devices, a customized interrogation method is required. Typical high-resolution spectrometers cannot scan this fast on the source or receiver side. Usually the wavelength modulation will be converted to an intensity change using either an edge filter or other WDM filtering devices. This will enable the sensing system to accurately measure and reproduce the time representation of the event.

12.3 FBG-based Optical Sensors

A basic building block and base reference for optical fiber-based pressure measurement analysis and understanding is shown in Fig. 12.5. The figure depicts an optical fiber containing a Bragg grating. The fiber containing the grating is assumed to be infinitely long so that when exposed to a hydrostatic pressure field there are no end effects contributing to the strain (or compression) along the longitudinal direction of the fiber. For reference, this

type of arrangement for a 125-μm-diameter standard silica-based structure yields a scale factor of ~13 psi/pm. This means that it takes approximately 13 psi of hydrostatic pressure to shift the peak wavelength of the Bragg grating 1 pm in spectral wavelength space.

It can be shown that for an infinitely homogeneous, isotropic long rod (or silica optical fiber in this case) exposed to a hydrostatic pressure, the longitudinal strain is[3,4]

$$\varepsilon = \frac{P}{E}(1 \quad 2\nu), \tag{12.1}$$

where
ε = the longitudinal strain,
P = the hydrostatic pressure surrounding the fiber (psi),
E = Young's modulus of fiber material (1.04×10^7 psi), and
ν = Poisson's ratio for fiber material (0.17).

We will define scale factor (SF) as the per unit change in a parameter per unit change in the physical mechanism responsible for the change. The SF for wavelength as a function of pressure is provided as

$$\frac{\Delta\lambda}{\lambda} = 0.78 \times \varepsilon, \tag{12.2}$$

or

$$\frac{\Delta\lambda}{P} = \frac{1\text{pm}}{13\,\text{psi}}. \tag{12.3}$$

Depending on the application, it may be desirable to change this scale factor of 13 psi/pm to something either lesser or greater. This scale factor must be taken into consideration when choosing an interrogator. The interrogator will need to have the appropriate optical source bandwidth and receiver electronics to measure over the entire modulation wavelength range, which is directly related to the pressure range of interest. In practical designs, there are certainly going to be end effects that come into play with any configuration. These create a more complex mechanical system to analyze with closed-form expressions and usually require the aid of a finite element modeling tool. These end effects can be intentionally designed into the transducer in such a way that they are the dominant contributors to any strain (or compression) that may occur as a result of exposure to a hydrostatic pressure field. Using this strategy, FBG-based sensors have been designed with scale factors of ~2 psi/pm. When used as a 0 10,000 psi pressure gauge, the total wavelength change is ~5nm. For WDM-type architectures, where more than one pressure gauge is attached to the same fiber, this sensing bandwidth of 5 nm must be taken into account and allocated to that particular sensor along with a given budgeted tolerance level.

A parameter that is useful for understanding the cross sensitivity of strain and temperature and therefore, indirectly, the performance of the sensor as a pure pressure gauge is

$$\frac{P_{\mathrm{SF}\left(\frac{\mathrm{pm}}{\mathrm{psi}}\right)}}{T_{\mathrm{SF}\left(\frac{\mathrm{pm}}{^{\circ}\mathrm{C}}\right)}}.$$

For example, in the case of the infinitely long fiber exposed to a hydrostatic P, the $P_{\mathrm{SF}} = 0.08$ pm/psi, whereas the $T_{\mathrm{SF}} = 10$ pm/°C. This would mean that a temperature measurement uncertainty of only 1 °C would correspond to a pressure uncertainty of 130 PSI, clearly an unacceptable level for such a device. After a quick analysis of this relationship, it is obvious that a different mechanical structure is required for fabricating a gauge with acceptable performance. It is also important to point out that the main contributor to the temperature scale factor is the dn/dT (where n is the refractive index and T is temperature) coefficient of the fiber core material. This particular property of the FBG-based sensors is not present with the air-gap F-P–type sensor, as the dn/dT coefficient of air is practically negligible when analyzing the sensor response. It quickly becomes obvious that temperature effects will need to be compensated for in the sensor design.

Different configurations of FBG-based sensors have been fabricated and tested. Shown in Fig. 12.6 is a version of an FBG design that utilizes a large-diameter-waveguide element.[21] This geometry provides a lot of design flexibility with respect to adjustment of scale factor. Different end geometries and diameters can be fabricated to make a sensor that is both able to mechanically stand up to high pressures and provides a reasonable peak wavelength change over the measurement. This particular design also shows a feature of having the grating in the thin portion of the body so that the majority of the load appears across this section resulting in a quasi-amplification of the pressure level.

Similar to what will be described with the F-P sensors, the most successful approaches have involved designs that come as close as possible to approximating

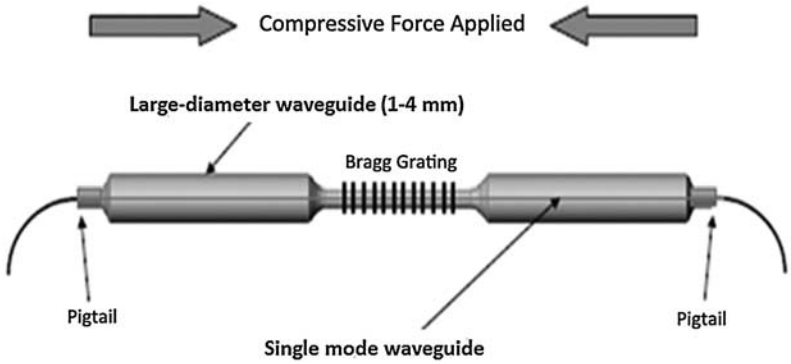

Figure 12.6 Bragg Grating-based fiber optic pressure sensor (reprinted from Ref. 21 with permission).

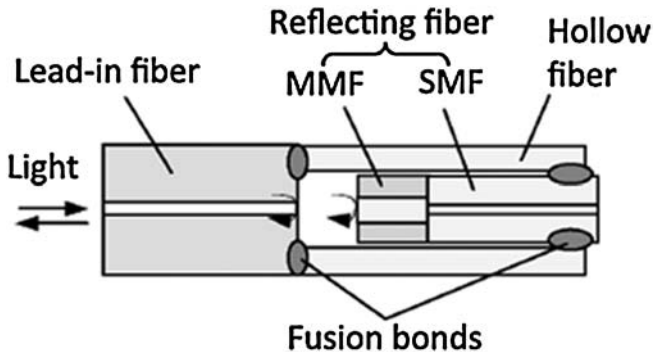

Figure 12.7 Monolithic fiber optic pressure gauge (MMF is multimode fiber, SMF is single-mode fiber) (reprinted from Ref. 11 with permission).

a monolithic construction of glass. The use of common materials for the various sections minimizes stress effects from coefficient of thermal expansion (CTE) mismatch as well as minimizing modulus nonuniformities. This is an important feature when exposing these devices to high forces. To date this has mainly been achieved using laser welding processes to fuse the various glass components together. Especially for harsh environments where there are extreme temperature changes and high pressures, the all-glass construction appears to hold up the best. Together with its low CTE and high elastic limit, these components are a good match for extreme conditions. Figure 12.7 shows an example of a monolithic design implemented into a F-P architecture.[11]

12.4 Fabry–Pérot-based Optical Sensors

Fabry–Pérot-based sensors typically incorporate more disruptions in the optical path than do the FBG architectures. Commonly there is an air path as part of the sensing system. This increases the sensitivity of the F-P designs to parameters such as vibration and shock, which are an important consideration in most applications. Whenever light exits the fiber and is re-injected, alignment of components becomes an important and sometimes challenging consideration to deal with in the sensor design.

Scale factors for F-P–type sensors are similar to those for FBGs to a first approximation. However, even the basic mechanical structure of the simplest F-P sensor is much more complex than that of the simple FBG sensor, creating immediate scale-factor variables that make it challenging to have an apples-to-apples comparison of the two types. Other challenges with the F-P approach also involve control over the etalon reflectivities as well as precise control over the fabrication of the initial or ambient condition cavity length. Efforts to leverage semiconductor fabrication processes have proven very successful in overcoming some of the manufacturing challenges. Figure 12.8 shows a typical design for a fiber-based F-P pressure sensor.[6]

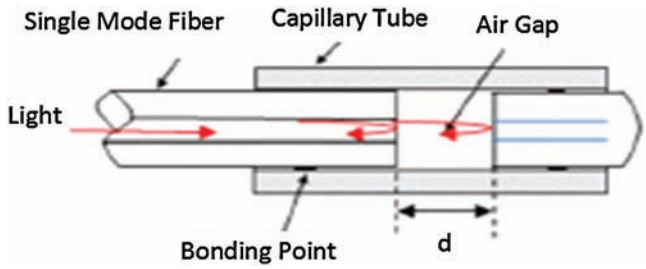

Figure 12.8 Fabry–Pérot fiber optic pressure sensor (reprinted from Ref. 5 with permission).

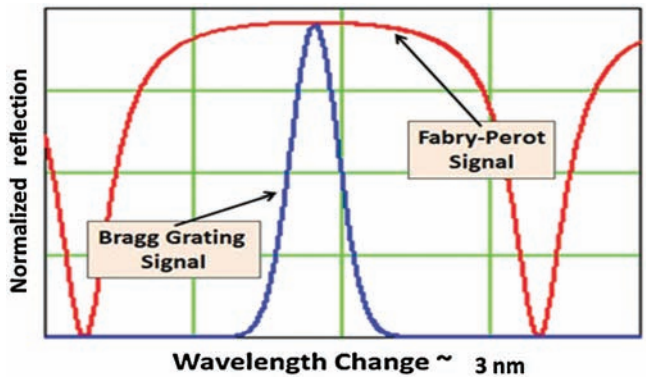

Figure 12.9 Comparison F-P and FBG reflection signals.

The spectrum in Fig. 12.9 shows the optical response of a typical F-P sensor interrogated in reflection compared to that of an FBG signal. In most cases these sensors are single ended and analyzed and, therefore, interrogated in reflection mode. As can be seen in the plot, an important difference between the two signals is the bandwidth and shape of the reflection peak. Together with processing opto-electronics, these optical characteristics will determine the resolution or minimum detectable change of the sensing system. The narrower and sharper peak of the FBG provides a higher-quality signal to measure small changes with and thus, in general, provides finer resolution than F-P devices.

12.5 Packaging

The basic building blocks of a complete optical pressure gauge are shown in Fig. 12.10. The key parts of the design are the transducer and the optical feedthrough. The feedthrough, which allows the optical fiber to pass through to the cable side of the housing must provide a pressure seal over the rated pressure and temperature range. The main challenges with this portion of the sensor can be exposure to cold ($< \ 30\,^{\circ}\mathrm{C}$) and temperature cycling and shock. Material selection is limited, as the device must block pressure over a wide temperature range but not be so mechanically stiff to create unacceptable loss in the optical path by inducing

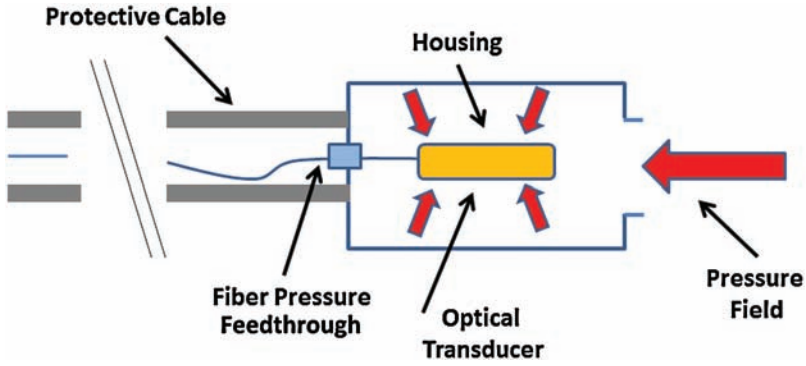

Figure 12.10 Basic building blocks of a fiber optic pressure gauge.

Figure 12.11 Packaged optical pressure gauges courtesy of Weatherford, Oxsensis, and Opsense.

large macro- and microbends in the optical fiber that is passing through it. Commercially packaged optical pressure gauges are shown in Fig. 12.11.

The transducer must be designed to convert the hydrostatic pressure field into a longitudinal strain across either the grating or F-P cavity structure. In addition, the environment immediately surrounding the transducer, the inside of the housing, must be chosen so as to be compatible with the target measurement environment. Depending on whether the target measurement environment is gas or fluid, this transfer medium must be able to communicate the outside pressure to the transducer. The housing design must also prevent the loss of the internal transfer medium.

12.6 Field Installation

The field installation of fiber optic pressure gauges in oil and gas wells can be somewhat complex. Depending on installation architecture, different types of

cable and sensor management will be required. For example, in the most common method of installation, the sensing cable is attached to the outside of the production tubing using either clamps or sometimes a banding technique. Another method involves assembling the cable into coil tubing first and then installing the entire string into the inside of the production tubing or another well-completion component. In some cases, the systems will need to be fed through packers in the completion, adding even more complexity to the installation.

Extreme care and engineering must be applied toward the particular method used for communicating the target fluid or gas pressure to the

Figure 12.12 Field installation of fiber optic sensors (courtesy of Petrospec Engineering).

Figure 12.13 Fiber optic pressure gauge installation (reprinted from Ref. 3 with permission, © 2003 Elsevier).

tranducer. In some cases this will require a separate mandrel or carrier for the sensor itself. The fiber optic cable must then be fed through the wellhead in order to be connected to the interrogating surface instrumentation. This may be located at the wellhead or remotely in a distant control room. These wellhead feedthroughs are similar to the fiber feedthrough at the transducer level in that they need to allow the fiber (or cable) to pass through from a high-pressure area to a low-pressure area and effectively block the pressure over a specified temperature range. Depending on field requirements, this may need to be incorporated at the fiber level or preferably at the cable level.

The photos in Fig. 12.12 and 12.13 show actual installations of fiber optic equipment and sensors into the oil wells. In these photos, the various hardware can be seen, as well as the harsh environments in which the fiber optic hardware must be able to survive and operate. These installations are performed in many types of weather and environmental conditions. Among offshore installations in both arctic and tropical temperatures, the operating specifications can span a very wide range.

Packaging and shipment of the equipment must be considered as well. The components must be packaged at the factory so that they can be safely installed once received on site. Typically, the transducer is attached to the cable at the factory and then spooled off and installed at the site.

References

1. M. G. Xu et al., "Optical in-fibre grating high pressure sensor," *Electronics Letters* **29**(4), 398–399 (1993).
2. G. B. Hocker, "Fiber-optic sensing of pressure and temperature," *Applied Optics* **18**(9), (1979).
3. P. M. Nellen et al., "Reliability of fiber Bragg grating based sensors for downhole applications," *Sensors and Actuators A: Physical* **103**(3), 364–376 (2003).
4. K. O. Hill and G. Meltz, "Fiber Bragg grating technology fundamentals and overview," *Journal of Lightwave Technology* **15**(8), 1263–1276 (1997).
5. W. Zhang, F. Li, and Y. Liu, "FBG pressure based on the double shell cylinder with temperature compensation," *Measurement* **42**(3), 408–411 (2009).
6. Q. Yu and X. Zhou, "Pressure sensor based on the fiber-optic extrinsic Fabry–Pérot interferometer," *Photonic Sensors* **1**(1), 72–83 (2011).
7. D. C. Abeysinghe et al., "A novel MEMS pressure sensor fabricated on an optical fiber," *IEEE Photonics Technology Letters* **13**(9), 993–995 (2001).
8. X. Wang et al., "All-fused-silica miniature optical fiber tip pressure sensor," *Optics Letters* **31**(7), 885–887 (2006).
9. H. Ming et al., "Signal-processing algorithm for white-light optical fiber extrinsic Fabry–Pérot interferometric sensors," *Optics Letters* **29**(15), 1736–1738 (2004).

10. Y. Zhu et al., "High temperature fiber-tip pressure sensor," *Journal of Lightwave Technology* **24**(2), 861 (2006).
11. J. Xu et al., "Miniature temperature-insensitive Fabry–Pérot fiber-optic pressure sensor," *IEEE Photonics Technology Letters* **18**(10), 1134–1136 (2006).
12. R. D. Pechstedt et al., "Fiber optic pressure and temperature sensor for applications in harsh environments," *Proc. SPIE* **8794**, 879405 (2013) [doi: 10.1117/12.2025725].
13. X. Wang, J. Xu, Y. Zhu, B. Yu, M. Han, K. L. Cooper, G. R. Pickrell, and A. Wang, "An optical fiber tip pressure sensor for medical applications," *Quantum Electronics and Laser Science Conference*, JTuC46 (2005).
14. Y. Zhang, D. Feng, Z. Liu, Z. Guo, X. Dong, K. S. Chiang, and B. C. B. Chu, "High-sensitivity pressure sensor using a shielded polymer-coated fiber Bragg grating," *IEEE Photonics Technology Letters* **13**(6), 618–619 (2001).
15. A. D. Kersey et al., "Fiber grating sensors," *Journal of Lightwave Technology* **15**(8), 1442–1446 (1997).
16. Y. Kim and D. P. Neikirk, "Micromachined Fabry–Pérot cavitv pressure transducer," *IEEE Photonics Technology Letters* **7**(12), 1471–1473 (1995).
17. W. T. Zhang, F. Li, Y. L. Liu, and L. H. Liu, "Ultrathin FBG pressure sensor with enhanced responsivity," *IEEE Photonics Technology Letters* **19**(19), 1553–1555 (2007).
18. D. L. Gysling and F. X. Bostick III, "Changing paradigms in oil and gas reservoir monitoring: the introduction and commercialization of in-well optical sensing systems," *Optical Fiber Sensors Conference Technical Digest* **1**, 43–46 (2002).
19. P. E. Sanders, T. W. MacDougall, F. Birritta, M. R. Melnychuk, K. M. Molzan, and G. V. Chalifoux, "Field evaluation of dual-ended, high temperature, hydrogen tolerant fiber optic DTS sensor with compact fiber Loop assembly," *Proc. World Heavy Oil Congress* (2011).
20. P. Sanders and T.W. MacDougall, "Recent developments in fiber optic sensor technology for high temperature well monitoring," *Proc. GeoThermal Research Council Annual Meeting* **33**, 859–864 (2009).
21. T. W. MacDougall and P. Sanders, "Large-diameter waveguide Bragg grating components," *Proc. SPIE* **5589**, 221 (2004) [doi: 10.1117/12.579165].
22. N. Wu, X. Zou, Y. Tian, J. Fitek, M. Maffeo, C. Niezrecki, J. Chen, and X. Wang, "An ultra-fast fiber optic pressure sensor for blast event measurements," *Meas. Sci. Technol.* **23**, 055102 (2012).

Chapter 13
Flow Sensors

13.1 Introduction

Flow measurement is a critical process-control parameter in a wide range of applications such as engine control, power generation, industrial processes, and oil and gas production optimization. Often the environment is difficult. The sensor can be subjected to high electrical noise, explosive environments, relatively high temperature, and areas of difficult access. Fiber optic sensors have the ability to perform under these environmental conditions and to be the basis for several sensing approaches.

Six basic sensing concepts have been used for flow detection using fiber optics:[1]

1. Rotational frequency monitoring of a paddle wheel or turbine in the flow field,
2. A cantilevered beam that bends in the flow path,
3. Differential pressure measurement across an orifice,
4. Frequency monitoring of a vortex-shedding device,
5. Laser Doppler velocimetry, and
6. Indirect flow monitoring.

These concepts will be discussed in terms of how they can be implemented with fiber optics.

13.2 Turbine Flowmeters

Turbine flowmeters require that they be put in the flow path, which causes a flow obstruction. The meter also has moving parts. Both of these features are generally undesirable, but the approach is accurate and repeatable and has broad industrial acceptance. Turbine flowmeters have a rotating device called a rotor, which is positioned in the flow stream. The rotor velocity is proportional to the flow velocity of the fluid passing through the device.[2] A simple device is shown in Fig. 13.l. The rotor rotational speed is monitored using a reflective fiber optic probe.

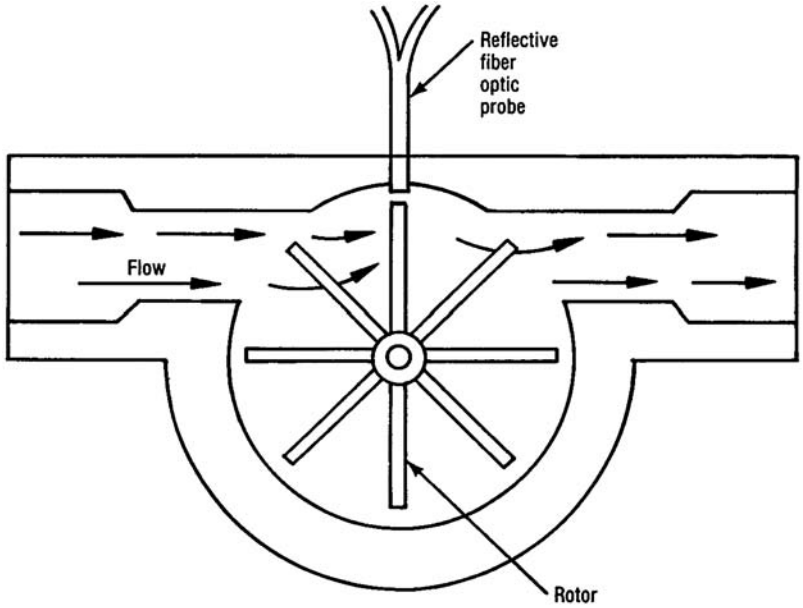

Figure 13.1 Turbine flowmeter with a reflective fiber optic sensor.

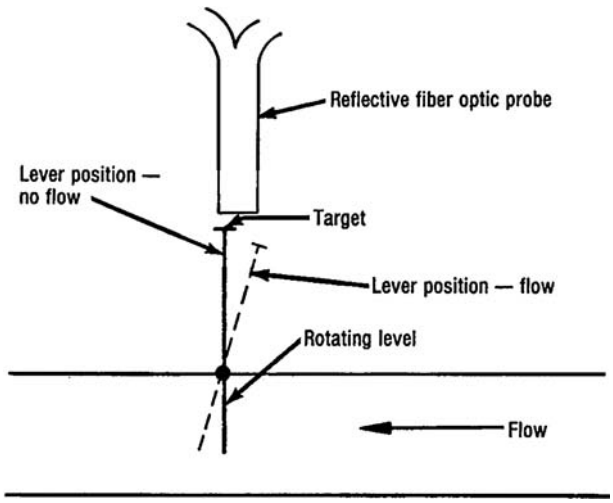

Figure 13.2 Rotating-lever flowmeter.

As each vane of the rotor passes the probe, a reflected optical pulse is generated. Since the sensor is digital in nature, the problems associated with fiber optic, intensity-modulated analog signals are eliminated.

An extension of a turbine flowmeter could be a lever that partially rotates due to fluid flow.[3] The position of the target attached to the end of the lever indicates that flow is occurring (digital switch function) as shown in Fig. 13.2. If the lever provides resistance proportional to the flow level, the rotation of the target results in an analog measurement of flow.

13.3 Cantilevered-Beam Flow Sensors

Cantilevered-beam flow sensors can be used for a wide range of flow detection applications, from industrial pipes in a refinery to microscale flow for lab-on-a-chip. For the industrial application, the system must be robust. Figure 13.3 shows a cantilever flow sensor using white-light interferometry.[4,5]

The cantilevered beam shown has two fiber leads with an air gap that forms an interferometric cavity on both sides of the beam. As the beam bends in the flow path, the air gap changes as a result of the deflection. The air gap of the sensor on the side facing the flow will increase because it is pulled in tension, and the air gap on the other side will decrease due to compression. The air-gap change is measured by the reflected light intensity from each interferometric cavity. The flow rate is a function of the difference between the two air-gap changes and is dependent on the geometry of the cantilevered beam. Figure 13.4 shows the general relationship between the air-gap changes and the flow rate. Since temperature changes that may occur are experienced by both the front and back sensors, their effect is cancelled, and, as a result, the temperature compensation is automatic.

Microflow sensors are a critical element of lab-on-a-chip.[6] The objective is to create a microflow sensor with high sensitivity and wide dynamic range. In a configuration similar to the cantilevered design discussed previously, the

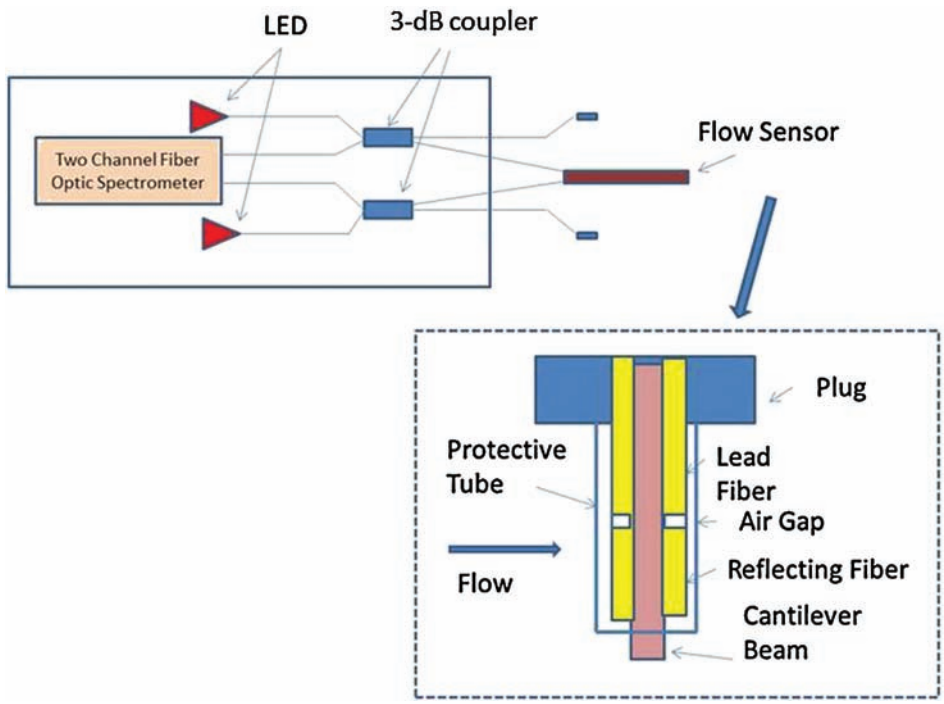

Figure 13.3 Fiber flow sensor using a cantilevered beam in conjunction with white-light interferometry.[4]

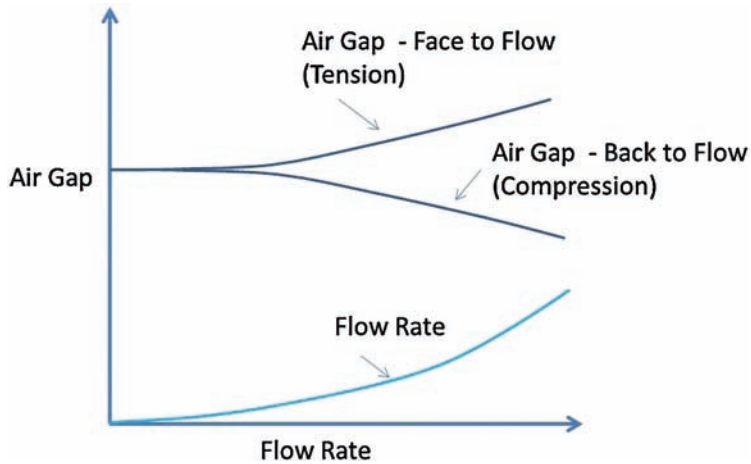

Figure 13.4 Cantilevered-beam flow sensor showing air gap versus flow rate relationship.[4]

fiber now is the integrated cantilever beam and sensor.[7] The sensing concept involves the displacement of the transmitting single-mode fiber and the change in coupling to the receiving multimode fiber. The cantilevered single-mode fiber is displaced by the flow drag. The displacement is a function of the fluid density, flow rate, and the stiffness of the cantilevered fiber, which is a function of the fiber diameter, cantilevered length, and Young's modulus. The concept is shown in Fig. 13.5.

Figure 13.6 shows the transmitted light intensity versus volumetric flow rate for liquids with different densities and viscosities. The cantilevered fiber displacement is lower in low viscosity, low-density liquids and higher in high-viscosity, high-density liquids. As a result, the transmitted light intensity decreases more rapidly as the flow rate increases for high-viscosity, high-density liquids. If the light source does not provide a uniform Gaussian pattern (side lobes), then nonuniformity can occur in the response curves.

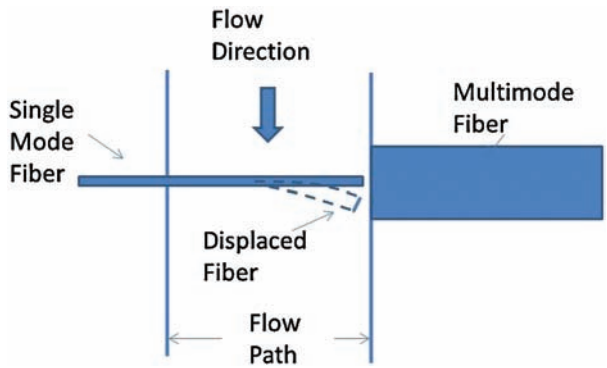

Figure 13.5 Microflow sensor based on a cantilevered fiber.

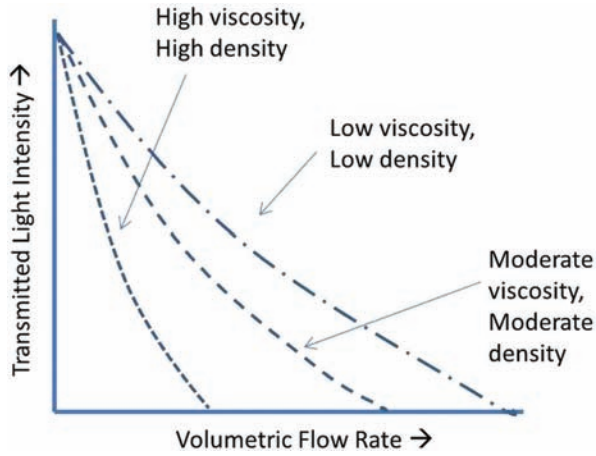

Figure 13.6 Transmitted light intensity versus volumetric flow rate for liquid with different densities and viscosities.

13.4 Differential-Pressure Flow Sensor

For a differential-pressure flow sensor, the volume of fluid is forced to flow through a restriction area with reduced cross section. The restriction causes an increase in flow rate at that point. The net effect is a pressure drop associated with the restriction. The change in pressure is proportional to flow. A general description of differential pressure-flow measurement can be found in Refs. 2 and 8.

Figure 13.7 shows the concept of a differential-pressure flow monitor using fiber optic pressure sensors. The pressure prior to the restriction is P_1, and the pressure after the restriction is P_2 with $P_1 > P_2$.

The simplicity of differential-pressure flow sensors gives them the potential for widespread use. They are especially well suited for low-viscosity fluids and gases.

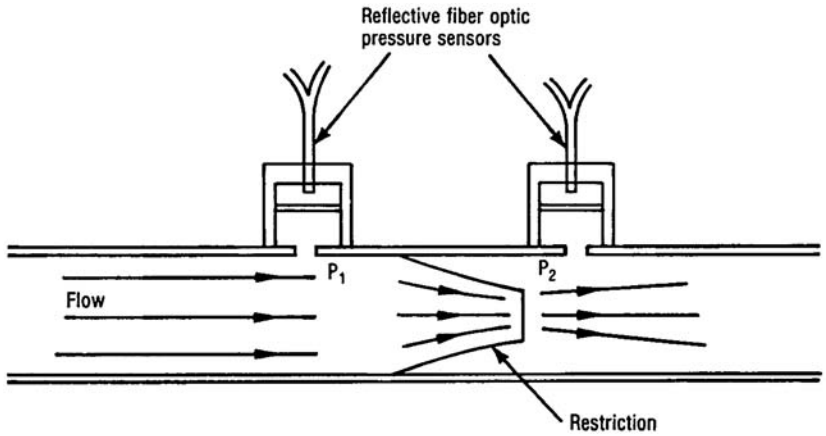

Figure 13.7 Differential-pressure flow sensor using reflective fiber optic pressure sensors.

13.5 Vortex-Shedding Flow Sensor

Figure 13.8 illustrates the concept of a vortex-shedding flow monitor. As a fluid passes over a bluff body, alternating vortices are generated from each side of the bluff body. The vortex formation causes a pressure pulse. The frequency of pressure pulses is proportional to the fluid velocity, as shown in the following equation:

$$f = SVd, \tag{13.1}$$

where f is the pressure-pulse frequency, S is the Strouhal number, a dimensionless constant that is flow-rate dependent, V is the flow velocity, and d is the width of the bluff body. A detailed description of the approach is found in Ref. 2. A unique feature of this sensor is that it is inherently digital. Therefore, only a pressure excursion, not actually the magnitude of the pulse, needs to be determined.

The position of the sensors is shown in Fig. 13.9. Generally, access is limited. Therefore, the reflective fiber optic technique for monitoring diaphragm movement is a logical choice for this application.

Another approach uses a microbending concept in a very simple configuration, as shown in Fig. 13.10.[9] The optical fiber itself is the bluff body. Chapter 3 discussed intensity modulation by means of microbending. This microbending approach uses the excitation pattern of light as the modulation mechanism. Changes in the pattern can be detected using a photodetector array, then pressure-perturbation frequency associated with vortex formation is determined.

Figure 13.11 shows a plot of shedding frequency (pressure pulse frequency) versus fluid flow rate (300-μm core fiber with NA = 0.37, water flow in 2.5-cm diameter pipe). The dashed line is the theoretically predicted curve. The measured flow is close to the theoretical case.

The distinct advantage of this approach is the very small size of the sensing element obstructing the flow path. A disadvantage is that it appears to

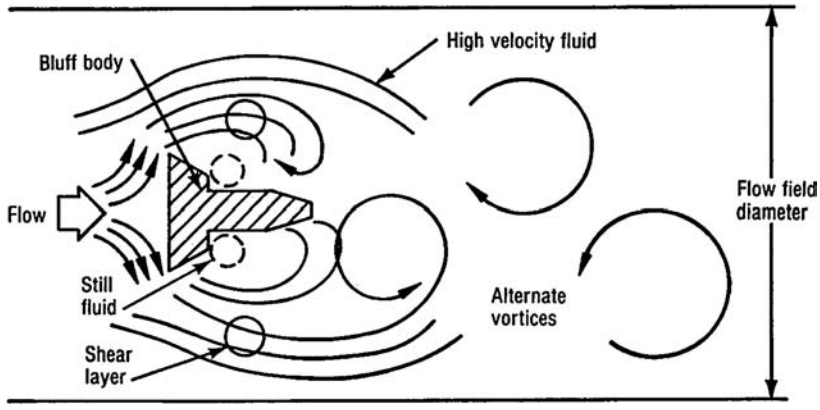

Figure 13.8 Shedding-vortex concept.

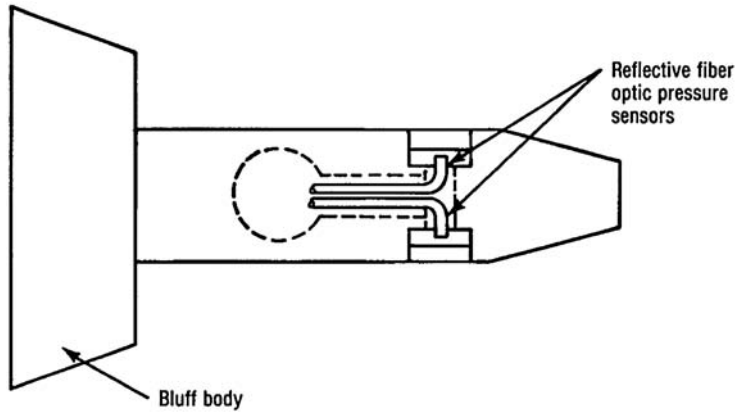

Figure 13.9 Reflection fiber optic pressure sensor in a shedding-vortex flow monitor (reprinted from Ref. 9 with permission).

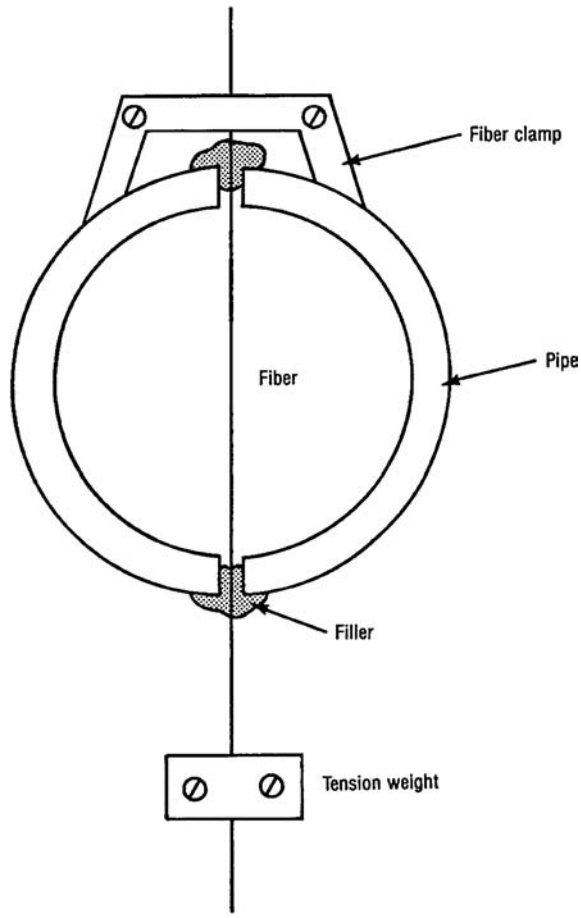

Figure 13.10 Shedding-vortex monitor using a microbending sensor (courtesy of IEEE, © 1981).

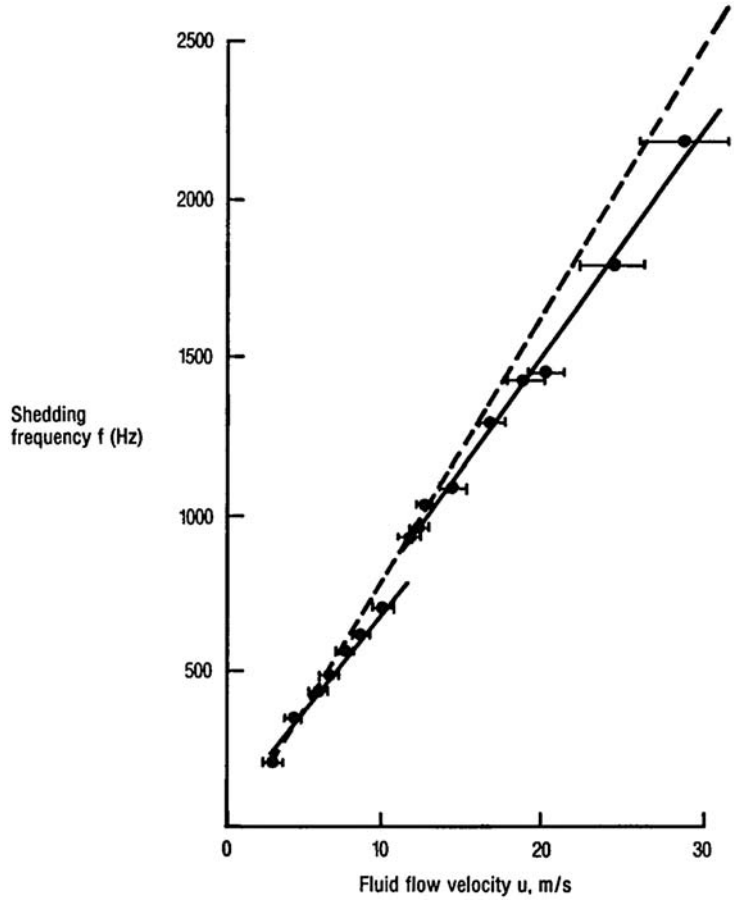

Figure 13.11 Shedding frequency versus fluid flow rate (courtesy of IEEE, © 1981).

be possible to have dead zones, which are associated with natural resonant frequencies in the sensor response.

13.6 Laser Doppler Velocity Sensors

Laser Doppler velocimetry (LDV) provides for a noninvasive mechanism to measure fluid flow.[10] The dual-beam method [see Fig. 13.12(a)] provides two beams of equal intensity focused at a common point. The intersection of the two beams creates an interference with the fringes being generated. The fringe pattern is parallel to the bisector of the beams. As a particle passes through the fringe pattern (dark and light regions), light is scattered. The intensity across the laser beam associated with scattering is Gaussian, as shown in Fig. 13.12(b). In Fig. 13.12(c), if the distance between fringes is df, and the time to pass from one fringe to another is t, then the velocity component in a direction normal to the fringe is U_x, therefore,

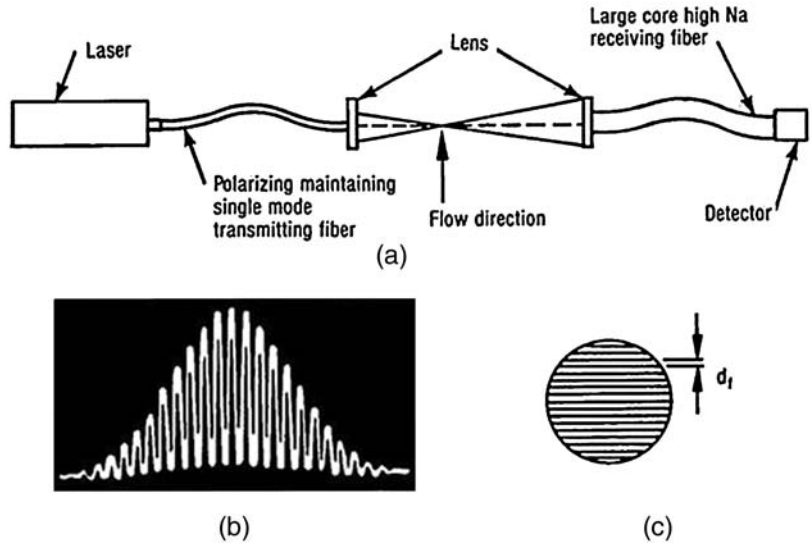

Figure 13.12 Principle of operation of an LDV system. (a) Sensor configuration (dual beam), (b) light intensity across laser beam, (c) fringe pattern at beam crossing point.

$$U_x \quad \frac{d_f}{t} = d_f F, \tag{13.2}$$

where F is the frequency of fluctuation in scattered light intensity, referred to as the Doppler frequency.

The arrangement in Fig. 13.12(a) requires constant polarization of the input light. Therefore, a polarization-maintaining fiber is on the input side. A large-core, multimode, high-NA fiber is used for maximum collection efficiency.

Fiber-optic-based LDV systems have distinct advantages. The use of fiber optics eliminates the need for bulkier optical components and allows for a very compact sensor. The technique is noninvasive and measures velocity directly. It does not use flow properties in the measurement and, therefore, does not require calibration. The concept also has a very broad dynamic range, from low-speed biological flows to supersonic levels.

13.7 Indirect Flow Monitoring

Flow can cause changes in temperature along the flow path and create a vibration signature (acoustic signals) that is characteristic of the flow rate. Therefore, distributed temperature sensors can detect changes in temperature that can be correlated with changes in flow. Detecting the acoustic emission can be correlated with flow rate or other flow changes such as liquid viscosity or density changes as well as obstructions in the flow path. These approaches are minimally invasive and have been very useful in oil and gas operations.

Monitoring where stimulation fluids are flowing is very beneficial in multizone completions for oil wells. An accurate understanding of where fracture initiation is occurring allows stimulation fluids to be diverted to other parts of the reservoir that need enhanced stimulation. The flow data helps improve completion efficiency. Real-time flow data allows operators to intervene and repair malfunctions in the well before a major disruption occurs.

The flow data is generated indirectly by monitoring temperature changes with Raman-based DTS systems and acoustic changes with Rayleigh-based DAS systems. The flow of liquids and gases can be determined for the various zones of the well.[11]

13.8 Applications

Generally, the flow-sensor concepts described have potential use primarily for industrial and power-utility applications. Engine-control applications are in an earlier product development stage, due in part to this application being more cost sensitive. Miniature fiber-optic-based flow sensors can be used for biological lab-on-a-chip applications.

The immunity from electrical and environmental noise as well as the inherent safety of fiber optic sensors will be the driving force for their use. The laser Doppler flow sensor has a much broader application range. It has been used for monitoring blood flow, biological cell flow, flow associated with industrial processes such as paper and steel manufacturing, and flows associated with ultrahigh-speed processes such as are found in aircraft applications. As previously mentioned, flow can be monitored indirectly with temperature and acoustic sensors. The latter approach is especially attractive for oil and gas well monitoring in which the harsh environment limits most conventional techniques.

References

1. I. G. Giallorenzi, J. A. Buccaro, A. Dandridge, and J. H. Cole, "Optical-fibers sensors challenge the competition," *IEEE Spectrum* **23**(9), 45–49 (1986).
2. D. W. Spitzer, *Industrial Flow Measurement*, ISA, Research Triangle Park, N.C., pp. 311–323 (1990).
3. J. C. Anderson, R. Eberlein, and M. J. Davies, "Fiber optic flow indicator system," U.S. Patent 4,596,442 (1986).
4. K. Cooper, G. Pickrell, and A. Wang, "Optical fiber sensor technology for efficient and economical oil recovery," Technical Report, DOE Contract: DE-FG26988C15167 (2003).
5. W. Peng, G. Pickrell, Z. Huang, J. Xu, D. Woong, B. Qi, and A. Wang, "Self-compensating fiber optic flow sensor system and its field applications," *Applied Optics* **43**(7), 1752–1760, (2004).

6. V. Lein and F. Vollmer, "Microfluidic flow rate detection based on integrated optical fiber cantilever," *Lab on a Chip* **7**(10), 1352–1356 (2007).
7. C. P. Renschen, "Fiber optic flow sensor with high dynamic range," *Proc. SPIE* **1795**, 325 (1993) [doi:10.1117/12.141261].
8. D. R. Gillum, *Industrial Pressure Measurement,* ISA, Research Triangle Park, N.C., pp. 54–62 (1982).
9. J. H. Lyle and C. W. Pitt, "Vortex shedding fluid flowmeter using optical fiber sensor," *Electronics Letters* **179**(6), 244–245 (1981).
10. R. K. Menon, "Velocity measurement using fiber optics," *Proc. ISA*, 1185–1195 (1986).
11. Anonymous, "Fiber Optic Sensing Technologies for Well Monitoring to Reservoir Management," www.Halliburton.com, (2012).

Chapter 14
Magnetic and Electric Field Sensors

14.1 Introduction

The main application for magnetic and electric field fiber optic sensors has been the electric power industry.[1 13] The ability to dielectrically isolate equipment and personnel from high power provides an attractive feature in terms of safety and, ultimately, cost for fiber optic systems versus those using conventional technology. In terms of performance, the theoretical bandwidth of the physical processes occurring within the optical techniques is much faster than the corresponding conducting devices. Also, effects such as hysteresis and saturation (dynamic range), which are common issues with magnetic materials, are, for all practical purposes, absent from the optical components. The size and weight of these devices are also an advantage over iron-core-based designs. All of these characteristics have inspired the vast amount of research and engineering devoted to the development and commercialization of optical-based products.

Several sensing approaches have been successfully conceived using fiber optics for both magnetic and electric field sensing. For magnetic field sensing (of which current is a special case), the majority of the designs exploit the Faraday effect and are polarization based.[15 33] Interferometric approaches using metallic glass and other various magnetostrictive coatings on fibers have also been demonstrated in the past.[35 46] More recently, the Sagnac interferometer configuration has proven to be the architecture that has found the most commercial acceptance.[12,59] For electric field and voltage sensing, polarization-based schemes have been described using electro-optical materials to utilize the Pockels and Kerr effects. Interferometric phase-modulation techniques for electric field monitoring have centered on piezoelectric fiber coatings.[47 53]

14.2 Magnetic Field

14.2.1 Faraday rotation-based sensors

The Faraday effect is a rotation of the plane of polarization of light propagating in certain transparent materials.[13] A transmissive fiber optic sensor can be used to measure the magnetic field and to determine the current of a nearby conductor (or, preferably, an encircled conductor) if a magneto-optical material is placed in the light path. The material can be incorporated intrinsically in the fiber or within a bulk material that is inserted between two fibers in a transmissive mode as shown in Fig. 14.1.

The underlying mechanisms of the Faraday effect are related to Zeeman splitting and the Lorentz force applied to material electrons. The splitting of the absorption lines in the Zeeman process can be also thought of as splitting the complex index of refraction function in "circular" space. The end result of all this is a change in refractive index that shows up as a circular birefringence within the material.[13] An interesting characteristic of the Faraday effect is that it is nonreciprocal, meaning that the rotation angle is the same in either direction. For example, if a light signal is reflected back on itself through the magneto-optic material it will double the amount of rotation as opposed to cancelling it out.

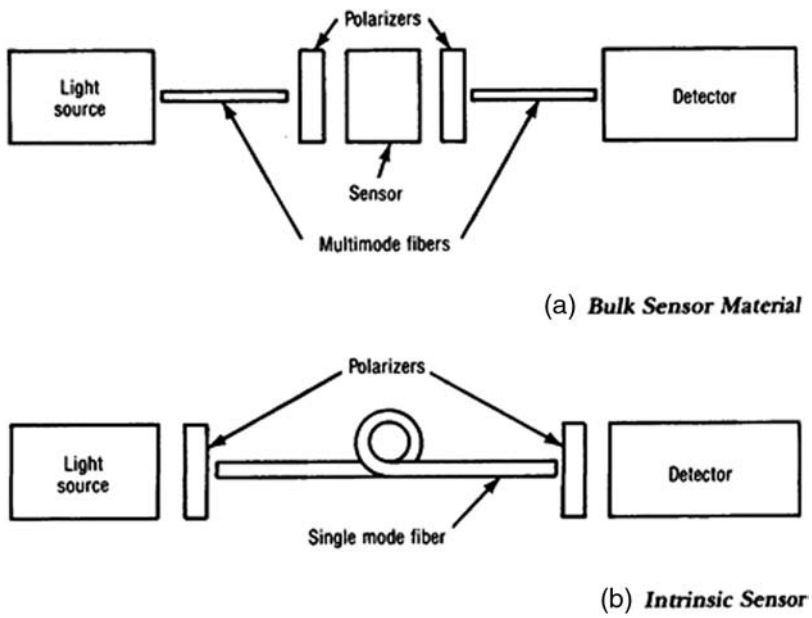

Figure 14.1 Fiber optic magnetic field sensor architectures.

Mathematically the Faraday rotation is defined as[16]

$$F = \mu V \int_0^l \mathbf{H} \cdot d\mathbf{l}, \tag{14.1}$$

where:

F = Faraday rotation (rad),
μ = Material permeability (H/m),
V = Verdet constant of material (rad/T-m),
l = Path length of light (m), and
$\mathbf{H}$ = Applied magnetic field (A/m).

When the optical path completely encloses the conductor,

$$\mathbf{H} = \frac{I}{2\pi\rho}\ \hat{\varphi}, \tag{14.2}$$

and

$$d\mathbf{l} = \hat{\varphi}\rho d\varphi, \tag{14.3}$$

where:

I = Conductor current (A),
ρ = distance between conductor and light path element (m).

The Faraday rotation then reduces to

$$F = \mu VNI, \tag{14.4}$$

where N = number of turns of fiber loops around the conductor.
When the magneto-optic material is placed between polarizers, the transmitted signal is proportional to

$$\cos^2(F). \tag{14.5}$$

Such a configuration is shown in Fig. 14.2, with a typical installation shown in Fig. 14.3.

The material-dependent Verdet constant is an important parameter in the performance of these sensors. For typical germanium-doped fiber materials, the Verdet constant value is approximately 3–4 times lower than that of flint glass bulk optic sensors and about 50 times lower than that of iron-garnet-doped crystals. The higher-Verdet-constant crystal structures allow for short sensor path length (or reduced number of turns), which enables the sensor to be compact. This sensor concept is not susceptible to birefringence noise but requires bulk optical components in the vicinity of the actual sensing point. Due to the fact that it is difficult to form bulk optic components into a closed path geometry, these materials are better suited for pure field sensing as opposed to current sensing. Due to lower sensitivity associated with a low Verdet constant, an intrinsic fiber sensor requires a long path length to achieve sensitivity, but the sensor configuration is quite flexible and allows for

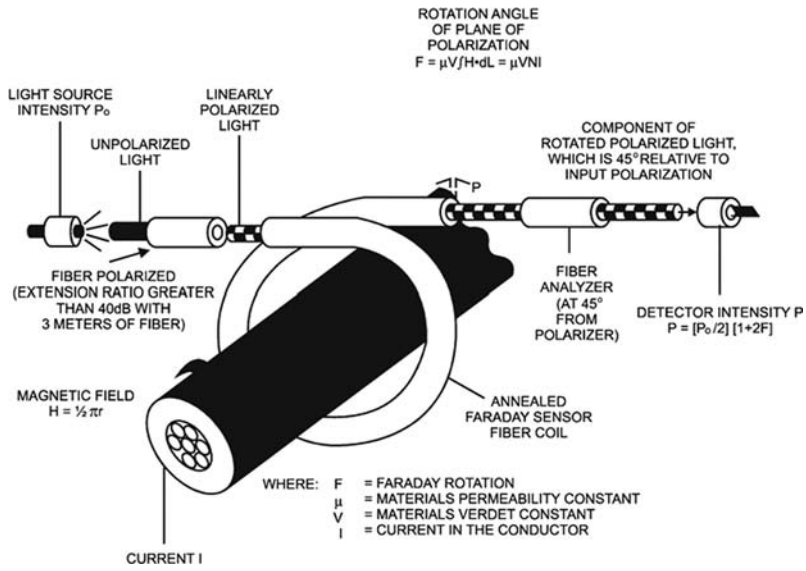

Figure 14.2 Faraday rotating optical fiber with attached polarizing optics.[31]

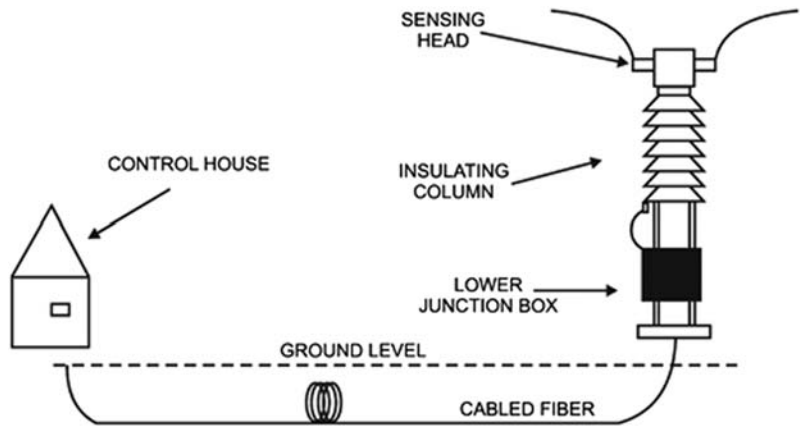

Figure 14.3 Typical installation of fiber optic current sensor.[31]

ampere-type loop current sensing. The higher-Verdet-constant materials typically demonstrate a higher level of Verdet constant dispersion as well as an increased sensitivity to temperature.

Historically, the fiber-based approach has had to manage linear birefringence as a major error source for Faraday-rotation-polarization-based systems. Linear birefringence is present in optical fiber cores due to many sources such as core ovality, intrinsic differential stress, and core nonuniformities. When the fiber is bent to form a loop, bend-induced birefringence is added to the already present intrinsic birefringence. For Faraday-based sensors, the objective is to measure the circular birefringence induced by an

applied magnetic field. When multiple sources are added to the medium, it becomes a more complex process to isolate and measure a relatively small amount of circular birefringence alone using polarimetric techniques. It can be shown that for situations where the linear birefringence δ is greater than F, the effective sensitivity of the sensor is reduced according to

$$F_{\text{effective}} = F\frac{\sin\delta}{\delta}. \tag{14.6}$$

From this relationship it can be seen that for very large δ values the signal can be completely washed out. Several solutions have been proposed and implemented to manage the presence of linear birefringence. Early on, a variety of spun fibers were developed with the goal of increasing the dominance of circular birefringence per unit length versus that of linear birefringence. This strategy was realized both with high-birefringence (linear) fibers and low-birefringence fibers. Both showed improvement in sensitivity, with the low-birefringence version proving more stable with temperature. In addition to the spun fiber work, fiber annealing methods pioneered at NIST[14] were engineered to form very high performing and stable sensing coils. Linear birefringence also affects the sensitivity of closed-loop sensors to external currents. Figure 14.4 provides a diagram of the setup, and Fig. 14.5 provides results of external current measurements as a function of linear birefringence. A detailed explanation of this effect is presented in Ref. 34. Another technique using polarization modulation to measure and track linear birefringence has also been proposed as a solution.[30]

Bulk glass designs that form complete loops using flint glass have also been realized. These devices have shown very good vibration isolation and shock performance. Compared to fiber-based devices, they have less flexibility in dynamic range, as they practically are limited to a single turn since they do not have the flexibility of an optical fiber. Also, coupling to polarization and fiber components can present its own challenges.

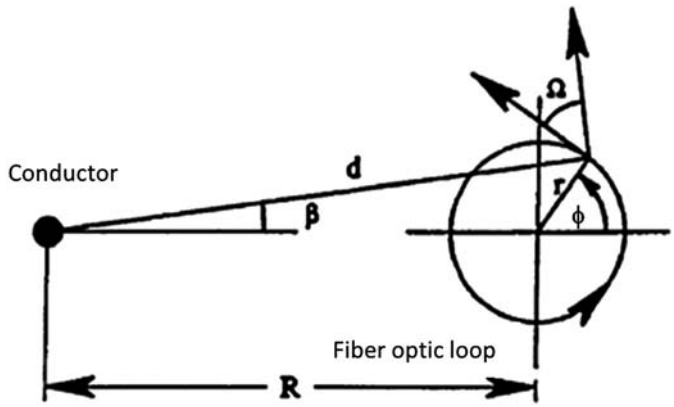

Figure 14.4 Geometry for performing analysis of external current effects.[34]

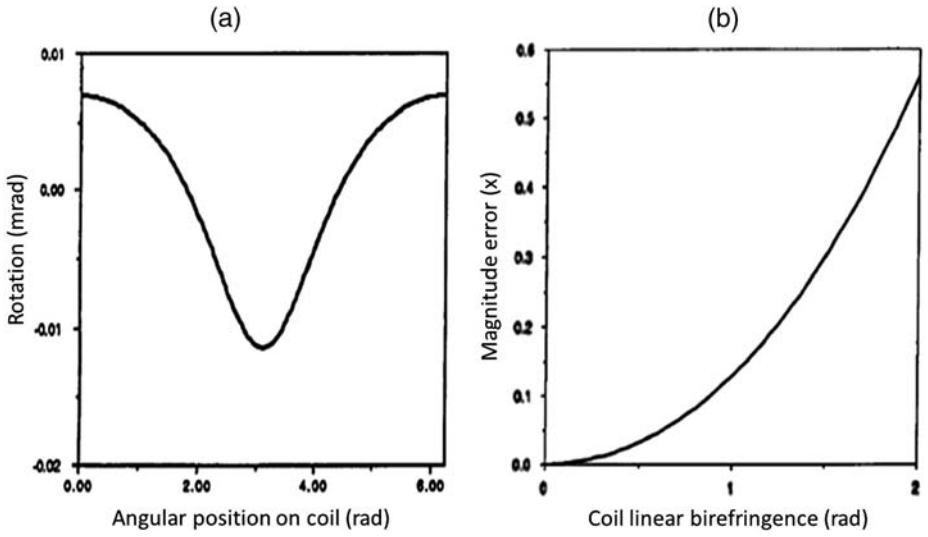

Figure 14.5 (a) Rotation in fiber loop and (b) effect of linear birefringence from external current.[34]

Figures 14.6 and 14.7 present a few different architectures for loop-based sensors. Shown in Fig. 14.6 is a bulk optic design along with a reflective mode design. The design shown in Fig 14.7 is yet another architecture using the concatenated sensing idea proposed by Dawson et al.[18]

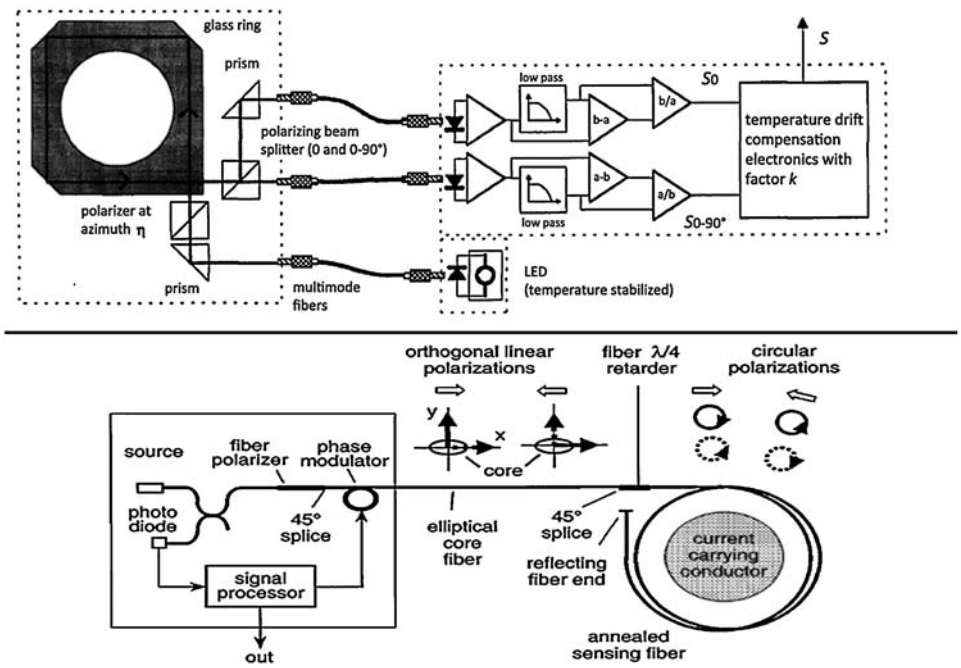

Figure 14.6 Bulk optic and reflective mode sensors.[20,22]

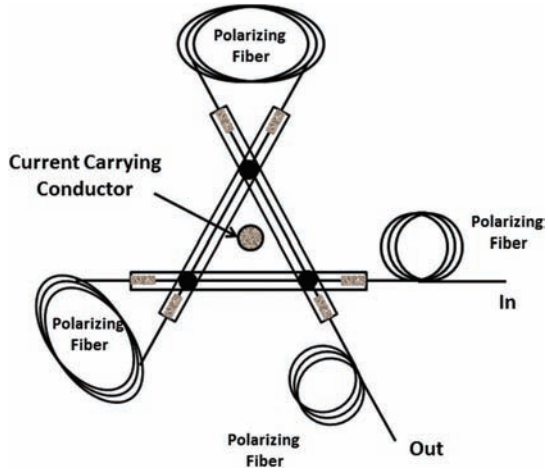

Figure 14.7 Concatenated quasi-current sensor.[18]

Commercial sensing systems with a dynamic range of 1–5000 A with a 0.3% accuracy or a dynamic range of 5,000–50,000 A with an accuracy of 0.3% to 10% have been achieved. These systems function at an operating wavelength of 830 nm with a temperature operating range of 40 to 80 °C. Figure 14.8 shows an application for measuring the currents in an electrowinning process and in a high-voltage utility.[11,12]

14.2.2 Phase modulation

Interferometric techniques for measuring magnetic fields have been used primarily in conjunction with magnetostrictive materials.[47 53] Magnetostrictive materials

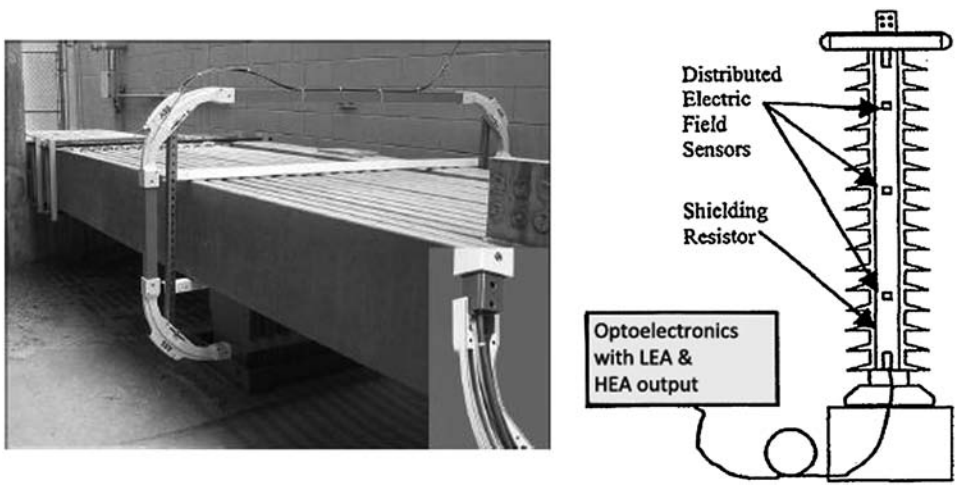

Figure 14.8 Industrial applications of fiber optic current sensors.[11,12]

expand or contract, depending on the material, in the presence of a magnetic field. Figure 14.9 depicts the geometry of the coating on a single-mode silica fiber. Ideally, the magnetostrictive coating is in a fiber form, but bulk materials can be used such as stripes or cylinders with the fiber bonded to the material. Several available alloys exhibit magnetostrictive properties, such as nickel alloys, cobalt-iron alloys, and metallic glasses. The sensor architectures have typically included a Mach–Zehnder configuration with the magnetostrictive material perturbing the sensing fiber. This basic configuration is shown in Fig. 14.10.

There is an optimum bias condition to achieve maximum sensitivity. This DC magnetic field bias has been shown to increase sensitivity by a factor of four. The frequency response of a phase-modulated magnetostrictive fiber optic sensor is very dependent on the material as well as the geometry. However, above approximately 1 kHz, a general decrease in sensitivity is observed.

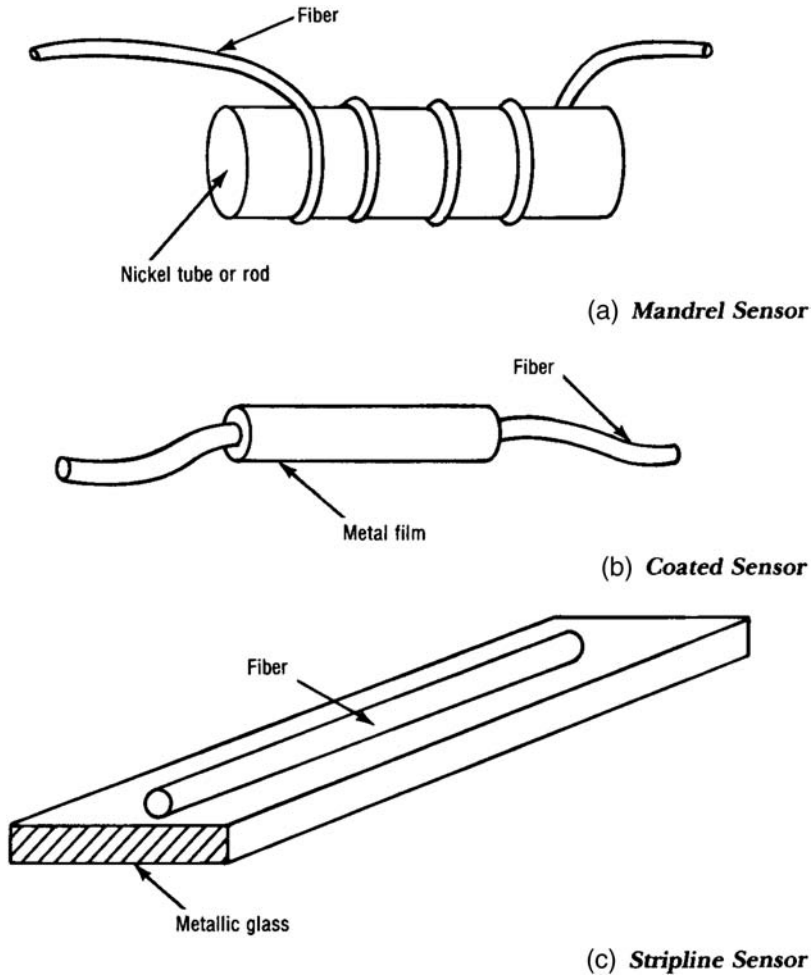

Figure 14.9 Phase modulation processes by magnetostriction (©1982 IEEE; reprinted with permission).[51]

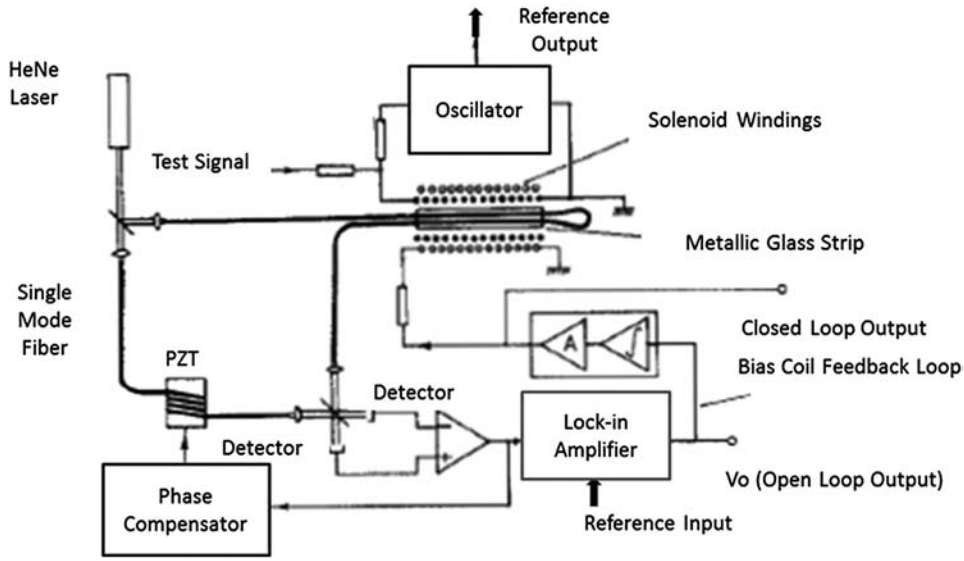

Figure 14.10 Mach–Zehnder interferometric configuration.[57]

The work of Koo and Sigel[49] resulted in very high-sensitivity magnetic field sensors. The minimum detectable field is approximately 5×10^{-12} *O*e/m. The magnetostrictive jacket concept can also be applied to a Bragg grating sensor. The displacement or strain associated with the magnetic field would cause a wavelength shift.

A Sagnac interferometric approach has been developed for use in current sensing.[12] The function of the sensor is very similar to that of a gyroscope and is shown in Fig. 14.11 and 14.12. The counter-propagating waves are generated by

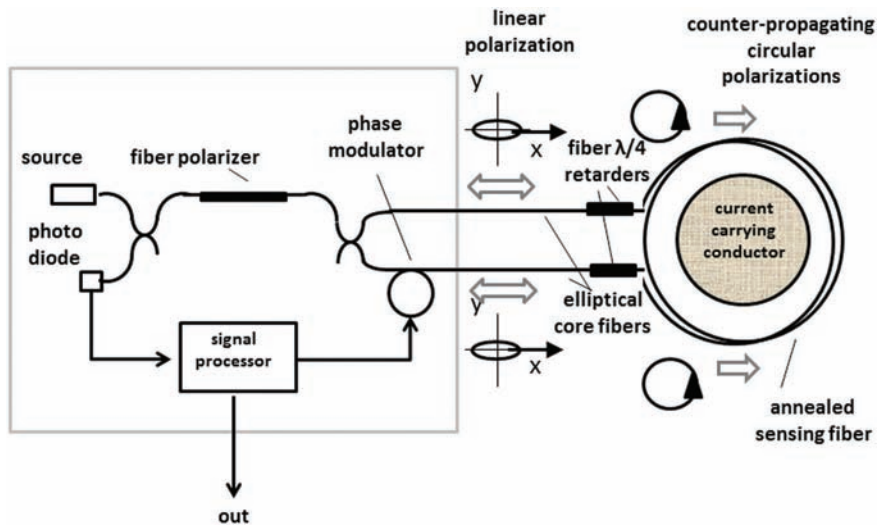

Figure 14.11 Sagnac interferometer configuration A.[22]

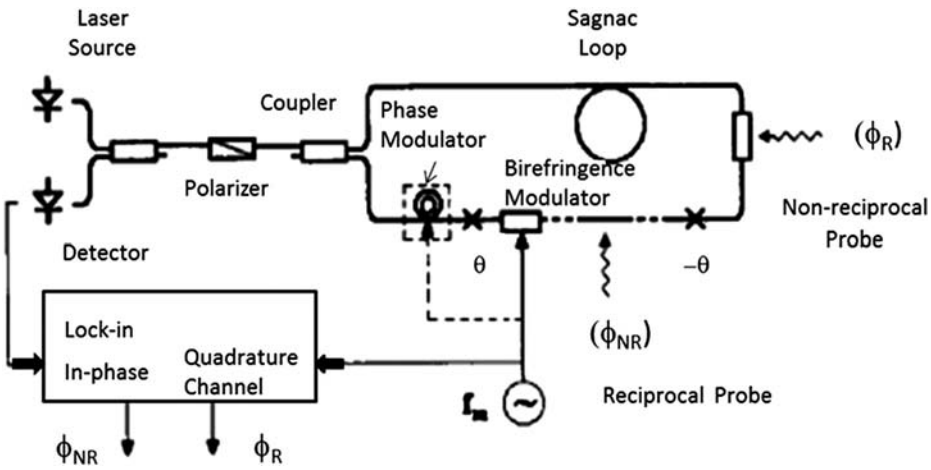

Figure 14.12 Sagnac interferometer configuration B.[59]

injecting left- and right-hand circularly polarized light from a polarizing-maintaining fiber into the single-mode (SM) sensing coil. The current flowing in the conductor induces a magnetic field, which creates a differential phase shift. The Sagnac interferometer has demonstrated excellent performance in measuring nonreciprocal effects. The theoretical bandwidth and dynamic range of such a design is more than adequate for performing high-precision current measurements.

Since the two interfering waves pass through the system simultaneously, there is a good common-mode rejection of vibration and other acoustic noise. However, care must be taken in the packaging to prevent linear birefringence, which can alter the scale factor.

14.3 Electric Field

14.3.1 Polarization modulation

In a manner similar to measuring a magnetic field, a transmissive fiber optic sensor can be used to measure an electric field if an electro-optic material is placed in the light path.[35 46] Unlike magneto-optical materials, there has been minimal success in adding dopants to optical fibers that have been effectively added to a glass fiber to achieve intrinsic sensing. Therefore, the majority of the sensors reported in the literature use electro-optic crystals. However, some use of liquid crystal materials within photonic crystal fiber has been reported. This is shown in Fig. 14.13.

Electro-optic materials generally are classified as exhibiting the Pockels effect or the Kerr effect. For the Pockels effect in the presence of an electric field, the index of refraction change is directly proportional to the field. Materials that exhibit the Kerr effect have a refractive index change that is proportional in the square of the field. The Kerr effect is more prevalent in liquids as compared to other material states. A variety of crystals exhibit the

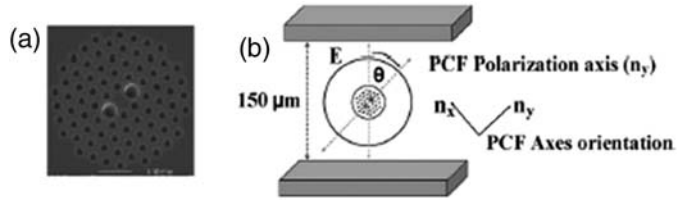

Figure 14.13 Liquid crystal electric field sensor.[41] (a) Photonic crystal fiber cross section, and (b) sensor configuration.

Pockels effect;[43] for this reason, most experimental work on the concept relates to the Pockels sensor.

Figure 14.14 shows a transmissive Pockels sensor. The incoming light is plane polarized. In the presence of an electric field, the orthogonally polarized beams propagate with different velocities, due to the refractive-index difference associated with the Pockels effect. A phase difference is generated, which, with the aid of a biasing quarter-wave plate, rotates the plane of polarization as a function of voltage. The transmitted intensity I is given by[45]

$$I = \frac{1}{2} I_0 \left[1 + \sin\left(\frac{V}{V_0} \right) \right], \tag{14.7}$$

where I_0 is the input light intensity, V_0 is the half-wave voltage of the Pockels material (a property of the material), and V is the applied voltage.

Pockels cell sensors using $Bi_{12}GeO_{20}$ as the electro-optic material have shown good linearity over nearly three orders of magnitude. Several techniques for measuring electric field or voltage using a reflective technique

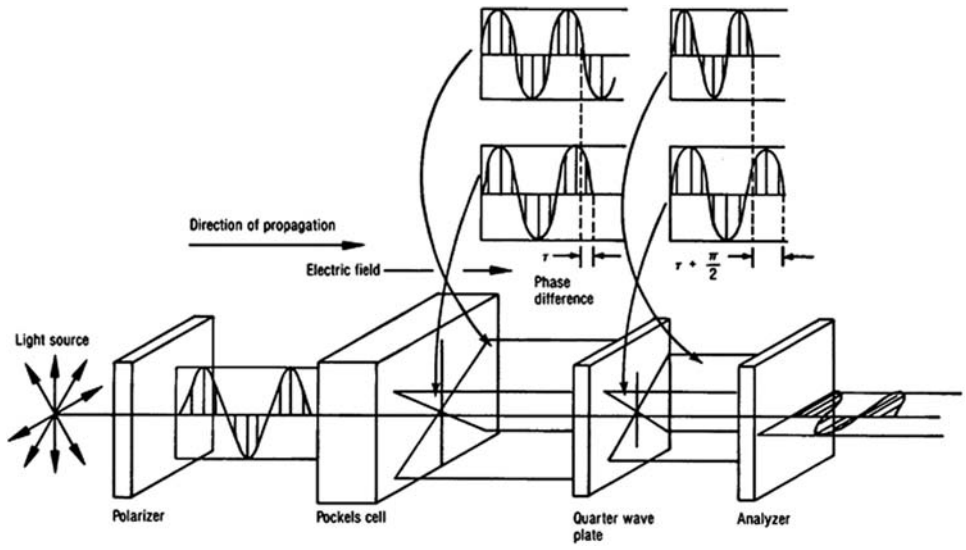

Figure 14.14 Pockels cell electric field sensor.[6]

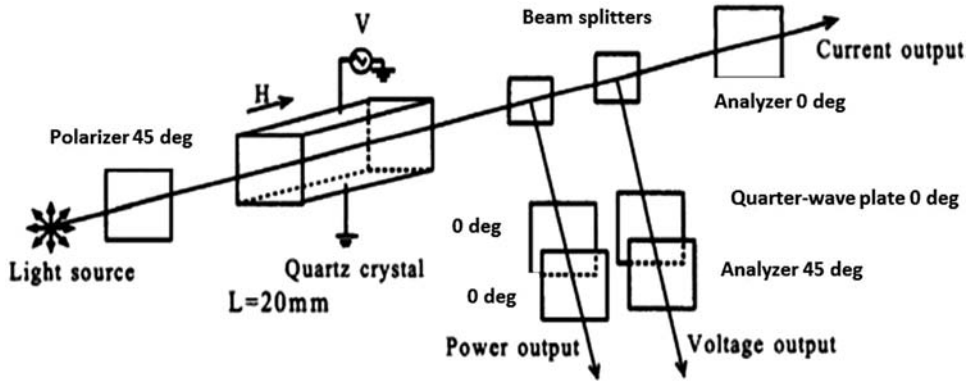

Figure 14.15 Setup for measuring both current and voltage (Compensation angle of optical activity is 14 degrees).[45]

are reported in the literature.[42 46] Figure 14.15 shows a schematic representation of a crystal current and voltage sensor.

14.3.2 Phase modulation

Phase modulation techniques for measuring electric fields have been used with electrostrictive materials, primarily piezoelectrics.[35 46] In a manner similar to magnetostrictive materials in a magnetic field, piezoelectric materials can expand and contract in the presence of an electric field. Piezoelectric materials interact with the sensing fiber in a Mach–Zehnder interferometer by being bonded to the fiber. The configuration can be a coated fiber, a fiber bonded or embedded in a sheet of the material, or a fiber wrapped around a mandrel. Most of the reported experimentation has been done with polyvinylidene fluorine (PVF_2) as the piezoelectric material.

Interferometric configurations are shown in Figs. 14.16 and 14.17 for both coating and transducer type sensors, respectively. The fiber can be coated with a PVF_2 coating and poled to optimize the molecular orientation in the

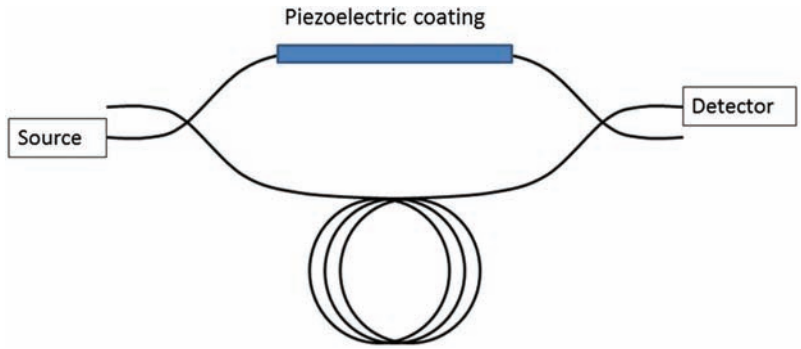

Figure 14.16 Electric field sensor with piezoelectric coatings.

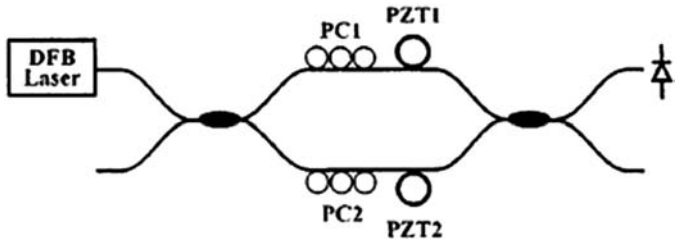

Figure 14.17 Electric field sensor utilizing piezoelectric transducers.[46]

polymer and maximize the piezoelectric effect. DeSouza and Mermelstein[40] found that the sensitivity increases with coating thickness up to about 300 μm. Coatings thicker than 300 μm have little added advantage. The projected minimum detectable field is 6 μV/m for a sensor with a 1-km sensing fiber length.

Pure voltage sensing is a more complicated process than current sensing. The underlying physical properties of electric fields versus those of magnetic fields create a situation where electric field sensors are really field sensors and not voltage sensors. In fact, Faraday current sensors have been used to split off a sensing current across a known resistance to indirectly measure voltage.[12] As mentioned earlier, the theoretical potential of these devices, especially for high voltage and current measurement, cannot be ignored. Their advantages in both cost and performance will eventually drive their commercial acceptance.[53–55]

References

1. R. Malewski and D. Erickson, "Fiber optic applications in electrical power systems, measurement applications (Part 1)," *IEEE Tutorial Course*, IEEE, Piscataway, NJ (1985).
2. R. E. Habner, "Fiber optic applications in electrical power systems, measurement application in electrical power systems, measurement application (Part 2)," *IEEE Tutorial Course*, IEEE, Piscataway, NJ (1985).
3. R. D. Habner, "Optical technology applications in gas and electric utilities," presented at the Newport Conference on Fiber Optic Markets (1985).
4. Anonymous, "Lasers and fibers monitor current and voltage at high power stations," *Laser Focus*, pp. 48–56 (1980).
5. R. Ullrich, "Fiber optical arrangement for measuring the intensity of an electric current," U.S. Patent 4,255,018 (1981).
6. Y. Kuroda et al., "Field test of fiber optic voltage and current sensor applied to gas insulated substation," *Proc. SPIE* **586**, 30–37 (1985) [doi: 10.1117/12.951134].

7. R. A. Fernandes, "Fiber optic electric utility applications present and future," in *Fiber Optic Applications in Electrical Utilities*, IEEE, Piscataway, NJ (1984).
8. M. Adolfsson and T. Brogradeh, "Fiber optic sensor for measuring current or voltage," U.S. Patent 4,547,729 (1986).
9. Anonymous, "Fiber sensors impact on power utilities," *Lightwave*, p. 12 (1984).
10. V. N. Filippov, A. N. Starodumov, V. P. Minkovich, and F. G. Peña Lecona, "Fiber sensor for simultaneous measurement of voltage and temperature," *IEEE Photonics Technology Letters* **12**(11), 1543–1545 (2000).
11. K. Bohnert, P. Gabus, J. Nehring, H. Brändle, and M. G. Brunzel "Fiber-optic current sensor for electrowinning of metals," *Journal of Lightwave Technology* **25**(11), 3602–3609 (2007).
12. G. A. Sanders, J. N. Blake, A. H. Rose, F. Rahmatian, and C. Herdman, "Commercialization of fiber optic current and voltage sensors at NxtPhase," *Optical Fiber Sensors Conference Technical Digest* **15**, 33–34 (2002).
13. T. MacDougall, R. Wandmacher, and D. Lutz, "Development of a fiber optic current sensor for power systems," *IEEE Transactions on Power Delivery* **7**(2), 848–852 (1992).
14. D. Tang, A. H. Rose, G. W. Day, and S. M. Etzel, "Annealing of linear birefringence in single-mode fiber coils: application to optical fiber current sensors," *Lightwave Technology* **9**(8), 1031–1037 (1991).
15. J. W. Dawson, T. W. MacDougall, *and* E. Hernandez, "Verdet constant limited temperature response of a fiber-optic current sensor," *Photonics Technology Letters* **7**(12), 1468–1470 (1995).
16. G. W. Day and A. H. Rose, "Faraday effect sensors: the state of the art," *Proc. SPIE* **0985,** 1–13 (1989) [doi: 10.1117/12.948837].
17. V. Annovazzi-Lodi, S. Donati, and S. Merlo, "Coiled-fiber sensor for vectorial measurement of magnetic field," *Lightwave Technology* **10**(12), 2006–2010 (1992).
18. J. W. Dawson, T. W. MacDougall, and E. Hernandez, "High-performance magnetic field and quasi-current sensors," *Conference on Lasers and Electro-Optics* (1996).
19. W. J. Tabor and F. S. Chen, "Electromagnetic propagation through materials possessing both Faraday rotation and birefringence: Experiments with ytterbium orthoferrite," *Journal of Applied Physics* **40**(7), 2760–2765 (1969).
20. P. Menke and T. Bosselmann, "Temperature compensation in magneto-optic AC current sensors using an intelligent AC-DC signal evaluation," *J. Lightwave Technol.* **13**(7), 1362–1370 (1995).

21. K. Hotate and Y. Konishi, "Formulas describing error induced by fiber linear-birefringence in fiber-optic current sensors," *Proc. Optical Fiber Sensor Conference* **15**, 557–560 (2002).
22. K. Bohnert, P. Gabus, J. Nehring, and H. Brändle,"Temperature and vibration insensitive fiber-optic current sensor," *Lightwave Technology* **20** (2), 267 (2002).
23. G. Y. Chen, G. Brambilla, and T. P. Newson, "Spun optical microfiber," *Photonics Technology Letters* **24**(19), 1663 (2012).
24. K. Kurosawa, S. Yoshida, and K. Sakamoto, "Polarization properties of the flint glass fiber," *Journal of Lightwave Technology* **13**(7), 1378–1384 (1995).
25. A. H. Rose, S. M. Etzel, and K. B. Rochford, "Optical fiber current sensors in high electric field environments," *Journal of Lightwave Technology* **17**(6), 1042–1048 (1999).
26. M. C. Oh, J. K. Seo, K. J. Kim, H. Kim, J. W. Kim, and W. S. Chu, "Optical current sensors consisting of polymeric waveguide components," *Journal of Lightwave Technology* **28**(12) 1851 (2010).
27. P. Kaminow, "Polarization in optical fibers," *Journal of Quantum Electronics* **QE- 17-1**(1), 15–22 (1981).
28. M. S. Maklad, "Fiber optic current and magnetic field sensor," *ISA Transactions* **27**(1), 25–29 (1988).
29. G. W. Day, L. R. Veeger, and R. W. Gernosek, "Progress in the design of optical fiber sensors for the measurement of pulsed electric currents," *Proc. of the Workshop on Measurement of Electrical Quantities in Pulse Power Systems* **1** (1986).
30. Z. B. Ren and P. Robert, "Discrimination of linear birefringence and Faraday rotation in optic fiber current sensors by polarization multiplexing," *Proc. SPIE* **1169**, 226–232 (1989) [doi: 10.1117/12.963036;].
31. 3M Technology, "Fiber optic current sensors," *3M Technology Brief* (1997).
32. N. Itoh, H. Minemoto, D. Ishiko, and S. Ishizaka, "Commercial current sensor activity in Japan," 12th International Conference on Optical Fiber Sensors, *Technical Digest Series* **16**, 92–95 (1997).
33. K. Kyuma et al., "Fiber optic current and voltage sensors using a Bi_2GeO_2, single crystal," *Journal of Lightwave Technology* **LT-1**(1), 93–97 (1983).
34. T. MacDougall and T. Hutchinson, "Stray magnetic-field response of linear birefringent optical current sensors," *Journal of Applied Optics* **34** (21), 4373–4739 (1995).
35. R. Johnson, "Fiber optic electric field meter," *NASA Tech. Briefs*, pp. 39–40 (1985).

36. R. Byberg, K. Herstad, K. B. Larsen, and T. E. Hansen, "Measuring electric field by using pressure sensitive elements," *IEEE Transactions on Electrical Insulation* **El-14**(5), 250–254 (1979).
37. M. D. Mermelstein, "Optical fiber copolymer-film electric-field sensor," *Applied Optics* **22**(7), 1006–1009 (1983).
38. K. P. Koo and G. H. Sigel, Jr., "An electric field sensor utilizing a piezoelectric polyvinylidene fluoride (PVF2) film in a single-mode fiber interferometer," *IEEE J. Quantum Electronics* **QE-18**(4), 670–675 (1982).
39. L. J. Donalds, W. G. French, W. C. Mitchell, R. M. Swinehart, and T. Wei, "Electric field sensitive optical fiber using piezoelectric polymer coating," *Electronics Letters* **18**(8), 327–328 (1982).
40. P. D. DeSouza and M. D. Mermelstein, "Electric field detection with a piezoelectric polymer -jacketed single-mode optical fiber," *Applied Optics* **21**(23), 4214–4218 (1982).
41. S. Mathews, G. Farrell, and Y. Semenova, "Directional electric field sensitivity of a liquid crystal infiltrated photonic crystal fiber," *IEEE Photonic Technology Letters* **23**(7), 408–410 (2011).
42. M. Mozafari1, Z. Sanjabi1, N. Granpayeh, and K. N. Toosi "Design and fabrication of piezo-optical Fabry-Pérot voltage sensor," *IEEE Avionics, Fiber Optics and Photonics Technology Conference*, 39–40 (2008).
43. C. Li and T. Yoshino, "Optical voltage sensor based on electrooptic crystal multiplier," *J. Lightwave Technol.* **20**(5), 843 (2002).
44. Z. Wang, Y. Zhang, L. Song, X. Wang, and A. Wang, "Optical high DC voltage sensor based on white-light interferometry," *IEEE Photonics Technology Letters* **18**(19), 2002–2004 (2006).
45. H. Miyashita and Y. Fujii, "Measurement of current, voltage and power using single quartz crystal," *IEEE Optical Fiber Sensors Conference Technical Digest*, 491–494 (2002).
46. L. Martínez-León, A. Díez, J. L. Cruz, and M. V. Andrés, "Frequency-output fiber-optic voltage sensor for high-voltage lines," *IEEE Photonics Technology Letters* **13**(9), 996–998 (2001).
47. G. L. Tangonan, D. I. Persechini, R. J. Morrison, and J. A. Wysocki, "Current sensing with metal-coated multimode optical fibers," *Electronic Letters* **16**(25), 958–959 (1980).
48. A. Yariv and H. V. Winsor, "Proposal for detection of magnetic fields through magnetostrictive perturbation of optical fiber," *Optics Letters* **5** (3), 87–89 (1980).
49. P. Koo and G. H. Sigel, "Characterizations of fiber optics magnetic fields sensors employing metallic glasses," *Optics Letters* **7**, 334–336 (1982).
50. A. Dandridge, A. B. Tvetan, G. H. Sigel, E. J. West, and T. G. Giaorenzi, "Optical magnetic field sensors," *Electronic Letters* **16**, 408–409 (1980).

51. J. Jarzynski, J. H. Cole, J. A. Bucaro, and C. M. Davis, "Magnetic field sensitivity of an optical fiber with magnetostrictive jacket," *Applied Optics* **19**(22), 3746–3748 (1980).
52. T. G. Giallorenzi et al., "Optical fiber sensor technology," *IEEE Journal of Quantum Electronics* **QE-18**(4), 626–665 (1982).
53. C. M. Davis, *Fiber Optic Sensor Technology Handbook,* Dynamic Systems, Inc., Reston, Virginia (1982).
54. W. W. Morey, "Development of fiber Bragg grating sensors for utility applications," TR 105/90 EPRI Research Project RP 8004-09 (EPRI Report).
55. S. X. Short, J. U. deArruda, A. A. Tselikou, and J. Blake, "Stable scale factor performance of an in-line Sagnac interferometer current sensor," *12th International Conference on Optical Fiber Sensors*, *Technical Digest Series* **16**, 100–103 (1997).
56. F. Bucholtz, C. A. Villarmel, A. R. Davis, C. K. Kirkendall, D. M. Dagenais, J. A. McVicker, S. S. Patrick, K. P. Koo, G. Wang, H. Val, T. Lund, A. G. Andersen, R. Gjessing, E. J. Eidem, and T. Knudsen, "Multichannel fiber-optic magnetometer system for undersea measurements" *J. Lightwave Technol.* **13**(7), 1385 (1995).
57. A. D. Kersey, D. A. Jackson, and M. Corke, "Single-mode fibre-optic magnetometer with DC bias field stabilization," *J. Lightwave Technol.* **3** (4), 836–840 (1985).
58. D. Y. Kim, H. J. Kong, and B. Y. Kim, "Fiber-optic DC magnetic field sensor with balanced detection technique," *IEEE Photonics Technology Letters* **4**(8), 945 (1992).
59. R. T. de Carvalho and J. Blake, "The Sagnac interferometer as a two-parameter sensor," *J. of Lightwave Technol.* **13**(7), 1250–1255 (1995).

Chapter 15
Chemical Analysis

15.1 Introduction

Fiber optic techniques for chemical analysis have several distinct advantages.[1] Analysis can often be done *in situ* in real time. The sensing techniques generally do not disturb the process. The sample size can be extremely small, and the sensing locations can be in remote areas that are normally difficult to access. Potential disadvantages include sensitivity to ambient light, relatively slow response time due to the required reaction with various reagents, and shortened lifetime if high incident radiation is used to enhance sensitivity. Also, interaction with a chemical agent is generally not reversible; therefore, the sensor will require replacement if triggered.

Several approaches can be used for qualitative and quantitative chemical analysis. These techniques are fluorescence, scattering, absorption, color change, evanescent wave interaction, and refractive-index change.

In general, chemical analysis techniques employ either a transmissive or a reflective fiber optic configuration. Figure 15.1 illustrates the two concepts. The reflective concept uses a bifurcated probe, as shown in Fig. 15.1(a). Light travels down the transmitting leg, reflects off the target material, and is accepted in the receiving leg, which is attached to a photodetector. The amount of light transmitted or reflected is a function of the nature and amount of chemical species present. In the transmissive system shown in Fig. 15.1(b), light travels down a transmitting fiber optic (a single fiber or a bundle of many fibers), passes through a gap that contains the material to be analyzed, and is captured in a receiving fiber optic, which, in turn, transmits the light to a photodetector. Distributive chemical sensors can function by detection of a transmitted or reflective signal.

15.2 Fluorescence

The use of fiber optic fluorescence techniques for chemical analysis is generally referred to as remote fiber fluorimetry (RFF).[2–8] A typical RFF system couples a high-intensity light source into a single, large-core silica fiber.

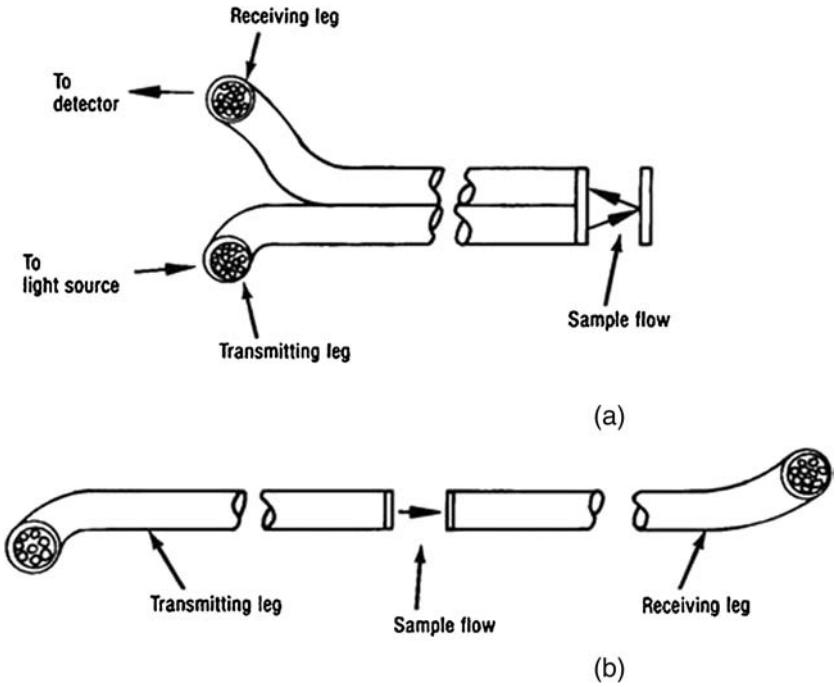

Figure 15.1 Fiber optic sensing system. (a) Relective system, (b) transmissive system.

Light travels along the length of the fiber as a result of total internal reflection, with little optical loss. Upon exiting the fiber, the rays of light impinge on the sample, which in turn gives off a characteristic fluorescence emission. The concept of absorbing energy to excite fluorescent elements, with subsequent fluorescence emission, is shown in Fig. 15.2. The fluorescence is at a lower energy level (higher wavelength) than required for excitation.[9] The emission is detected by the same fiber and travels back to a photodetector, which, with the aid of interrogation software, can provide both qualitative and quantitative information (see Fig. 15.3).

The fiber immersed in the sample is called an optrode. The fluorescence can be enhanced with the aid of a sapphire microlens, as shown in Fig. 15.4.

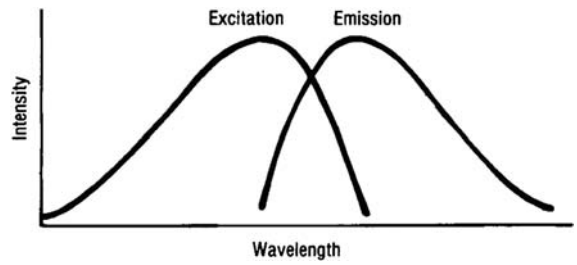

Figure 15.2 Excitation and emission spectrum for a fluorescence sensor.[9]

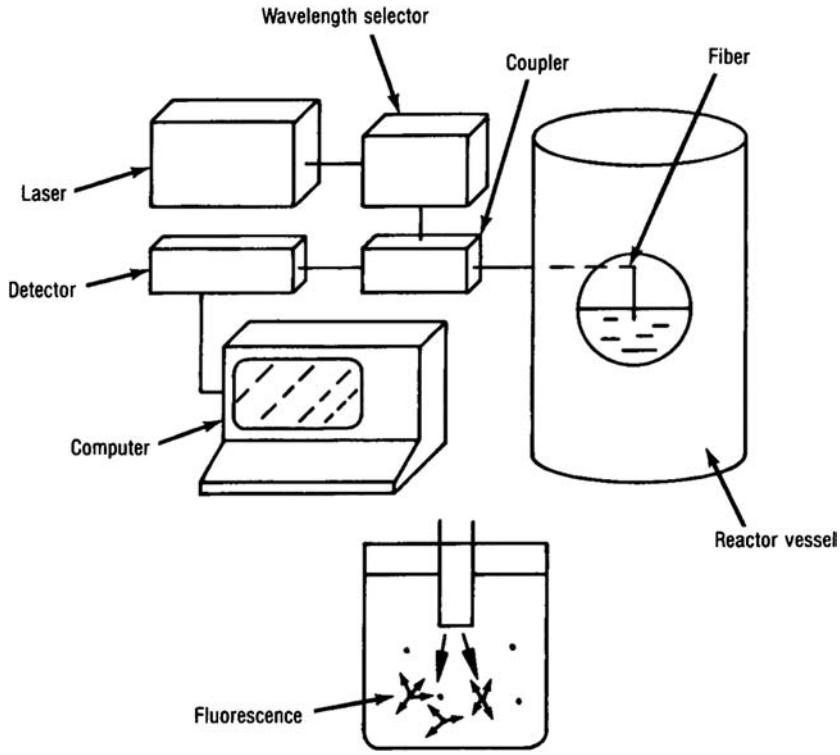

Figure 15.3 Remote fiber fluorimetry.

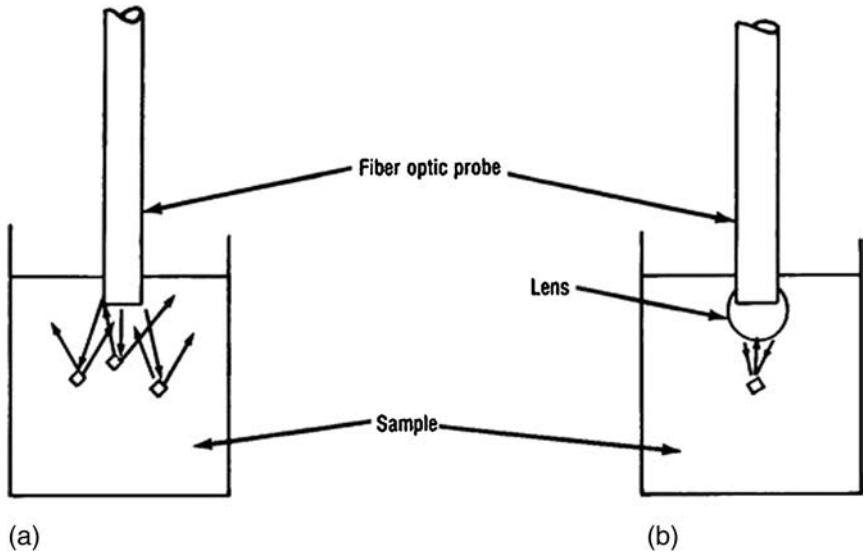

Figure 15.4 (a) Unfocused and (b) focused remote fiber fluorimetry probes.

Using the RFF technique, measurements have been demonstrated with uranyl, chloride, iodide, iron, plutonium, and sulfate ions.[4] Ground water contamination, such as from toluene and xylene associated with gasoline spills and leakage,[10,11] has also been detected by this technique.

Graff[2] has pointed out that a material does not have to be fluorescent to work with the technique. A target of known fluorescence can be used. The sample in question can react with the target and enhance or diminish its fluorescence. Aluminum and other metals have been analyzed by using a reagent immobilized in the form of a powder and attached to a bifurcated fiber optic probe.[12] The metal reacts with the reagent, giving a fluorescence signal. The response time was 1 to 2 min with a detection limit of 0.027 ppm.

Oxygen partial pressure has been measured by a fluorescence technique.[13] The technique uses a fluorescent dye that is quenched in the presence of oxygen. Fluorescence quenching works well for oxygen detection.[14] Oxygen as a triplet molecule is able to efficiently quench the fluorescence of certain luminophores. If an oxygen molecule collides with an exited-state fluorophore, the transfer of energy is nonradiative. The degree of fluorescence quenching is a function of collision frequency, and therefore is also the function of the concentration, pressure, and temperature of the oxygen-containing media.

The device is shown in Fig. 15.5. A high-intensity blue light is transmitted to the dye through one leg of a bifurcated fiber optic probe. The blue light, upon impinging the dye, gives off a characteristic green fluorescence. The level of fluorescence diminishes with the increasing levels of oxygen that pass through the gas-permeable membrane, which in turn, reacts with the dye. The partial pressure of oxygen is a function of the ratio of blue-light intensity to green-light intensity. Over a range of 0–150 torr, the sensor was accurate to better than 1%, with a response time of about 2 min. Seitz[14] has used a similar technique for measuring the concentration of glucose. Halide contaminations such as iodide, bromide, and chloride were also detected using fluorescence quenching.[16] The detection limit was about 2 ppm for iodide, 6 ppm for bromide, and 200 ppm for chloride.

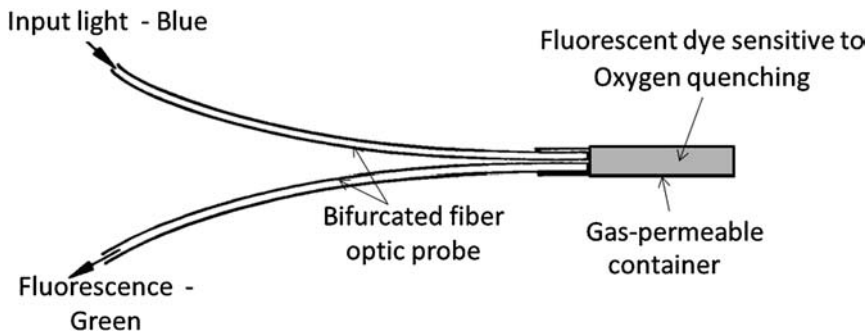

Figure 15.5 Construction of fiber optic fluorescence probe.

The fluorescence technique has been expanded to measure pH. Saari and Seitz,[17] using a fiber optic bifurcated probe in conjunction with an immobilized reagent, found that the fluorescence intensity changed with pH and/or the concentration of metal ion. The apparatus is shown in Fig. 15.6. The device had good sensitivity over the pH range of 3–8.

The fluorescence technique described has included only direct impingement on the target. However, evanescent wave interaction with fluorescent dyes can be especially useful for distributed systems. In this case, as shown in Fig. 15.11, the reagent is in direct contact with the fiber core. Sensitivity is somewhat limited because only the tail of the evanescent field interacts with the reagent coating. The resulting low-level fluorescence is scattered in all directions. Only those rays that fall within the critical angle for total internal reflection in the fiber core can be used for sensing. Since most of the light rays are not captured in the fiber, the sensitivity of the detection system must be very high to detect the captured light.[18]

Two-stage fluorescence coupling can be used to significantly increase the sensor efficiency. The concept is shown in Fig. 15.7.[18] The fiber coating contains a fluorescent dye as in the previous case. However, the core (usually in plastic fiber) contains a secondary fluorescent compound that can be excited by the primary coating dye fluorescence, as shown in Fig. 15.8.[18] The secondary fluorescence emission, being within the fiber core, should provide for a more efficient collection of the sensor-modulated light. Preliminary indications are that two-stage fluorescence sensing may provide sensitivity one hundred fold greater than single-stage fluorescence.[18]

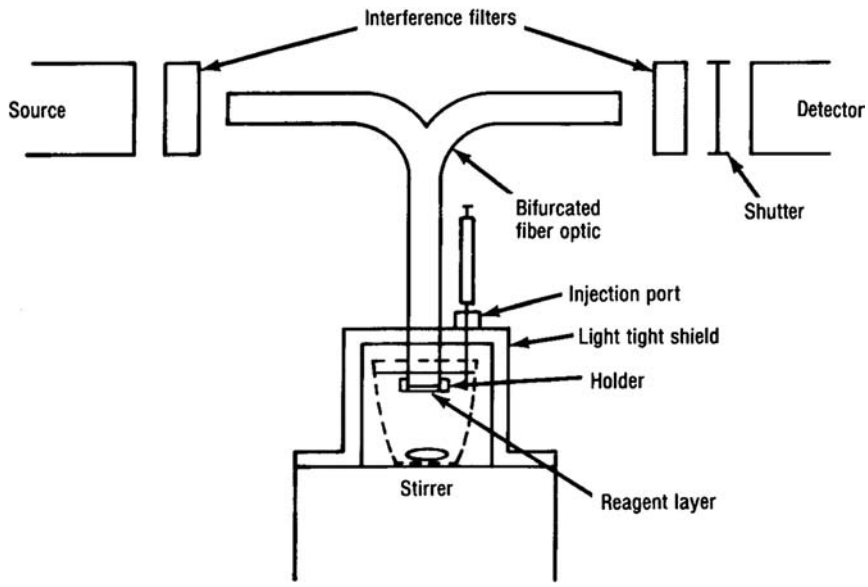

Figure 15.6 Diagram of pH sensor based on fluorescence and associated instrumentation.

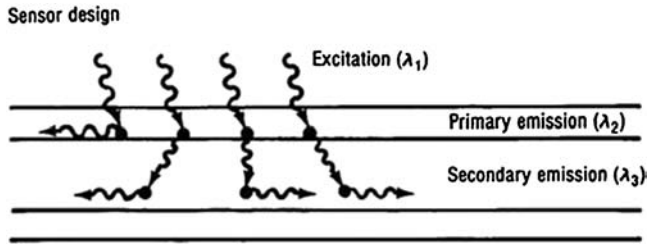

Figure 15.7 Two-stage fluorescence coupling.[18] (Principle: Sensing dye in cladding results in excitation at λ_1 and emission at λ_2. Coupling dye in core results in excitation at λ_2 and emission at λ_3. The advantage is an increased signal.)

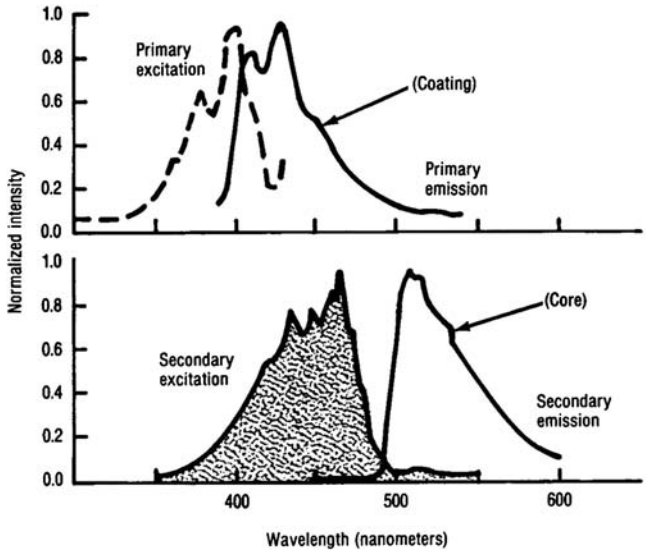

Figure 15.8 Spectral overlap between coating emission and core excitation.[18]

15.3 Absorption

Absorption can be used as an analysis approach.[4,19] Figure 15.9 shows a reflective system in which a gas sample to be measured is in the optical path. Gases have characteristic absorption bands. If the fiber optic sensor is used in conjunction with a spectrophotometer, both qualitative and quantitative analyses are achievable. For a weakly absorbing gas, the light path through the gas may have to be long to enhance the required sensitivity. This problem can usually be solved by use of a faceted target, which allows multiple reflections through the material being analyzed.

There is a major limitation in any fiber optic system. The best-quality fiber can transmit only between the UV and the mid-IR range. Therefore, the primary absorption peaks of many gases are beyond the range of present fiber optic systems. However, many gases have weaker overtone absorption bands

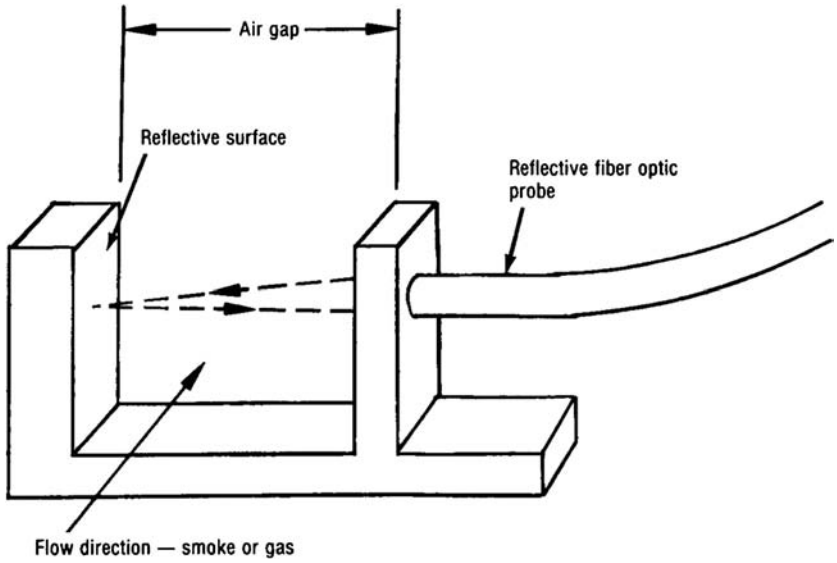

Figure 15.9 Gas/smoke sensor.

in the near IR that can be used in analysis.[4,20,21] The same device, shown in Fig. 15.9, can be used in a scattering mode for smoke detection (switch) in both military and industrial applications.

The usefulness of absorption-based fiber optic sensors can be enhanced if reagents that react with the substance to be detected are used.[15,22,23] The reaction can be designed to occur within the operational wavelength range of the sensor, even if the substance has no characteristic absorption bands within the operational wavelength range. Figure 15.10 shows a configuration of such a sensor. The reagent is immobilized, which entraps the reagent and allows the sensor to function in a reversible manner. The sensor design allows the analyte to diffuse through the membrane surrounding the reagent. The reagent is typically a dye that changes its absorption as a function of concentration. At a given wavelength, the reflected light is diminished in intensity as a function of

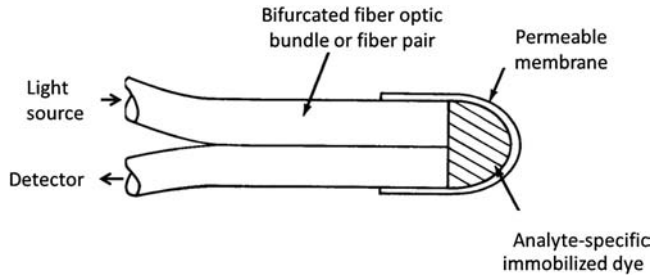

Figure 15.10 Reflective fiber optic probe using an immobilized dye for absorption-based sensing.

analyte concentration. The sensor concept is further enhanced if a second wavelength that does not attenuate the light level is used. The intensity associated with the nonabsorption wavelength is used as a reference to normalize the intensity associated with absorption wavelength.

It has been shown that the reagent can be in the light path of a reflective-type sensor or a transmissive sensor. However, it is also possible to have the reaction occur along the wall of the fiber since some of the light penetrates beyond the wall (evanescent wave).[15] The reaction can be enhanced if a short section of fiber has the cladding removed and the reagent is in direct contact with the core, as shown in Fig. 15.11. The distinct advantage of this approach is that the sensor has lower inherent losses compared to a reflective or a transmissive sensor, since the light path is unbroken and loss at the sensing point is minimized (but detectable). This approach also has an advantage in a distributive sensor configuration, which will be discussed in Section 15.8.

An improvement to the sensor described above is the use of a long-period grating to get the light to leave the core efficiently and interact with chemically sensitive coatings.[24] For this case, the cladding did not require removal, which significantly improved fiber strength. Figure 15.12 depicts the concept

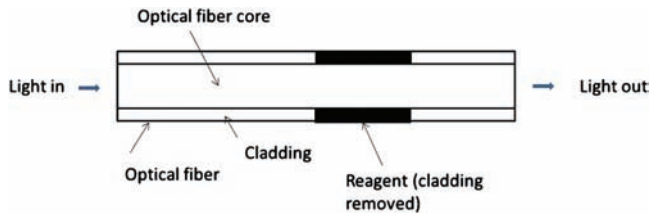

Figure 15.11 Transmissive fiber optic sensor with reagent in direct contact with the core along its walls.

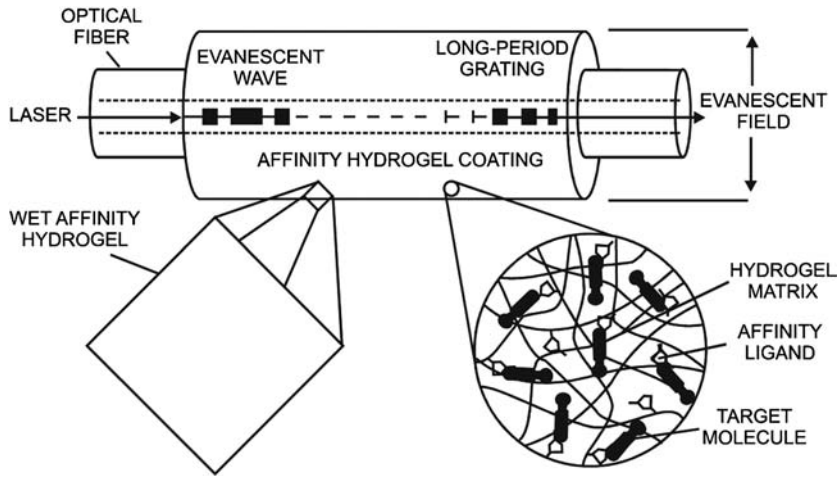

Figure 15.12 Chemical sensor using a long-period grating.[24]

showing a hydrogel coating, which is capable of detecting the poison endotoxin at 500 ppt.

A reversible sensor capable of detecting toxic gases was developed using a reagent on the side wall of a waveguide.[25] The reagent was an immobilized dye that changed color in the presence of the gas. Specifically, ammonia vapors were detected to levels of 60 ppm. The response time to reach 90% of the intensity for a given concentration was approximately 1 min. When the gas was removed, the sensor relaxation time to the zero concentration level was approximately 20 sec.

Fiber optic colorimetry in its simplest form uses a basic absorption/transmission concept.[26] Many processes, such as antifreeze manufacturing, monitor color at various process stages. Figure 15.13 shows a basic colorimeter. The device uses a bifurcated fiber optic reflective probe and a mirror target. The material to be measured is between the probe tip and the mirror. By using specific-wavelength interference filters on the receiving leg of the probe, specific colors can be monitored. More detailed color characterization is also possible, providing Commission Internationale d'Eclairge standard color coordinates, but a more complicated sensor configuration is required.

15.4 Scattering

Many applications require the measurement of the opacity associated with airborne particulate matter. For an opaque particulate, the loss in transmission is due to scattering. For a particulate that is semitransparent, the loss in transmission is due to both scattering and absorption. Opacity is defined as[27]

$$\%\ \text{opacity} = 100\%\ \text{transmission} \quad \%\ \text{actually transmitted}. \tag{15.1}$$

A measure of the ability of airborne particulate to attenuate light is the optical density defined by

$$\text{Optical Density} = \log_{10} \frac{1}{1 \quad \text{Opacity}}. \tag{15.2}$$

Figure 15.14 shows a transmissive sensor used to characterize smoke in a stack. The opacity is correlated with the efficiency of the manufacturing process. Generally, an increase in opacity indicates that the process being monitored is running at less than optimum conditions.

There is a shift in wavelength of reflected light as a result of smoke particles.[28] Figure 15.15 shows a schematic representation of the sensor. The sensor detects reflected light that has passed through the smoke path. The shift to longer wavelengths in the presence of smoke is identified. The opto-electronics detects the reflected signals associated with both short wavelengths and longer wavelengths, and the ratiometric results are a direct function of smoke density.

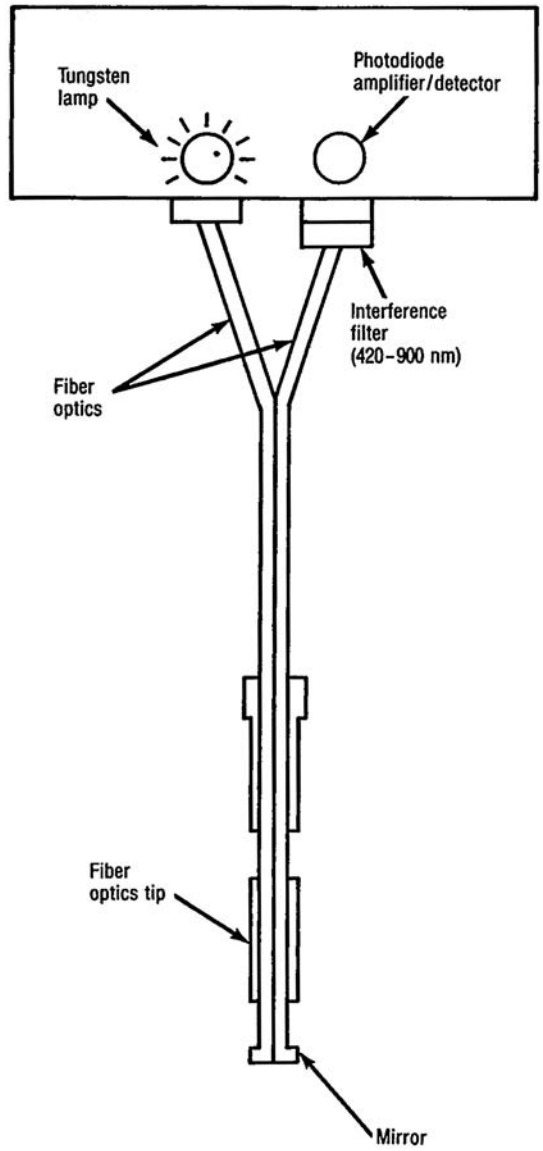

Figure 15.13 Operational schematic diagram for a fiber optic probe colorimeter.[26]

The scattering concept can be expanded to determine the volume fraction of one immiscible liquid in another.[20] Figure 15.16 shows a sensor designed for detecting oil droplets in water. The oil–water mixture flows into a chamber where a light beam is projected perpendicular to the path of the flow. The ratio of the light entering the off-axis probe to the light entering the on-axis probe is a measure of the oil concentration.

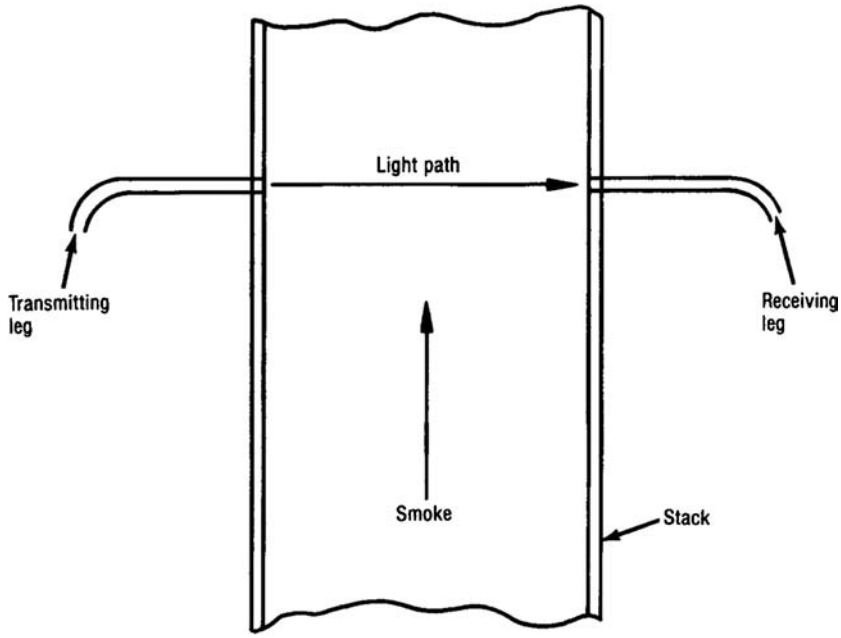

Figure 15.14 Transmissive sensor for smoke characterization in a smoke stack.

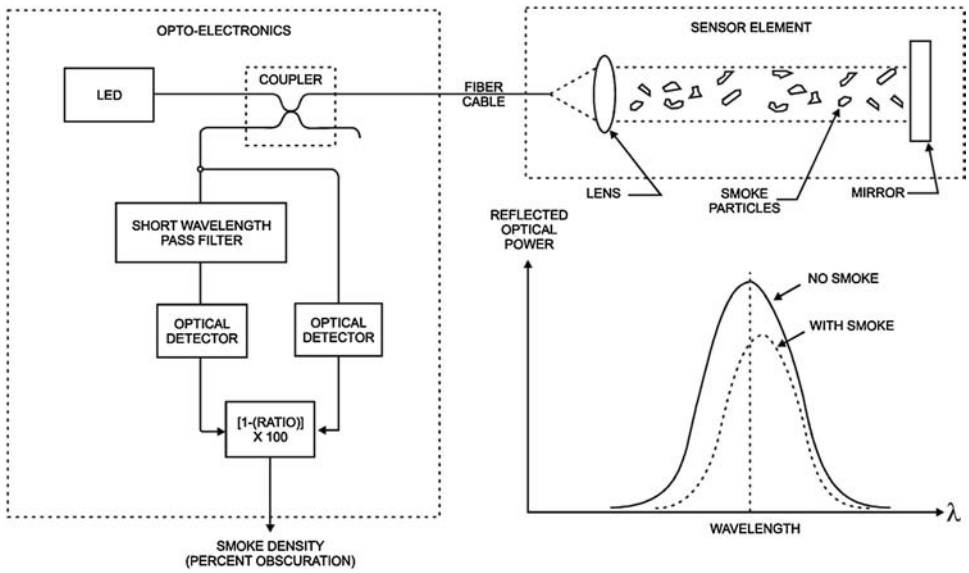

Figure 15.15 Schematic diagram for a spectrometric fiber optic smoke sensor.[28]

Scattering has also been used to detect physical transitions such as melting, the glass transition, and crystallization.[29] If the material to be characterized is transparent in one state, the change in state generally results in the formation of scattering sites, which denotes the physical change.

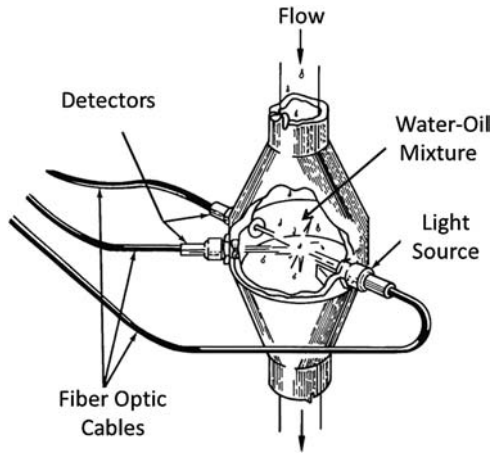

Figure 15.16 Transmissive sensor for the detection of oil in water using scattering.

Since the physical change of state usually occurs at a specific temperature, the scattering phenomena can be used as the basis for a temperature switch. Devices that use this concept have a pellet of material in a reflective container. In the transparent state, the reflection is detected from the container. In the high-scattering state, the reflectivity is greatly diminished.

Scattering has been used in a transmissive system to fabricate dosimeters that detect radiation level. In the presence of nuclear radiation, many glasses form color centers that act as scattering sites. The transmission level in a radiation-sensitive glass fiber is a measure of radiation exposure.

Molecular constituents can be identified by their Raman-scattered spectra. A major advantage of this approach is that the signal is directly proportional to concentration.[29] Raman laser scattering has been used to detect small concentrations of various gases.[30] The system employs a high-intensity monochromatic light source coupled to the transmitting fiber that illuminates the gas sample. The receiving fiber collects the Raman-scattered radiation that is characteristic of the particular gas being measured.

Applications of this technique include monitoring methane vapor, which can, in turn, identify a possible liquid natural gas spill. Detection of 1% or less of methane vapor is achievable.

To increase the overall system sensitivity, a multipass sampling cell is used, as shown in Fig. 15.17.[30] The spherical mirrors labeled M1 provide for multiple passes of the light beam. A portion of the scattered light is injected directly into the receiving fiber, while additional scattered light reflects from mirror M2 into the receiving fiber. The fiber chosen for this sensor was glass, not plastic, due to the fact that the fibers themselves have a characteristic Raman scattering spectrum. Plastic fiber has many intensity peaks that mask the gas spectra being measured. Another problem is the scattering wavelength dependence in optical fibers.[31] At short wavelengths, the problem is more pronounced.

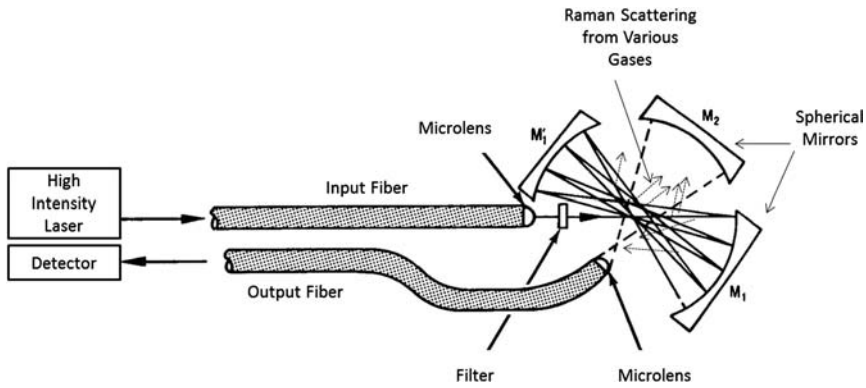

Figure 15.17 Multipass reflection sensor configuration for Raman scattering.

15.5 Refractive Index Change

The output level and the pattern of light are related to the difference between the index of refraction of the core and that of the cladding. Figure 15.18 shows the effects of the three principal index-of-refraction conditions and the resulting ray paths.[32] Sensors using this concept have been devised either by

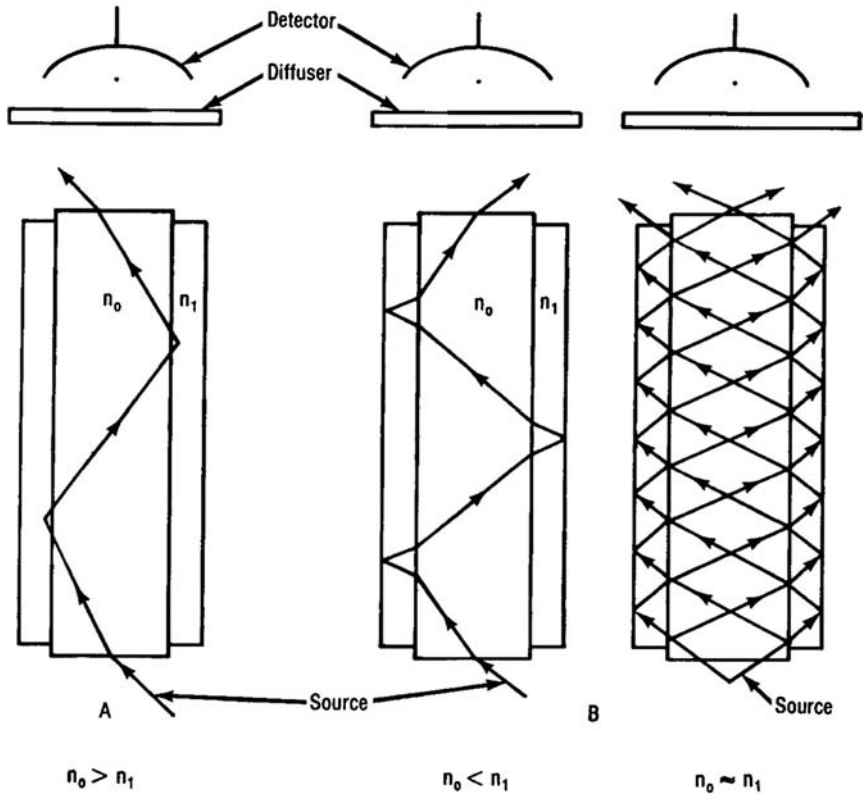

Figure 15.18 Ray paths associated with various index of refraction conditions in the cladding.[32]

having the substance (gas or liquid) in contact directly on an unclad glass rod (or prism) that acts as the core, or by reacting with a permeable coating on the glass rod. Gases such as NH_3, HCN, and H_2S have been detected by this approach.[33] Similar techniques have been devised for monitoring the combustion of jet fue1.[34]

Figure 15.19 shows a reflective fiber optic probe coupled to a prism. In air, the index of the prism is sufficiently higher than that of air, and a condition of total internal reflection exists within the prism. Therefore, light transmitted to the prism is reflected efficiently back into the fiber optic probe. However, if the prism is immersed in a liquid with a refractive index approaching the prism value, the reflected light significantly decreases. If the index of the liquid is higher than the prism, the intensity will drop to even lower values, typically less than 10% of the initial value.

While the concept is normally used for liquid level switch-type sensors, it can provide an analog signal proportional to the refractive index of the liquid. Since many components of a solution alter the refractive index of the liquid as a function of concentration, such a device can provide a measure of concentration. An example would be the concentration of sulfuric acid, which has a refractive index of just above 1.33 in low concentrations and 1.46 for a 90% concentration level. The device can also be used to differentiate liquids of different refractive indices, such as gasoline and water.

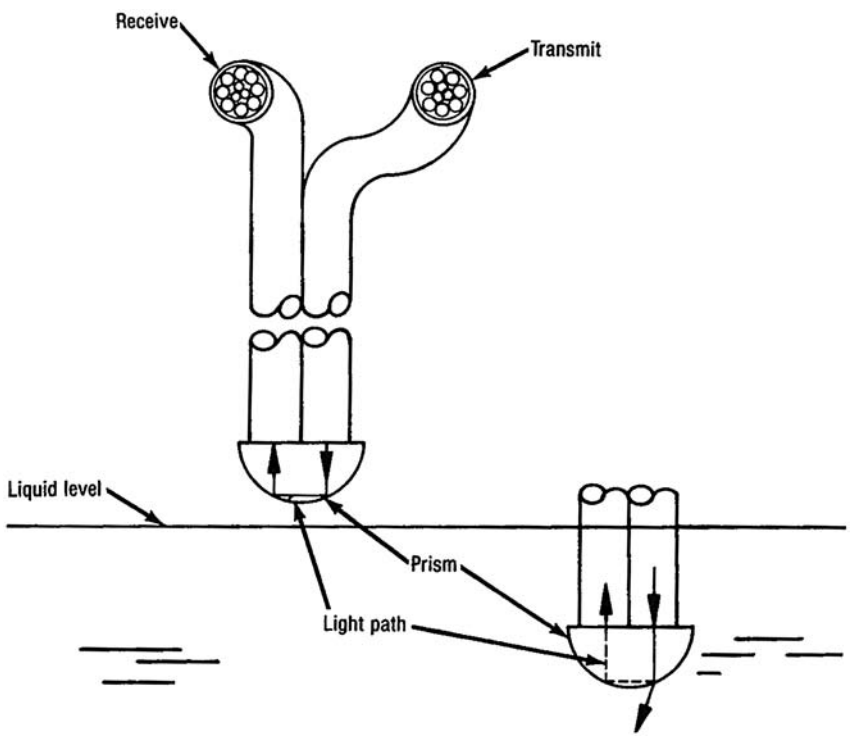

Figure 15.19 Refractive index change sensor using a reflective fiber optic probe.

The prism approach has also been used to measure void fraction.[33,35] As a bubble or void passes by the prism in a volume of material, the liquid and the voids have different refractive indices. This provides a signal corresponding to the condition at the probe tip. The probe, in effect, is used as a counter per unit time that determines the void fraction. The accuracy is estimated to be 0.5%.

A similar approach to the prism uses a tapered fiber as shown in Fig. 15.20.[6] The tapered section has the cladding removed so that the core can interact directly with the surrounding liquid. The power transmitted in the tapered region decreases with the square of the index of refraction of the liquid, as shown in Fig. 15.21. Sensitivity as high as 6×10^{5} index of refraction units has been determined.

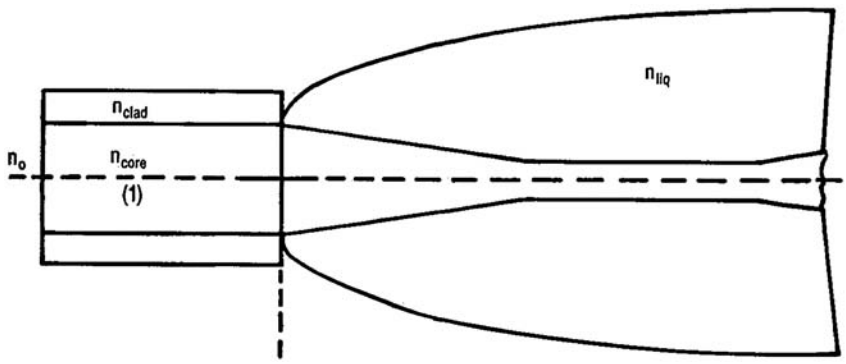

Figure 15.20 A tapered optical fiber with the cladding removed and the tapered section immersed in a liquid of refractive index n_{liq}.[6]

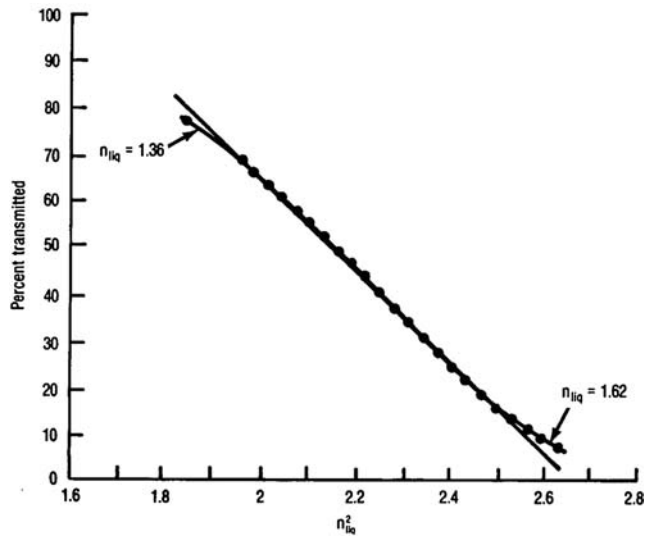

Figure 15.21 Percent of transmitted light versus n^2_{liq}.[6]

15.6 Color Changes

Fiber optic pH sensing systems use a bifurcated probe that, at the probe tip, contains an immobilized dye that changes color in a manner that is specific to the pH of the fluid being tested.[36] The process speed is limited by the diffusion rate associated with the fluid penetrating the film containing the immobilized dye. The response time is faster if the fluid is stirred or is at higher temperatures. These probes can function in both clear and turbid fluids.

15.7 Interferometry

Nearly all chemical sensors use intensity-modulation schemes. However, some chemical reagents swell when the reaction occurs. The potential of a mechanical (axial) movement corresponding to the concentration of a chemical species allows interferometric sensors to be considered. The principle is identical to electric and magnetic field interferometric sensors using piezoelectric and magnetostrictive coatings. Butler[37] has reported coating a fiber with palladium. The palladium is a hydrogen absorber that expands with hydrogen concentration. The palladium-coated fiber is the sensing leg in a Mach–Zehnder interferometer.

15.8 Distributed Fiber Optic Chemical Sensors

DICAST® (Distributed, Intrinsic, Chemical Agent Sensing and Transmission, a registered trademark of Intelligent Optical Systems) is a distributed fiber optic chemical detection system.[38] Figure 15.22 shows the concept. The coating is chemically active. The evanescent wave associated with the incoming light interacts with specifically targeted chemical agents such as chlorine or hydrogen cyanide or other toxic agents. The interaction of the incoming light with the target emits a specific wavelength of light characteristic of the toxin, and this light is injected back into the fiber core and can be detected.

DICAST cables achieve distributed chemical detection over tens of meters of coverage without the limitations of point sensor systems. Chemically sensitive optical fibers, each designed to detect a specific chemical agent, are housed in a ruggedized cable assembly. DICAST sensor cables can be

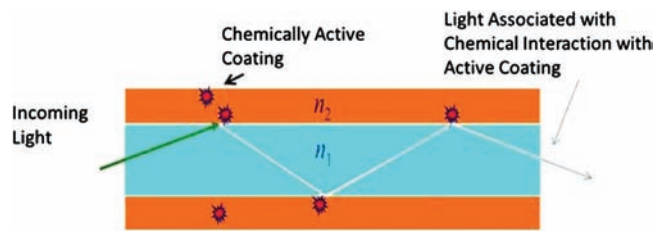

Figure 15.22 Distributed fiber optic chemical sensor (DICAST) operation.

designed to detect one or more multi-analytes in one cable. This approach is very sensitive and provides quick response to IDLH (immediate danger to life and health) levels. In practical applications it may not be necessary to have long lengths of the chemical sensing fiber. However, the active areas can be spliced with standard fibers so that discrete sections of the cable are functional chemical sensors.

Distributed Bragg grating sensors can be sensitized to a specific chemical.[39] It is possible to coat a fiber Bragg grating so that the coating induces a strain within the grating as a result of a chemical reaction with the coating and a target analyte. For example, hydrogen can be monitored by coating the fiber Bragg grating with palladium. Palladium absorbs hydrogen and expands as the hydrogen level increases, thereby, causing a strain on the fiber. This process is reversible, so, as the hydrogen level decreases, the palladium degasses, and the FBG then returns to its normal shape, relieving the induced strain.

The FBG can be coated with a variety of reactive materials that will react only to a specifically targeted chemical. This is especially applicable in cases of bio-agents, where the absorption of the bio-agent by the coating on the FBG would cause the grating to expand in proportion to its absorption of the bio-agent. This approach has the potential to detect a multiplicity of bio-agents on a single fiber at multiple locations.

15.9 Fiber-Optics-Enabled Spectroscopy

The development of advanced fibers and robust fiber optic cables has allowed remote spectroscopy to penetrate into harsh environments such as oil wells.[40] Multichannel spectrometers can be configured to accept over 100 separate channels simultaneously. Data from all channels is collected at the same time, allowing the user to measure multiple samples. The general concept is shown in Fig. 15.23, where each chemical sample is assessed through a fiber optic probe.

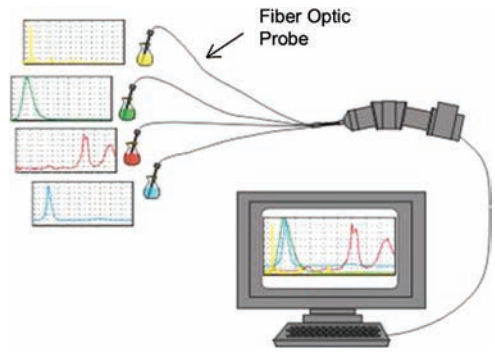

Figure 15.23 Fiber-optics-enabled multichannel spectroscopy.[40]

15.10 Applications

The applications for chemical analysis fall primarily into three categories: industrial process monitoring, medical monitoring, and security. The primary advantage for industrial and medical categories is *in situ* real-time measurement with minimal perturbations to the process being monitored.

Remote chemical analysis has a distinct advantage in a chemical plant. Centralized analyzers using remote fiber optic sensors can potentially replace costly inline conventional analysis equipment. The evolution of the sensor technology will be slowed by the fact that most materials do not fluoresce or have absorption or scattering phenomena in the desired wavelength range. Therefore, reagents have to be developed that are compatible with optical techniques for the vast majority of materials and processes to be monitored.

The medical sensor area is of keen interest because of the potential of extremely small-size sensors for direct use within the body. Fluorescence techniques are much more widely applicable in biological processes. For instance, fluorescence can differentiate between diseased and normal arterial tissue, as well as between many cancerous and noncancerous tissues.

Security is creating a growing need for chemical sensors. It is difficult to cover large areas such as perimeter security with a series of point sensors. Distributed chemical sensing approaches such as DICAST can provide solutions. Figure 15.24 shows a series of applications.[38] The first example shows an actual deployment in an air traffic control tower. The second example is a subway station, and the third example is perimeter security for an airport.

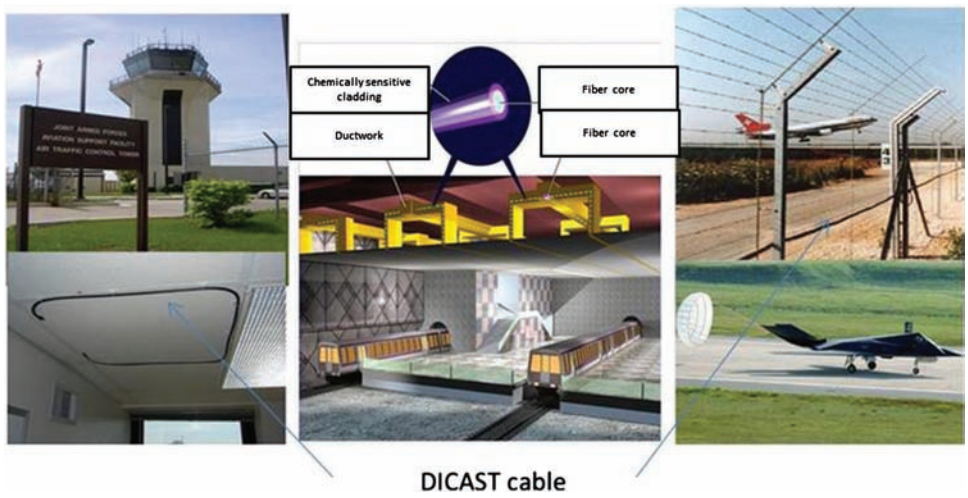

Figure 15.24 DICAST® Deployment.[38]

References

1. I. Chabay, "Optical waveguides," *Analytical Chemistry* **54**(9), 1071A–1080A (1982).
2. G. Graff, "Fiber optics analyze chemical processes," *High Technology*, 24–25 (1983).
3. T. H. Maugh, "Remote spectrometry with fiber optics," *Science* **218**, 875–876 (1982).
4. W. B. Grant, "Laser spectroscopy techniques make industrial appearance," *Industrial Research and Development*, 154–57 (1983).
5. Anonymous, "Fiber optics simplify remote analyses," *C& EN*, 28–30 (1982).
6. L. C. Bobb, H. D. Kurmboltz, and J. P. Davis, "An optical fiber refractometer," *Proc. SPIE* **990**, 164–169 (1988) [doi: 10.1117/.12.959989].
7. D. W. Lubbers, "Chemical *in vivo* monitoring by optical sensors in medicine," *Sensors and Actuat. B* **11**, 253 (1993).
8. S. McCulloch and D. U. Hamchandani, "A fiber optic micro-optrude for dissolved oxygen measurement," 12th International Conference on Optical Fiber Sensors, *Tech Digest Services* **16**, 428–431 (1997**)**.
9. J. I. Peterson, "Fiber optic chemical sensor development," *Proc. SPIE* **990**, 2–17 (1988) [doi: 10.1117/12.959967].
10. W. Chudyk, K. Kenhy, G. Jarvis, and K. Pohlig, "Monitoring of ground water contaminants using laser fluorescence and fiber optics," *Proc. ISA*, 1237–1243 (1986).
11. W. Chudyk, K. Pohlig, N. Rico, and G. Johnson, "Ground water monitoring using laser fluorescence and fiber optics," *Proc. SPIE* **990**, 45–47 (1988) [doi: 10.1117/12.959972].
12. L. Sarri and W. Weitz, "Immobilized morin as fluorescence sensor for determination of aluminum (111)," *Analytical Chemistry* **55**, 667–670 (1983).
13. J. Peterson, R. Fitzgerald, and D. Buckhold, "Fiber optic probe for *in vivo* measurement of oxygen partial pressure," *Analytical Chemistry* **56**, 62–67 (1984).
14. W. Seitz, "Chemical sensors based on fiber optics," *Analytical Chemistry* **56**(1), 19A–34A (1984).
15. Anonymous, "Fiber optic oxygen sensors: theory of operation", www .oceanoptics.com (2013).
16. E. Urbano, H. Offenbacher, and O. Wolfbeis, "Optical sensor for continuous determination of halides," *Analytical Chemistry* **56**(3), 427–429 (1984).
17. L. Sarri, and W. Seitz, "pH sensor based on immobilized fluoresceinamine," *Analytical Chemistry* **54**, 821–823 (1982).

18. R. A. Liebermann and K. E. Brown, "Intrinsic fiber optic chemical sensor based on two-stage fluorescent coupling," *Proc. SPIE* **990**, 104–110 (1988) [doi: 10.1117/12.959980].
19. C. Komives and J. S. Schultz, "Optical fiber biochemical sensors for continuous monitoring," *Medical Design and Material*, 24–27 (1991).
20. R. Chamberlin and J. Nellist, "The applications of fiber optics in worldwide offshore oil and gas industry operations," Gulf Fibercom, Inc., Irvine, CA (1985).
21. R. Schirmer, "On-line, fiber optic-based near infrared absorption spectrophotometry for process vontrol," *Proc. ISA*, 1229–1235 (1986).
22. R. Murry, D. Smith, and P. Wright, "Fiber-optic sensors for the chemical industry," *Optics News*, 31–33 (1986).
23. W. Seitz, "Chemical sensors based on fiber optics," *Sensors*, 7–9 (1985).
24. H. K. Whitesel, J. K. Overby, M. S. Ransford, and P. Tatem, "Smoke and mirrors, a fiber optic smoke sensor," *Proc. SPIE* **2292**, 133–133 (1994) [doi: 10.1117/12.191826].
25. J. Giuliani, W. Wohltjen, and N. Jarvis, "Reversible optical waveguide sensor for ammonia vapors," *Optical Letters* **8**(1), 54–56 (1983).
26. R. Munsinger, "Fiber optic colorimetry," *Electro-Optical Systems Design* **13**(2), 43–47 (1981).
27. Anonymous, "Smoke opacity monitoring systems," *Applications Engineering Handbook*, Dynatron, Wallingford, CT (1982).
28. S. Pilevar, C. C. David, and F. Portugal, "Tapered optical fiber using near-infrared fluorpheores to assay hybridization," *Anal Chem.* Article UC 9709965 (April 1998).
29. W. A. Leugers and R. D. McLachlan, "Remote analysis by fiber optic Raman spectroscopy," *Proc. SPIE* **990**, 88–95 (1988) [doi: 10.1117/12.959978].
30. R. Chang and R. Benner, "Laser-Raman point monitoring of CH_4 vapor in the LNG storage field," Gas Research Institute, Research Grant No. 5014-363-0146 (1979).
31. M. L. Myrick and S. M. Angel, "Normal and surface-enhanced Raman scattering with optical fibers," *Proc. SPIE* **1172**, 38–48 (1990) [doi: 10.1117/12.963171].
32. E. Handy, D. David, N. Kapany, and F. Unterleitner, "Coated optical guides for spectrophotometry of chemical reactions," *Nature* **257**, 646–647 (1975).
33. E. Handy and D. David, "Optical analytical device, waveguide and method," U.S. Patent 4,050,895 (1977).
34. D. K. Dandge, T. M. Salinas, S. M. Klaina, K. Gaswami, and M. Butler, "Fiber optic chemical sensors for jet fuel," *Proc. SPIE* **1172**, 132–139 (1989) [doi: 10.1117/12.963182].

35. P. Graindorge, G. LeBoudex, D. Meyet, and H. Arditty, "High bandwidth two-phase flow void fraction fiber optic sensor," *Proc. SPIE* **586**, 211–214 (1985) [doi: 10.1117/12.951167].
36. Anonymous, "Fiber optic pH sensors," www.oceanoptics.com (2013).
37. M. Butler, "Chemical sensor uses optical fibers," *C&EN*, 22–23 (1984).
38. R. Lieberman, "DICAST distributed chemical sensor system," www.intopsys.com (2009).
39. Anonymous, "Micron optics optical sensing guide," www.micronoptics.com (2005).
40. O. Pawluczyk, "Non scanning multichannel spectroscopy in biomedical applications," *OIDA Photonic Sensor Symposium*, Boston, MA, December 8 (2010).

Chapter 16
Biophotonic Sensors

16.1 Introduction

There is an increasing demand for biophotonic sensors in applications that include military, homeland security, industrial process, and biomedical, as well as a wide range of other applications. Biophotonic technology expands the sensing concepts to include the detection of chemical and biological agents (toxins) as well as the monitoring of biological processes. Biophotonic sensors are based on a broad range of photonics technologies. Not all of the sensing concepts require fiber optics for their implementation. However, the scope of this chapter will cover concepts that use optical fiber or waveguide technology.

The following quote from Tuan Vo-Dinh, Director, Center for Advanced Biomedical Photonics, Oak Ridge National Laboratory, clearly states the importance of biophotonic sensors: "An important area in chemical and biological sensing is the sensitive detection and selective identification of toxic chemical compounds (carcinogens, pollutants, etc.) or living systems (bioaerosols, bacteria, viruses or related components) at ultra-trace levels in complex samples. Combining the exquisite specificity of biological recognition probes and the excellent sensitivity of laser-based optical detection, biophotonic sensors are capable of detecting and differentiating bio/chemical constituents of complex systems in order to provide unambiguous identification and accurate quantitation, and open new horizons for chemical and biological sensing."[1]

Biophotonic sensors can be defined in two basic categories. In the first, the sensing function is created by the modulation of light using the embedded biomolecular properties of a sensing element (intrinsic). In the second category, biological processes are monitored by conventional photonic (fiber optic) sensing approaches (extrinsic).

16.2 Intrinsic Biophotonic Sensors

Using the biomolecular properties of the sensing element, a variety of intrinsic sensor approaches has been developed. The basic concept is shown in Fig. 16.1. The recognition layer has chemical or bio-receptors that react with the target

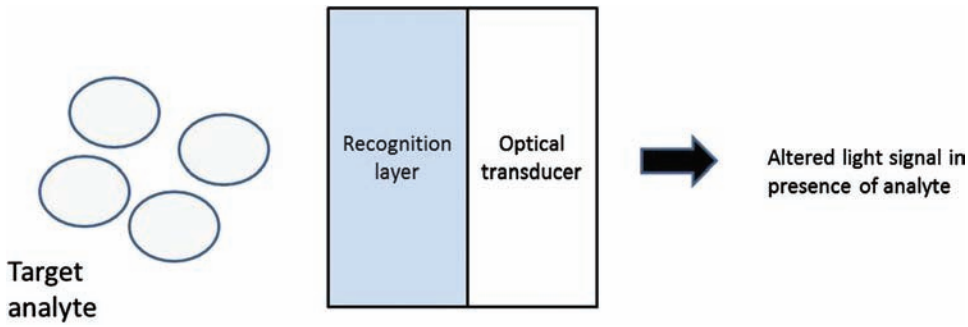

Figure 16.1 Biosensor concept.[2]

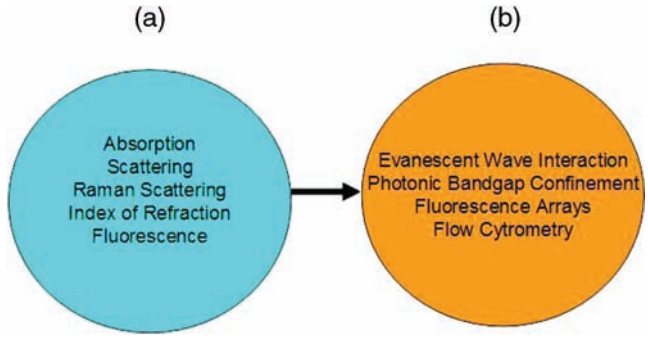

Figure 16.2 Intrinsic sensing (a) mechanisms and (b) concepts.

analyte. The interaction alters the response of the transducer. The various sensing mechanisms and concepts that can be used are defined in Fig. 16.2.

16.2.1 Intrinsic biophotonic sensors: evanescent wave interaction

Many of the sensor configurations that have been described are based on evanescent field interaction. Attaching a chemical/bio-receptor to the surface of a waveguide or other photonic device causes some optical perturbations when the target analyte is encountered. A change in refractive index, absorption, or fluorescence can alter the light transmission in the device. One approach uses an active coating on a metal waveguide in a Mach–Zehnder configuration. The metal waveguide provides a surface useful for the sensing function. The surface of the metal is coated with a receptor molecule that binds with the target analyte molecule. The receptor is one component of a biospecific pair (antibody–antigen) and is immobilized to the sensor surface. The receptor–analyte layer changes the propagation characteristics of the waveguide. The optical fields associated with the metal waveguide are greatest at the metal surface with the maximum fields (TM) in the interaction region, as shown in Fig. 16.3. The sensor architecture using an interferometer is shown in Fig. 16.4.

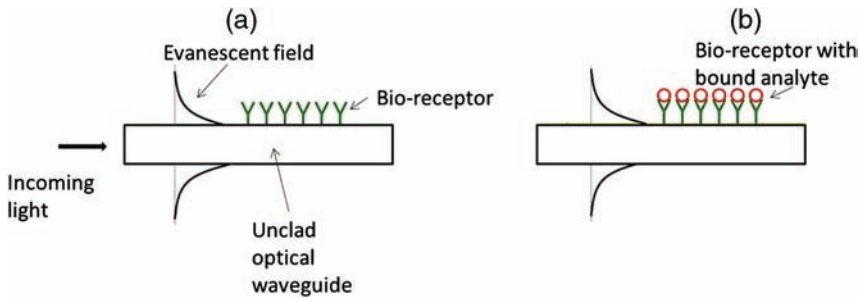

Figure 16.3 Waveguide (a) prior to and (b) after binding with analyte.[3]

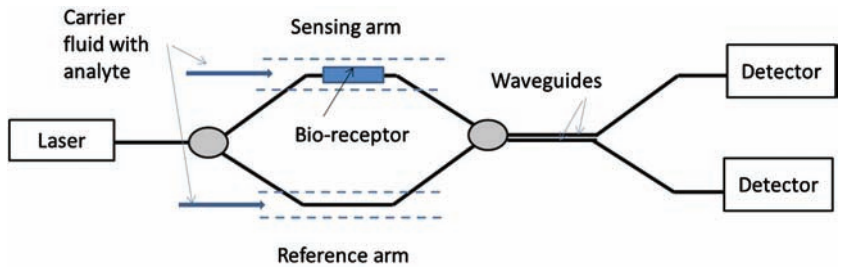

Figure 16.4 Biophotonic interaction-modulated Mach–Zehnder interferometer.[3]

The reference arm compensates for thermal and strain variations along the device, changes in carrier fluid index, and nonspecific binding. Single or multiple outputs can be achieved. Also, integration of microfluidics and electronics are possible. There are many benefits related to this approach. The sensitivity is high. Analyte detection occurs directly in one step. The receptor provides for specificity, and the modulation of optical properties is a measure of concentration. Binding kinetics can be determined in real time. Chemical treatments to facilitate monitoring are unnecessary. Other techniques, such as absorption, require identification of specific absorption bands. For this approach, a distinct advantage is that target analytes do not require special features. As with all photonic sensing approaches, there is an absence of electromagnetic interference. In addition, array configuration architectures can be employed that greatly expand the measurement capability.

Fluoroimmunoassay technology is another evanescent wave interaction methodology. The concept is shown in Fig. 16.5. The target analyte is a fluorospore that gives off a fluorescence signal that alters the transmitted light through the evanescent field. One of the main applications for this technology is aerosol bio-agent monitoring in a negative-pressure environment (semi-clean room). This approach is capable of continuous operation and can provide statistically significant airflow sampling. The sensor can detect bacteria, spores, viruses and toxins. Potentially, the sensor can monitor for multiple target analytes. The fluorescence target approach is insensitive to

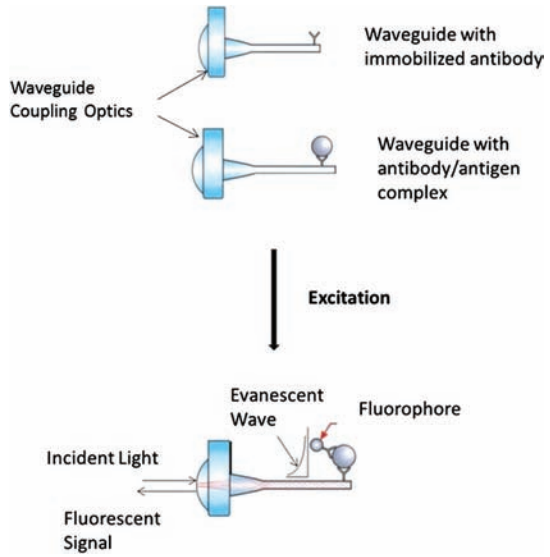

Figure 16.5 Evanescent wave fluoroimmunoassay concept.[4]

dirty environments, resulting in a low false-alarm rate. It has low per-assay costs and, due to its compact size, is field deployable. The results of an actual field test resulted in a false alarm rate of less than 1% while tracking five target elements at low concentration levels.

Bragg grating sensors can be expanded beyond strain and temperature to include chemical sensing. This approach can greatly enhance the ability to do distributed chemical sensing over long spans. If the fiber containing a Bragg grating is squeezed, stretched, or heated, this will cause a wavelength shift in the reflected spectrum, which typically responds to temperature, strain, or pressure. However, if a chemical reaction can alter the strain in the fiber or interact with the cladding modes, it can be detected as shown in Fig. 16.6.

The Bragg grating sensing concept can be greatly expanded using tilted fiber gratings as shown Fig 16.7.[5] The concept is to generate several distinct resonances from a single grating and to make these resonances respond differently to perturbations. This allows for the measurement of multiple parameters from a single sensor.

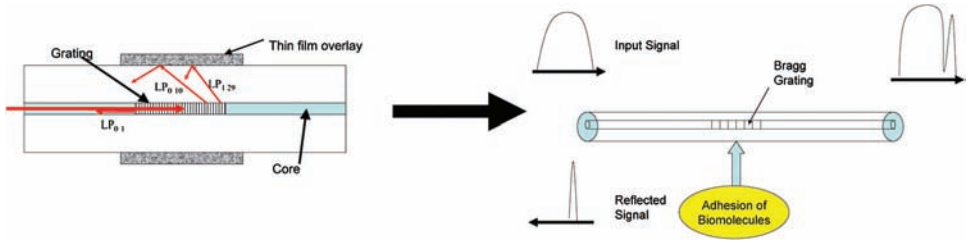

Figure 16.6 Biomolecularly modulated Bragg grating sensors.[5]

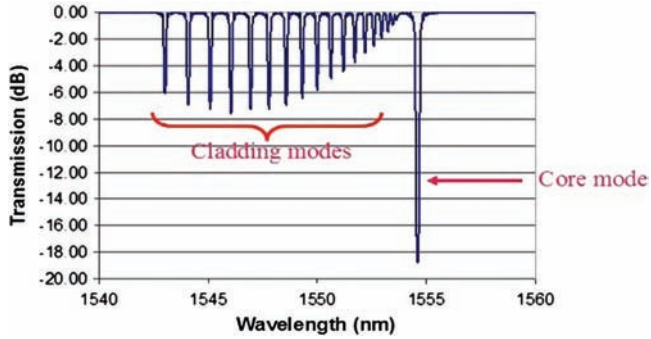

Figure 16.7 Transmission spectrum of a Fiber Bragg grating with slightly tited (1 to 4 degrees) reflection planes.[5]

Changes in refractive index, fluorescence, or absorption perturb the cladding modes. Each cladding mode resonates differently due to perturbations to the thin film. Bioreceptors attached to the fiber coating perturb the light transmission modes in the fiber in the presence of a target analyte. A sensing scheme using evanescent absorption in a transmissive configuration is represented schematically in Fig. 16.8. The sensor is sensitive to small changes in absorption and wavelength. In field configurations, the attachment is flexible in that it can be in a fluid flow in a pipe or on any surface. As an example, the detection of hydrogen cyanide (HCN) gas is shown in Fig. 16.9.

The extent of the absorption change is proportional to the analyte concentration. A specific enzyme is chosen (recognition) that binds to the target analyte, thereby providing specificity.

16.2.2 Intrinsic biophotonic sensors: using photonic crystal fibers

A photonic crystal fiber bio/chemical sensing platform is shown in Fig. 6.10.[7] The photonic crystal fiber (PCF) has a dual function. PCF acts simultaneously as an efficient waveguide and an analyte-carrying gas or liquid transmission cell. There is a long interaction path with the bound analyte on the air-filled cladding and the core as illustrated. The concept uses vibrational Raman scattering that occurs when light interacts with a molecule. A small amount of wavelength-shifted light is scattered, creating a distinct spectral

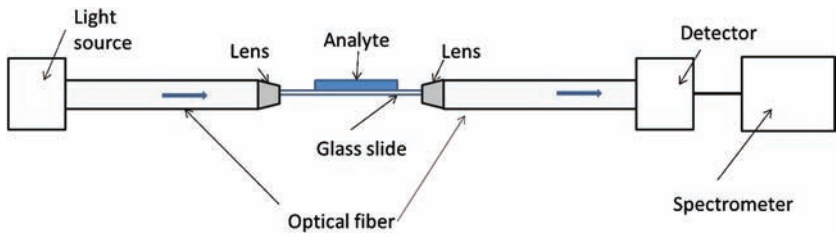

Figure 16.8 Fiber optic-based evanescent absorption sensor.[6]

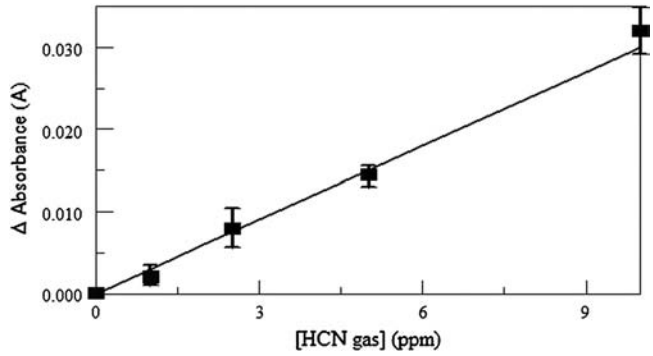

Figure 16.9 HCN gas detection by evanescent absorption.[6]

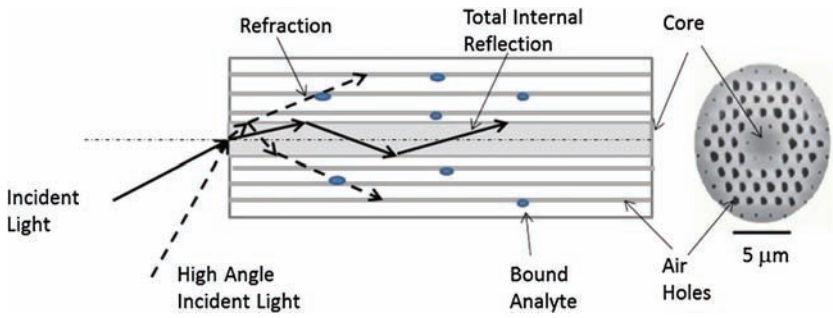

Figure 16.10 Photonic crystal fiber sensor concept with nanoparticles (diam. ~30 nm) immob lized on the air hole surface.[7]

fingerprint. Molecular- and nano-scale surface modification of PCF air holes for surface-enhanced Raman scattering (SERS) enables high analyte selectivity and specificity. The anticipated benefit is ultrasensitive (ppb–ppt) detection and molecular fingerprinting. The SERS principle is given in Fig. 16.11.

There are some issues with PCF platforms. Gas/liquid flow in PCF is constrained, limiting sampling volume and thus requiring a pressure gradient for flow management. The sensor response rate corresponds to the filling of the air holes over the fiber length.

The use of PCF as sensors makes them very attractive devices for biomedical applications, since a broad range of analytes and optical interaction schemes can be used to provide monitoring and detection.[8,9]

16.2.3 Intrinsic biophotonic sensors: fluorescent microsphere array sensors

Typically, with a single sensor, one measurement is performed per given time. Multiple measurements must be done sequentially. With an array of sensors, the same measurement or multiple measurements can be performed

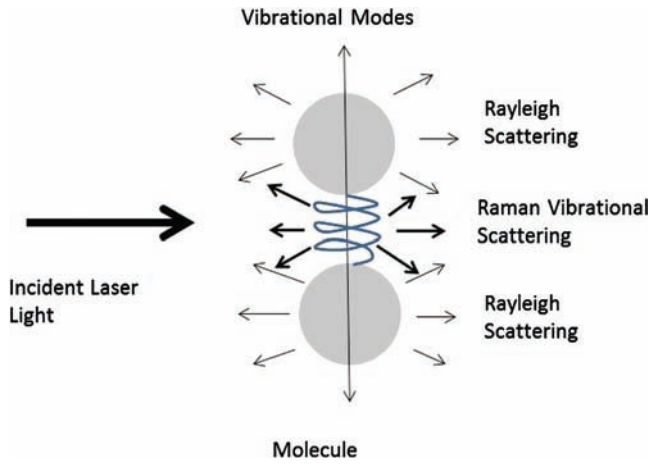

Figure 16.11 SERS Principle.[7]

many times simultaneously. Arrays increase selectivity and lower the detection limit due to the presence of multiple sensor types and signal averaging. The challenge is to develop an array that is compact and useful for sensing. A distinct advantage of fluorescence-based sensing is the rapid response time.

The approach is to use a fiber array on which fluorescent microspheres are attached.[10] The fiber cores can be selectively etched, which leaves an array of microwells. The addition of an analyte-sensitive fluorescent dye results in analyte-sensitive microspheres as depicted in Fig. 16.12. Attaching multiple fluorescent dye micospheres to a fiber bundle with etched wells at one end provides for a variety of target analytes and results in a multiplexed array.

Microsphere arrays enable high-throughput screening. Figure 16.13 depicts an array in multi-well microtiter plate format. The array is designed

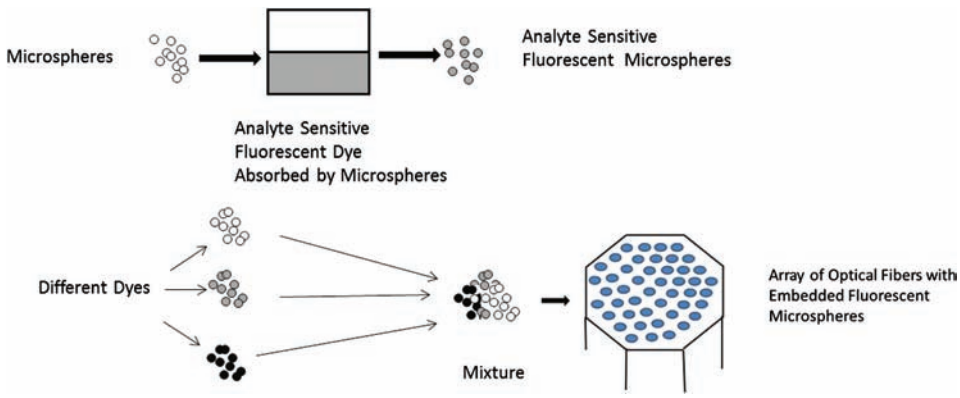

Figure 16.12 Fluorescent array microsphere sensors.[10]

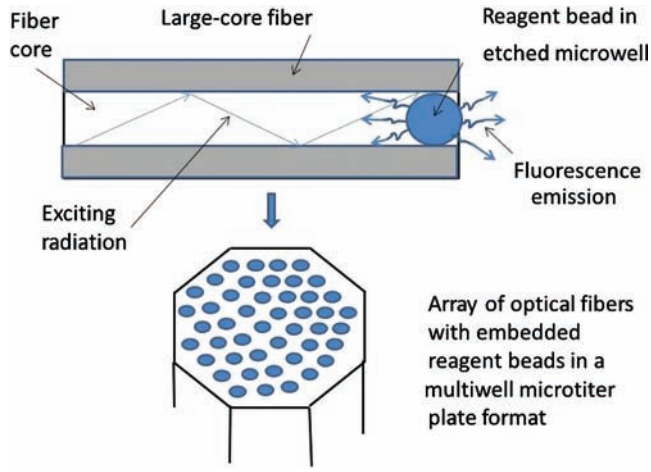

Figure 16.13 Fiber-optic-enabled arrays using fluorescence for high-speed screening.[1]

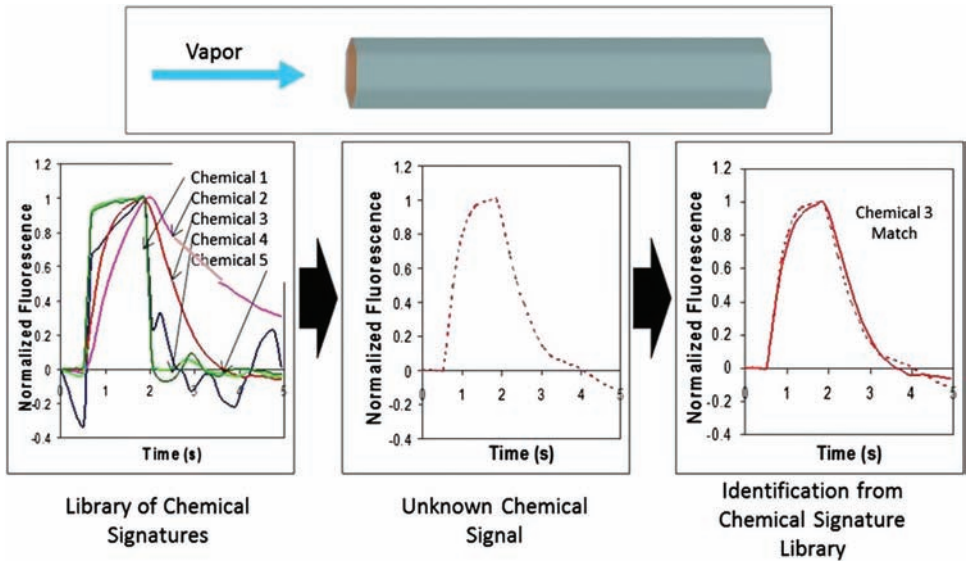

Figure 16.14 Fluorescent array microsphere sensors.[10]

to have low background fluorescence to maximize the fluorescent signal from each bead. The array has many beads modified with different chemistries. The multiplexed array has increased selectivity due to cross reactivity. The detection limit is improved as a result of signal averaging many sensors. An example of using the fluorescence-based microsphere array is vapor sensing. The fluorescent signature is known for gases and is stored. Therefore, the sample can be identified by comparison with the stored fluorescent signature library, as shown in Fig. 16.14.

16.2.4 Intrinsic biophotonic sensors: distributed sensor concepts

As discussed in Chapter 15, an intrinsic sensing concept in which a doped cladding turns a passive fiber into a chemical sensor is referred to as "Distributed Intrinsic Chemical Agent Sensing and Transmission" or DICAST®.[11] The entire fiber is the sensor.

The DICAST approach provides a sensing capability that is fully distributed, intrinsically sensitive, chemically active, cladding based, and provides seamless coverage. The multifiber/multichemistry approach provides a dramatic reduction in false alarms. The alarm signal is achieved with phase-locked-loop optoelectronic detection that is self-referenced and has high sensitivity. Visible wavelength OTDR provides the threat location.

Active DICAST fibers have been developed for chlorine, hydrogen sulfide, hydrogen cyanide, and sarin/soman. The fiber integrates total exposure over the short term and resets after 24 hours (HCN, H_2S). The system performance requirements are tabulated in Table 16.1. The sensor concept provides for specificity and low false-alarm rate. LCt_{50} is defined as the lethal concentration that will cause incapacitation within typically 1 minute. IDLH is an acronym for Immediately Dangerous to Life or Health, and is defined by the US National Institute for Occupational Safety and Health (NIOSH).

16.2.5 Intrinsic biophotonic sensors: surface plasmon resonance

Blood group detection errors can lead to serious medical problems. To address this issue, an errorless blood group detection probe has been designed.[12] The probe provides rapid results with a smaller blood sample than required with other approaches.

Table 16.1 DICAST system performance specificiations.[11]

System Parameter	Requirement
Sensitivity	Will alarm at 10% of LCt_{50} integrated dosage; zero false negatives
Specificity	Will not alarm to interferants anticipated to be found in indoor, outdoor, and military environments
Accuracy/Linearity/Resolution	Alarm system: • Triggers when 3 ft exposed anywhere • 50 ft distance resolution OTDR system: Linear concentration versus length plot • 10% concentration accuracy • 3 ft distance resolution
Response Time	• 10 sec 100% LCt_{50}/IDLH • 20 sec 50% LCt_{50}/IDLH • 45 sec 25% LCt_{50}/IDLH
Cable Length	200 ft (chemically sensitive) Can be interspersed with >1,000 ft of conventional fiber cable
Cable Lifetime	1 year
Calibration	Electronic compensation
False Alarm	Less than 1% (not to exceed 1 per year)

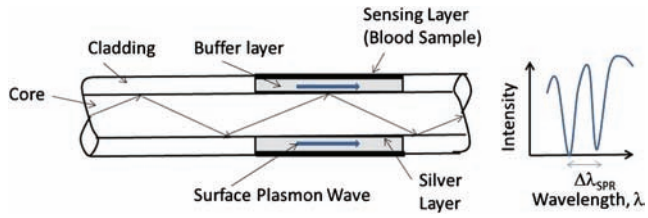

Figure 16.15 A proposed fiber optic SPR sensor probe for detecting human blood groups.[12]

The probe design consists of coating a small segment of optical fiber (typically 10 to 15 mm) with a surface plasmon resonance (SPR) active metal such as silver. The coating thickness is a few nanometers. The thin metal layer is then coated with a buffer that prevents any contaminants from being deposited on top of the metal, as shown in Fig. 16.15. For measurements, the blood sample is brought into contact with the probe, and light is launched into the input end of the optical fiber. The resulting light emitted at the other end of the probe provides information such as resonant wavelength, from which the blood group can be deduced. Specifically, in the presence of a blood sample, the output signal exhibits a sharp dip at a resonance wavelength because of strong optical absorption by the surface plasmon wave (occurrence of SPR). The shift in resonance wavelength $\Delta\lambda_{SPR}$ is shown in Fig. 16.15.

Optimum results were obtained using an optical fiber with a large core diameter and small sensing regions with silver layer thicknesses typically around 50 nm. Another important feature is that with an appropriate buffer solution, the probe was reusable. This basic concept can be used in a distributed configuration.

Tilted Bragg gratings can be used efficiently with surface plasmons in a metal-coated fiber similar to the configuration shown in Fig. 16.15, where the fiber has a thin silver coating. The tilted Bragg enhances the evanescent wave interaction. Minute changes at the surface of the fiber facilitate biochemical reactions. As an example, micromolar concentrations of proteins have been detected by attaching synthetic DNA sequences on a gold-coated fiber using a tilted Bragg grating incorporated in an SPR sensor.[16]

16.3 Extrinsic Biophotonic Sensors

Conventional photonic sensing techniques can also be used for monitoring biological processes extrinsically. In general, extrinsic biophotonic sensors provide indirect chemical process measurement such as changes in pressure, temperature, or polarization state. White-light interferometry (WLI) technology can be used for biomedical pressure monitoring.[14] The concept is shown in Fig. 16.16.

There are several benefits of white light interferometric sensors. They can be made extremely small. They are resistant to harsh chemical and thermal environments. Absolute or relative measurements are possible. Several types

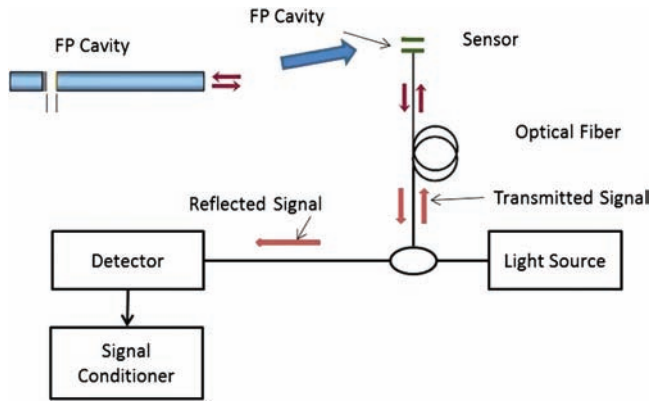

Figure 16.16 White light interferometry for medical applications.[14]

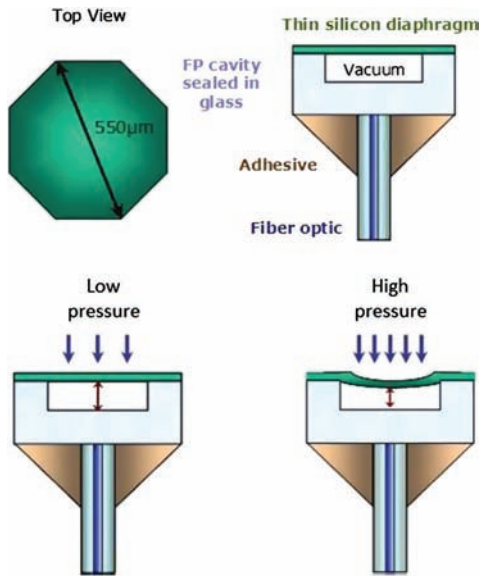

Figure 16.17 Pressure sensor design.[14]

of sensors can be used with the same signal analyzer (pressure, temperature, strain, force/load, displacement, refractive index, etc.). They have a high tolerance to fiber losses such as fiber bending, fiber attenuation, and source fluctuations. The technology promotes cost-effective sensors. The pressure sensor design is shown in Fig 16.17.

The pressure sensor performance is defined below:[14]

- Absolute pressure measure (0.25 mm Hg)
- Physiologic pressure range (±300 mm Hg)
- Robustness: Proof pressure (> 6 atm)
- Linear pressure response (NL < 1%)

- Good sensitivity (~2 nm/mm Hg)
- Stability (low drift <1 mm Hg)
- Predictable low thermal shift (<0.4 mm Hg/°C)
- Fully biocompatible materials
- Sterilization [ethylene oxide (EtO), electron-beam, etc.]

As discussed in the chapters on temperature and pressure, several fiber optic technologies can provide measurements suitable for biomedical applications. As an example, a Bragg-grating-based sensor can be integrated with an endoscope to provide pressure or temperature data in conjunction with imaging.[15] Bragg grating temperature sensors have been used to enhance the effectiveness of laser-induced thermotherapy. A problem with thermotherapy is detecting the temperature distribution of the treated tissue in real time. Bragg grating sensors were able to provide the temperature distribution with a spatial resolution of 0.25 mm within 10 sec. The temperature distribution information allowed more precise control of the laser parameters and a better therapeutic result.[16]

Medical applications for pressure sensors include: intracranial pressure monitoring, intrauterine diagnostics, pediatric surgery, bleed control during surgery, intraocular pressure control, and urodynamics. An example of using a fiber optic pressure sensor in counter-pulsation [intra-aortic balloon (IAB)] therapy is shown in Fig. 16.18.

The biophotonic concepts can function over a broad spectral range including UV, visible, near IR, and mid-IR. The advanced stage of component availability in the C band due to telecommunications investment has generated biophotonic sensing schemes that utilize this established technology. Those applications that can function in the UV, visible, and near IR also benefit greatly from optical fiber technology and are for the most part compatible with optical fiber integration. However, biophotonic sensors that have unique chemical sensing properties in the mid-IR are no longer compatible with silica-based optical fibers, which are limited to wavelengths less than 2 μm. However, fibers are available that function into the mid-IR range.

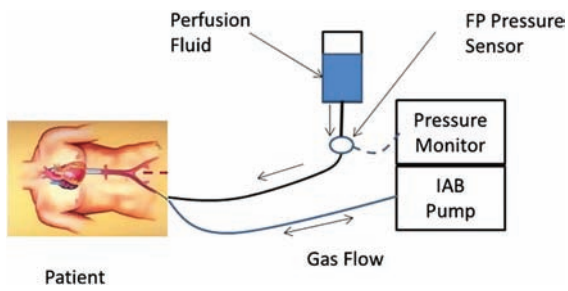

Figure 16.18 Fluid pressure transduction.[14]

References

1. T. Vo-Dinh, "Advanced biophotonics: from biochip to nanosensor, Plenary Keynote, 2nd Asian Pacific Rim Symposium on Biophotonics, Taipei, Taiwan, December 15, 2004.
2. P. Berini, "Photonic biosensors," *OIDA Biophotonic Sensors and Smart Fiber Optic Sensor Networks Workshop*, p. 9 (August, 2005).
3. E. Saaski, "Optical biosensor monitoring systems," *OIDA Biophotonic Sensors and Smart Fiber Optic Sensor Networks Workshop*, p. 11 (August, 2005).
4. P. Lefebvre, "Tilted-grating-based optical fiber multi-parameter sensing," *OIDA Biophotonic Sensors and Smart Fiber Optic Sensor Networks Workshop*, p. 17 (August, 2005).
5. H. J. Harmon,"Optical detection using protein and enzyme monolayers on planar waveguides,"*OIDA Biophotonic Sensors and Smart Fiber Optic Sensor Networks Workshop*, p. 21 (August, 2005).
6. H. Du,"Nanotechnology-enabled photonic crystal fiber sensing platform," *OIDA Biophotonic Sensors and Smart Fiber Optic Sensor Networks Workshop*, p. 23 (August, 2005).
7. V. V. Tuchin, J. S. Skibina, and A. V. Malinin, "Photonic crystal fibers in biophotonics," *Proc. SPIE* **8311**, 83110N (2011) [doi: 10.1117/12.902647].
8. F. Berghmans et al., "Photonic crystal fiber Bragg grating based sensors: opportunities for applications in healthcare," *Proc. SPIE* **8311**, 831102 (2011) [doi:10.1117/12.901240].
9. D. Monk, "An overview of biophotonic and fiber optic sensing in the walt laboratory at Tufts University," *OIDA Biophotonic Sensors and Smart Fiber Optic Sensor Networks Workshop*, p. 22 (August, 2005).
10. R. Lieberman, "DICAST distributed chemical sensor system," www.intopsys.com (2009).
11. M. Freebody, "Fiber optic probe provides errorless blood group detection," *BioPhotonics* (April 19, 2010).
12. J. Albert, "Tilted fiber Bragg gratings as multi-sensors," *OPN Optics & News*, 28 (2011).
13. C. Hamel, "Miniature fiber optic pressure sensors for intra aortic balloon pumping applications," *OIDA Biophotonic Sensors and Smart Fiber Optic Sensor Networks Workshop*, p. 15 (August, 2005).
14. S. Heyvaert, "Fiber optic sensors as guidance and diagnostic tools for epiduroscopy: P4L industrial project," *Scientific Meeting of Photonics4Life* (2010).
15. C. Li, N. Chen, and T. Wang, "Fully distributed chirped FBG sensor and application in laser-induced interstitial thermotherapy," *Proc. SPIE* **7634**, 76340D (2009) [doi: 10.1117/12.852040]

Chapter 17
Rotation Rate Sensors (Gyroscopes)

17.1 Introduction

The major advantages of a fiber optic gyroscope over mechanical devices include: no moving parts, no warm-up time, unlimited shelf life, minimal maintenance, large dynamic range, and small size.[1,2] Fiber optic gyroscopes are used broadly in inertial navigation systems, and tactical and strategic missiles.[3] New applications are emerging, such as in oil well drilling. The scope of applications is quite broad with a wide range of specifications. Figure 17.1 graphically shows the various applications in relation to the required dynamic range and sensitivity.[4] As an example, aircraft navigation gyroscopes have requirements of 0.1 to 0.001 deg/hr. The earth's rotation rate, $\Omega_E = 15$ deg/hr. Therefore, aircraft navigation needs expressed in earth's rotation rate are 10^{-2} to $10^{-4}\Omega_E$. Geophysical applications require detection of rotation rates at $10^{-6}\Omega_E$.[4] All optical rotation sensors are based on the Sagnac effect, which is described in Chapter 4.

17.2 Sensor Mechanism

The Sagnac effect uses an interferometric technique for rotation-rate detection.[6] The initial light beam is split into two beams that travel along a single fiber in a coiled configuration, as shown in Fig. 17.2. One path is clockwise, and the other is counterclockwise. When the fiber ring rotates in a clockwise direction, the light propagation in the clockwise direction is longer. This situation is due to the fact that the starting point has now moved due to rotation, and the light beam must travel a greater distance to reach the starting point. Conversely, the counterclockwise light beam travels a shorter distance. The path length difference results in a phase difference that affects the output of the Sagnac interferometer in a manner that is related to the rotation rate (angular velocity).

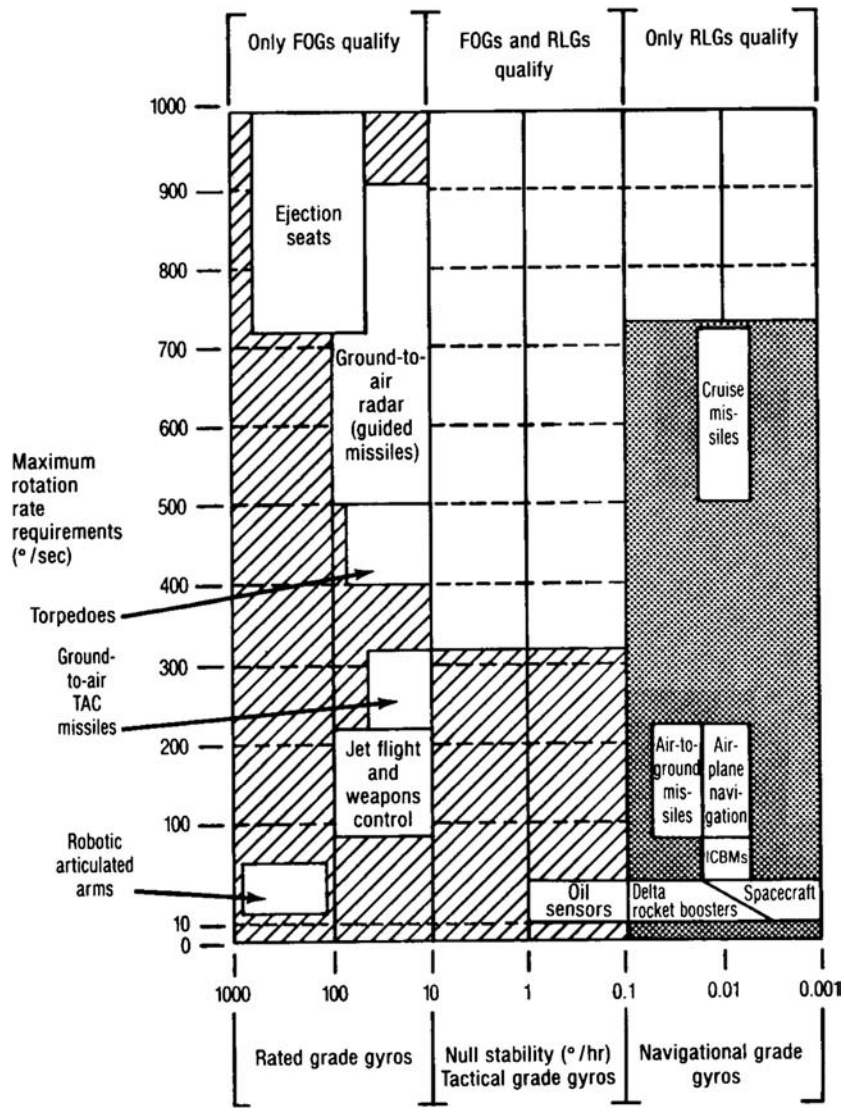

Figure 17.1 Applications of optical gyroscopes with the required specifications.[4]

Figure 17.3 provides the definition for the mathematical relationship between the path length difference L and the rotation rate Ω. The rotation rate corresponds to an angular velocity, ω. The angular velocity is expressed in radians/sec. The magnitude in radians defines the length of the arc traveled:

$$\theta = \Delta S/R, \tag{17.1}$$

where θ is the subtended angle in radians (dimensionless), R is the radius of the arc, and ΔS is the arc length. Using the angular velocity, the path length is given by[2]

$$\Delta L = (4A/c)\omega \tag{17.2}$$

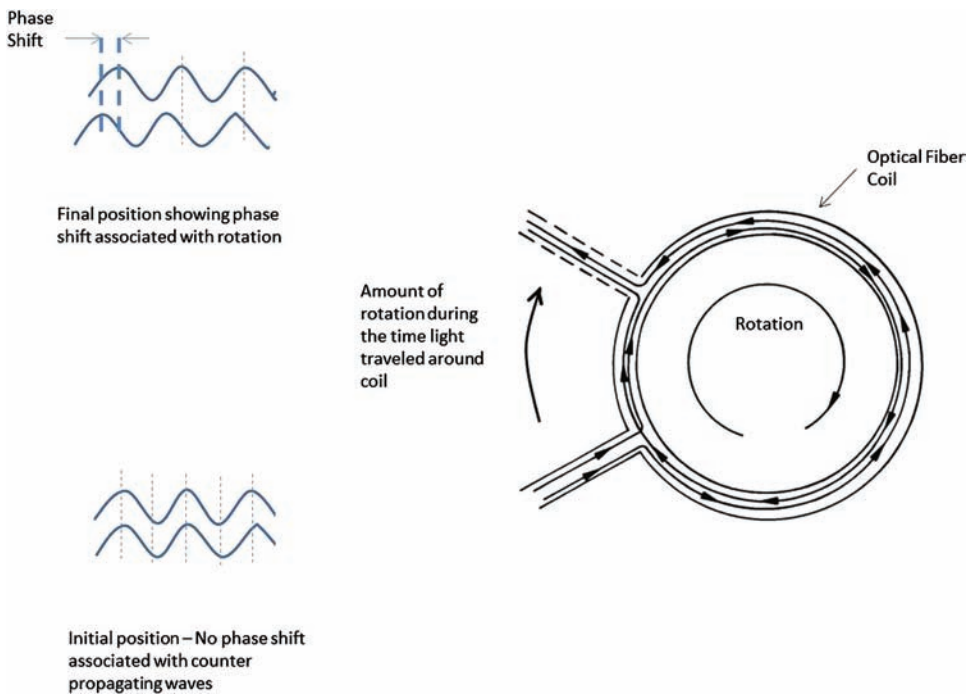

Figure 17.2 Sagnac effect in a coiled fiber used for rotation-rate sensing.

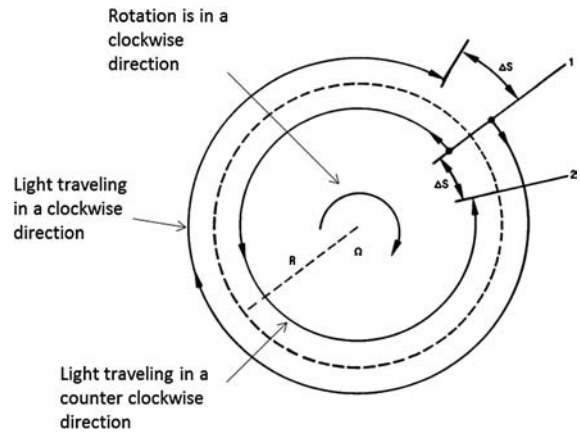

Figure 17.3 Sagnac configuration with geometric parameters defined (courtesy of Dynamic Systems, Inc.).

where A is the area enclosed by the light path (of radius R), and c is the velocity of light in vacuum. For a clockwise rotation, starting at point 1 and moving to point 2, the clockwise path length is $2\pi R + \Delta S$. The counterclockwise path length is $2\pi R - \Delta S$. ΔS is the change in circumferential path length. Therefore,

$$\Delta L = 2\pi R + \Delta S - (2\pi R - \Delta S) = 2\Delta S. \tag{17.3}$$

The path length traveled by the light in a time t is given by

$$\Delta L = c\Delta t = (4A/c)\omega. \tag{17.4}$$

Both definitions of L and t defined above in vacuum are applicable in a medium of refractive index n.[2] For a fiber coil with N turns, t then becomes

$$\Delta t = (4AN/c^2)\omega. \tag{17.5}$$

A phase-shift change is defined as

$$\Delta\phi = 2\pi\Delta t \frac{c}{\lambda_0}. \tag{17.6}$$

Since $\lambda_0 = \lambda_n$ (λ_0 is the wavelength in vacuum),

$$\begin{aligned} \Delta\phi &= 2\pi\Delta t \frac{c}{\lambda n} \\ &= \frac{(8\pi AN)\omega}{(\lambda_0 c)}, \end{aligned} \tag{17.7}$$

and ΔL is defined by

$$\Delta L = \left(\frac{4AN}{c}\right)\omega. \tag{17.8}$$

For a fiber with a coil diameter D and length L, the following equations apply:

$$A = \pi D^2/4, \tag{17.9}$$

and

$$N = L/\pi D, \tag{17.10}$$

therefore,

$$\Delta\phi = (2\pi LD/\lambda_0 c)\omega, \tag{17.11}$$

and

$$\Delta L = (LD/c)\omega. \tag{17.12}$$

Using typical values in Eq. 17.11, the magnitude of L is very small for a single fiber loop.[2] To increase L to a more reasonable value, the number of turns in the fiber loop needs to be quite large.

As discussed in Chapter 4, the maximum sensitivity occurs when the phase changes are $\pi/2$ or some multiple thereof. Therefore, to maximize the sensitivity for small rotations, a nonreciprocal, stable $\pi/2$ phase shift must be introduced between the counter-rotating beams.[3,7] Figure 17.4 shows two biasing approaches. The first approach [Fig. 17.4(a)] applies a bias so that at small rotation rates the inherent insensitivity of the sensor, due to the output being near a maximum point (little slope change), is shifted to a maximum slope-change point. A more common approach is to sinusoidally modulate the

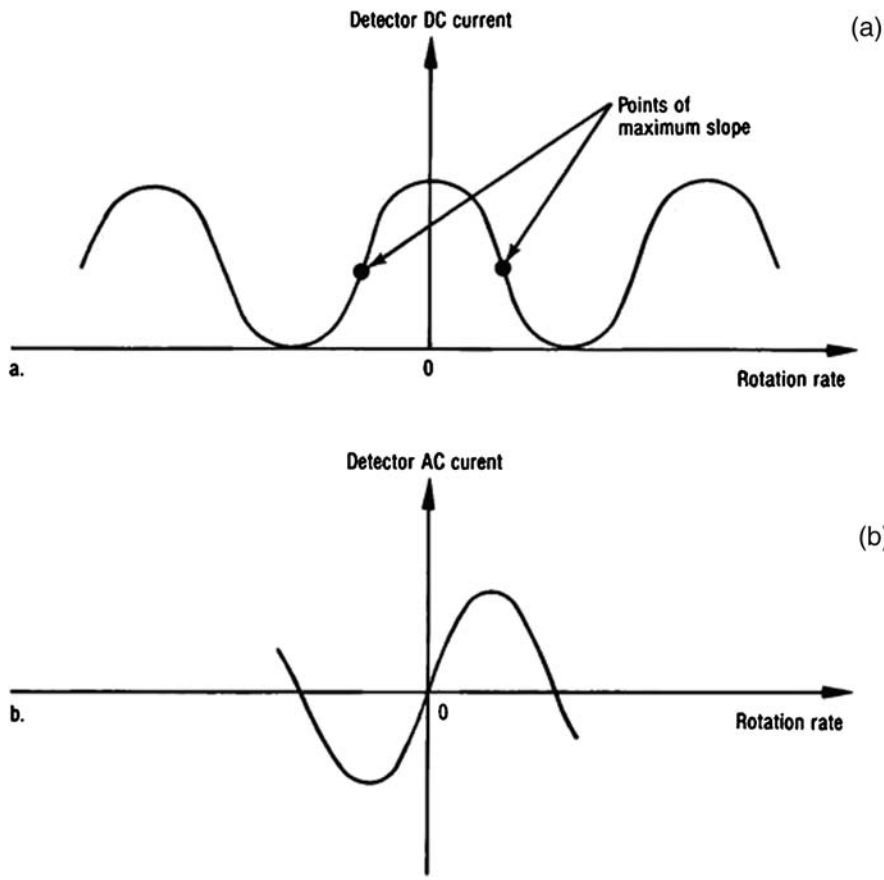

Figure 17.4 Biasing approaches (courtesy of IEEE, © 1986).[1]

phase difference between counterpropagating light beams. The AC detector current versus rotation rate is shown in Fig. 17.4(b). The sensing system now has a maximum sensitivity at zero rotation. The response is linear over a limited region of the response curve, and direction can be determined.

The fiber optic gyroscope using a modulator is shown in Fig. 17.5.[8] The spatial filter and polarizer ensure that the light paths for the counter-propagating waves are the same. The nonreciprocal phase modulator (NRPM) is typically a fiber wrapped on a piezoelectric cylinder. Through a feedback circuit, the piezoelectric cylinder, and hence, the fiber length, are altered in a sinusoidal manner to achieve the desired nonreciprocal phase shift, which in turn provides the bias. Those that use this configuration are referred to as analog, or open-loop, gyroscopes. A major disadvantage of this gyroscope configuration is that the calibration is dependent on the intensity of the light source. Open-loop gyroscopes are limited to applications with moderate dynamic range, sensitivity, and drift. The phase-shift change and length change are defined by Eqs. 17.6 and 17.8 respectively.

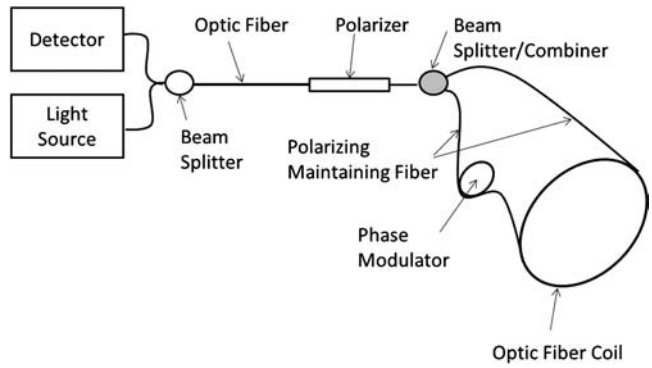

Figure 17.5 Analog fiber optic gyroscope configuration.

Closed-loop fiber optic gyroscopes are used for applications that require high dynamic range, sensitivity, and low drift. The closed-loop sensor configuration is shown in Fig. 17.6(b) with an open-loop sensor in Fig. 17.6 (a).[4] In contrast to the open-loop configuration, the closed-loop configuration is always operated at null, i.e., the net change in phase is zero. The null is accomplished by having the output of the modulator drive a nonreciprocal phase transducer (NRPT). The phase shift created by the NRPT is equal to but opposite in sign to the phase shift associated with the rotation. The closed-loop sensor can simulate frequency shifting with a digital approach, in which case it is referred to as a digital gyroscope.[8–10] The NRPT phase shift is accomplished by introducing a frequency difference Δf between the counter-propagating beams. The path length difference ΔL results in a frequency difference Δf as defined by

$$\Delta L = \frac{\Delta f L \lambda_0}{c}. \tag{17.12}$$

For the system to be at null with maximum sensitivity, the change of path length due to rotation must equal the path difference associated with the frequency shift; therefore,

$$\Delta f = \frac{4NA\omega}{\lambda_0 nL}. \tag{17.13}$$

The analog (open-loop) fiber optic gyroscope has a dynamic range of 10^3–10^5 with a scale factor correction (sensor accuracy) of 0.3%, which is characteristic of a medium-accuracy heading and attitude reference application.[3] The digital (closed-loop) gyroscope has a dynamic range of 10^8 and a scale factor correction of 0.03%.[8] A closed-loop navigation gyroscope design with an integrated optical chip is shown in Fig. 17.7.[11] The integrated optical chip imparts the phase modulation and splits the light into the clockwise and counterclockwise directions. The loop is closed by imparting a ramp, which causes the phase shift between the

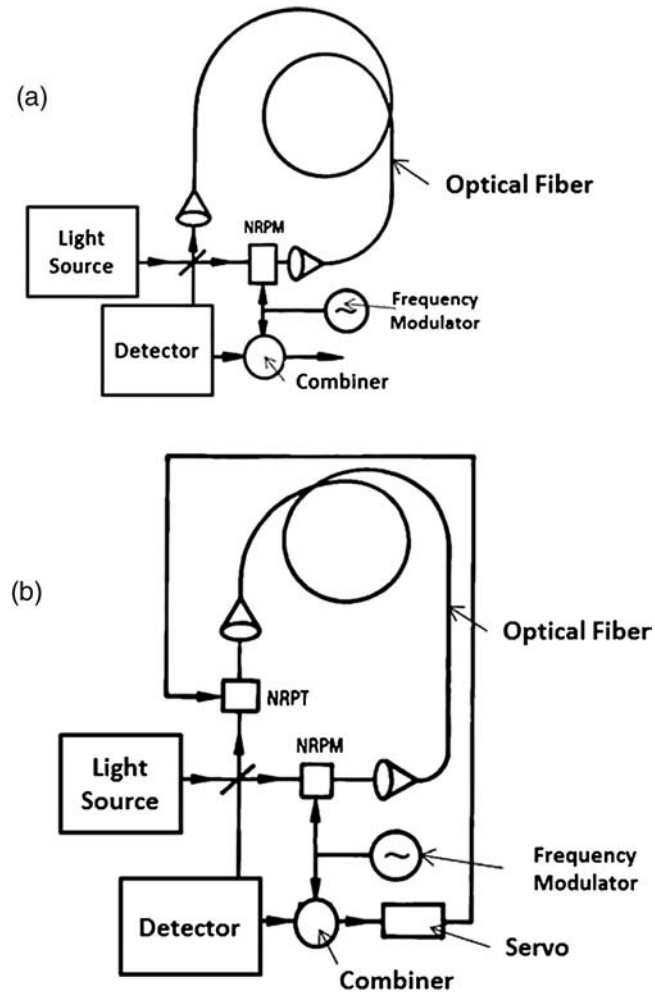

Figure 17.6 Fiber optic gyroscope configurations: (a) simplified open loop, and (b) simplified closed loop.[5] (NRPM: Non-reciprocal phase modulator, NRPT: Non-reciprocal phase transducer).

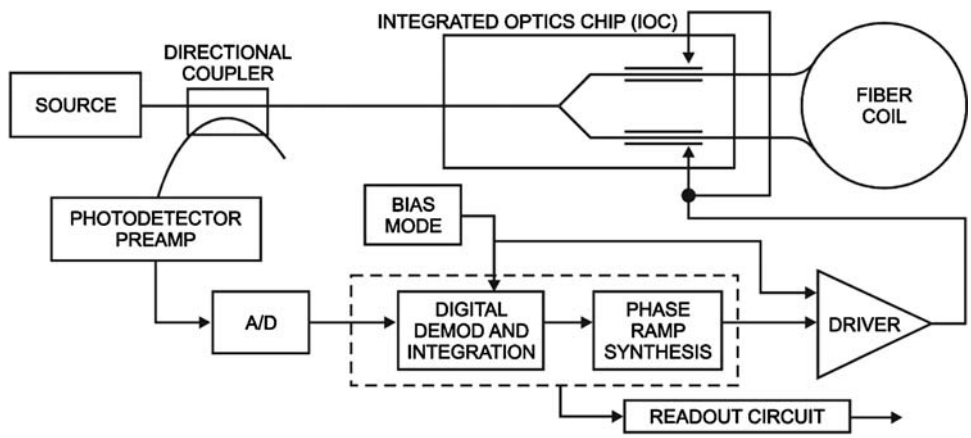

Figure 17.7 Schematic of a typical closed-loop navigation-grade gyroscope design.[11]

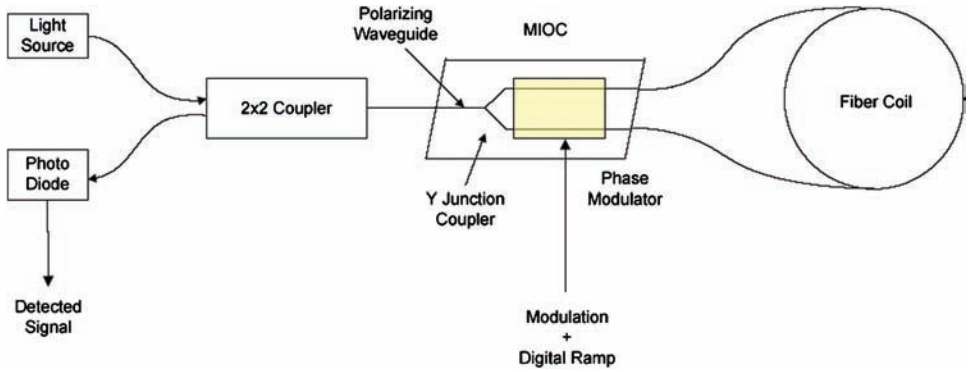

Figure 17.8 Schematic of a typical closed-loop fiber optic gyroscope used at Northrop Grumman.[12]

counterpropagating waves. This phase shift maintains the sensor at its zero-rotation condition. Designs for a depolarized, navigation-grade, fiber optic gyroscope have been reduced to practice.[11] The purpose for such designs is to reduce the cost of the sensor by replacing the polarizing-maintaining fiber with more conventional single-mode fiber. However, the necessity of using two depolarizers[12] and special coatings on the single-mode fibers mitigates some of the cost advantage.

Figure 17.8 is a schematic of the optical circuit of a typical Northrop Grumman fiber optic gyroscope.[12] It is a closed-loop design. The gyroscope optical circuit uses a multifunctional integrated optical chip (MIOC). The chip uses $LiNbO_3$ and proton exchange technology to generate the polarizing waveguides. The MIOC contains a polarizer, a Y-junction coupler, and an electro-optic phase modulator. The light source is a broadband light source that operates at different wavelengths depending on the specific application and gyroscope design. Typical wavelengths are in the 800-nm and the 1500-nm bands, where optical fibers and optical components are readily available. Gyroscopes can be designed to use a single light source per gyroscope axis or share a single light source between two or three axes. A semiconductor photodetector is used to convert the light exiting the gyroscope into an electrical signal so that it can provide the rotation measurement.

Figure 17.9 shows a commercial inertial measurement unit (IMU) manufactured by Northrop Grumman. The picture unit consists of three fiber optic gyroscopes, three micromachined silicon accelerometers, and a microprocessor. It senses rotation and acceleration about three orthogonal axes.[12,13] The dimensions are approximately 9 cm in diameter and 9 cm in height. The sensitivity is less than 0.1 deg/hr and the dynamic range is 1000 deg/sec.

Figure 17.9 Northrop Grumman commercial IMU with three fiber optic gyroscopes.[13]

17.3 Reciprocity

The concept of reciprocity is critical to the use of a Sagnac fiber optic interferometer.[7] The reciprocity concept simply states that the phase that is accumulated when light is injected in one end of the sensor exactly equals the phase accumulated when light is injected in the other end of the sensor. The two waves, which have propagated through the same optical path, have the same phase delay if nonreciprocal effects are absent. This approach also implies that there is some immunity to environmental perturbations.

Polarization effects can cause nonreciprocity.[7,14–17] Single-mode fibers have two degenerate polarization modes. All fibers have random birefringence normally associated with slight geometric variations generated in fabrication. Twisting and bending of the fiber provides additional birefringence. Since these effects are nonuniform along the fiber, the polarization that is affected by the birefringence varies with fiber length. Therefore, the two propagating waves will have a phase shift associated with polarization effects. These effects can cause errors that are significantly larger than the phase shift resulting from rotation. This problem can be eliminated if a polarizer is at the ends of the fiber. With the polarizing filter in place, birefringence effects in the fiber do not contribute to a phase shift. However, birefringence in combination with the polarizing-maintaining fiber can be used to minimize external birefringence and maintain high transmitted-light levels. To achieve the highest levels of sensitivity, high-quality polarizing filters and polarizing-maintaining fibers are required.

Time-varying temperature gradients across the fiber coil can also cause drift. Thermal gradients can create strain, which introduces nonreciprocal polarization effects. The gyroscope package design can potentially maximize temperature homogeneity across the loop and eliminate temperature gradient problems.

The Faraday effect is another nonreciprocal phenomenon.[3] Magnetic fields can cause rotation of the polarized light (Faraday rotation). This effect can cause a rotation-rate error in a fiber optic gyroscope; the error is a function of the direction and magnitude of the field. Therefore, for sensitive rotation-rate measurements, magnetic shielding is required.

Non-reciprocities can also be associated with the Kerr effect, which results in a change in refractive index of the fiber core as a function of light intensity. The refractive index change results in a rotation-rate error if the propagation constants of the two counter-rotating waves are not identical. It has been shown[7] that using a duty cycle of 50% will eliminate this effect.

17.4 Noise Limitations

In addition to the sources of noise associated with nonreciprocity, several other sources exist, as shown in Fig. 17.10. The fundamental limitation is

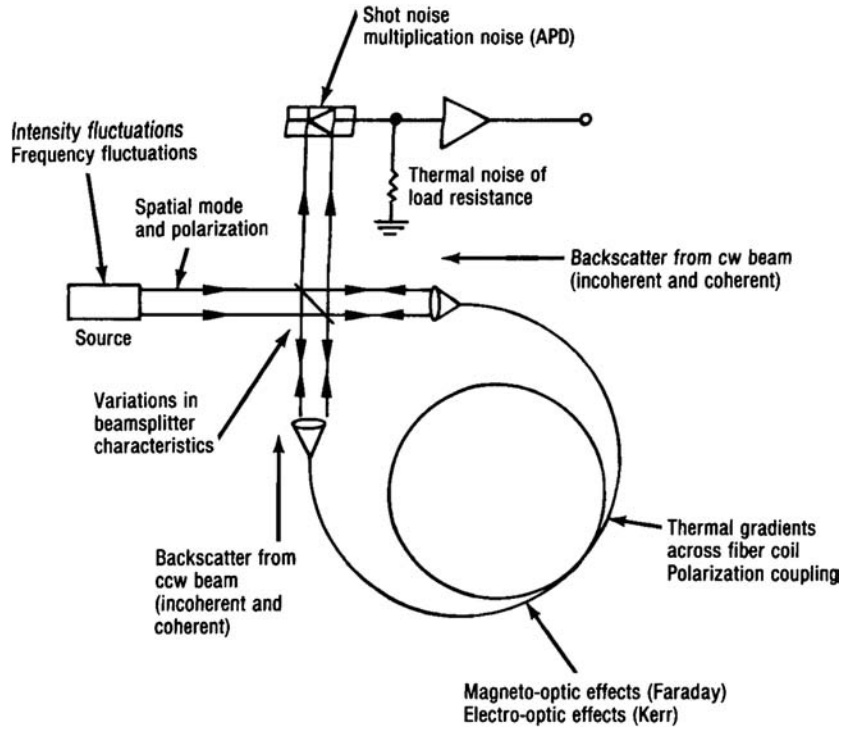

Figure 17.10 Noise sources in an optical fiber gyroscope.[7]

photon shot noise. Compensation for shot noise is not possible because it is a random process manifested in random fluctuations in the detector output. A typical gyroscope application with 500 m of fiber in the sensing coil would have a rotation rate threshold associated with shot noise of 0.01 deg/hr. Light-source-intensity fluctuations are another noise source. Errors associated with variations in the light source intensity, however, can be removed by various compensation schemes.

Rayleigh scattering and scattering from interfaces have the same basic effect.[17–19] The scattered light, if it is at least partially coherent with the transmitted light, can interfere and cause noise. Light sources with long coherence lengths, i.e., sources in which the light beam wavefront stays coherent for long distances, create a severe backscatter noise problem. Light sources that have shorter coherence lengths (more diffuse) reduce this noise problem.[20]

Fiber optic gyroscopes have distinct advantages over mechanical and other optic gyroscopes. Sensitivity ranges have been reported for 1 deg/hr to 0.01 deg/hr.[8,17,21] The ultimate sensitivity, based on realistic fiber properties, is calculated to be 3×10^{-4}deg/hr.[22]

For navigation-grade, fiber optic gyroscopes, the desired stability throughout flight should be better than 0.006 deg/hr.[7,11,24,25] The scale factor requirements are as little as 10 ppm over a rotation range of 1000 deg/s. The environmental conditions are problematic. The sensor is subjected to random vibration. Temperature gradients occur over a temperature range of -50 °C to $+70$ °C. The sensor may experience magnetic fields of 10 G. Actual sensors have achieved a 0.0081-deg/hr. stability over the defined environmental conditions.[25]

For a precision fiber optic gyroscope such as is required for a spacecraft and submarine, the accuracy requirement is better than 0.001 deg/hr.[26,27] The fiber optic gyroscope must offer very low angle random walk (ARW), very long life, and excellent reliability. A schematic representation of a precise gyroscope is shown in Fig. 17.11.[27] The primary causes of angle random walk

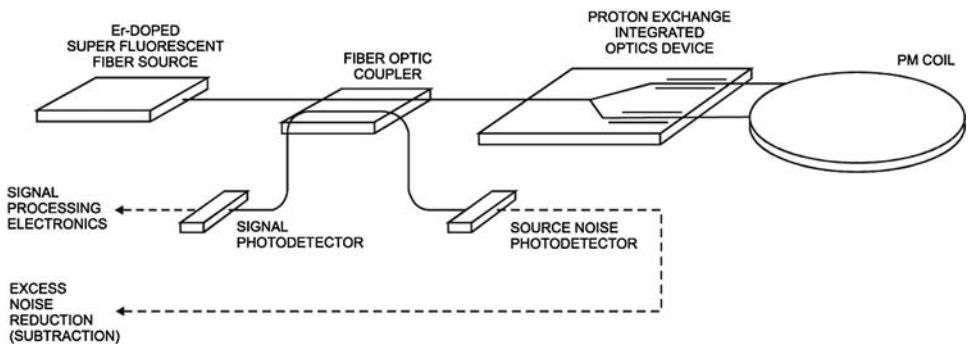

Figure 17.11 Typical precision fiber optic gyroscope design.[27]

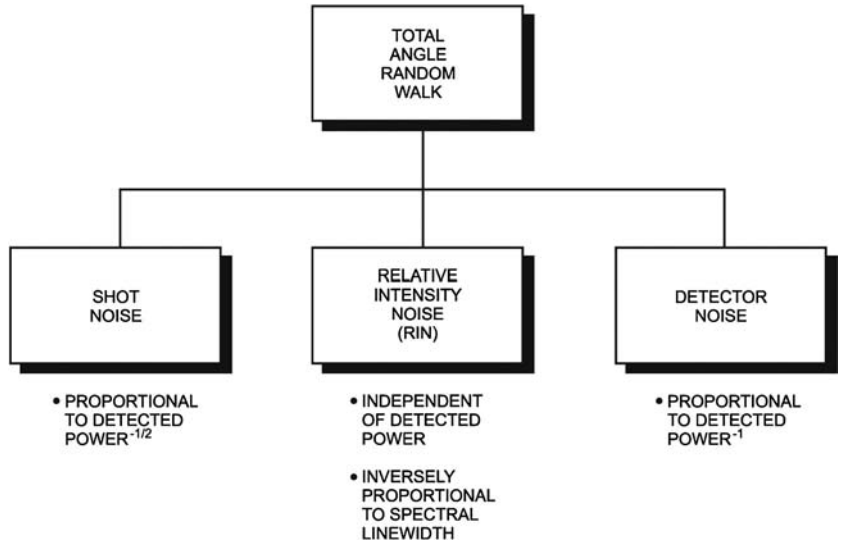

Figure 17.12 Leading angle-random-walk contributors.[27]

are shown in Fig. 17.12.[26] A superfluorescent, erbium-doped-fiber light source produces the 1.53- to 1.56-nm wavelength required for sensor function. This light source allows a broadband spectrum output to reduce relative intensity noise (RIN). Since it has sufficiently higher power, it can be derated to function at 50% power to maintain long lifetime.

17.5 Resonators

Sagnac rotation sensors can be classified as either interferometers or resonators.[27] Consider a resonator as shown in Fig. 17.13. Light is input into port 1 and coupled into ports 3 and 4; the light circulates around the loop through port 2 to port 3 until equilibrium is reached. The equilibrium corresponds to the light input at port 1, balancing the energy dissipation through the directional coupler and losses in the loop. The port 4 output will exhibit sharp minima whenever the continuously varied input light frequency

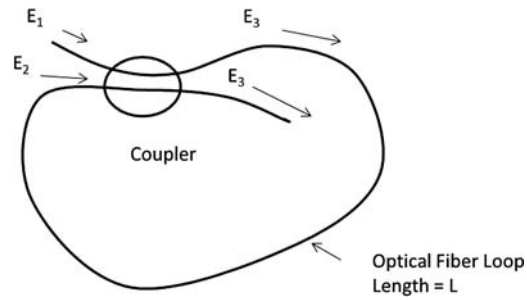

Figure 17.13 Schematic of an all-single-mode fiber resonator.[27]

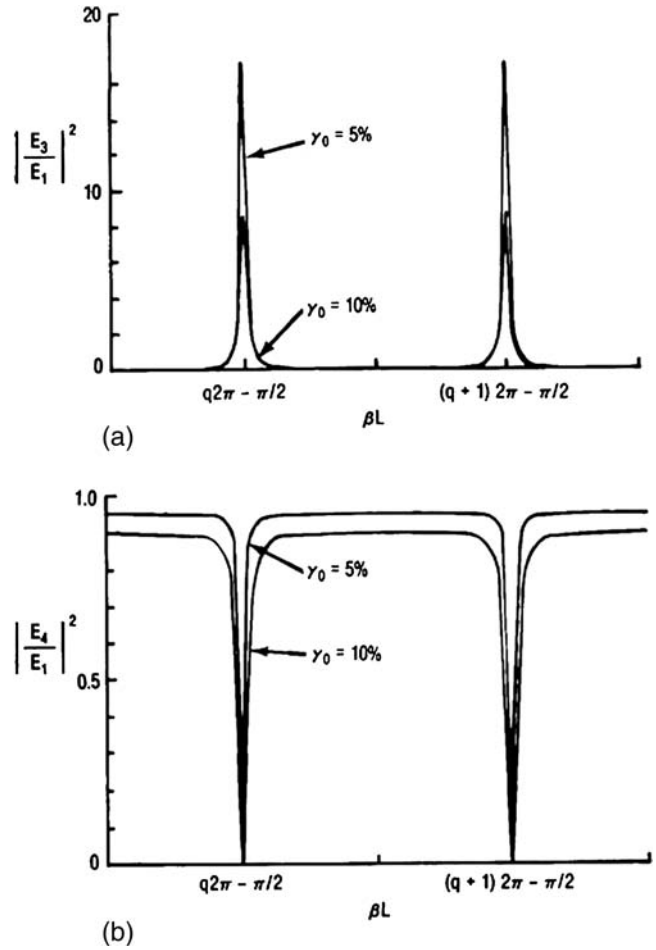

Figure 17.14 Resonator intensity. (a) Theoretical resonator circulating intensity. (b) Output intensity for a 5 and 10% coupler insertion power.

matches the resonance condition. The output intensity is shown in Fig. 17.14.[27] The output shown is the ratio of the field intensity E_4 at port 4 (output port) to the field intensity E_1 at port 1 (input port). The resonance occurs when

$$\beta L = \frac{nwL}{c} = q2\pi - \frac{\pi}{2}, \tag{17.14}$$

where
n = the refractive index of the fiber core,
β = a propagation constant,
w = the optical frequency,
c = the speed of light,
L = the fiber loop length, and
q = an integer.

The curves shown are for different, fractional-coupler, intensity-loss (λ_0) values. As the loss decreases, the resonance minima become sharper. The sharpness of the resonance is defined as the ratio of the peak spacing (2_π) to the width of the half-peak height of a given resonance curve. The term is called finesse F and is given by[28]

$$F = \frac{2\pi}{\Gamma}. \tag{17.15}$$

As the finesse increases, so does the sensitivity of the fiber resonator gyroscope. A fiber resonator gyroscope is shown in Fig. 17.15.[29] The output laser beam is split into two beams, both of frequency f_0. Frequency shifts in the two beam paths shift the two beams to $f_0 + f_1$ and $f_0 + f_2$, respectively. The two frequency-shifted beams are coupled into counter-rotating paths in the fiber resonator. A second coupler is used to channel the two beams to their respective photodetectors. The feedback loops lock the frequency to the resonance condition and provide the maximum output. The resonant frequency spectrum Δf which is associated with rotation, is given by

$$\Delta f = \frac{4A\omega}{\lambda L}. \tag{17.16}$$

In the resonance gyroscope, Δf is independent of the number of turns in the fiber coil. Figure 17.l6 shows the output-intensity-versus-frequency curves. [9] The shifts in resonance peak to frequency Δf are clearly defined.

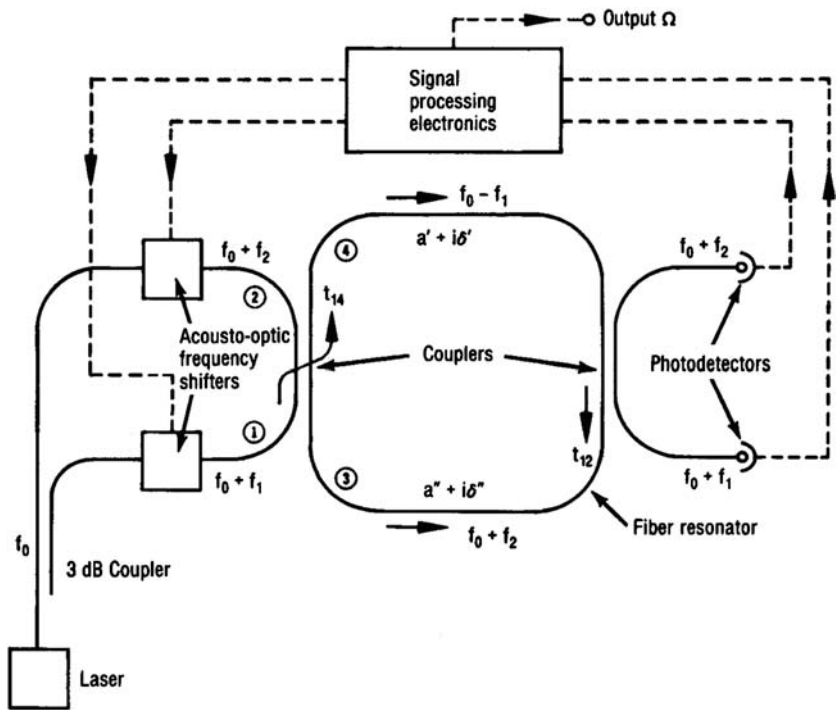

Figure 17.15 Diagram of the fiber resonator gyroscope.[29]

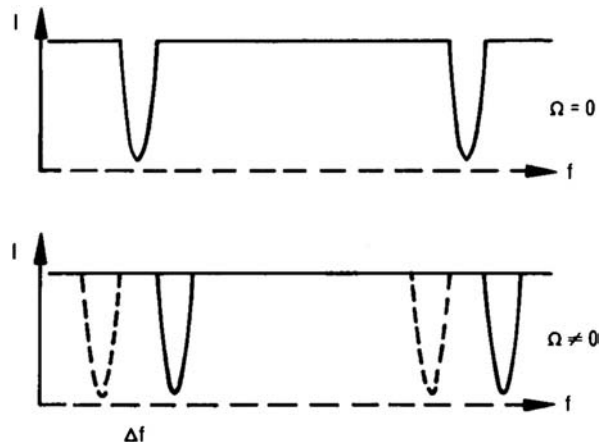

Figure 17.16 Intensity-versus-frequency curve for a fiber resonator.[9]

17.6 Comparison of Resonator (RFOG) and Interferometer (IFOG) Gyroscopes

It has been shown that the calculated sensitivities of the two fiberoptic gyroscope (FOG) approaches are similar, based on shot-noise limitations.[30–32] The fiber resonator has some distinct advantages. The high sensitivity can be achieved with a much shorter optical fiber than for the interferometer. Thermally induced nonreciprocity is reduced by as much as a factor of ten. Since the coil fiber is one of the major contributors to gyroscope cost, reduction in fiber length will have a significant cost impact.

Nonlinear optical effects are a major source of errors for the resonator when compared to the fiber interferometer.[9] To avoid such errors, the input power must be severely limited. The RFOG must use a light source with narrow line width and high spectral density. The IFOG can use a lower-cost light source in which coherence specifications can be relaxed. The high power level in the RFOG will have a sensitivity limitation as a result of the Kerr effect. To avoid this occurrence, the finesse must be reduced, which also degrades performance.

Another nonlinear optical effect is stimulated Brillouin scattering. The high-coherence light source required for the resonator function can result in this stimulation process, in which the gyroscope can become a laser with significant noise increase. The IFOG has much lower sensitivity to nonlinear optical effects since the spectral density of suitable light sources is orders of magnitude lower than required for the RFOG.

References

1. B. Kim and H. Shaw, "Fiber-optic gyroscopes," *IEEE Spectrum*, 54–60 (1986).

2. C. M. Davis et al., *Fiber Optic Sensor Technology Handbook*, Dynamic Systems, Reston, VA (1982).
3. V. Vukmirica, "Interferometric fiber optic gyroscope: principle of operation and basic parameters determination," *Scientific Technical Review* **3**, 83–90 (2008).
4. J. Kreidl, "Northrop's new RLG to rival the FOG," *Lightwave*, 58 (1987).
5. S. Ezekiel and H. J. Arditty, *Fiber-Optic Rotation Sensors and Related Technologies*, Springer-Verlag, Berlin, pp. 2–26 (1982).
6. J. Hecht, "Fiber optics turns to sensing," *High Technology*, 49–56 (1982).
7. R. A. Bergh, H. C. Lefevre, and H. J. Shaw, "An overview of fiber-optic gyroscopes," *J. Lightwave Technol.* **2**(2), 91 (1984).
8. E. Udd, "Fiber optic vs. ring laser gyros: an assessment of the technology," *Laser Focus/Electro-optics* **21**(12), 64–74 (1985).
9. N. J. Frigo, "A comparison of interferometric and resonant ring fiber optic gyroscopes," *Proc. SPIE* **0985**, 270 (1988) [doi: 10.1117/12.948868].
10. H. C. Lefeure, S. Vatocie, M. Papucheon, and C. Puech, "Integrated optics: a practical solution for the fiber optic gyroscope," *Proc. SPIE* **0719**, 101 (1987) [doi: 10.1117/12.937545].
11. G. A. Sanders, B. Szafraniec, L. Strandjord, R. Bergh, A. Kaliszek, R. Dankwort, L. Lange, and D. Kimmel, "Progress in high performance fiber optic gyroscopes," 12th International Congress on Fiber Optic Sensors, *OSA Technical Digest Series* **16**, pp. 116–121 (1997).
12. G. A. Pavlath, "Fiber-optic gyros: the vision realized," www.ngc.com (2004).
13. Anonymous, "LN-200 FOG Family," www.ngc.com, 2013.
14. J. Blake, "Magnetic field sensitivity of repolarized fiber optic gyros," *Proc. SPIE* **1367**, 81–86 (1990) [doi: 10.1117/12.24731].
15. W. Burns, R. Moeller, C. Villarruel, and M. Abebe, "Fiber-optic gyroscope with polarization-holding fiber," *Optics Letters* **8**(10), 540–542 (1983).
16. G. A. Pavlath and H. J. Shaw, "Birefringence and polarization effects in fiber optic gyroscopes," *Applied Optics* **21**(10), 1752–1757 (1989).
17. T. G. Giallorenzi, J. Bucaro, A. Dandridge, G. H. Sigel, J. Cole, S. Rashleigh, and R. Prest, "Optical fiber sensor technology," *IEEE Journal of Quantum Electronics* **QE-18**(4), 626–664 (1982).
18. I. Giles, J. McMillan, J. Mackintosh, and B. Culshaw, "Coherence in optical fiber gyroscopes," *Proc. SPIE* **586**, 180–186 (1985) [doi: 10.1117/12.951158].
19. K. Bohn, P. Marten, K. Petermann, and E. Weidel, "Low drift fiber gyro using superluminescent diode," *Electronics Letters* **17**(10), 352–353 (1981).

20. W. Burns, C. Chen, and R. Moeller, "Fiber-optic gyroscopes with broad band sources," *J. Lightwave Technol.* **LT-1**(1), 78–104 (1983).
21. E. Dianov et al., "Rotation sensors based on single-mode fibers with low and high birefringence," *Third International Conference in Optical Fiber Sensors Technical Digest*, 120 (1985).
22. L. Jeunhomme, *Single-Mode Fiber Optics*, Marcel Dekker, New York, pp. 251–269 (1983).
23. H. Kajioka, T. Kumagui, H. Nakai, T. Dohsho, H. Soekawa, and T. Yuhare, "Commercial applications of mass produced fiber optic gyros," *Proc. SPIE* **2837**, 18–23 (1996) [doi: 10.1117/12.258177].
24. K. Sukuma, "Application of fiber optic gyros at JAE," *Proc. SPIE* **2837**, 72–79 (1996) [doi: 10.1117/12.258209].
25. A. Cordova, R. Patterson, J. Rahu, L. Lam, and D. Roselle, "Progress in navigation grade IFOG performance," *Proc. SPIE* **2837**, 61–71 (1996) [doi: 10.1117/12.258181].
26. K. Killian, M. Bermenko, and W. Hollinger, "High performance fiber optic gyroscopes with noise reduction," *Proc. SPIE* **2292**, 255–263 (1994) [doi: 10.1117/12.191838].
27. L. F. Stokes, M. Chodones, and H. S. Shaw, "All single-mode fibers resonator" *Optics Letters* **7**(6), 288–270 (1982).
28. Y. Uhtsuka, "Analysis of a fiber-optic passive loop resonator gyroscope," *J. Lightwave Technol.* **LT-3**(2), 378–384 (1985).
29. D. M. Shupe, "Fiber resonator gyroscope: sensitivity and thermal nonreciprocity," *Applied Optics* **20**(2), 286–289 (1981).
30. R. Carroll, D. Coccoli, D. Cardarelli, and G. T. Coate, "The passive resonator fiber optic gyro and comparison to interferometric fiber gyro," *Proc. SPIE* **0719**, 169–177 (1985) [doi: 10.1117/12.937554].
31. O. Laznicka, L. Freier, J. Gilmore, and M. Fontanella, "Interferometric fiber optic gyro (IFOG) technology achievement at draper laboratory," *Proc. SPIE* **2292**, 177–191 (1994) [doi: 10.1117/12.191832].

Chapter 18
Distributed Sensing Systems

18.1 Introduction

The concept of distributed sensors was first introduced in the 1980s with the development of the optical time-domain reflectometer (OTDR) and its application to the sensor field. OTDR refers to the use of a single optical fiber as a linear continuous sensor, providing multiple measurement points distributed spatially in a continuous sequence over the entire fiber length as depicted in Fig. 18.1. A single optical fiber cable can, *de facto*, replace thousands of traditional single-point sensors such as thermocouples or strain gauges, saving complex installation, calibration, and maintenance costs. As a result, temperature and/or strain information is made available through profiles as a function of distance in one shot, providing simultaneous temperature/strain information of thousands of locations with a single instrument. More recently the measurement of acoustic and vibrational signals has also been performed with these distributed architectures.

The geometry of optical fibers makes them ideal candidates for long-range distributed sensors. Furthermore, the wide range of commercially available fiber cable embodiment offers suitable solutions for various monitoring applications, even in the case of extreme environmental conditions (robust design for rough conditions, resistant to corrosion, compatible with temperature range from 0 K to 970 K, intrinsically safe in hazardous environments, etc.). Standard fiber optic cables offer decades of guaranteed lifetime even in demanding environments such as for subsea applications.

Distributed sensing techniques are based on the recording and the analysis of the scattered light at every location along the fiber. Light scattering is associated with inhomogeneities in the propagation medium. Different types of inhomogeneities give rise to different scattering phenomena, ranging from density fluctuation generating Rayleigh scattering (both coherent and incoherent) to thermally excited acoustic waves (or phonons) and molecular vibrations causing Brillouin and Raman scattering.[1–10] The details of the scattering processes discussed here have been fully covered in Chapter 6.

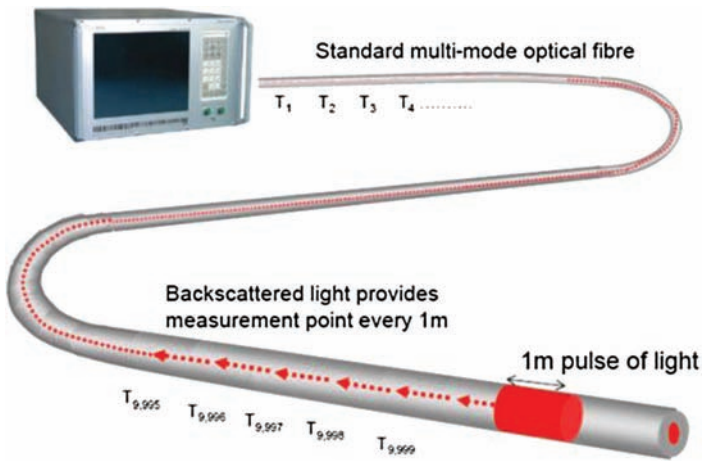

Figure 18.1 A distributed fiber optic sensor is capable of performing a multitude of spatial measurements along the entire length.

18.2 Applications

The main applications for fiber optic distributed sensors have been as follows: temperature (using mostly Raman mixed with a small percentage of Brillouin), strain, vibration, and acoustic. The industrial focus of these systems has included fire protection, power cable monitoring, pipeline monitoring, security, and leak detection. By far, Raman-based temperature sensing has seen the majority of commercial installations with most of these being installed in oil and gas applications. Next in line would be Brillouin technology, primarily for strain pipeline and structural monitoring. More recently, technical advances in distributed acoustic sensing (DAS) technology have created a considerable amount of commercial excitement and activity. The dividing line between vibration sensing and acoustic sensing is those applications requiring actual movement of the sensing fiber (vibration) versus those solely responding to an acoustic pressure (DAS). The DAS technology has found success in perimeter security and oil, gas, and railway monitoring.

Over the last few years, optical fiber sensors have received widespread acceptance within the oil industry due to their reliability, flexibility, and low operating cost, as well as the benefits brought by their multipoint and distributed sensing capabilities. Initial applications have focused on downhole oil well temperature and pressure sensing, while newer ones are geared toward multiparameter sensing as well as distributed temperature, strain, and pressure sensing in both downhole and subsea environments.

In general, the most common applications for fiber sensors in the production segment of the oil industry will be in downhole pressure and temperature measurements. Typically, the measurements will be performed at the bottom of the well using permanently installed gauges. However, with the

advent of multizone wells, horizontal wells, and intelligent completions, it will also become necessary to perform distributed and multipoint pressure and temperature readings. Below is a simplified list of the most common and appropriate applications of distributed, multipoint fiber optic sensors within the oil and gas industry:

- Well bore temperature profiling (reservoir and permeability profiles, multizone detection),
- Water injection (injection dynamics, permeability variations, zonal identification),
- Artificial lift optimization (water/steam/gas monitoring),
- Steam flooding management (thermal recovery analysis, detection and tracking of steam flow),
- Water/gas breakthrough detection and localization, and
- Flowline monitoring (wax or hydrate blockage detection, thermal profiling, modeling validation),
- Pipeline monitoring (intrusion detection, leak monitoring),
- Reservoir subsidence and compaction monitoring,
- Casing deformation monitoring,
- Riser stress and lifetime monitoring (hot-spot detection, axial and hoop strains),
- Acoustic sensing and hydrophones, and
- 3D and 4D seismic sensing.

One of the key attractive features of optical fiber sensors is the fact that they can serve the function of a transducer as well as that of a signal transmission medium. In the case of optically-based downhole instrumentation, optical fiber cables will be used as leads to carry optical power into the sensor and data signals from it. Typically, the optical light source and processing electronics will be located at the control house on the platform. The distance between the system electronics and the sensor itself can be several kilometers.

18.3 Distributed Temperature Sensing Applications in the Oil and Gas Industry

Fiber optic sensors can be considered a new tool for reservoir engineers and a future key enabling technology for the acquisition of real-time data on a variety of well parameters such as temperature, strain, pressure, sand detection, and acoustic signals, facilitating the optimization of a reservoir's production capabilities through its entire life cycle.

To date, relatively few system developers, integrators, services companies, and oil companies are interested and engaged in the research, development, utilization, and installation of fiber-optic-based sensing systems for diverse oil and gas applications. It is expected that the number of players, activity, and

Table 18.1 List of common DTS measuring applications within the oil and gas industry

Oil Wells	**Gas Wells**
Production monitoring	Production entry monitoring
Zonal production contributions over time	Inflow location
Comingling monitoring	Produced gas rates
Water and gas cap breakthrough detection	Detection of water breakthrough
Acid or fracture treatments	Tubing/casing leak detection
Tubing/casing leak detection	De watering management
Compaction and subsidence monitoring	
Casing compaction and deformation	**Thermal Recovery Modelling**
Cement monitoring	SAGD
	Thermal monitoring of producer, injectors and
Artificial Lift Monitoring	observation wells
ESP monitoring	Monitoring of steam cavity
Steam, gas, water injection	Monitoring and diagnosis of steam injection process
Zonal injection distribution	Detect steam/water breakthroughs
Fluid levels	Pattern steamflood
Gas lift location and operation evaluation	Zonal distribution
	Steam fromt distribution and dynamics
Flow Assurance	Thermal monitoring of producer, injectors,
Detection and localization of blockages	and observation wells
Heating monitoring	
Thermal insulation monitoring	
Leak detection	
Intrusion detection	

overall diffusion of the technology will increase as these sensors continue to be proven effective and reliable, and their operational and cost benefits are weighted against unmonitored reservoirs and the use of conventional sensors.

Within the oil and gas industry, distributed temperature sensing (DTS) measurements will be of use in both upstream and downstream applications. In upstream cases, potential applications include: monitoring electrical submersible pumps (ESPs); detecting cold or hot spots along oil/gas pipelines, flowlines, and umbilical risers for flow assurance applications; optimizing artificial lift operations; oil/gas well bore temperature profiling; thermal profiling in steam-assisted gravity drainage (SAGD) management; and many others. Downstream, there are ample opportunities to exploit the capabilities of a DTS system in process monitoring and control by measuring temperatures in vessels, reactors, crackers, furnaces, pipelines, and other components. Table 18.1 shows several physical parameters that distributed temperature measurements can indirectly detect in oil and gas industry applications.

As shown in Fig. 18.2, an optical fiber cable can be strapped along the entire length of a vertical or horizontal well's production tubing. DTS measurements can be performed remotely, from the topside, using a permanent DTS electronics unit or by connecting to the preinstalled cable at periodic intervals. Taking DTS readings this way produces a real-time

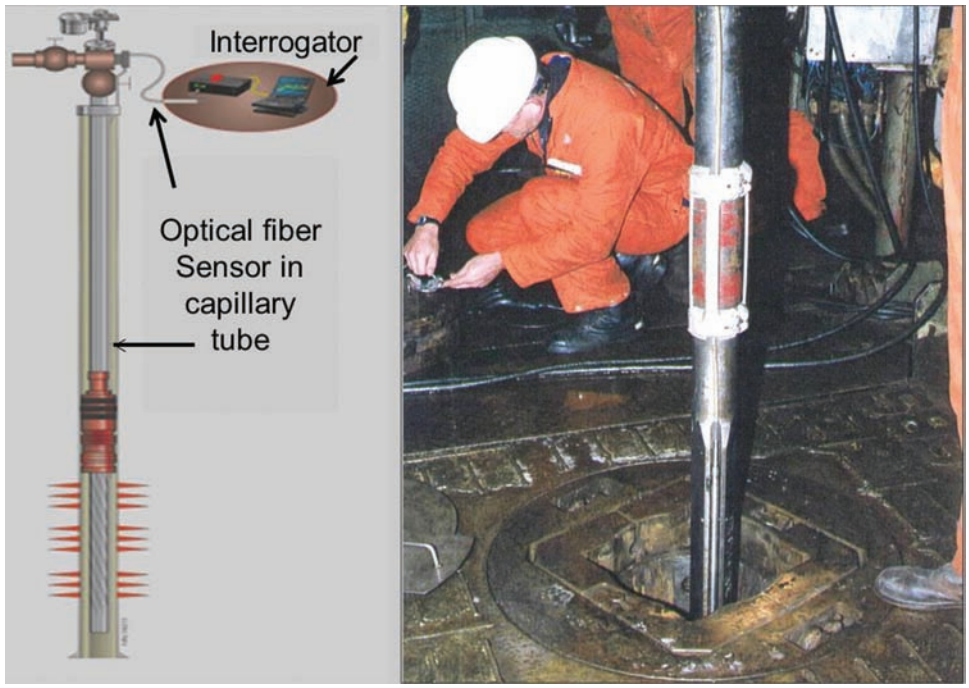

Figure 18.2 Aspect of a fiber optic cable installed along a production tubing to perform DTS measurements along its length (Source: Shell).

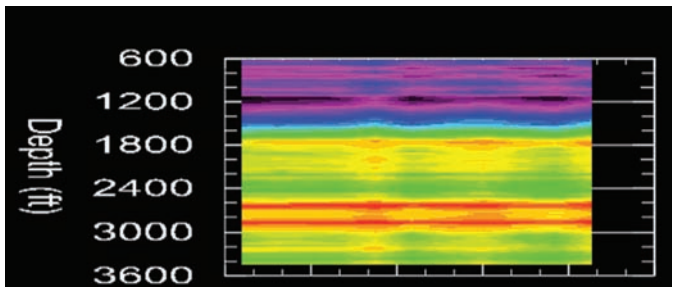

Figure 18.3 2D temperature plot based on accumulated, time-lapse DTS data on a well reservoir. The temperature profile evolution can be observed over time (horizontal axis) along the well's depth (vertical axis). Color represents temperature (Source: Petrospec/ QOREX Engineering).

thermal profile along the entire length of the well, thus enabling optimal inflow conformance by the online detection of any specific downhole thermal event. Figure 18.3 shows a plot of temperature in the well. DTS can identify and monitor, among many others, the following effects:

- Flow profiling,
- Zonal identification,
- Injection profiling and monitoring,
- Casing/tubing leak detection,
- Water/steam breakthrough detection, and
- Fluid levels.

One of the growing enhanced-recovery approaches is steam-assisted gravity drainage known simply as SAGD. The process involves the injection of steam through injector wells; the steam permeates oil sands, increasing their temperature. This in effect lowers the oil viscosity and allows the oil to flow more effectively into slotted production liner tube completions. As the steam builds up, a pressure increase helps sustain pressure levels in the reservoir, as pressure is lost from the produced oil. This method is particularly attractive in geophysical regions with high oil viscosities or cold temperatures, such as Canada and Venezuela. SAGD installations are also characterized by localized high temperatures >300 °C resulting from the injected steam.

Sensing fiber elements can be deployed along both the producing and the steam injector tubings in single or dual SAGD installations to obtain temperature profile readings (see Fig. 18.4). Fibers can also be deployed in observation wells if needed. As with conventional steam flooding, knowledge of temperature data over time would facilitate a more effective online management of steam injection in SAGD operations and determination of heat dynamics and breakthrough events, as illustrated in Fig. 18.5, which is a 3D plot of the temperature DTS measurements taken in a SAGD reservoir over a period of time. The DTS benefits and power of temperature data

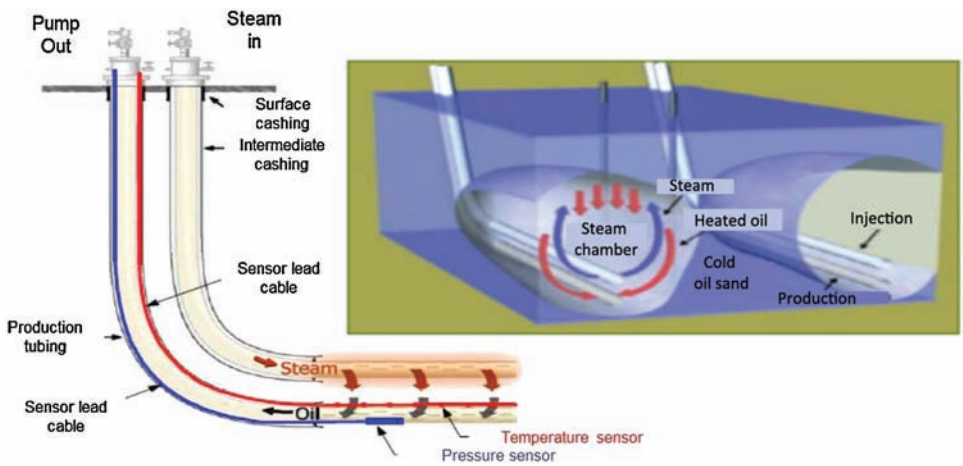

Figure 18.4 Aspect of a SAGD well and use of installed fibers and DTS for thermal monitoring (Source: Sabeus).

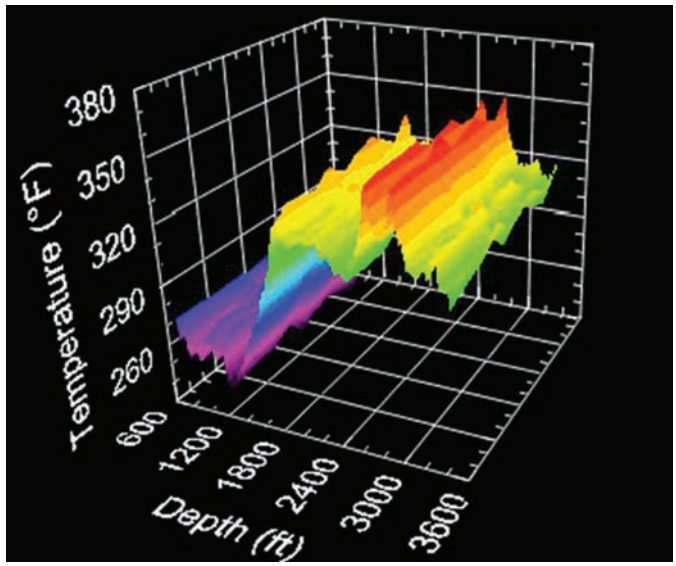

Figure 18.5 3D plot of DTS measurements over a three-month period showing the dynamics of the thermal chamber in a SAGD reservoir (Source: Petrospec/QOREX Engineering).

visualization can immediately be realized with this graph. For instance, temperature measurements provided by a DTS system can help monitor:

- Steam temperature and injection dynamics,
- Temperature and growth of the steam chamber,
- Steam cone boundaries, and
- Potential blockage of the slotted liners in injector and producer tubes.

Given their physical lengths, long offsets, and the impossibility of deploying logging tools into them, horizontal wells are ideal candidates for the installation and use of fiber sensing systems. With the advent of liquid injection techniques, there is no impediment to the deployment of long lengths of fiber inside capillary metallic tubes along any vertical, lateral, inclined, or truly horizontal well bore.

Besides obtaining temperature profiles along the length of the well bore itself, it would also be possible to obtain geothermal profiles of the surroundings, as well as the evolution of the profiles over time. Measured temperature gradients can be compared soon after drilling to those during actual oil production. This can help diagnose well-production problems as well as optimize stimulation and cleanup operations. Application of mapping techniques to multipoint temperature profiles from across different zones can help identify bypassed oil regions.

From an operational standpoint, real-time temperature data would allow for more effective reservoir control and detection of the onset of gas or water breakthroughs by localization of regions with unusual hot or cold spots. Any

entry point of steam, gas, or water would induce localized cooling as a result of the Joule–Thompson thermodynamic effect, and thus could be easily detected and their position located by continuous monitoring of temperature profiles over time.

Deployed optical fibers allow the possibility to obtain temperature profiles along well bores and zones of interest, as well as the capability to detect actual injection, entry, and breakthrough points. This information will be of aid in the monitoring and operation of artificial lift systems such as rod pump, ESP, steam, gas, and others. Typically, the detection of these events will be made possible by the localized cooling or heating produced by the lift fluid flowing under pressure. In the case of gas lift installations, it would be possible to monitor the operation of gas valves, alerting operators of potential leaks, blockages, or well pluggings.

As part of the overall process of oil extraction and processing, it becomes necessary to transport the liquid hydrocarbons from their reservoirs—whether inland or subsea—to remote plants for chemical processing. This transport process is usually conducted using flow and pipelines that can be anywhere from several hundred meters to various kilometers in length. However, the transport of liquid hydrocarbons is faced with some serious problems such as: the buildup of wax and scale in the pipe walls; internal pipe erosion and corrosion; formation of hydrates and asphaltenes; and several others.

A practical monitoring technique for the detection and localization of wax and hydrate buildup and blockages in oil pipelines consists of the installation of a fiber along a pipeline to perform DTS measurements. As wax layers build up on the internal walls, the heat-transfer characteristics change over time producing an irregularity along the pipeline's longitudinal temperature profile, as shown in Fig. 18.6. Hence, an incipient blockage can be detected and its position along the pipeline determined by comparing periodic distributed-temperature readings against an original baseline temperature profile. The same technique can be used to detect and locate leaks in pipelines.

As DTS installations grow and the technology proves its value, the performance demand will also increase. Common error sources such as hydrogen ingress into cables, and limited range and resolution continue to be addressed and improved on. Techniques using new coding technologies, as shown in Fig. 18.7, as well as new cable designs and installation processes, have proven to accelerate the technology's acceptance.

18.4 Brillouin Sensors

Distributed fiber optic sensors based on Brillouin scattering, although sensitive to temperature, have found more widespread application as distributed strain sensors.[11 18] Being a frequency-encoded process allows these systems to work over a much longer range than Raman-based intensity devices. Typical operating ranges of >50 km have been reported. Figure 18.8 shows the basic operating principle of Brillouin sensing.

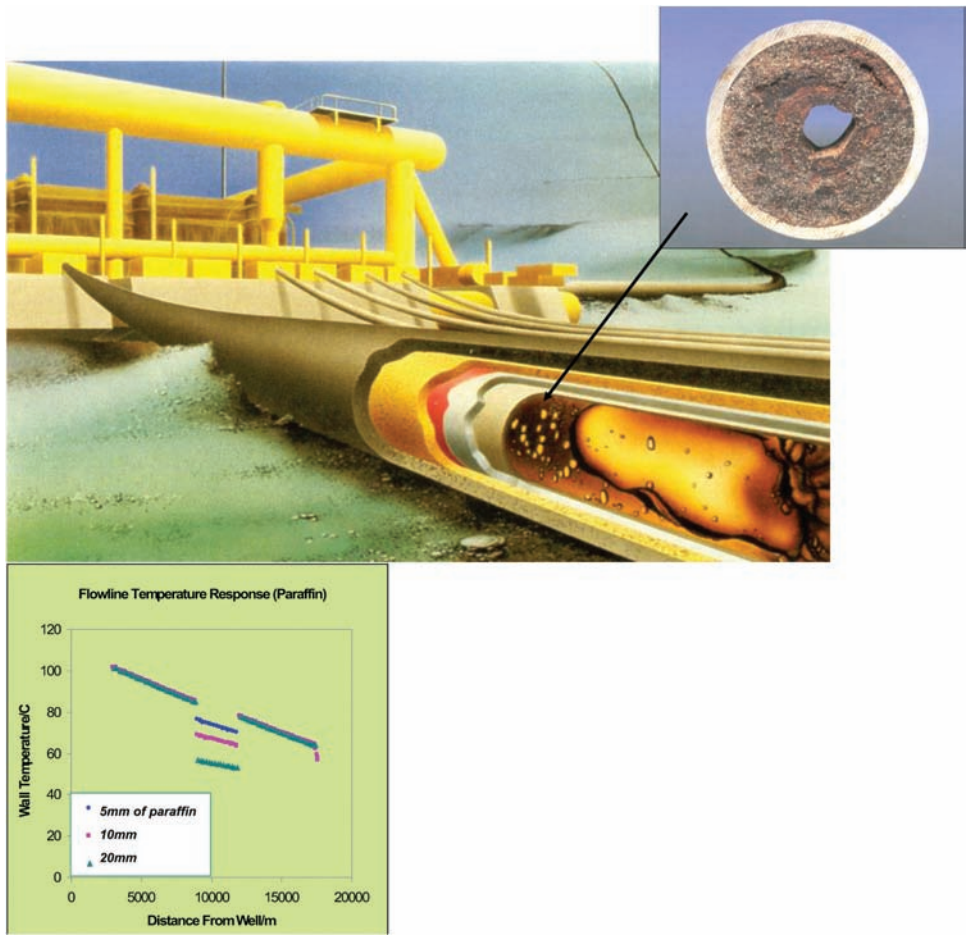

Figure 18.6 Blockages in a pipeline (from either wax or hydrates) can be monitored for and located by performing continuous DTS measurements.

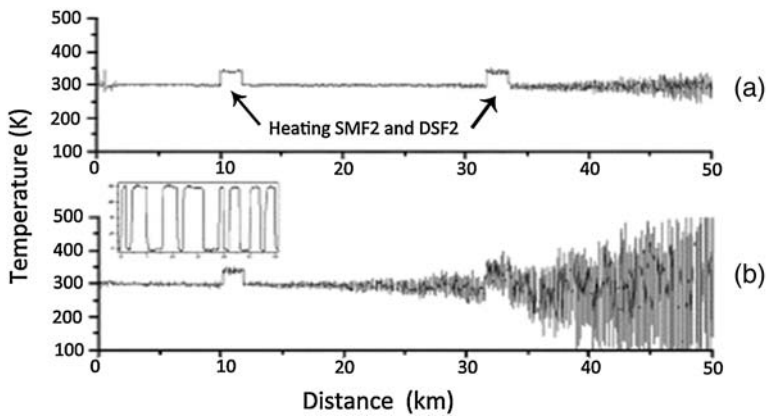

Figure 18.7 Effect of advanced coding techniques on signal integrity.[4]

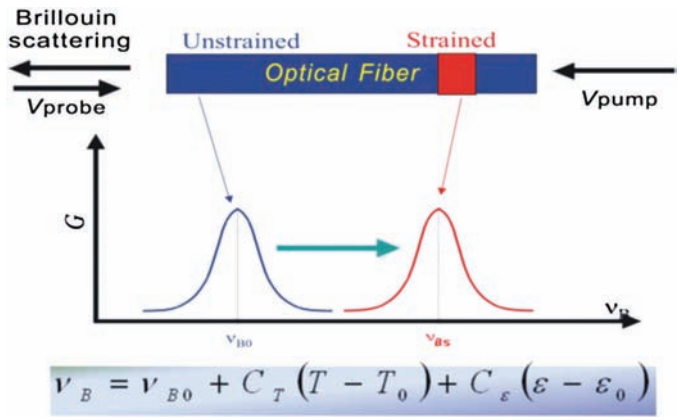

Figure 18.8 Brillouin principle of operation (courtesy of OZ Optics[19]).

Two main architectures have been used for deployment of these sensors. One uses a single fiber that monitors the backscattered Brillouin signal with an OTDR setup and determines frequency shifts corresponding to strain and temperature along the length of the cable. The second uses an optical loop design that employs a pump/probe method to determine the frequency peak of the stimulated interaction. This is generally known as the Brillouin optical time-domain analysis (BOTDA) method. The BOTDA systems, since they are in effect mixing power from both a pump and probe to generate a strong response signal, can operate for very long distances. The drawback of the BOTDA is that it requires a closed optical loop, which can be problematic for some applications.

The main applications for distributed Brillouin sensors have been pipeline, bridge, and structural monitoring, as well as transmission line monitoring. Figures 18.9 and 18.10 show the recommended placement of distributed

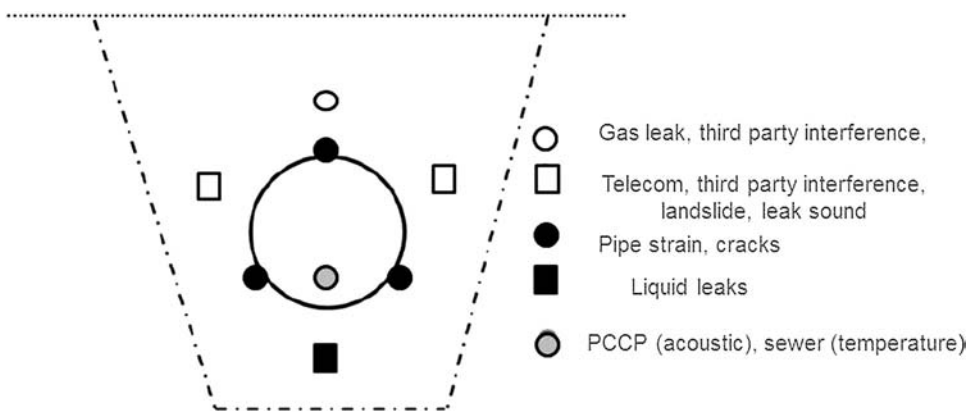

Figure 18.9 Pipeline sensor placement (PCCP is prestressed concrete cylinder pipe).[21]

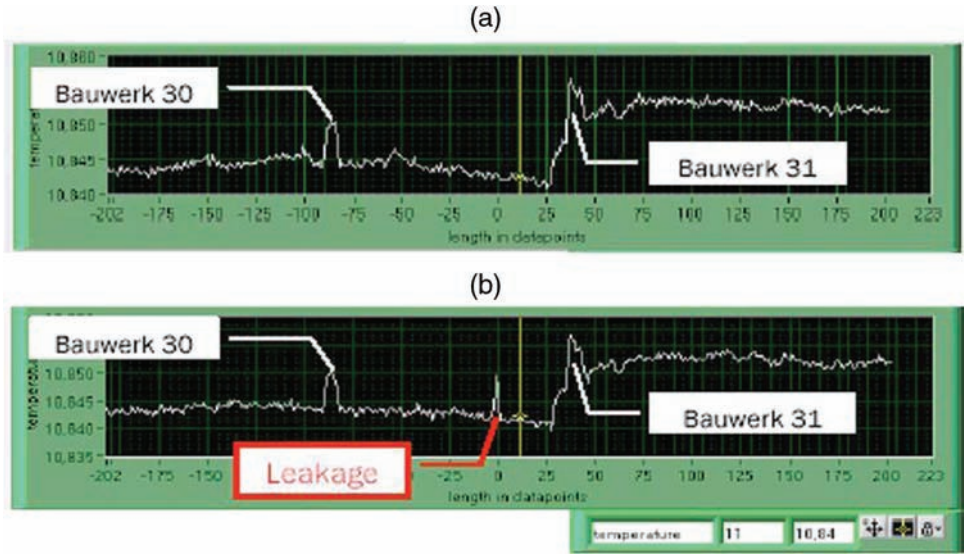

Figure 18.10 Pipeline leak detection. (a) Temperature profile before leak and (b) temperature profile when leakage is detected (image courtesy of Omnisens).[22]

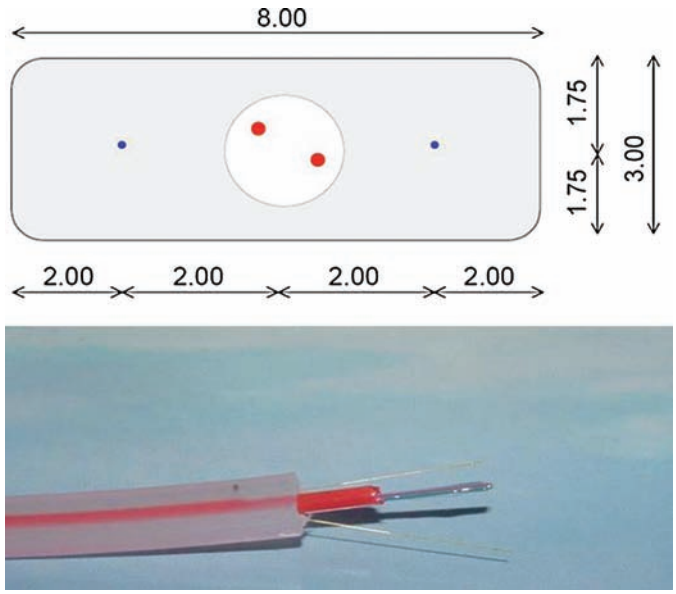

Figure 18.11 Fiber optic sensing tape.[22]

sensors to correctly monitor the length of an operating pipeline and the detection of a possible leak.

For attachment to these structures, a tape has been developed that contains the sensing fiber and a mechanically stable transducing layer for adherence. This is shown in Fig. 18.11. Figure 18.12 shows an application for monitoring strain in power cables.

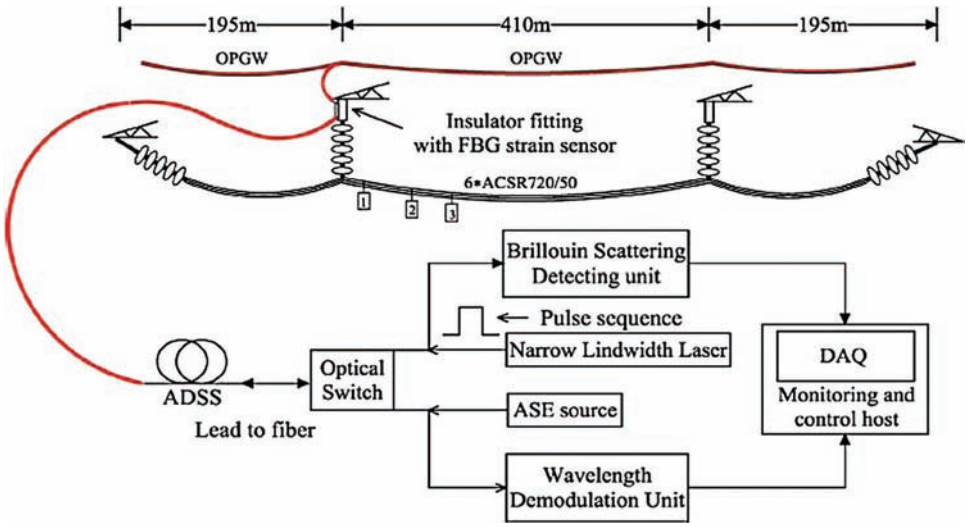

Figure 18.12 Strain monitoring of power cables (OPGW is optical ground wire, ADSS is all-dielectric self-supporting, ASE is amplified spontaneous emission, and DAQ is data acquisition).[20]

As previously mentioned, structural health monitoring has become a major application for the Brillouin-based distributed sensors. Figure 18.13 shows the response of a concrete column being stressed in various directions.

In addition to the applications covered here, new opportunities for monitoring the structural health and performance of large structures are constantly surfacing. Applications for wind turbines, ground movement, and ship hull monitoring are just a few that have recently received attention. As the technology develops and the value is demonstrated, other applications will certainly benefit from using these systems.

18.5 Distributed Acoustic Sensors

Fiber optic DAS systems have seen a dramatically increased level of attention over the last several years. The ability of these systems to detect incredibly small acoustic disturbances has made them very attractive for use as intrusion detectors as well as for monitors of several oil and gas processes.

Security applications have included perimeter and pipeline monitoring. In the oil and gas industry, these sensors have been used to monitor fracking processes, search for leaks in existing completions, and determine distributed flow.

As mentioned earlier, the operating principle relies on the coherent interference of the Rayleigh-scattered signals. With spatial resolutions approaching the meter level, this is equivalent to interrogating nearly 1000 interferometers for a 1-km cable. Recalling previous discussions on interferometers, the challenges required to perform this amount of signal

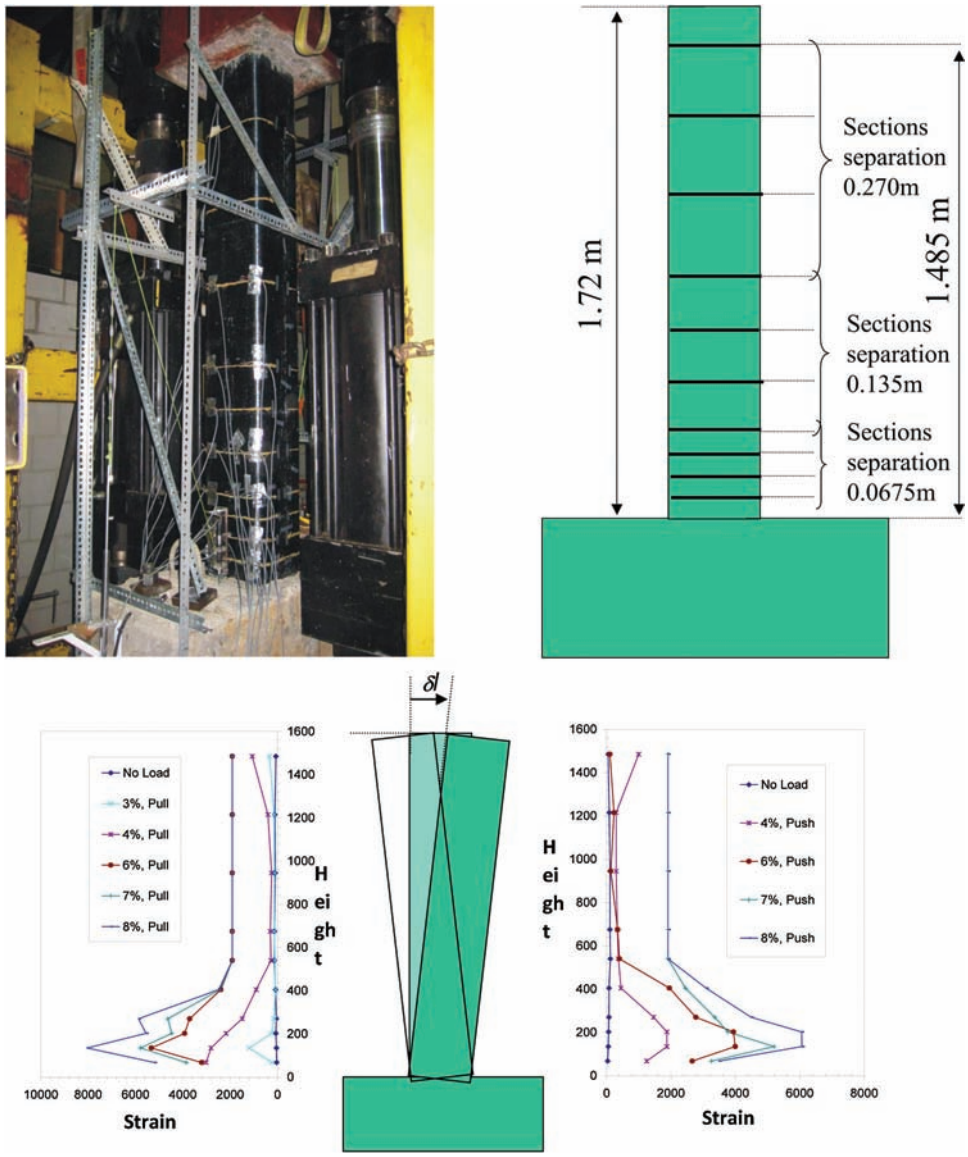

Figure 18.13 Concrete column strain monitoring.[23]

processing become fairly obvious. Component performance for both the optical source and detector, as well as for timing circuitry, becomes quite complex and the requirements quite high. These sensors are sensitive to the overall instantaneous acoustic pressure; therefore, ambient noise also needs to be addressed. Complex algorithms have been developed to eliminate unwanted ambient noise and isolate particular acoustic sources and determine their locations, frequency, and amplitude content.

Table 8.2 shows the relative pressure levels for various acoustic events and environments. DAS systems have shown that they are able to measure ~ .0001 Pa as a minimum detectable signal.

Figure 18.14 shows a simplified system layout of a DAS system for security monitoring.

The acoustic signatures for various events can be recorded and used as a library to correlate against for determination of the signal details. The plots shown in Fig. 18.15 display a sample of some of these different events, along with Fig. 18.16, which shows a perimeter-monitoring setup.

Table 18.2 Pressure levels for various acoustic events and environments.

Level	References	
0 dB	0.00002 Pa	Threshold of Hearing
60 dB	0.02 Pa	Business Office
80 dB	0.2 Pa	Shop Noise
94 dB	1 Pa	Large Truck
100 dB	2 Pa	Jackhammer
120 dB	20 Pa	Airplane Take Off
140 dB	200 Pa	Threshold of Pain
100,000 Pa		Atmospheric Pressure

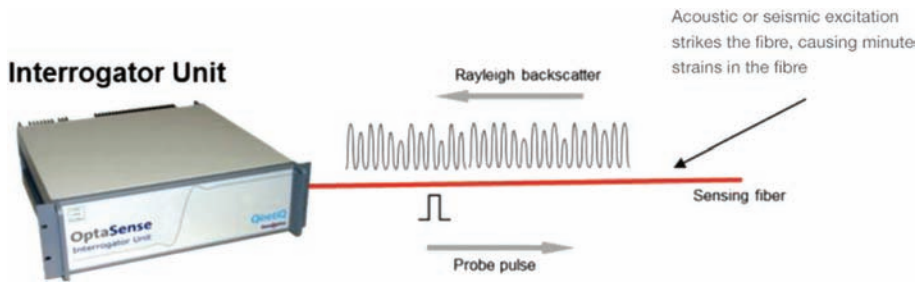

Figure 18.14 System components of DAS system (courtesy OptaSense).

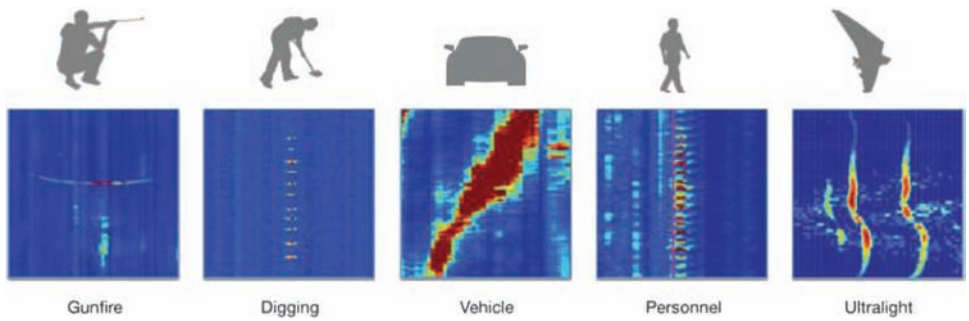

Figure 18.15 Acoustic signatures for various intrusion events (courtesy OptaSense).

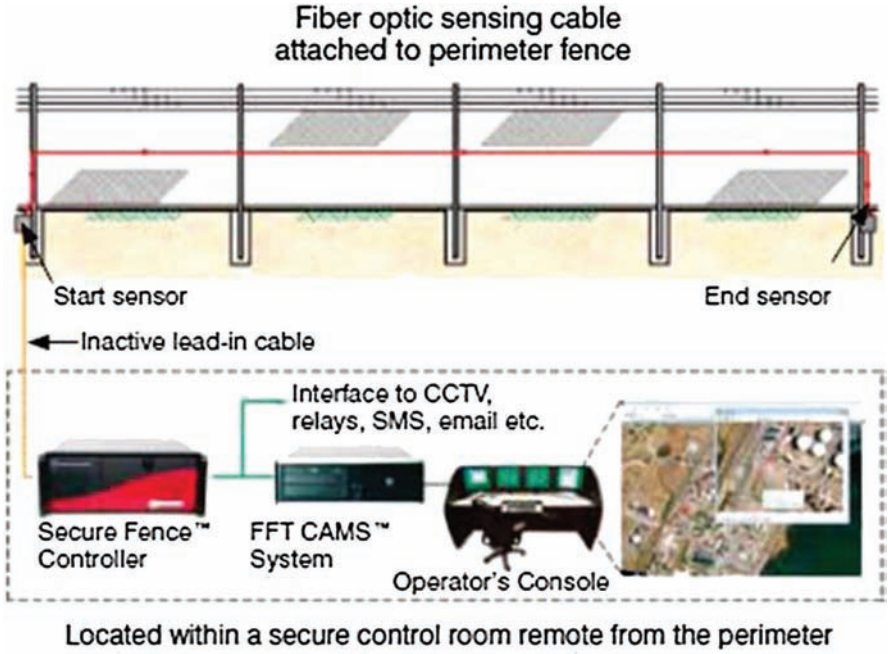

Figure 18.16 Fence perimeter sensor (courtesy FFT).

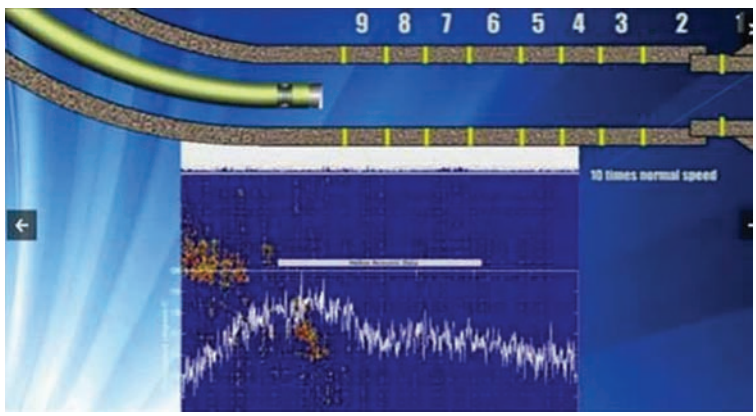

Figure 18.17 In-well seismic and acoustic measurements (courtesy of Fotech Solutions).

A sample DAS acoustic measurement in an oil well is shown in Fig. 18.17, where the acoustic signature for the hydraulic fracturing well is being monitored; a leak detection response detected with DAS[24] is shown in Fig. 18.18. Figure 18.19 shows a railway monitoring system. In this plot the two disturbances are trains approaching one another.

To date the Raman-based DTS systems have gained the greatest commercial acceptance compared to the other fiber optic distributed sensors. The

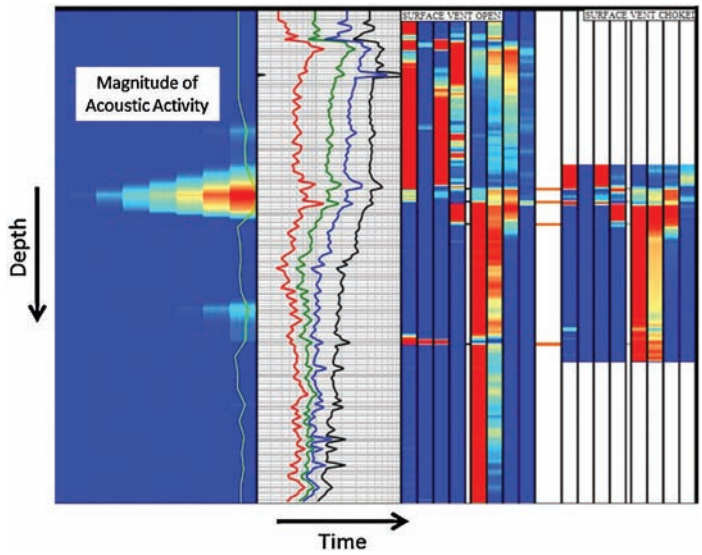

Figure 18.18 Detection of sporadic events over time (Courtesy of HiFi Engineering).

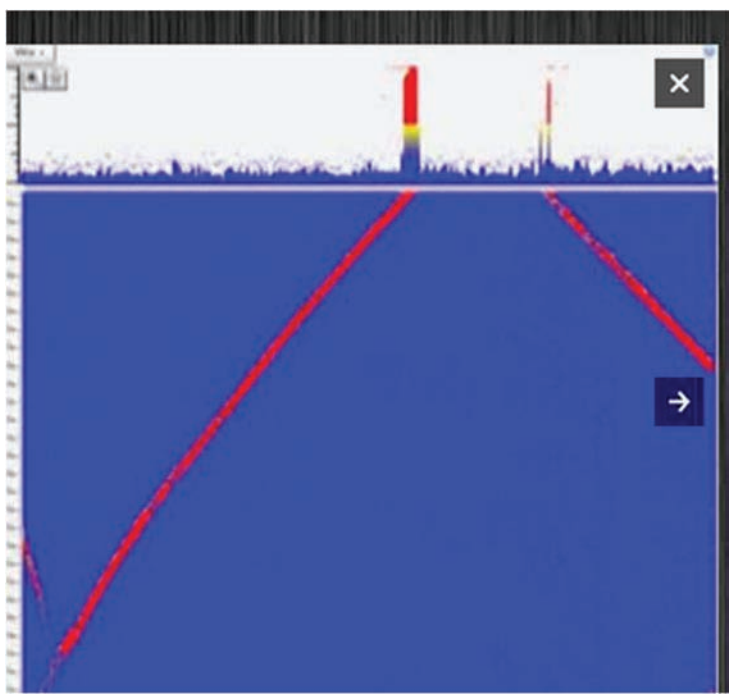

Figure 18.19 DAS railway monitoring (courtesy of Fotech Solutions).

instrumentation for these sensors is the least complex, allowing affordable and field-hardened units to be built and installed. Furthermore, the need for distributed temperature measurements in many industrial applications and the value that obtaining information in real-time brings, especially in oil and gas applications, have accelerated the adoption and commercial success of Raman DTS systems. DAS systems will continue to be further developed and optimized for various applications. The ultimate achievement for these systems would be to truly measure distributed flow and composition within the oil and gas industry. The ability to make such a measurement would easily justify the economics required for installation. Brillouin technology is unique in that it can measure both temperature and strain, and is frequency encoded. Both the requirement of an optical loop for high-quality measurements and the instrumentation costs will need to be addressed in order to gain further commercial success.

18.6 Quasi-distributed Sensing Systems

The various scattering mechanisms give rise to distributed sensing systems in which every location in the fiber can be used as a sensor. While Bragg gratings and interferomtric sensors generally are characterized by discrete sensing points along a fiber, they can be configured to have many sensing points along a fiber and act as quasi-distributed sensing systems. More detailed information on these systems is given in Chapter 10.

References

1. J. P. Dakin et al., "Distributed optical fiber temperature sensor using a semiconductor light source and detector," *Electron. Lett*. **21**, 569–970 (1985).
2. B. K. Lagishetty and B. Srinivasan, "Development of a cost-optimized distributed temperature sensing system based on Raman scattering," *Twentieth International Conference on Optical Fiber Sensors*, OFS, Edinburgh (2009).
3. A. H. Hartog and M. P. Gold. "On the theory of backscattering in single-mode optical fibers." *J. Lightwave Technol.* **2**(2), 76–82 (1984).
4. J. Park, G. Bolognini, D. Lee, P. Kim, P. Cho, F. Di Pasquale, and N. Park, "Raman-based distributed temperature sensor with simplex coding and link optimization," *IEEE Photonics Technology Letters* **18**(17), 1879 (2006).
5. K. Vilhelmsson, "Simultaneous forward and backward Raman scattering in low-attenuation single-mode fibers," *J. Lightwave Technol.* **4**(4), 400–404 (1986).
6. J. Auyeung and A. Yariv, "Spontaneous and stimulated Raman scattering in long low loss fibers," *IEEE J. Quantum Electron*. **14**(5), 347–352 (1978).

7. M. A. Farahani and T. Gogolla, "Spontaneous Raman scattering in optical fibers with modulated probe light for distributed temperature Raman remote sensing," *J. Lightwave Technol.* **17**(8), 1379 (1999).
8. K. J. Blow and D. Wood, "Theoretical description of transient stimulated scattering in optical fibers," *IEEE J. Quantum Electron*. **25**(12), 2665–2673 (1989).
9. C. Yijiang and A. W. Snyder, "Saturation and depletion effect of Raman scattering in optical fibers." *J. Lightwave Technol.* **7**(7), 1109–1117 (1989).
10. K. Kikuchi, T. Naito, and T. Okoshi, "Measurement of Raman scattering in single-mode optical fiber by optical time-domain reflectometry," *IEEE J. Quantum Electron*. **24**(10), 1973–1975 (1988).
11. X. Zeng, X. Bao, C. Chhoa, T. Bremner, A. Brown, M. DeMerchant, G. Ferrier, A. Kalamkarov, and A. Georgiades, "Strain measurement in a concrete beam by use of the Brillouin-scattering-based fiber senor with single-mode fibers embedded in glass fiber reinforced polymer rods and bonded to steel reinforcing bars," *Applied Optics* **41**(24), 5105–5114 (2002).
12. L. Zou, X. Bao, F. Ravet, and L. Chen, "Distributed Brillouin fiber sensor for detecting pipeline buckling in an energy pipe under internal pressure," *Applied Optics* **45**(14), 3372–3377 (2006).
13. L. Zou, G. Ferrier, S. Afshar, Q. Yu, L. Chen, and X. Bao, "Distributed Brillouin scattering sensor for discrimination of wall-thinning defects in steel pipe under internal pressure," *Applied Optics* **43**(7), 1583–1588 (2004).
14. M. DeMerchant, A. Brown, X. Bao, and T. Bremner, "Structural monitoring by use of a Brillouin distributed sensor," *Applied Optics* **38**(13), 2755–2759 (1999).
15. L. Zou, X. Bao, Y. Wan, and L. Chen, "Coherent probe-pump-based Brillouin sensor for centimeter-crack detection," *Optics Letters* **30**(4), 370–372 (2005).
16. X. Bao, D. Webb, and D. Jackson, "Combined distributed temperature and strain sensor based on Brillouin loss in an optical fiber," *Optics Letters* **19**(2), 141–143 (1994).
17. X. Zeng, Q. Yu, G. Ferrier, and X. Bao, "Strain measurement of the load test on the Rollinsford bridge using distributed Brillouin sensors," *1st International Workshop on Structural Health Monitoring of Innovative Civil Engineering Structures*, Winnipeg, Canada, 265–274 (2002).
18. X. Zeng, Q. Yu, G. Ferrier, and X. Bao, "Strain and temperature monitoring of a concrete structure of nuclear reactor using a distributed Brillouin sensor," *1st International Workshop on Structural Health Monitoring of Innovative Civil Engineering Structures*, Winnipeg, Canada, 207–216 (2002).

19. Oz Optics Application Note APN0008, "Fiber Optic Distributed Brillouin Sensor Applications," September 2006.
20. J. Luo, Y. Hao, Q. Ye, Y. Hao, and L. Li, "Development of optical fiber sensors based on Brillouin scattering and FBG for on-line monitoring in overhead transmission lines," *J. Lightwave Technol.* **31**(10), 1559–1565 (2013).
21. J. Frings, "Enhanced pipeline monitoring with fiber optic sensors," *6th Pipeline Technology Conference*, Hannover, Germany (2011).
22. D. Inaudi and B. Glisic, "Long-range pipeline monitoring by distributed fiber optic sensing," *J. Pressure Vessel Technol.* **132**(1), 011701 (2010).
23. X. Bao, F. Ravet, and L. Zou, "Distributed Brillouin sensor based on Brillouin scattering for structural health monitoring," *Optical Fiber Communication Conference*, OFC 2006, Anaheim, CA (2006).
24. J. Hull, L. Gosselin, and K. Borzel, "Well integrity monitoring and analysis using distributed acoustic fiber optic sensors," *Proc. IADC/SPE Drilling Conference and Exhibition*, paper #128304, Society of Petroleum Engineering (SPE), New Orleans, Louisiana (2010).

Chapter 19
Market Opportunities

19.1 Introduction

The various sectors of fiber optic sensor technology are at different levels of maturity. Fiber optic switches and counters, which are an extension of optoelectronic devices, are more than 40 years old. The overall market for opto-electronic sensors, excluding telecommunications, was nearly $4 billion in 2012. The fiber optic segment is estimated to be in excess of $175 million. This family of products is at an advanced maturity level and has been proven and accepted in those niche market applications where it is appropriate.

Fiber optic gyroscopes have been a success in the military and avionics applications market segments. The primary gyroscope manufacturers, with strong government support, have developed Sagnac-based, interferometric-rotation-rate sensors with excellent performance and reliability that are cost competitive with existing technologies. Both military and civilian aircraft uses have performed exceptionally well. The 2012 market was estimated at about $125 million.

Distributed fiber optic sensing has created an opportunity for broad growth in a multiplicity of markets.[1] Distributed sensing systems allow a large number of sensing points to be monitored using a common electro-optic interface (interrogator) that has the potential for cost-effective solutions. Distributed fiber optic sensors are an enabling technology that creates smart systems in a variety of applications. For the most part, this is not a new technology. The initial commercialization efforts focused on military applications. However, the need to function in harsh environments and the development of optical fiber technology that can survive in these applications has significantly impacted the oil and gas industry. These smart sensing systems provide benefits throughout the life of a well, from exploration to drilling and completion, to production and reservoir management. There is no other technology that can provide critical process control information spatially throughout a well in real time over long periods. Without smart well technology, fracture monitoring and analysis, and applications like steam-assisted gravity drainage (SAGD) would be very difficult to effectively

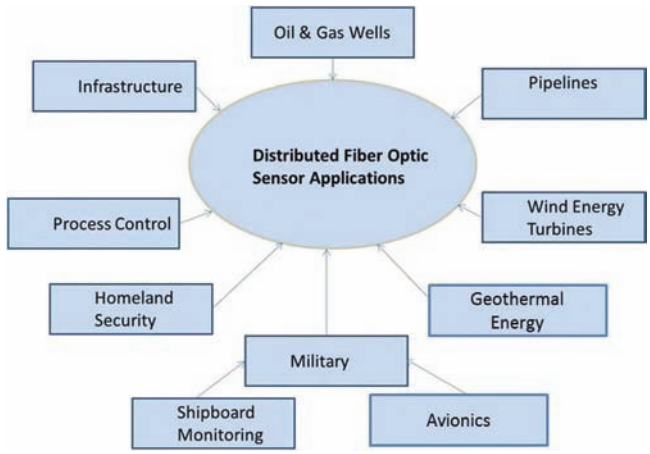

Figure 19.1 Distributed fiber optic sensor applications.

implement. A point that is understated is that distributed fiber optic sensing systems have enabled smart well technology which has created the North American energy boom. While energy is the leading market sector for this technology, it serves as a platform for many other applications (see Fig. 19.1).

The distributed fiber optic sensor market was estimated at $500 million in 2012. The smart oil well market segment (in-well) represented 41% of the total market in 2012 and is projected to reach 60% in 2017. In terms of the overall distributed fiber optic sensor market, Raman-scattering sensors have the largest market share (46%). Bragg grating technology sensors have 25% market share. Interferometric sensing approaches have about 25% market share, but half is for distributed acoustic sensing, which is rapidly gaining market share.[1]

19.2 Barriers to Market Growth[1]

The barriers to growth include:

- Cost,
- Competing technologies,
- Limited government funding,
- Lack of standards,
- Qualification testing, and
- Materials limitations.

Cost has been a major barrier to fiber optic sensor use. Many applications can be achieved with conventional technology, which is often significantly lower cost. Distributed sensing systems in which the electro-optic interface is shared with a large number of sensors can significantly impact the cost per sensing point. The use of high-volume components developed for the telecommunications industry can also impact cost. Kersey[2] stated that in areas such as process control, there are well-established, non–fiber-optic sensor technologies

that work well and are cost effective. The advantages of fiber optic sensors, such as immunity to EMI and high sensitivity, are not sufficient to replace a proven technological solution in most applications.

Government funding has played a key role in developing fiber optic sensor technology, the Department of Defense (Navy, Army, Air Force, DARPA) as well as the Department of Energy and the National Institute of Standards and Technology have funded hundreds of millions of dollars over the last 35 years. However, the potential for a government funding slowdown will have a negative impact on technology evolution.

Packaging is critical to sensor function and integration. Packaging problems are complicated by an overall lack of standardization. A high-performance sensor must be in a package that meets the needs of the end user. For instance, many industrial temperature sensors must be in a stainless steel sheath with proper fittings, so that replacement can be on a one-for-one basis with no retrofit problems. In a visit to a pressure transducer manufacturer, it was found that there were over 500 different pressure sensor (diaphragm) configurations. As a result, a new sensor technology has a significant package hurdle to overcome. As indicated throughout this book, many of the sensor technologies are sensitive to strain, temperature, polarization, and other effects that must be compensated for or isolated in the package design. Also, as sensor technology pushes into more difficult environments, new materials are required such as hydrogen-resistant fiber in oil wells and higher-temperature materials for industrial and avionic applications.

Another obstacle to the adaptation of fiber optic sensor technology is qualification testing. The cycle time to get a sensor into a test site and evaluated can be quite long. Long gestation periods for specific sensor applications must always be part of the planning process for commercialization. In addition, qualification testing can be expensive, as is, for example, the required flight testing for fiber optic gyroscopes.

19.3 Summary and Conclusions

Several factors have impacted the fiber optic sensor market growth.

On the positive side:

- The fiber optic gyroscope has been widely accepted;
- The price of oil supports growth of smart wells for oil and gas;
- Distributed fiber optic sensor technology has been proven to be robust and reliable in harsh environment applications;
- The success of smart well technology in increasing North American energy capacity has been a driver to expand the market; and
- Over the past several years, there has been a consolidation in the industry with a multiplicity of acquisitions and strategic partnerships.

On the negative side:

- Delays and reductions in government spending have impacted the market;
- In many market segments, adoption of new technology has been slow;
- The high cost of fiber optic sensing systems is a deterrent for many applications; and
- Competition from wireless systems will have an impact, especially in simple alarm applications.

After consideration of these positive and negative factors, all of the fiber optic sensor companies that were surveyed in a recent study are optimistic about future growth, with 100% of the companies surveyed forecasting market expansion at 10% or higher. An important conclusion of the survey was that strategic partners and reduced cost were the dominant growth drivers.[1]

The distributed fiber optic sensor market was estimated at $500 million in 2012. In 2017, the market is projected to be over $1.5 billion, with more than 70% associated with the oil and gas and other energy segments.[1]

References

1. D. A. Krohn, "Photonic Sensor Consortium Market Survey," Information Gatekeepers, www.igigroup.com, June, 2013.
2. A. D. Kersey et al., "Fiber optic sensors," *J. Lightwave Tech.* **15**(8), 1442 (1997).

Index

David Krohn has over 45 years' experience in the photonics industry. He is the Managing Partner of Light Wave Venture LLC, which is focused on developing telecommunications, sensor, power delivery, and energy-related business opportunities. He has assisted over 120 companies with activities in marketing, planning, and management functions, as well as technical input. In prior experience, he served as Global New Business Director for Photonics at 3M Company. From 1987 to 1998, he was the General Manager of the 3M Specialty Optical Fiber Business that included the Bragg Grating Technologies business acquired from UTC in 1995. He founded EOTec Corporation in 1979 that manufactured specialty fiber, sensors, cables, cable assemblies, and data links. He was the CEO of EOTec until the business was acquired by 3M in 1987. Currently, he is also very active in many technical societies and teaches short courses in technology and business development at various Universities. He started and is the current chairman of the Photonic (Fiber Optic) Sensor Consortium which has more than 60 participating companies and organizations. As the photonics marketplace has radically changed in the last few years, he has worked with several companies to diversify into non-telecommunication markets such as military, homeland security, biomedical, and green energy areas, such as alternative energy sources.

David Krohn has significant experience in the technical aspects of photonic design and fabrication and is currently active in the development of advanced photonic components and systems. He played a key role in the development of polarizing maintaining (PM) fiber that is a critical component in advanced fiber optic gyro systems.

David Krohn attended Rutgers University as an undergraduate (BS 1965). He obtained his MS from Case Western Reserve University in 1967 and his Ph.D. from Lehigh University in 1973. All his degrees are in materials science. He has written 5 books (4 on fiber optic sensors), over 60 papers and holds 27 patents relating to photonics.

Trevor MacDougall is Vice President of Fiber Optic Engineering and Operations at Petrospec Engineering. He has over 25 years of experience in the design and commercialization of fiber optic components and sensing systems. Trevor was a co-founder of QOREX, which was acquired by Petrospec in May of 2012. Prior to QOREX he held senior positions at Weatherford, CiDRA, and 3M. He currently directs the engineering and manufacturing of the Petrospec fiber optic sensing system product line. He holds a Bachelor of Science degree from the University of Rhode Island in Electrical Engineering (EE) as well as a Master of Science degree in EE. He has 48 patents and 20 publications in the field of fiber optics.

Alexis Mendez is President of MCH Engineering LLC, a consulting firm specializing in optical fiber sensing technology. He received a Ph.D degree in Electrical Engineering from Brown University, USA in 1992. He has over 25 years of experience in optical fiber technology, sensors and instrumentation. Dr. Mendez was the former Group Leader of the Fiber Optic Sensors Lab within ABB Corporate Research (USA) where he led R&D activities for the development of fiber sensors for use in industrial plant, oil & gas, and high voltage electric power applications. He has written 60 technical publications, given numerous invited talks and tutorials, taught several short courses on fiber sensors, holds 5 US patents and is recipient of an R&D100 award.

Dr. Mendez is a Fellow of SPIE and was past Chairman of the 2006 International Optical Fiber Sensors Conference (OFS-18); past Technical Chair of the 2nd Workshop on Specialty Optical Fibers and their Applications (WSOF-21010); and co-editor of the "*Specialty Optical Fibers Handbook*".